Jonctions tunnel magnétiques à aimantation perpendiculaire : anisotropie, magnétorésistance, couplages magnétiques et renversement par couple de transfert de spin

Lavinia Nistor

UNIVERSITÉ DE GRENOBLE

THÈSE

Pour obtenir le grade de

DOCTEUR DE L'UNIVERSITÉ DE GRENOBLE

Spécialité : **Physique des Matériaux**

Arrêté ministériel du 7 août 2006

Présentée par

Lavinia Elena NISTOR

Thèse dirigée par **M. Bernard RODMACQ**
et co-dirigée par **M. Bernard DIENY**

préparée au sein du **Laboratoire Spintec (INAC, CEA Grenoble)**
dans l'**École Doctorale de Physique**

Magnetic tunnel junctions with perpendicular magnetization: anisotropy, magnetoresistance, magnetic coupling and spin transfer torque switching

Thèse soutenue publiquement le **7 Octobre 2011**
devant le jury composé de:

M. James M. D. COEY
Prof., Trinity College, Dublin (Président)
M. Stéphane MANGIN
Prof., Université Henri-Poincaré, Nancy (Rapporteur)
M. Dafiné RAVELOSONA
D.R. CNRS, Institut d'Électronique Fondamentale, Orsay (Rapporteur)
M. Bernard RODMACQ
Ingénieur, Spintec, CEA Grenoble (Directeur de Thèse)
M. Bernard DIENY
Ingénieur, Spintec, CEA Grenoble (Co-Directeur de Thèse)
M. Olivier FRUCHART
D.R. CNRS, Institut Néel, Grenoble (Examinateur)
M. André THIAVILLE
D.R. CNRS, Laboratoire de Physique des Solides, Orsay (Examinateur)
M. Alain SCHUHL
Prof., Université Joseph-Fourier, Grenoble (Invité)

Remerciements

Je tiens à remercier en premier celui qui m'a ouvert la porte vers la recherche dans le domaine du magnétisme : **Viorel Pop**, Professeur à l'Université Babes-Bolyai de Cluj-Napoca (Roumanie), qui a suivi avec beaucoup d'attention, de bons conseils et d'encouragements tout mon parcours scientifique à l'Université de Cluj et à l'Université Joseph-Fourier de Grenoble. Je vous remercie de m'avoir accueilli dans votre équipe depuis mes premières années de Faculté en me donnant la possibilité de faire mes premiers pas dans le métier de chercheur à vos cotés et surtout de m'avoir toujours soutenu dans mes choix. Merci pour votre confiance.

Je voudrais remercier **Bernard Rodmacq**, mon directeur de thèse à Spintec, pour toute sa patience, sa disponibilité, son enthousiasme et ses conseils. Je vous remercie d'avoir été à mes côtés dans mon apprentissage du métier de chercheur, de m'avoir toujours encouragée pour dire mes idées, de m'avoir appris à bien argumenter chaque manip, chaque point de mesure et de m'avoir initiée à la physique très appliquée à travers les brevets. Merci de m'avoir encouragée aussi à explorer pendant la thèse des problématiques plus fondamentales à coté d'un but plus appliqué. Merci pour votre disponibilité, les discussions avec vous m'ont apporté beaucoup au niveau scientifique et m'ont aidé à développer mon esprit critique.

Je voudrais aussi remercier **Alain Schuhl**, Directeur de SPINTEC jusqu'en 2010, et **Bernard Dieny**, son adjoint et mon correspondant CEA, de m'avoir accueilli dans leur Laboratoire en me donnant la chance de découvrir un autre "monde" entre la physique fondamentale et les applications. **Alain Schuhl,** je vous remercie pour votre disponibilité et surtout pour vos conseils scientifiques mais aussi pédagogiques. **Bernard Dieny**, je voudrais vous remercier spécialement pour m'avoir suivi pendant ces années de thèse, pour vos conseils scientifiques concernant les articles et les présentations orales que j'ai faits pendant ma thèse. Je tiens aussi à remercier **Jean-Pierre Nozières,** actuel Directeur de Spintec, pour sa disponibilité, sa sincérité et les encouragements pour la suite de la thèse.

Je remercie **James M.D. Coey** d'avoir accepté de présider mon jury de thèse. Je remercie également **Stéphane Mangin et Dafiné Ravelosona** pour avoir accepté le travail de rapporteur pour ma thèse et pour leurs observations et suggestions. Merci également à **Olivier Fruchart** et **André Thiaville**, et à tous les membres du jury, pour le temps qu'ils ont consacré à la lecture mon manuscrit de thèse, pour leurs questions intéressantes lors de ma soutenance et leurs observations et commentaires qui ont été très bénéfiques pour l'amélioration de ce manuscrit.

Merci à **Stéphane Auffret** pour toutes ses heures passées devant la machine de dépôt dans la salle blanche PTA, pour nous fabriquer les échantillons dont on avait besoin pour cette étude. Je te remercie Stéphane, pour la confiance que tu m'as montrée en m'apprenant à utiliser la machine de dépôt Actemium en tenant compte des problèmes techniques qu'elle avait. Merci Stéphane aussi pour les discutions scientifiques ou pas qui m'ont fait un grand plaisir.

Je tiens à remercier également **Liliana Prejbeanu** pour m'avoir donné la chance de faire de l'enseignement, pour toutes ses encouragements et conseils et discussions scientifiques et pédagogiques.

Je remercie aussi **Mairbek Chshiev,** pour toute sa disponibilité, sa patience pour discuter avec moi et m'aider à mieux comprendre mes résultats à travers la théorie. Merci Mair aussi de m'avoir laissé un peu explorer le monde des simulations de transport de spin et structure électronique des matériaux.

Pendant cette thèse j'ai utilisé différentes techniques. Je voudrais remercier pour leur disponibilité et leur aide pour résoudre des petits problèmes de manip à **Stéphanie Pouget** pour la réflectivité de RX, **Jean-François Jacquot** pour le Squid et **Marité** pour m'avoir appris le process des jonctions tunnel à la PTA. Mes remerciements aussi au personnel **de la salle blanche PTA.**

Je voudrais aussi remercier **Crocus Technology** et spécialement **Clarisse Ducruet, Céline Portemont et Lucian Prejbeanu** pour leur collaboration sur certaines études et pour m'avoir fabriqué des échantillons et m'avoir laissé utiliser leur outil CAPRES pour faire des mesures de transport sur couches continues et pouvoir avancer plus vite (sans passer par l'étape lithographie) dans la fabrication des jonctions tunnel magnétiques.

Je remercie également tout le personnel du Laboratoire pour l'accueil et pour la bonne humeur et surtout les secrétaires qui m'ont beaucoup aidé avec tous les papiers qu'on a dû faire pendant ces 3 années de thèse.

Je vous souhaite une bonne lecture !

Introduction

MATERIALS. THE SPINTRONICS AGE. MOTIVATION

Materials, more or less sophisticated, are present in Man's life since several thousand years. Man's intelligence, in the need to improve his life condition, contributed to the evolution of the materials used in our daily life (from the simplest ones like the wood and stone to more complex ones like bronze and iron). The impact of materials in Man's evolution was so strong than we can assert it helped to model civilisations. For instance, in the case of Hittites (18th century before Christ), the improvement of the technique to fabricate very good quality iron made them one of the most advanced and powerful civilisations of the antiquity and helped them to dominate the Mediterranean region **[Hum_04]**. The appreciation of the materials impact in Man's history and evolution was illustrated in the History by naming each era after the material used:

- stone age - 4500 bc
- bronze age - 1700 to 0 bc
- iron age – 1500 bc to 1950 ac

Nowadays we are more directed towards the use of functional materials (electronic materials, materials for optics, hydrogen storage materials) for technological applications but also for fundamental research because these materials are full of interesting phenomena to be understood and valorised.

We will focus in this manuscript on the electronic materials in which electrons are the first responsible for their physical properties. Some examples of electronic materials: **magnetic materials, metals, insulators**.

Magnetism is the property of materials which respond to an applied magnetic field and is related to the electron motion and parity of electrons in the atom. In a simplified picture according to Ampère and Oersted the electron motion (orbital motion around the nucleus, and spin motion around his axis) results in an electric current from which a magnetic field will rise. But spin comes out of quantum mechanics combined with relativity and can be detected by its **magnetic moment,** $m=g\,\mu_B\,s$, or the average spin of an ensemble of electrons in a given volume, the **magnetization** (M). Considering the electrons numbers, the Pauli's law for filling the atomic energy levels (which allows one paired spin up and down electrons on each energy level in the atom) and spin-orbit coupling, one obtains the atomic momentum, J. So in the case of diamagnetic materials (which have no unpaired electrons and filled energy levels in their atoms, J=0) the magnetism will arise from the interaction between the external applied field and the electron motion in the atom through the Lentz law, resulting in a magnetic moment which will be opposite to the applied field. More interesting are materials with an atomic momentum like paramagnetic and ordered ferromagnetic or antiferromagnetic materials. In paramagnetic materials the uncompensated orbital momentum (L) and spin angular momentum (S) result in independent atomic moments contrary to the ferromagnetic materials which have cooperating atomic moments. This is why the response to an applied magnetic field will be different: paramagnetic materials will be ordered only in the presence of a magnetic field, while ordered materials will stay aligned even after the applied field is removed.

Electrons are also responsible for the metallic or insulating properties of materials. In this case electrons have the role of charge carrier. So in a simple picture one can distinguish such materials by their charge mobility. While metals present high electron mobility, insulators do not.

The fabrications techniques can change and model material properties. This is why they are an important factor in the materials evolution. Another example from history: the bronze discovery was due to the insertion of 10% tin (Sn) in copper (Cu) in order to decrease its melting temperature, making easier the elaboration of different objects. Today, joining together magnetic materials with metals or insulators by using new techniques of fabrication of thin films (with layer thicknesses of the order of the electron scattering length) like Molecular Beam Epitaxy or sputtering, made possible to evidence new physical phenomenon like:
- Interfacial perpendicular magnetic anisotropy (PMA) [Gra_68]
- Giant MagnetoResistance (GMR) [Bai_88, Bin_89]
- Tunnel MagnetoResistance (TMR) [Moo_95]
- Oscillatory character of RKKY exchange coupling [Par_91].

All these fascinating phenomena consider the spin of the electron in addition to its charge, associating magnetism and electronic transport in a new research area: the **spin electronics or Spintronics**. Taking into account both charge and spin of electrons make the physics of materials more complex but gives an additional advantage to applications providing more possibilities to conceive new devices and reinvent the electronics.

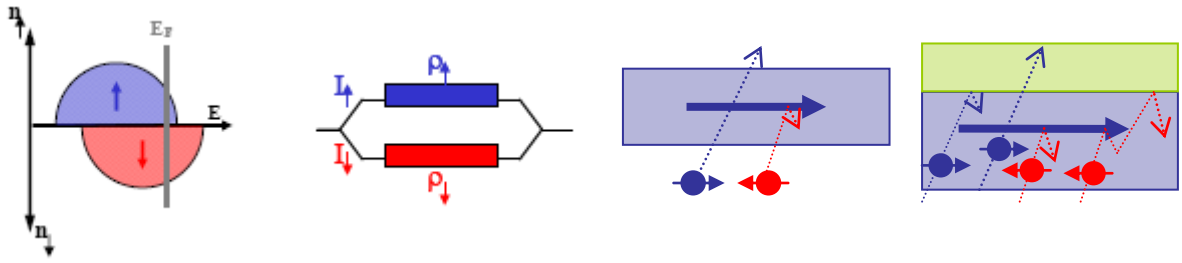

Figure 1: Spintronics bricks: (a) Spin asymmetry; (b) Mott approximation; (c) Spin dependent diffusion; (d) Spin accumulation.

Spintronics is based on four effects (see **Figure 1**) which, when combined, are at the origin of all the properties observed in thin magnetic layers:
1) **Spin asymmetry (d electrons)**: in the density of states for localized d electrons of a ferromagnetic material the number of spin up (↑) of d electrons is different from that of spin down (↓) ones.
2) **Mott approximation**: the electron spin is conserved (low probability of spin inversion after electron diffusion on the layer defects). As a consequence, two conduction channels exist in parallel for spin up and spin down [Mot_36].
3) **Spin dependent diffusion (s electrons):** as a consequence of the spin asymmetry there will be a different probability of diffusion for the s spin up and spin down electrons (conduction electrons) when they are parallel (P) or antiparallel (AP) to the magnetization of the layer.
4) **Spin accumulation (s electrons)**: s electrons will be diffused at a magnetic/nonmagnetic interface (because of the difference between the spin disequilibrium-equilibrium states). According to the Mott approximation s electrons will have large diffusion lengths.

Among all these properties of ferromagnetic-metal multilayers, the discovery of the GMR had the strongest impact on both fundamental and applied physics. From a fundamental point of view, GMR can be explained by the **spin dependent diffusion of the electrons** due to the relative orientation of the magnetisation in the magnetic layers. So when the layer's magnetizations are parallel, only the electrons with the spin parallel to the magnetization can pass through the sample because they are weakly diffused resulting in a low resistance (R_{low}) state. In the case when the layer's magnetizations are antiparallel, both electrons with parallel/antiparallel spin will be diffused resulting in a high resistance (R_{high}) state. The large resistance variation between the AP and P orientation inspired the name of GMR. The schematic principle for a simplified case of two ferromagnetic layers (F1 and F2) separated by a nonmagnetic metallic layer (NM) is presented in **Figure 2**.

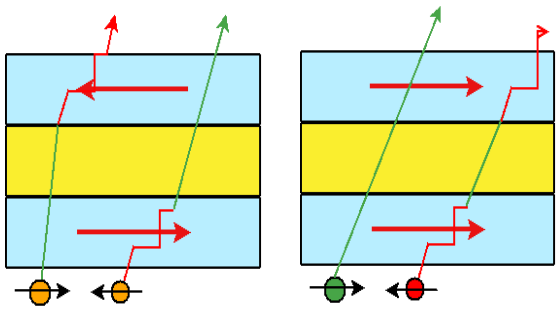

Figure 2: Schematic explanation of the GMR effect.

From an application point of view the GMR discovery offered a new concept for magnetic sensor device: the **spin valve** [Die_91]. Giving a much improved sensitivity at nanoscale than inductive or even anisotropic magnetoresistance sensors, the spin valves were rapidly integrated in the read/write heads of the hard disk drive (HDD) industry. This allowed a fast increase of the HDD areal density, as it can be observed in **Figure 3,** and inspired a new device for industrial applications, the **Magnetic Tunnel Junction**.

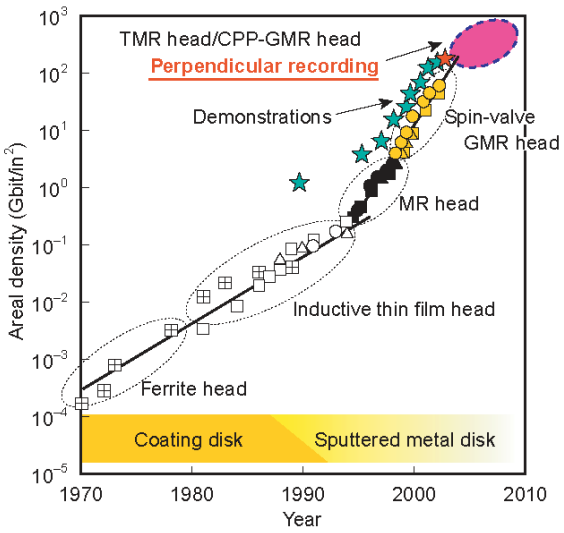

Figure 3: Read/Write heads technologies which contributed to the areal density increase in hard disk drives [Fuj_06].

The magnetic tunnel junctions (MTJ) are spintronic devices derived from spin valves just replacing the metallic spacer by a very thin insulator (oxide) layer so that electrons can pass from one ferromagnetic layer to the other by tunnelling. In this case the **spin filtering** effect is dominant compared to spin diffusion and the result is a very high relative resistance variation called Tunnel MagnetoResistance (TMR). This is why MTJ devices have a higher output signal than spin valves, making them very attractive for industrial applications. The difference in the resistance values between the P and AP configuration of the magnetic layers can be used for binary coding so that new recording media applications or logic circuits can be imagined.

Today computers use four means of data storage: dynamic random access memory (DRAM), high density memory which needs to be constantly refreshed (high power consumption); static random access memory (SRAM, used in cache memories), with fast reading and writing cycles; Flash memories, non-volatile but with a low writing access; and hard disk drives (HDD), presenting high density but relying on moving parts, which impose size and speed limitations.

In the future, consumer needs for recording media will demand to combine **high access speed, reduced noise, reliability, portability, non volatility and low power consumption in a smallest as possible chip with high density. However, one also has to consider stability against thermal fluctuations and long-term data retention** (**Appendix 1**).

Spintronics give us a candidate for this universal memory based on MTJ technology: the **Magnetic Random Access Memory (MRAM).** MRAM is attractive for industrial applications because it could, in principle, replace all other kinds of memories. For instance using a MRAM in a computer, data could be loaded directly into the working memory and wouldn't have to juggle between main memory (SRAM) and hard disk. This could make possible instant-on systems and innovate in the computer architecture.

First MRAM architectures using in-plane magnetized thin films separated by a thin oxide provide some key advantages: the **non volatility and unlimited read/write endurance (10^{15} read-write cycles),** in addition to those of conventional RAM memories (speed of SRAM). The energy used for operating (data retention for writing/reading process) is much smaller than that of FLASH because the time required per operation is much shorter. But, even if MRAM writing technique seems the simplest one using an applied field to switch the free layer magnetization, the architecture required is complicated and requires a lot of space making impossible to reach high densities. In addition, Field Induced Magnetic Switching MRAM architectures reach their limits when the cell size is reduced below 100 nm. Decreasing the cell size will increase the current density necessary to produce the switching field and also the write power, the selection errors for writing the memory cells will also increase, as the impact of the thermal fluctuations on the data stability. A 4Mb-MRAM was commercialized by Freescale Motorola (now EverSpin) in 2006 **[Eve_06]** and finds applications in satellite, aerospace, automotive/ telecommunications industries or memory embedded in controllers or printers.

A high density/stable/fast MRAM memory is the dream to the universal memory which could be used in all applications and replace all different recording media and memories of present times. But it requires a new MRAM technology.

A new physical phenomenon for magnetization switching, the **spin transfer torque switching (STT)** predicted by Slonczewski in 1996 **[Slo_96, Ber_96]** and first measured in spin valves **[Kat_00, Sun_02, Puf_03],** gives the possibility to reach storage densities of DRAM's. An STT-MRAM architecture can be imagined and can bring considerable advantages: no more addressing errors because only the pillars traversed by the pulse current will be written; increasing the memory density, by suppressing write line, enables 1 Transistor-1 MTJ per cell similar to DRAM and makes possible the MTJ cell size reduction.

In the case of nano-magnetic elements with in-plane magnetization, the thermal stability limit is not related to the current induced switching parameters, but to their shape. In materials without preferred in-plane axis for the magnetization (without crystalline anisotropy), a specific elliptical shape is required to stabilize the magnetization along the long in-plane axis in order to minimize the magnetostatic energy. Reducing cell size makes impossible to keep the elliptical shape and to prevent from magnetization curling due to thermal fluctuations. One solution is to define the magnetization direction of the free layer by coupling it to an antiferromagnetic layer (AF). The switching of the free layer is realized by heating the MTJ cell above the blocking temperature of the antiferromagnet. Based on this phenomenon Spintec proposed a new write technique based on thermally-assisted spin transfer torque switching (STT-TAS-MTJ) **[Pre_04, Oun_02, Noz_06, Her_10]**.

Using materials with out-of-plane anisotropy could be an alternate solution to keep the magnetization along one well-defined axis in MTJ and enhance the robustness against thermal fluctuations **[Mor_06, Car_08, Yoo_05]**. The size and shape limitations of planar MTJ elements with respect to magnetization curling are eliminated by using p-MTJs. Furthermore studies **[Man_06, Nak_08]** have shown that STT perpendicular structures may present lower critical switching currents and higher STT efficiency.

These new out-of-plane MTJ elements are promising for industrial applications and interesting for fundamental physics. The pMTJ combine both magnetic properties as out-of-plane anisotropy of the layers and tunnel transport properties across an insulator barrier. In conventional MTJ the high TMR performances are given by the good match between the crystal structure and texture of barrier and electrodes, interfaces quality, low roughness of the barrier. PMA can have different origins, either bulk (in hcp CoCrPt, heavy rare earth/transition metal alloys, or FePt $L1_0$ ordered alloys, or interfacial (in Pt/Co, Pd/Co, or Co/Ni multilayers). It has also been observed that a quite large PMA can be induced at the interfaces between the ferromagnetic electrodes and an oxide **[Mon_02, Rod_03]**. One can take advantage of this PMA from the oxide magnetic electrode interface to fabricate out-of-plane MTJ.

In conclusion pMTJ are very promising for increasing storage areal density, still keeping good data stability and low power consumption. But even if the stability problem seems to be solved other questions can arise:

1) *Are nanofabrication techniques able to produce very small nanopillars having the size of one transistor of our days (30nm)?*
2) *Can we fabricate adapted electronics around a 1T-STT-MTJ cell?*

STT-pMRAM will be able to compete with FLASH memories and HDD if these technical aspects are solved at similar production cost. Otherwise MRAM will be used in special markets like Battery-Backed SRAM replacement and would be attractive in applications where speed and permanent data storage are needed, eliminating the use of combined memories. Some examples of applications are the replacement of components of server systems, networking and data-storage devices, home-security systems and computer printers. The consequences are enormous considering the circuit size reduction, low system energy resulting in increased battery life, enhanced performance by improving efficiency of data transfer (the computer start speed). Even more, with MTJ it will be possible to take advantage of precessional dynamics for low power operation or to obtain tuneable radiofrequency oscillators leading to new RF devices for the mobile phone industry.

This thesis summarizes all the efforts done during the last three years, from the fabrication of pMTJ elements to the demonstration of low STT switching currents obtained by using outofplane magnetic anisotropy.

The engineering of pMTJ is a real challenge and a difficult task because good TMR and PMA properties will impose constraints and limit the working window of the device. It also demands a good understanding of PMA and TMR origins, and a good mastering of the thin film growth and characterization techniques in order to be able to optimize the characteristics of materials to obtain their best properties in a given sample. Thin film growth and characterization showed me the physics complexity and wealth of structures made of different materials with different properties. One can obtain a lot of combinations of these properties using different materials, changing their layers thicknesses, performing annealing treatments, applying magnetic fields or current pulses.

We will present here the most significant studies and results in four chapters. **Chapter I** will be dedicated to the fabrication of materials having PMA contribution also from the interface with an oxide. Both magnetic metal/oxide and oxide/magnetic metal structures will be studied. The PMA origin in these two kinds of materials will be studied by varying different parameters like nature of magnetic material, annealing temperature, layer thicknesses. **Chapter II** will be dedicated to full pMTJ structures and two kinds of materials will be presented: those with very high PMA based on Pt/Magnetic Metal/Oxide and those with low PMA like Ta/Magnetic Metal/Oxide. Magnetic and transport properties of both structures will be studied in order to choose the best candidate for the MRAM applications. A correlation between TMR and PMA was observed and it helped to confirm the PMA origin from the magnetic metal/oxide interface. **Chapter III** is a more fundamental study of pMTJ and concerns interlayer exchange coupling in the presence of out-of-plane anisotropy. A detailed study was made comprising annealing

temperature and layers thickness dependence of the coupling in order to understand its origin. Finally the STT-pMTJ concept will be validated in **Chapter IV**, after sub-micrometric patterning of magnetic tunnel junctions.

References

[Bai_88] M.N. Baibich, J.-M. Broto, A. Fert, F. Nguyen Van Dau, F. Petroff, P. Etienne, G. Creuzet, A. Friederich and J. Chazelas, *Giant magnetoresistance of (001)Fe/(001)Cr magnetic superlattices,* **Phys. Rev. Lett.** **61** (1988) 2472.

[Ber_96] L. Berger, *Emission of spin waves by a magnetic multilayer traversed by a current,* **Phys. Rev. B** **54** (1996) 9353.

[Bin_89] G. Binasch, P. Grünberg, F. Saurenbach and W. Zinn, *Enhanced magnetoresistance in layered magnetic structures with antiferromagnetic interlayer exchange,* **Phys. Rev. B** **39** (1989) 4828 (R).

[Car_08] B. Carvello, C. Ducruet, B. Rodmacq, S. Auffret, E. Gautier, G. Gaudin and B. Dieny, *Sizable room-temperature magnetoresistance in cobalt based magnetic tunnel junctions with out-of-plane anisotropy,* **Appl. Phys. Lett.** **92** (2008) 102508.

[Die_91] B. Dieny, V.S. Speriosu, B.A. Gurney, S.S.P. Parkin, D.R. Wilhoit, K.P. Roche, S. Metin, D.T. Peterson and S. Nadimi, *Spin-valve effect in soft ferromagnetic sandwiches*, **J. Magn. Magn. Mat.** **93** (1991) 101.

[Eve_06] **http://everspin.com/press.php?ppo=2006&qtype=press**

[Fuj_06] *Storage Systems and HDD Technologies,* **Fujitsu Sci. Tech. J.** **42** (2006) 122.

[Gra_68] U. Gradmann and J. Müller, *Flat ferromagnetic epitaxial 48Ni/52Fe(111) films of few atomic layers*, **Phys. Stat. Sol.** **27** (1968) 313.

[Her_10] J. Alvarez-Hérault, PhD Thesis, Grenoble University (2010).

[Hum_04] R.E. Hummel, *Understanding Materials Science - History, Properties, Applications*, 2nd Edition, Springer-Verlag, New York, (2004).

[Kat_00] J.A. Katine, F.J. Albert, R.A. Buhrman, E.B. Myers and D.C. Ralph, *Current-driven magnetization reversal and spin-wave excitations in Co/Cu/Co pillars,* **Phys. Rev. Lett.** **84** (2000) 3149.

[Man_06] S. Mangin, D. Ravelosona, J.A. Katine, M.J. Carey, B.D. Terris and E.E. Fullerton, *Current-induced magnetization reversal in nanopillars with perpendicular anisotropy,* **Nature Mater.** **5** (2006) 210.

[Mon_02] S. Monso, B. Rodmacq, S. Auffret, G. Casali, F. Fettar, B. Gilles, B. Dieny and P. Boyer, *Crossover from in-plane to perpendicular anisotropy in Pt/CoFe/AlO_x sandwiches as a function of Al oxidation: A very accurate control of the oxidation of tunnel barriers,* **Appl. Phys. Lett.** **80** (2002) 4157.

[Moo_95] J.S. Moodera, L.R Kinder, T.M. Wong and R. Meservey, *Large magnetoresistance at room temperature in ferromagnetic thin film tunnel junctions*, **Phys. Rev. Lett.** **74** (1995) 3273.

[Mor_06] A. Morisako and X.X. Liu, *Sm-Co and Nd-Fe-B thin films with perpendicular anisotropy for high-density magnetic recording media,* **J. Magn. Magn. Mater.** **304** (2006) 46.

[Mot_36] N.F. Mott, *The electrical conductivity of Transition Metals,* **Proc. Roy. Soc. A** **153** (1936) 699.

[Nak_08] M. Nakayama, T. Kai, N. Shimomura, M. Amano, E. Kitagawa, T. Nagase, M. Yoshikawa, T. Kishi, S. Ikegawa and H. Yoda., *Spin transfer switching in TbCoFe/CoFeB/MgO/CoFeB/TbCoFe magnetic tunnel junctions with perpendicular magnetic anisotropy,* **J. Appl. Phys.** **103** (2008) 07A710.

[Noz_06] J.-P. Nozières, B. Dieny, O. Redon, R.C. Sousa and I.L. Prejbeanu, *Magnetic memory with a magnetic tunnel junction written in a thermally assisted manner, and method for writing the same*, **US Patent 7,411,817** (2006).

[Oun_02] K. Ounadjela, B. Dieny and O. Redon, *High density MRAM using thermal writing*, **US Patent 20020281603** (2002).

[Par_91] S.S.P. Parkin, *Systematic variation of the strength and oscillation period of indirect magnetic exchange coupling through the 3d, 4d, and 5d transition metals*, **Phys. Rev. Lett.** **67** (1991) 3598.

[Pre_04] I.L. Prejbeanu, W. Kula, K. Ounadjela, R.C. Sousa, O. Redon, B. Dieny and J.-P. Nozières, *Thermally assisted switching in exchange-biased storage layer magnetic tunnel junctions*, **IEEE Trans. Magn.** **40** (2004) 2625.

[Puf_03] M.R. Pufall, W.H. Rippard and T.J. Silva, *Materials dependence of the spin-momentum transfer efficiency and critical current in ferromagnetic metal/Cu multilayers,* **Appl. Phys. Lett.** **83** (2003) 323.

[Rod_03] B. Rodmacq, S. Auffret, B. Dieny, S. Monso and P. Boyer, *Crossovers from in-plane to perpendicular anisotropy in magnetic tunnel junctions as a function of the barrier degree of oxidation,* **J. Appl. Phys.** **93** (2003) 7513.

[Slo_96] J.C. Slonczewski, *Current-driven excitation of magnetic multilayers,* **J. Magn. Magn. Mater.** **159** (1996) L1.

[Sun_02] J.Z. Sun, D.J. Monsma, D.W. Abraham, M.J. Rooks and R.H. Koch, *Batch-fabricated spin-injection magnetic switches,* **Appl. Phys. Lett.** **81** (2002) 2202.

[Yoo_05] I. Yoo, D.K. Kim and Y.K. Kim, *Switching characteristics of submicrometer magnetic tunnel junction devices with perpendicular anisotropy,* **J. Appl. Phys.** **97** (2005) 10C919.

Chapter I

PERPENDICULAR MAGNETIC ANISOTROPY AT MAGNETIC METAL/OXIDE INTERFACE

Chapter I

PERPENDICULAR MAGNETIC ANISOTROPY AT MAGNETIC METAL/OXIDE INTERFACE

In magnetic materials the spontaneous magnetization can have preferred orientation axes. This anisotropy can be quantified as a magnetic energy dependence on the magnetization direction. More precisely the orbital momentum of the electrons (L) is coupled to the lattice by electrostatic interactions with the charge distribution of ions in materials (crystalline electric field E). Since the orbital momentum direction is established by crystal field it will also affect the spin (S) magnetic moment through the spin-orbit interaction resulting in the magnetization alignment along the preferred lattice axis. This is known as the magnetocrystalline contribution to the anisotropy. When the magnetization lies perpendicular to the layer (sample) plane we talk about perpendicular magnetic anisotropy (PMA).

PMA can have different origins, either bulk (in hcp CoCrPt, heavy Rare Earth-Transition Metal, or $L1_0$ FePt ordered alloys), or interfacial (in Pt/Co, Pd/Co, or Co/Ni multilayers). In this latter case it has also been observed that a quite large PMA can be induced at the interface between a ferromagnetic electrode and an oxide **[Mon_02]**.

Materials with PMA already proved their advantage for increasing storage density in Hard Disk Drives. Another application is envisaged in the case of MTJ based memories taking use of the anisotropy arising from the interface between the magnetic layers and the oxide barrier. From a basic point of view perpendicular magnetized materials are fascinating and can be used to investigate field/current induced domain wall motion, spin torque switching phenomena, control of magnetic properties by an applied electric field **[Man_06, End_10, Ike_10, Mir_10, Wei_07]**. But this needs a good understanding of the anisotropy origin in thin films, especially at the magnetic metal/oxide interface.

This chapter will present the essential PMA properties of magnetic metal/oxide and oxide/magnetic metal structures. First the origin of PMA at magnetic metal/oxide interface will be discussed. We will then present the principles of PMA determination in thin magnetic films.

I-1. Origin of PMA in magnetic metal / oxide bilayers

In magnetic thin films, the interfaces have a high impact on their magnetic properties, due to the reduced bulk contribution. This is even more relevant in the case of the perpendicular magnetic anisotropy (PMA) for which the interface between the magnetic and non-magnetic layer is the driving mechanism, as predicted by Néel **[Née_54]** and experimentally observed several years later **[Gra_68]**. In a very simple picture the measured effective anisotropy energy (K_{Eff}) will have two major contributions (**Figure I-1**), the volume anisotropy (K_V) and the surface/interface anisotropy (K_S/K_I), whose relative contribution increases as the thickness t of the magnetic film decreases.

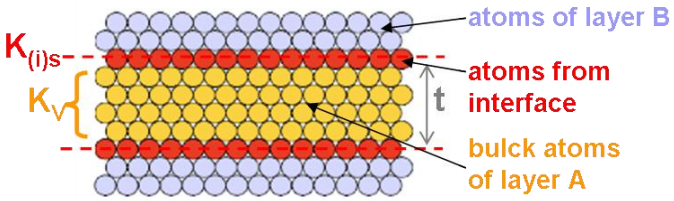

Figure I-1: Interface/surface and volume anisotropy contributions in thin films.

The volume anisotropy in transition metal thin films has two major contributions: magnetocrystalline volume anisotropy (K_V) and shape anisotropy (K_D). The magnetocristalline anisotropy in the case of Co, Fe and Ni metals is due to the spin-orbit interactions. The orbital magnetic moment (m_{Orb}) is usually a small contribution to magnetism in 3d transition (due to the orbital moment quenching), resulting in low magnetocrystalline anisotropy contribution to the volume anisotropy (for Co K_V=4.1 10^5 J/m^3 (4.1 10^6 erg/cm^3)) **[Daa_94]**. For these materials the dipolar interaction energy (which depends on the orientation of the magnetization relative to the crystal axes) only contributes to the shape anisotropy since the sum of the dipole–dipole energies cancels in symmetric crystals (Fe, Ni cubic, and Co hcp with low c/a ratio deviation **[Daa_90]**). In thin films the long range magnetic dipolar interaction is sensitive to the outer boundaries of the sample giving rise to strong demagnetizing fields when the magnetization is tilted out of the film plane. In the absence of uniaxial anisotropy contribution, magnetization prefers to lie parallel to the film plane in order to minimize the magnetic energy.

These contributions to the effective anisotropy can be expressed as follows:

$$K_{eff} = K_V - 2\pi M_s^2 + \frac{K_{s1} + K_{s2}}{t} \qquad \textbf{Equation I-1}$$

From this empirical expression, one can see that the interfacial contribution of the anisotropy increases when the magnetic layer thickness (t) decreases. The interfacial anisotropy term $K_{S1}+K_{S2}$ is the sum of the contributions from both interfaces and could only be observed thanks to the improvement of deposition techniques which enabled the fabrication of very thin layers.

At the interface (surface) the crystal continuum is broken, so atoms from the interface (surface) have a different environment compared to those in the bulk (**Figure I-1**). Considering this fact, Néel **[Née_54]** predicted that the effective anisotropy of thin films should be different from that in the bulk due to the interfacial anisotropy contribution. However, Neel's approach is based on the simple pair interaction model (localized molecular orbitals) and is not the most appropriate for 3d transition metals like Co, Fe, Ni. The itinerant electron model (band model) introduced by Gay and Richter **[Gay_86]** to explain PMA in thin films gives a more appropriate

picture taking into account the position of the Fermi level together with the broken crystal symmetry at the interface/surface.

Let us first focus on the simplest case, **surfaces.** Bruno **[Bru_89]** predicted for Co, Fe, Ni monolayers a surface anisotropy of the order of 1 erg/cm^2 which strongly depends on the crystal-field parameters and on the filling of the 3d bands. Because of the strongly reduced symmetry at the surface, it will result in much larger shifts (Δ) in the d orbitals energy than in bulk materials (high symmetry) (**Figure I-2**). More precisely, the absence of coordination atoms results in a reduction of the 3d band which will more affect the out-of-plane orbitals than the in-plane ones (see **Figure I-2** for d orbitals). As a result, the bands population needs to be reconfigured by a charge transfer from the in-plane to the out-of-plane levels, thus changing the coulombian energy which will split the levels.

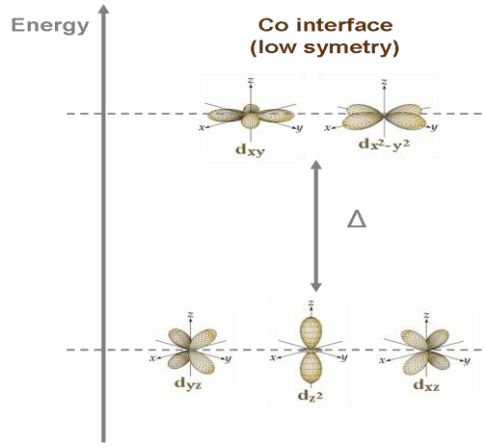

Figure I-2: Co d orbitals and effect of the surface/interface broken symmetry (no coordination atoms). Δ is the energy difference between out-of-plane yz, zx, z^2 and in-plane xy and x^2-y^2 orbitals.

The picture is more complicated in the case of **interfaces** due to the presence of different kinds of surrounding atoms. This is why at the interface one has to consider at the same time not only a change in the bulk symmetry but also a change of the nature of coordination (surrounding) atoms. Two examples are presented for different materials at the Co(Fe) interface, Pt with a strong spin-orbit coupling and a strong crystal field, and O with low spin-orbit coupling.

The presence of heavy atoms like Pt (or Pd) at the Co interface will induce a strong hybridization of 3d Co orbitals with 5d Pt orbitals **[Nak_98]** which, combined with the strong spin-orbit coupling of Pt, will produce an increase of the Co orbital momentum **[Wel_94]**, making possible to orient the spin momentum perpendicular to the interface. In more details, the interface hybridization can be viewed as an effective uniaxial crystal field acting on the Co/Pt interfacial atoms and modifying the material's band structure. At the Co interface side, the **crystal field** defines both in-plane orbitals $\mathbf{d_{xy}}$ and $\mathbf{d_{x2-y2}}$ states and out-of-plane orbitals with $\mathbf{d_{yz}}$ and $\mathbf{d_{xz}}$ states near the Fermi energy level. The **spin-orbit coupling** will split both in-plane and out-of-plane states at the interface. The energy separation for $\mathbf{d_{xy}}$ and $\mathbf{d_{x2-y2}}$ states is smaller than in bulk Co (due to the broken symmetry at the interface) but also smaller than the spin-orbit coupling separation in out-of-plane orbitals $\mathbf{d_{yz}}$, $\mathbf{d_{xz}}$. Due to the **strong splitting in out-of-plane orbitals, the Co out-of-plane perpendicular orbital momentum will be enhanced.** Wang et al **[Wan_93]** showed that **the d-d bonding** between Co and **Pd is mediated by d_{yz}, d_{xz} orbitals** and predicted even stronger bonding with Pt or Au since in these materials the spin-orbit interaction is larger. The crystal field effect on interfacial Pt layer will shift towards lower energies the Pt 5d bands of spin parallel to the Co majority spin, resulting in a **Pt spin momentum parallel to that of Co (Ms(Pt) // Ms(Co))**. The large Pt orbital momentum contributes to the interfacial Pt layers **magnetic moment** via a strong spin-orbit coupling, thus aligning it parallel to the Co total momentum.

In conclusion PMA at Co/Pt interface is due to the 3d-5d hybridization combined with spin-orbit coupling:

- for Co layers this results in a strong splitting of in-plane and out-of-plane orbitals favouring the lowest energy for the out-of-plane orbital.
- for Pt layers the effect is the occurrence of a **magnetic moment at the Pt** interface aligned with the **Co magnetic moment**.

The interfacial perpendicular anisotropy reported in the case of Co/Pt (Pt, Pd, Au, W, Mo) multilayers **[Bro_89, Yoo_05]** is principally due to a heavy metal layer (having a strong spin-orbit coupling) present at the interface. According to this observation it was believed that the presence of heavy metal at the magnetic metal interface is essential to obtain the PMA.

Recently a PMA interfacial contribution from the **MagneticMetal/oxyde interface** has been observed **[Mon_02, Rod_03]** despite the weak spin-orbit coupling. Experiments showed that this phenomenon is quite general **[Man_08a, Rod_09, Nis_09, Ike_10]** since it was observed at the interface between various magnetic transition metals and oxide layers and is independent of the crystalline structure of the oxide layers. In addition, X-ray photoemission spectroscopy **[Man_08b]** showed that oxygen plays an essential role in the PMA at magnetic metal-oxide interface by the formation of Fe(Co)-oxygen bonds. For a better understanding of the PMA origin at the Magnetic Metal/oxide interfaces an ab initio study was realized taking into account the weak spin-orbit coupling **[Yan_11]**.

The origin of the large PMA is ascribed to the combination of several factors:

- **degeneracy lift of out-of-plane 3d orbitals due to the weak spin-orbit coupling,**
- **hybridizations between dz^2 and d_{xz} and d_{yz} 3d orbitals induced by weak spin-orbit interactions**
- **hybridizations between Fe-3d and O-2p orbitals at the interface between the transition metal and the insulator.**

The strong overlap between Fe 3d and O 2p orbitals modifies the band structure giving rise to a strong crystal field at the interface. In **Figure I-3** (middle column) one can clearly see the band levels for the 3d Fe and 2p O orbitals, containing levels (blue/green levels) resulting from the hybridization of the Fe $\mathbf{dz^2}$ and O **pz** orbitals near the Fermi level energy. Even a **low spin-orbit coupling** is enough **to split the Fe(Co) band levels d_{xz}, d_{yz}, d_{z2} and O p_z** around Fermi energy in either the in-plane magnetization (right column in **Figure I-3**), or the out-of-plane magnetization configuration (left column in **Figure I-3**). After splitting, **band positions corresponding in energy for d_{z2}, d_{xz}, d_{yz} levels become hybridized**, resulting in the appearance of additional levels for both $\mathbf{d_{z2}}$ and $\mathbf{d_{xz,yz}}$ orbitals represented by numbers showing the percentage of the corresponding orbital character components within Wigner-Seitz spheres. For the out-of-plane magnetization orientation (left columns), the additional $\mathbf{d_{z2}}$ levels with 5, 2 and 44 percentage (red lines) originate from $\mathbf{d_{xz,yz}}$ orbital character due to SOI and the additional $\mathbf{d_{xz,yz}}$ band with 8 percents (blue line) comes from $\mathbf{d_{z2}}$ orbital. In addition for the out-of plane magnetization orientation (left subcolumns) of Fe $\mathbf{d_{z2}}$ we also observe energy levels with O-pz character (red levels) since the Fe $\mathbf{d_{z2}}$ orbitals have already been hybridized with the O $\mathbf{p_z}$ ones.

In conclusion PMA at metal/oxide interface comes from the combination of the **Fe-O bond formation** resulting in the mixing of $\mathbf{d_{z2}}$ and $\mathbf{p_z}$ levels and the **weak spin-orbit coupling** which will split the levels in the $\mathbf{d_{xz}}$, $\mathbf{d_{yz}}$, $\mathbf{d_{z2}}$ and $\mathbf{p_z}$ and especially mix the $\mathbf{d_{xz}}$ and $\mathbf{d_{yz}}$ orbitals with the $\mathbf{d_{z2}}$ ones.

So far, it was assumed that the layers have ideal flat interfaces. In reality, films cannot be grown perfectly even using epitaxial techniques. This leads to roughness and/or interdiffusion at the interface which will modify the magnetic properties.

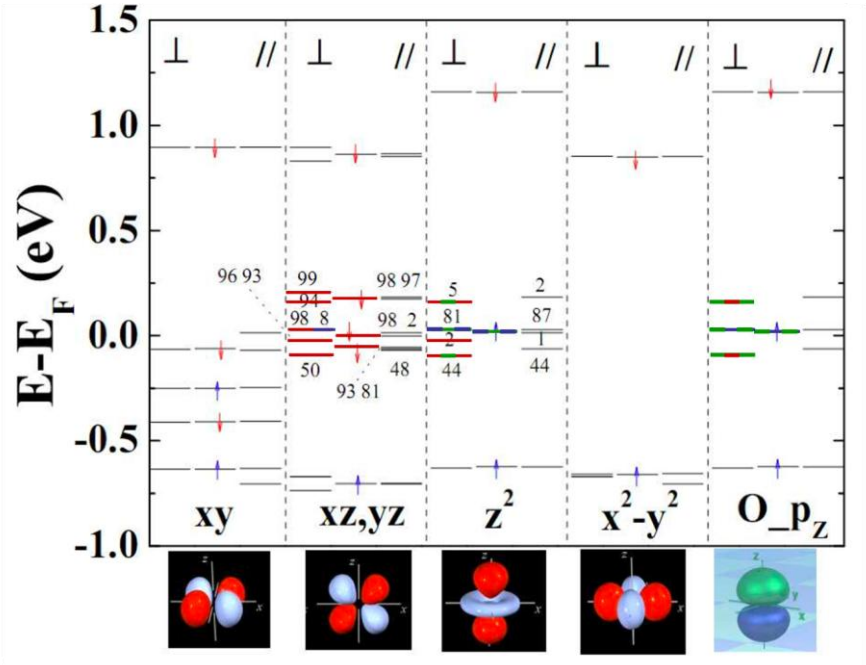

Figure I-3: Fe-O hybridization and spin-orbit coupling effects at Fe/O interface. Three sub-columns in each column show the band levels for out-of-plane (left) and in-plane (right) orientation of the magnetization as well as for the case with no spin-orbit interaction included (middle).

The effect of roughness on the dipolar anisotropy has been studied theoretically by Bruno [Bru_88]. He used an ideal rough surface (epitaxial layers case) which can be characterized by the roughness height h (which is the mean square deviation from the ideally flat surface) and the correlation length λ (the average lateral size of flat areas on the surface, terraces). Roughness creates in-plane demagnetizing fields at the edges of terraces reducing the shape anisotropy. The anisotropy contribution resulting from the roughness will, therefore, always be positive (favouring PMA). In addition, due to its presence at the interfaces only it will scale as 1/t. But roughness will also introduce step atoms at the interface. Contrary to terraces each step atom contributes to a decrease of the anisotropy. In general the roughness always reduces the anisotropy, it is just a matter of number of step atoms relative to the number of terrace atoms. However for sputtered samples, roughness effects may greatly alter the magnetic surface anisotropy.

The interdiffusion between layers, caused by the nature of the materials (immiscibility) or by annealing, is always detrimental to the interface anisotropy. For example it was experimentally observed [Man_08a, Rod_09, Nis_10] and calculated [Yan_11] that over/under-oxidation of the magnetic material/oxide interface will strongly reduce the interface anisotropy. In the case of over-oxidation at the interface (additional oxygen at the Co interface) the Fe $\mathbf{d}_{z2}$ and O $\mathbf{p}_z$ orbitals will no more mix due to the charge redistribution induced by the additional oxygen and the spin orbit coupling will cause stronger splitting for $\mathbf{d}_{xz,yz}$ states with in-plane orientation than with out-of-plane. The case of under-oxidized interface is characterized by no overlap between the Fe $\mathbf{d}_{z2}$ and O $\mathbf{p}_z$ orbital and $\mathbf{d}_{xz,yz}$ orbitals, and higher splitting for out-of-plane magnetization orientation compared to the in-plane one. Anisotropy in the under-oxidized case will be higher than in the over-oxidized case but much lower than in the case of ideal Fe/MgO interfaces. All this underlines the importance of the interface quality.

I-2. Experimental determination of perpendicular anisotropy

The effective anisotropy energy K_{eff} is the energy required to align the magnetization along the hard magnetization axis and it can be calculated by the difference in areas of the M(H) curves measured along the hard and easy axis directions [Joh_96]:

$$Keff = \int_{\substack{hard\\axis}} M \cdot dH - \int_{\substack{easy\\axis}} M \cdot dH \qquad \textbf{Equation I-2}$$

K_{eff} is usually taken as positive for out-of-plane magnetization. In the case of a linear M(H) variation along the hard axis, the saturation field H_{an} can be used to extract K_{eff} using $K_{eff} = H_{an} M_S/2$, where M_S is the saturation magnetization determined from VSM or SQUID measurements. Along the easy axis, only the reversible magnetization curve has to be considered as shown in **Figure I-4**. In the case of perpendicular magnetization with a multidomain structure in zero applied field, and because of the magnetostatic interactions between domains, saturation fields will have no direct relation with K_{Eff}. However K_{Eff} can still be determined from the differential area. In practice the anisotropy measured along the hard axis is always much larger than that measured along the easy axis, which can usually be neglected, except near the transition from perpendicular multidomain to in-plane magnetization, which however occurs on a very narrow thickness range.

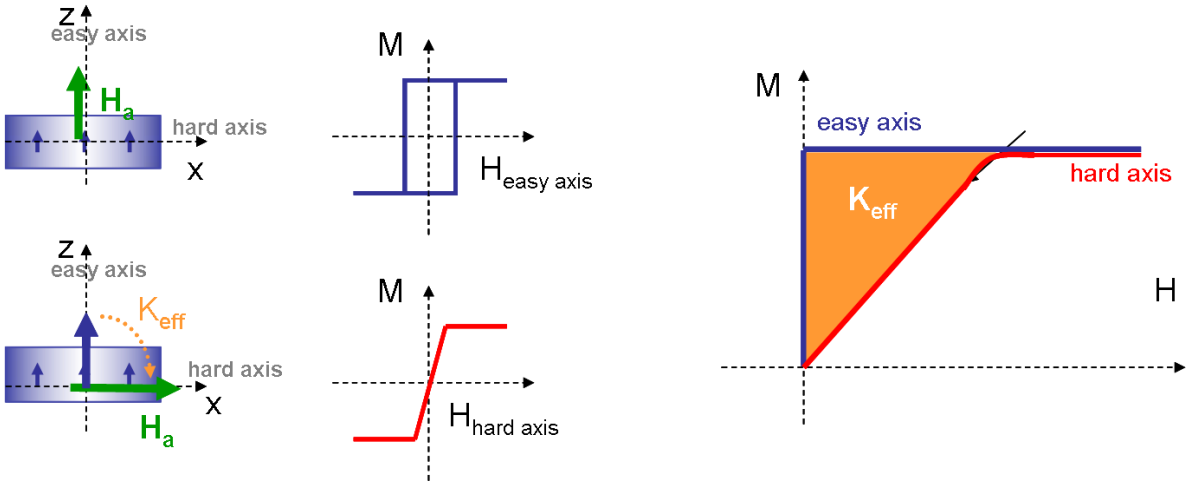

Figure I-4: (a) Magnetization measurements along easy and hard axis in the case of a sample with out of plane magnetization; (b) K_{Eff} determination by the the difference between areas above magnetization curves measured along hard and easy magnetic axis.

According to **Equation I-1**, a plot of K_{eff} t versus t, where t is thickness of the magnetic layer, should give a straight line if the total anisotropy can be reasonably separated into a volume and interface contribution. **Figure I-5** gives an example of such a plot in the case of Co/Pd multilayers [Bro_91]. The interface anisotropy $K_{S1}+K_{S2}$ is usually noted as $2K_S$ in the case of multilayers, where one supposes that both bottom and top interfaces contribute equally to the anisotropy. This is not straightforward if one considers possible differences between the growth of the magnetic material on the metallic spacer and the growth of the metallic spacer on the magnetic material. In our case it is even more questionable since we are dealing with two different interfaces (Pt/Co and Ox/Co for example). We will however, for convenience, call $2K_S$ the total interface anisotropy $K_{S1}+K_{S2}$.

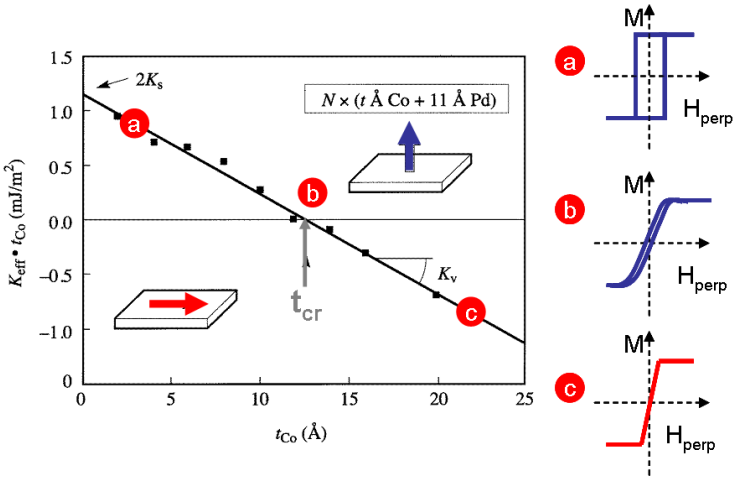

Figure I-5: Effective magnetic anisotropy times Co thickness versus Co thickness in Co/Pd multilayers: (a) Out-of-plane anisotropy; (b) Critical thickness; (c) In-plane anisotropy. The vertical axis intercept equals the sum of both interface anisotropies, whereas the slope gives the volume contribution [Bro_91].

The interface anisotropy $2K_S$ is obtained from the vertical axis intercepts, whereas the difference between the volume anisotropy and demagnetizing energy contribution (K_V-$2\pi M_S^2$) is given by the slope of the curve. The effective anisotropy can be:
a) **positive (Keff > 0)**: the interface anisotropy contribution $2K_S$ outweighs the volume contribution (K_V-$2\pi M_S^2$), resulting in a perpendicularly magnetized system. The strong demagnetizing fields which are created when tilting the magnetization out of the film plane, and which are usually responsible for the orientation of the magnetization parallel to the film plane, are overcome.
b) **zero (Keff = 0),** which marks the transition of the magnetization from out-of-plane to in-plane for a given magnetic thickness called critical thickness.
c) **negative (Keff < 0),** when the volume term dominates and the magnetization is in-plane.

The volume contribution K_V, which can be either positive or negative, is usually much smaller than the demagnetizing term, leading generally to a negative slope of the curves. Increasing the $2K_S/t$ term (increasing K_S and/or decreasing thickness) is thus the only way to obtain perpendicular magnetization.

There are different techniques sensitive to the magnetization which can be used to determine the magnetization variation either along the easy axis (coercive field) or the hard axis (magnetic anisotropy): magnetometry techniques (VSM and SQUID), magneto-optical techniques (Kerr Effect) and magneto-transport techniques (magnetoresistance or Hall Effect). Each technique has advantages and drawbacks, and the choice of the technique will depend on both sample composition and expected information.

Magnetometry measurement is in principle the best choice, since it gives an absolute values of the magnetization. However, the sensitivity is limited to magnetic thicknesses larger than about 1 nm. In addition, since it is a global measurement, all magnetic contaminations (substrate, sample holder) will contribute to the signal. SQUID measurements lead to a much better sensitivity, but suffer from the same contamination problems. It is also a very time-consuming technique.

Magneto-optical techniques are insensitive to external parasitic signals (except for possible surface contamination). The sensitivity to thin magnetic layers is very good, and measurements fast. However, because of the limited penetration depth of the laser radiation, the signal of buried magnetic layers will be small, especially when using capping layers made of heavy metals. In the case of multiple magnetic layers, the relative amplitudes of the Kerr signals will not

give the real ratio of magnetizations.

Transport measurements, especially Hall effect, are sensitive to the perpendicular component of the magnetization. Hall effect is a very sensitive technique, but only when the magnetic layer is in contact with metals such as Pt or Pd. As an example, a Co layer sandwiched between two oxide layers will gives almost no Hall signal. The Hall amplitude will thus depend on the magnetization, but also on the Hall coefficient, which is influenced by the environment of the magnetic layer. Such electrical measurements will also be of limited use when thick buffer or capping layers are used, because the large amount of current derived into these layers greatly decreases the signal from the magnetic layer itself.

Since most of the samples we studied contain Pt layers in contact with the magnetic ones, we extensively used Hall measurements to determine their magnetic properties. These experiments were conducted on macroscopic samples, in a conventional Van der Pauw geometry presented in **Figure I-6a**.

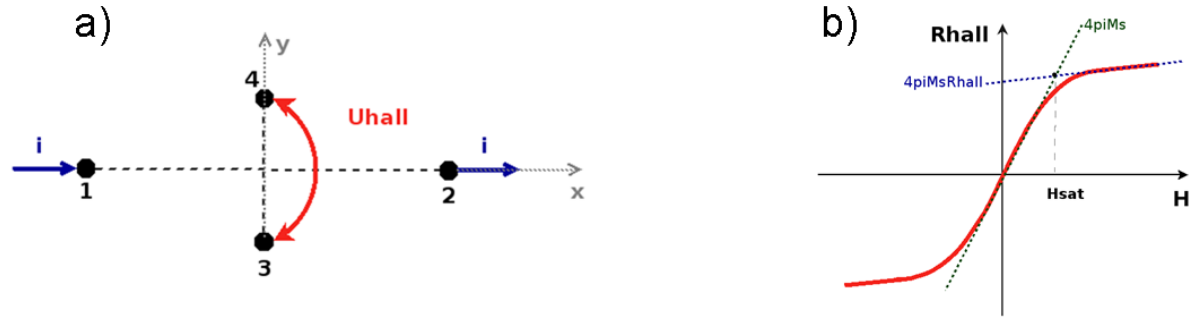

Figure I-6: (a) Schematic representation of the Hall configuration. Current is injected along the x direction, Hall voltage is measured along the y direction. The magnetic field is applied along the orthogonal z direction; (b) Typical R(H) curve along the hard axis direction.

In this perfect geometry the current is injected along the in-plane x direction and the Hall voltage is measured along the in-plane y direction. The Hall resistance is the sum of two contributions:

$$R_H = B\,R_0 + Mz\,R_E \qquad \textbf{Equation I-3}$$

where R_H is the Hall resistivity, B the magnetic induction, and M the magnetization. R_0 is the ordinary Hall coefficient related to the Lorentz force acting on moving charge carriers. R_E is the extraordinary Hall coefficient associated with a break of the right–left symmetry during the spin–orbit scattering in magnetic materials and can be much larger than R_0.

If the magnetic field is applied along the hard axis (**Figure I-6b**), the Hall resistance will first vary rapidly until the magnetization is saturated (extraordinary contribution). At larger field, the Hall resistance will vary linearly with field (ordinary contribution). The extraordinary contribution can be expressed as a function of the longitudinal resistivity as:

$$R_E = a\,\rho_{XX} + b\,\rho^2_{XX} \qquad \textbf{Equation I-4}$$

where a and b are the skew scattering [Smi_55] and side-jump [Ber_70] coefficients.

These two scattering mechanisms responsible for the extraordinary term have their origin in the spin-orbit interaction: the classical asymmetric scattering [Smi_55] (one scattering channel is favored over the other one), which gives a linear variation with longitudinal resistivity, and the non-classical side-jump mechanism [Ber_70] (different lateral displacement for spin up and spin down electrons) which has a quadratic dependence on the resistivity. Skew scattering and side jump action of spin-orbit coupling thus cause currents of up and down electrons to deflect in

opposite directions. If the current is spin-polarized (materials with high polarization), there will be more electrons moving in one perpendicular direction than the other, resulting in an actual transverse charge current, which in addition to the Lorentz force charge separation can be detected by voltage measurements.

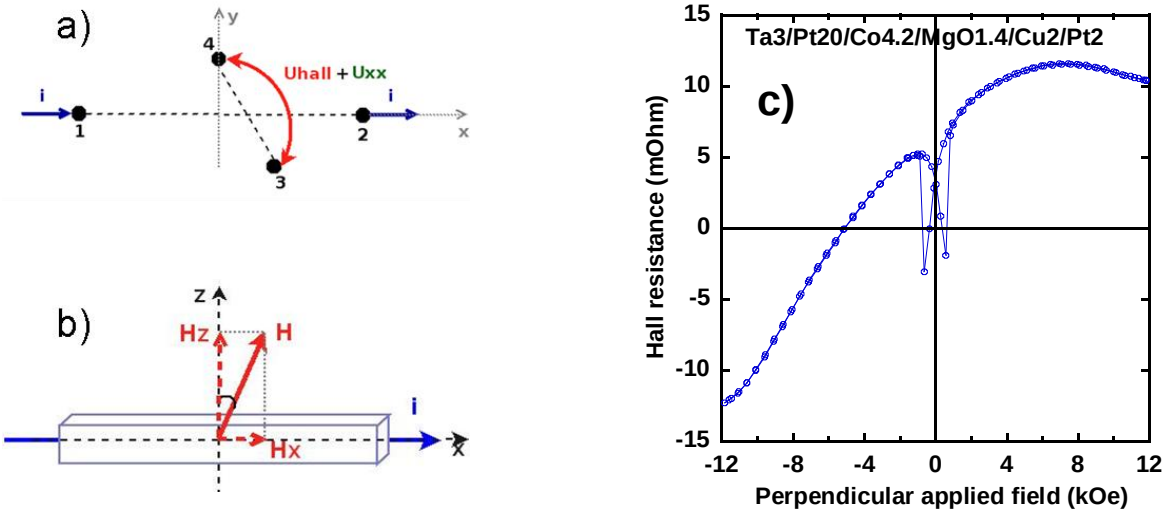

Figure I-7: (a) Deviation from the perfect Hall geometry between current and voltage directions and (b) Deviation of the direction of the applied field from the perpendicular direction; (c) Perpendicular Hall curve of a sample with in-plane magnetization. Deviation (a) leads to an even AMR contribution to the Hall signal. Additional deviation (b) leads to a low field AMR signal corresponding to the in-plane switching of the magnetization.

Hall effect measurements are sensitive to any deviation from the perfect orthogonality between current and voltage probes (**Figure I-7a**). In this case the Hall voltage will contain a contribution from the longitudinal resistivity ρ_{XX}. For a sample with in-plane magnetization (**Figure I-7c**), the total signal will be the sum of two contributions: an odd one coming from the Hall contribution, and an even one from the anisotropic magnetoresistance (AMR), which depends on the angle between magnetization and current [Tho_56]. Since magnetization progressively goes from parallel to perpendicular to the electrical current, both Hall and AMR contributions will saturate at the same field. A deconvolution of the curve allows to separate out the two contributions.

In addition, if the magnetic field is not perfectly perpendicular to the film plane (**Figure I-7b**), its in-plane projection will go from positive to negative. The in-plane magnetization will thus switch in a field $H = H_C / \sin\alpha$, where H_C is the in-plane coercive field and α is the angular deviation from the perfect perpendicular field orientation. This will leads to a supplementary AMR contribution (low-field negative signals in **Figure I-7c**).

For samples with in-plane anisotropy, a Hall measurement is equivalent to a magnetometry or a Kerr effect one. One just measures the field-induced increase of the M_Z component of the magnetization up to saturation. The problem is slightly different for an out-of-plane magnetized layer. One now measures the decrease of the M_Z component under the action of an in-plane field from its maximum value (saturated up or down state) down to zero where the magnetization lays in plane for a large enough in-plane field. In order to extract the effective anisotropy, the R(H) curve must be normalized, and then the M_X component is extracted from the M_Z variation by $M_X^2 = 1 - M_Z^2$. The area above the curve can thus be calculated in order to determine K_{Eff}.

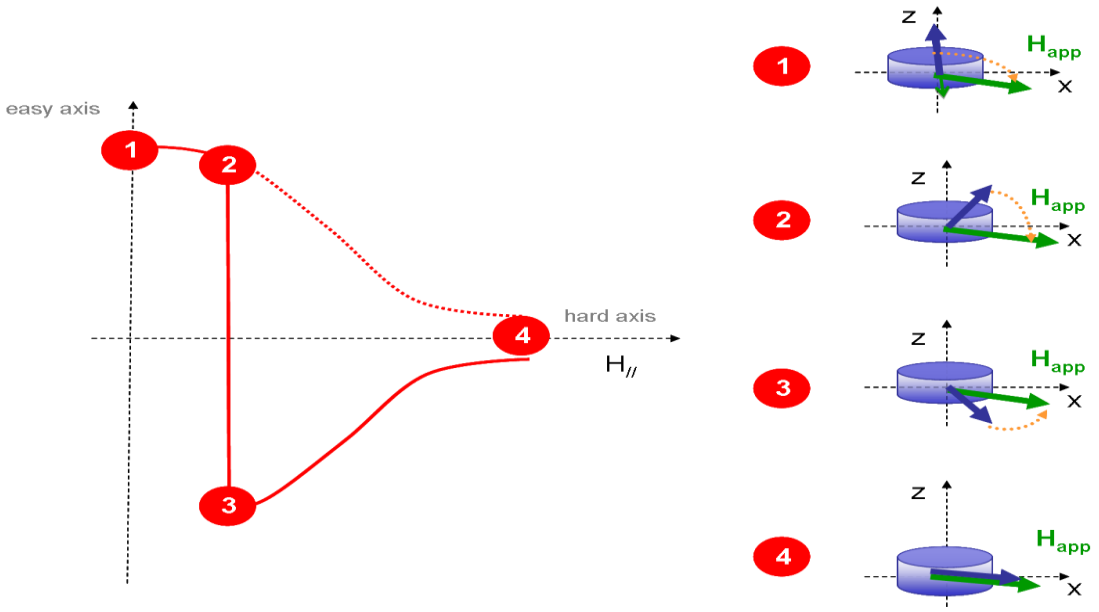

Figure I-8: Effect of a small (-z) component on the magnetization curve as a function of in-plane magnetic field.

When the magnetization is in a multi-domain configuration in zero field, for a magnetic thickness close to the critical one, the M_Z component will be zero whatever the applied field, and M_X cannot be determined from such measurements. One must note that if the applied field is not perfectly in-plane, the measurement will also perturbed, as was the case in **Figure I-7b**. **Figure I-8** illustrates this situation. Starting from positive saturation (**1**), and considering a small -z component of the H_X field, magnetization will switch from the +z to the -z direction (**2** → **3**) when the -z component of the applied field will be equal to the out-of-plane coercive field of the sample. In order to avoid this perturbation, experiments where always performed aligning the initial magnetization parallel to this H_Z component.

The transformation from M_Z to M_X does not hold anymore for a structure containing more than one magnetic layer. However, as shown in **Figure I-9**, the successive saturation of the magnetic layers leads to a larger change of slope for Hall measurements (M_Z) than for classical magnetometry ones (M_X). The anisotropy fields can thus be more easily estimated.

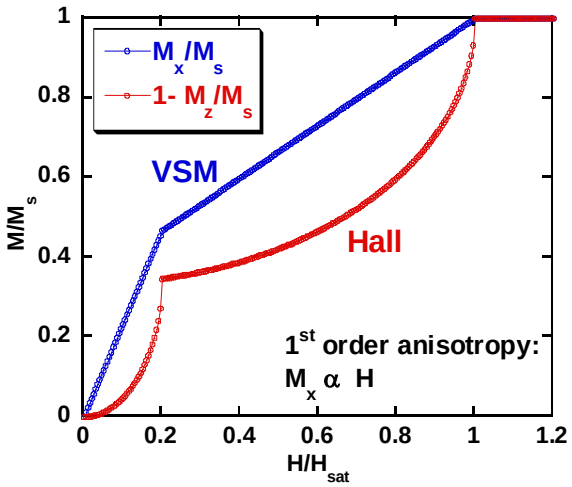

Figure I-9: Schematic variation of the magnetization as a function of in-plane field for a structure composed of two magnetic layers with perpendicular magnetization. The blue curve is a classical VSM curve (assuming a linear field response), the red one corresponds to Hall measurements.

I-3. Thin films preparation

Cathodic sputtering is a deposition technique used for the preparation of semiconductor and metallic thin films in industry and research. This technique is interesting for magnetic thin film deposition and fabrication of tunnel junctions because of its advantages over other existing techniques like Chemical Vapor Deposition (CVD) or Molecular Beam Epitaxy (MBE) methods:

- **deposition of all type of materials** (metals, alloys, refractory compounds, dielectrics)
- **high deposition rates,**
- **good adherence of the deposited films on the substrate,**
- **good thickness homogeneity over large substrates (up to 300mm),**
- **good control of layer thicknesses, down to a few tenths of nanometer.**

This technique consists in the deposition on a substrate of atoms mechanically extracted from a target bombarded with accelerated argon ions of a plasma as shown in **Figure I-10**. The sputtering chamber is under vacuum (a few 10^{-8} mbar) and an inert gas is introduced to a pressure of about 10^{-3} mbar. Argon is the most commonly used process gas for sputtering process, since it has a high sputter yield (ionized/sputtered atoms) for most metals, is chemically inert and non-toxic, and is relatively inexpensive (compared with other rare gases as krypton or xenon). The plasma is obtained by an electrical discharge made by applying a negative voltage between target (cathode) and surrounding shield maintained at zero potential. This electrical discharge will ionize the argon atoms by collisions with the electrons. Positive ions are attracted by the target and by elastic collisions will extract atoms from the target. Atoms extracted from the target will deposit on the substrate carrying a large kinetic energy (approximately 50 to 100 times that of neutral atoms generated from thermal evaporation sources). The incoming atoms are likely to mix at the interface with the underlying layer or substrate since their energies are large enough to break bonds in most solids. This large energy is thought to be the reason for the greater adherence of layers observed for sputter-deposited films compared to thermally evaporated films.

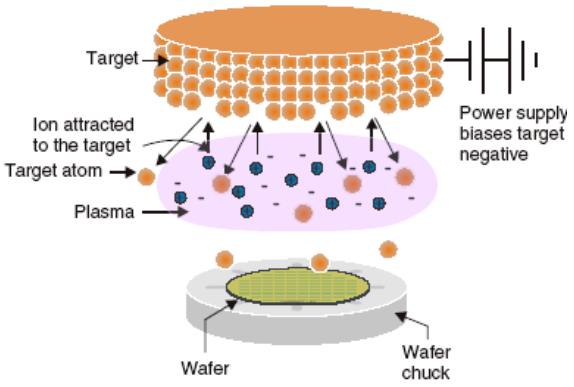

Figure I-10: Cathodic sputtering: accelerated Ar^+ ions extract atoms from the target.

After reaching the substrate surface, the pulverized atoms can diffuse and interact forming islands as a sign of thermodynamically non-equilibrium with the substrate. In this case the cohesion energy is higher between the sputtered atoms than between the sputtered atoms and the substrate surface. The growth mechanism of sputtering film is strongly influenced by several factors: chemical nature (surface energy) and crystallography of the substrate and deposited layer, interfacial energy, substrate temperature, background pressure, deposition rates.

The vacuum is very important for the film properties. In a poor vacuum (>10^{-7} mbar) the background pressure is mostly composed of water vapour. The water adsorbed on the surface

may increase the mobility of surface atoms and oxygen may be incorporated in the growing film. For example MgO deposited layers are very sensitive to water vapour changing its insulator or crystallographic properties.

The sputtering rate depends on the DC voltage, and can modify microstructural properties of the material. For example using high sputtering rates one can obtain polycrystalline or even more homogeneous amorphous materials, or modify the magnetic properties of magnetic materials.

Another way to increase the sputtering rates is to use permanent magnets located underneath the target. This magnetic field will concentrate the plasma near the target, thus protecting the substrate from possible heating by the plasma or inclusion of Ar atoms into the layers. This will also allow working with lower argon pressures still keeping high sputtering rates.

In the case of non-metallic targets like oxides, the deposition rates are usually lowered by the accumulation of positive charges on the target. This is why in this case a radiofrequency mode is used, applying alternatively positive and negative polarization on the target in order to evacuate the positive charges. Oxide layers deposited from an oxide target are usually non stoicchiometric. As a consequence another method can be used to fabricate thin oxide layers, which consists in depositing the metallic layer and oxidizing it. There are three ways to prepare oxides from a metallic layer: reactive sputtering (sputtering the metallic layer in an argon/oxygen atmosphere), plasma oxidation (exposing the metallic layer to an oxygen plasma after deposition) and natural oxidation (exposing the metallic layer to an oxygen atmosphere for a given time after deposition).

Our Actemium sputtering machine allows us to prepare layers presenting a thickness gradient. In the usual geometry, the centre of the substrate holder and the centre of the target are on the same vertical axis (**Figure I-11a**). In order to get rid of any plasma inhomogeneities (coming for example from the permanent magnets), the sample is rotated at 100 rpm around its axis. It is also possible to position the substrate holder off-axis (**Figure I-11b**) without rotation. In this case one obtains a thickness gradient on the substrate which depends on the distance d between target and sample normals. The usual geometry is when d equals 100 mm, leading to a thickness variation by a factor of about 2 on a 100 mm substrate.

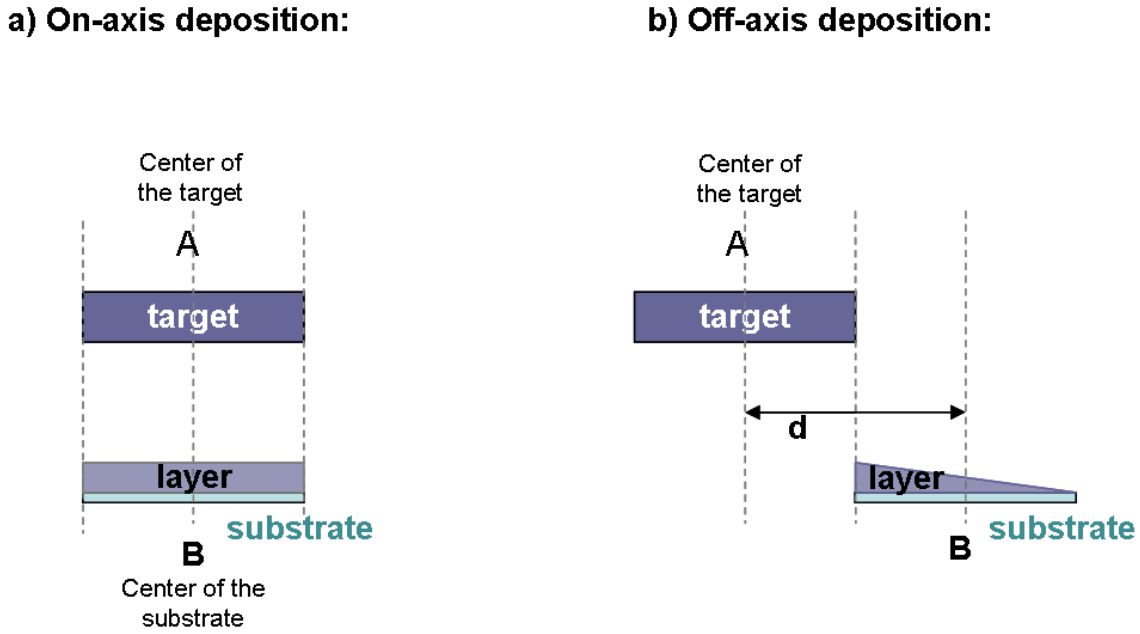

Figure I-11: Different deposition geometries in our Actemium sputtering machine.

I-4. Pt/Co(CoFeB)/Oxide trilayers

Since early work at Spintec on Pt/Co/AlOx structures **[Mon_02, Rod_09]**, which evidenced relationship between optimal oxidation conditions of the barrier and optimal perpendicular anisotropy, numerous investigations of PMA properties of Magnetic Metal/Oxide and Oxide/Magnetic Metal have been carried out, boosted by the growing interest in perpendicular magnetic tunnel junctions (see **Chapter II**), as well as in PMA modifications induced by an electrical field **[Wei_07]**. One can cite work on bottom Co(CoFeB)/MgO electrodes **[End_10, Jun_10a, Nis_09]**, on top MgO/Co(CoFeB) ones **[Fow_10, Fow_11, Jun_10b, Nis_09, Yam_11]**, as well as on (MgO/FePdB) multilayers **[Cho_10]**.

Bottom-type perpendicular (Pt/Co/AlOx) electrodes where recently developed in our laboratory **[Dah_08]**, with Co layers presenting perpendicular magnetization for thicknesses as large as 3 nm after annealing at 350°C. We present here a detailed study of the anisotropy properties of Pt/Magnetic material/Oxide stacks with two different magnetic materials (Co and amorphous $Co_{60}Fe_{20}B_{20}$) covered by an MgO oxide prepared by either natural oxidation of metallic Mg or by RF sputtering from an MgO target **[Nis_09]**.

I-4.1 Natural oxidation

Pt/Co/oxide trilayers were prepared by dc-sputtering onto thermally oxidized Si substrates. The Ta layer is used to ensure a good adherence of the trilayers on the silicon oxide substrate. Co layers of different thicknesses were grown on a thick Pt buffer in order to obtain a strong interfacial anisotropy at the Pt/Co interface. On the top of the Co layer a 1.4 nm thick Mg layer was deposited and naturally oxidized (10 minutes under 160 mbar oxygen pressure) in order to obtain an MgO oxide layer. A Cu2/Pt2 bilayer was sputtered on top in order to protect the trilayers from oxidation. The Pt layer is used to protect the structure from oxidation, and the Cu one prevents from any possible influence of the top Pt layer on the anisotropy of the Co layer (see Section **I-4.6**).

Figure I-12 presents Hall hysteresis loops for different Co thicknesses in Pt/Cox/MgO structures before and after annealing at 325°C. The magnetization of a Co layer 1 nm thick is already perpendicular in the as-deposited state since it grows on a thick Pt buffer. After annealing one observes a strong increase of the coercive field. For Co 1.8 nm the magnetization is in-plane before annealing. The critical Co thickness (transition from out-of plane to in-plane) is thus smaller than 1.8 nm before annealing. After annealing this transition occurs for a Co thickness larger than 2.6 nm. There is thus a large increase of the perpendicular anisotropy with annealing. It is ascribed mainly to the Co/MgO interface because of Co-O hybridization. In order to quantify this anisotropy evolution a detailed study was realized as a function of Co layer thickness for different annealing temperatures.

The variation of the effective anisotropy times the Co thickness as a function of Co thickness is presented in **Figure I-13**, as extracted from in-plane and out-of-plane Hall measurements. The interfacial anisotropy value, the volume contribution and the critical thickness can be determined from such plots as was shown in **Section I-2** (**Equation I-1**). One can clearly observe the increase of the interfacial anisotropy (intercept on the y axis) with annealing temperature as was observed in Pt/Co/AlOx structures **[Dah_08]**. On the contrary, the volume anisotropy does not vary so much, except after annealing at 375°C. The variations of interfacial and volume anisotropies are shown in **Figure I-14a**. Assuming a Co saturation magnetization of 1400 emu/cm^3, the volume anisotropy has a negligible contribution (1 10^6 erg/cm^3) up to 350°C annealing compared to that of the demagnetizing field (12.3 10^6 erg/cm^3). After annealing at 375°C the volume anisotropy decreases. However the continuous increase of

the interface anisotropy still dominates, leading to a continuous increase of the critical thickness, from 1.3 nm before annealing up to 3.5 nm after annealing at 350°C as can be seen in **Figure I-14b**.

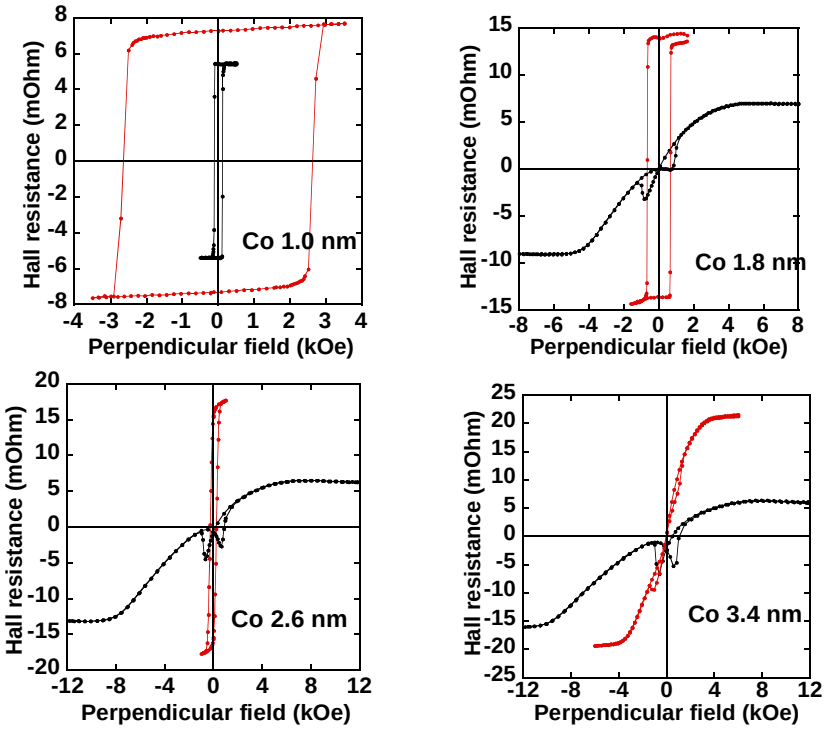

Figure I-12: Hall resistance as a function of perpendicular magnetic field in Ta3/Pt20/Cox/Mg1.4NatOx/Cu2/Pt2 (nm) structures with different Co thicknesses before (black) and after (red) annealing at 325°C.

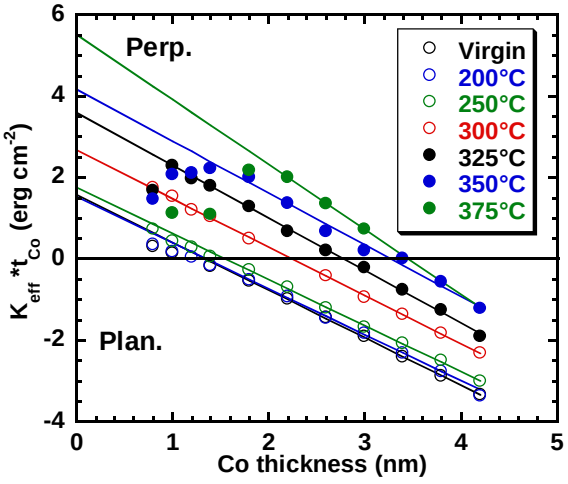

Figure I-13: Plots of Keff*t_{Co} as a function of Co thickness after annealing at different temperatures in Ta3/Pt20/Co/Mg1.4NatOx/Cu2 /Pt2 structures. Lines are fits to Equation I-1.

In the as deposited state the perpendicular anisotropy mainly comes from the Pt/Co interface due to the good growth of Co on metallic substrates. The Co top interface does not contribute so much to PMA in the as-deposited state, which can be explained by the low oxygen concentration at the Co/MgO interface due to the large Mg thickness (1.4 nm). After annealing, intermixing at the Pt/Co interface will cause a decrease of the interfacial anisotropy and an

increased contribution of volume anisotropy. This effect is compensated by the formation of Co-O bonds at the opposite Co interface with MgO since annealing leads to oxygen homogenization in the barrier. This results in a larger contribution from the Co/MgO interface to the perpendicular anisotropy.

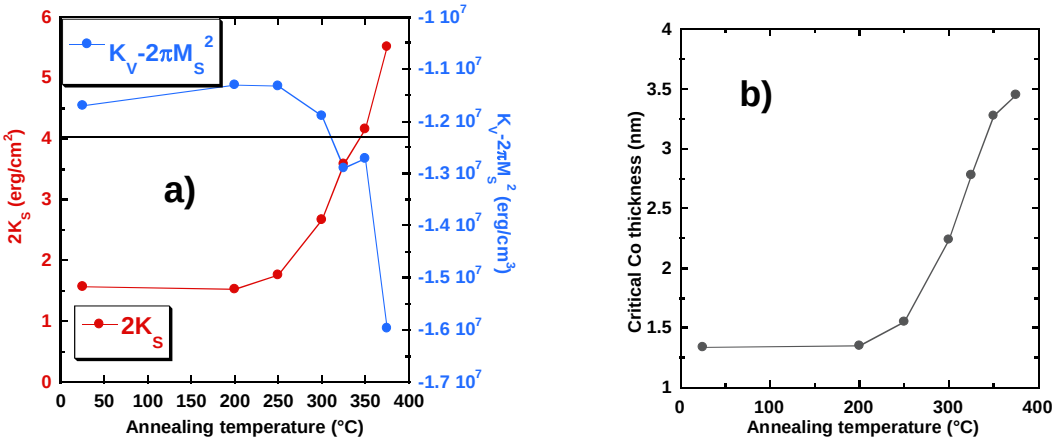

Figure I-14: (a) Interface and volume anisotropies as a function of annealing temperature in Ta3/Pt20/Co/Mg1.4NatOx/Cu2/Pt2 structures. The horizontal line corresponds to -2πM$_S^2$, where M$_S$ is the Co saturation magnetization (1400 emu/cm^3); (b) Critical Co thickness as a function of annealing temperature.

I-4.2 RF deposition of MgO

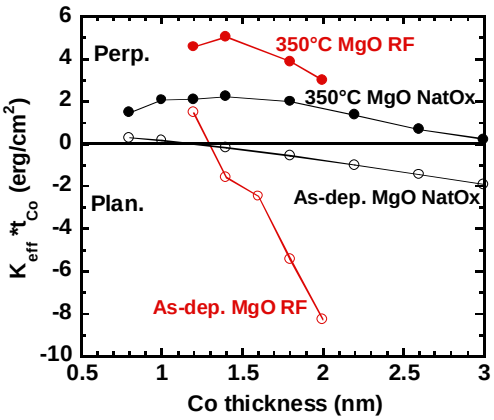

Figure I-15: Plots of Keff*tCo as a function of tCo before and after annealing at 350°C in Ta3/Pt20/Cox/Mg1.4NatOx/Cu2Pt2 (black) and Ta3/Pt20/Cox/MgO1.6RF (red) structures.

Replacing naturally oxidized MgO by an MgO oxide RF-deposited in Pt/Co/MgO trilayers leads to very different anisotropy properties. **Figure I-15** shows plots of K_{Eff}*tCo as a function of the Co layer thickness before and after annealing at 350°C for both oxide types. Samples with MgO RF present higher interfacial but lower volume anisotropy than MgNatOx in the as-deposited state. It is still the case after annealing, although the difference between oxides is reduced. For the Mg naturally oxidized sample, the smaller interfacial anisotropy before annealing can be explained by the under oxidation of the 1.4 nm thick Mg layer in the virgin state, leading to a lower concentration of oxygen at the Co-MgO interface. For MgORF the interfacial anisotropy seems to decrease after annealing whereas the volume anisotropy increases probably because of a slight Pt/Co interface mixing. Despite the large difference between anisotropy contributions in both samples, they lead to very comparable critical thicknesses (about 1.2 nm in the virgin state and 3 nm after annealing).

I-4.3 Comparison between Co and CoFeB

The variation of the anisotropy field as a function of magnetic thickness for Co and CoFeB in the as-deposited state and after annealing at 350°C in Ta3/Pt20/Co(CoFeB)x/MgO1.6RF structures is presented in **Figure I-16**. In the as-deposited state, samples with Co and CoFeB have comparable anisotropy fields. After annealing at 350°C the anisotropy field of the Co sample strongly increases, whereas that of CoFeB is almost unchanged. The slope change with annealing in the case of CoFeB electrodes could be related to structural changes upon CoFeB crystallization and B diffusion resulting in an increased magnetization.

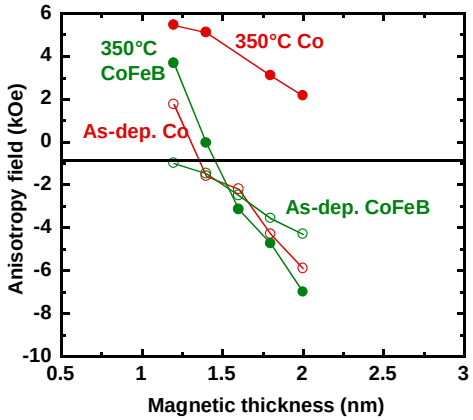

Figure I-16: Variation of the anisotropy field with magnetic thickness before and after annealing at 350°C in Ta3/Pt20/Cox/MgO1.6RF (red) and Ta3/Pt20/CoFeBx/MgO1.6RF (green) structures.

Figure I-17 shows the variation of the anisotropy field with annealing temperature for Ta3/Pt20/Co0.5/CoFeBx/MgO1.6RF samples. The Co layer 0.5 nm thick was used in order to keep the anisotropy brought by the Pt/Co interface. The CoFeB layer thickness varies from 0.6 to 2.6 nm. For all temperatures the anisotropy field goes through a minimum, which progressively shifts to higher annealing temperature with increasing CoFeB thickness. This could indicate that the CoFeB crystallization temperature increases with increasing thickness. Boron diffusion out of CoFe towards the Pt interface could explain the anisotropy minimum. These results are coherent with those presented in **Figure I-16**. For small CoFeB thicknesses, the anisotropy field increases with annealing, whereas it is the reverse for large thicknesses.

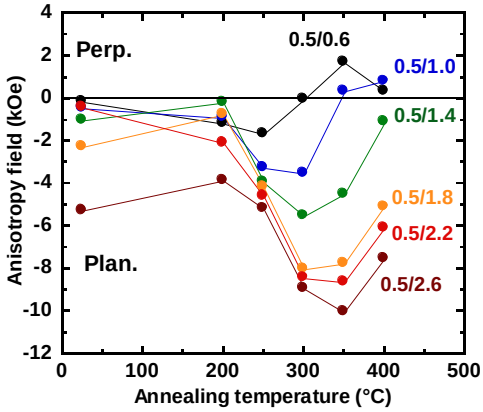

Figure I-17: Variation of the anisotropy field with annealing temperature in Ta3/Pt20/Co0.5/CoFeBx/MgO1.6RF structures with different CoFeB thicknesses.

I-4.4 RF deposition of MgO in different machines

The properties of thin films are very sensitive to deposition conditions, as for instance residual vacuum before sputtering, target quality, sputtering geometry and sputtering power. **Figure I-18** gives an example of two identical samples with the following structure: Ta3/Pt30/Co0.5/CoFeB1/MgO2RF prepared in our two sputtering machines. The sample fabricated in the Plassys machine has 100% perpendicular remanence, whereas the magnetization of the sample fabricated in the Actemium machine is in-plane, although with a low saturation field of 4 kOe. The base vacuum in the Plassys sputtering machine (3.2 10^{-7} mbar) is higher than in the Actemium one (10^{-7}mbar). There are a lot of differences between both machines (base pressure, sputtering power of all targets, target-substrate distance, geometry of the CoFeB deposition), which make difficult to identify the real origin of the difference observed in perpendicular anisotropy for two identical MgO targets.

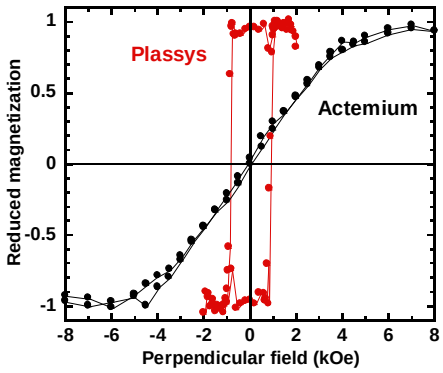

Figure I-18: Reduced magnetization as a function of perpendicular magnetic field, after annealing at 300°C, in two Ta3/Pt30/Co0.5/CoFeB/MgO2RF structures deposited in our Actemium (black) and Plassys (red) sputtering units.

I-4.5 Influence of Pt buffer

The choice of a thick Pt buffer in our structures wasn't arbitrary. It has already been observed in the case of Co/Pt multilayers grown on a Pt buffer [Tan_91, Lan_01] that increasing the buffer thickness increases the multilayer anisotropy and coercive field. This has been related to a smoother top Pt surface for larger buffer thicknesses coming from the improvement of the (111) texture and the larger grain size. X-ray rocking curves show a decrease in the mosaicity of the Pt layer by increasing its thickness from 4.4 to 19 nm [Lan_01]. The same tendency was also observed in our samples with the following structure: Ta3/Ptx/Co0.5/MgO2RF/Ta1.5.

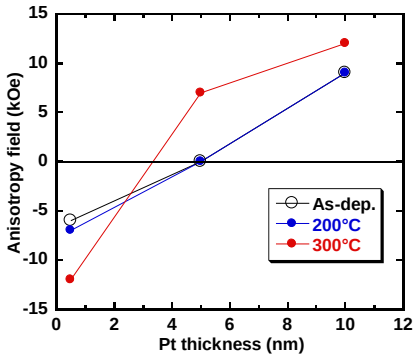

Figure I-19: Variation of the anisotropy field with Pt buffer thickness in Ta3/Ptx/Co0.5/ MgO2RF/Ta1.5 structures for different annealing temperatures.

The variation of the anisotropy field with Pt thickness is shown in **Figure I-19** for different annealing temperatures. Whatever annealing temperature, the anisotropy increases with Pt thickness. For Pt thicknesses of 5 and 10 nm, anisotropy increases with annealing, as usually observed in these Pt/Co/Oxide structures. It is not the case for a Pt layer 0.5 nm thick, where anisotropy decreases with increasing annealing temperature. For such a small thickness, one can suspect that Ta diffusion towards the top Pt interface plays a role in such a degradation. So annealing can also contribute to the improvement of the Pt interface.

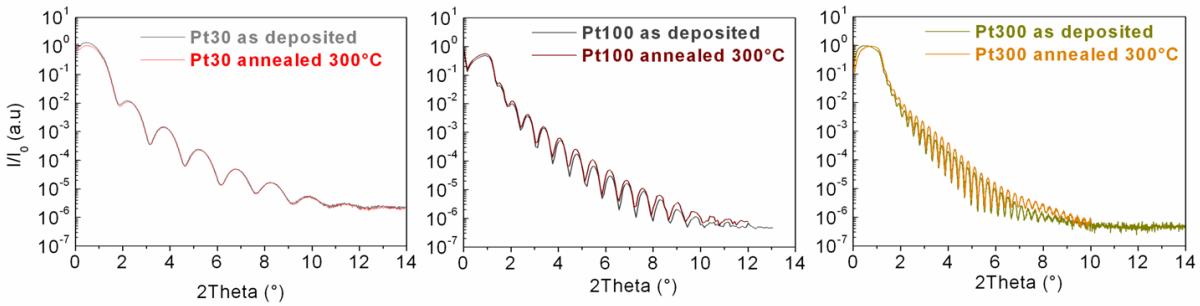

Figure I-20: X-ray reflectivity curves for SiO_2/Ta3/Pt structures for different Pt thicknesses before and after annealing at 300°C

X-ray reflectivity curves for Ta3/Pt layers deposited on Si/SiO_2 substrates for different Pt thicknesses (3, 10 and 30 nm) before and after annealing at 300°C are presented in **Figure I-20**. These experiments werre carried out by H. Garad and F. Fettar at Néel's Institute. All curves display a large number of oscillations, indicating a very low surface roughness. Fits of these curves, in terms of roughness, give about the same results whatever Pt thickness or annealing: from 0.25 nm (rms) for SiO_2, the roughness increases up to 1.4 nm for the top Ta surface, and decreases again to about 0.25 nm for the top Pt surface, even for the smallest Pt thickness. It can be concluded that the increase of the perpendicular anisotropy with increasing Pt thickness or annealing temperature is not linked to a large modification of the Pt surface roughness, but rather to slight modifications of the parameters cited above (texture, grain size, mosaicity).

I-4.6 Influence of capping layer

Since we are looking at very thin oxide layers, of the order of 1 nm, we decided at the beginning of this study to protect them with a capping metallic layer. It was already observed in the case of Pt/Co/AlOx structures [Dah_08] that the anisotropy strength can vary as a function of the capping material. **Figure I-21** shows the Hall curves as a function of perpendicular applied field in Ta3/Pt20/Co2.2/Mg1.0NatOx/X structures with different X capping layers (Pt2, Cu2/Pt2 and Ta2/Pt2).

Before annealing (**Figure I-21a**), the Pt capping layer gives the smallest saturation field (-5 kOe) compared to the Cu/Pt (-6 kOe) and Ta/Pt (-8 kOe) ones. After annealing (**Figure I-21b**), the anisotropy increases for all three samples, but the order between cappings is not modified.

We suggest two possible explanations for the influence of capping layer on the magnetic anisotropy. The first one is based on the affinity of the capping layer to the oxygen from the oxide barrier. Oxygen affinity increases when going from Pt to Cu to Ta. One can thus imagine that the MgO barrier will be more oxygen-deficient when capped with a Ta layer, leading to a smaller anisotropy. Mg oxidation is certainly not homogeneous before annealing, with a maximum oxygen concentration at the top Mg interface. Since Ta is known to be an oxygen-getter material, the oxygen concentration at the bottom Co/MgO interface will be then smaller than in the case of Pt capping, which has no affinity for oxygen. This Ta oxide will be stable enough to lead to still lower anisotropy after annealing. In the case of Cu capping, the same reasoning holds in the as-

deposited state. However, since Cu oxide is less stable than Ta oxide (see **Appendix 2**), de-oxidation of the Cu interface upon annealing could explain that perpendicular anisotropy of the Cu-capped sample now approaches that of the Pt-capped one.

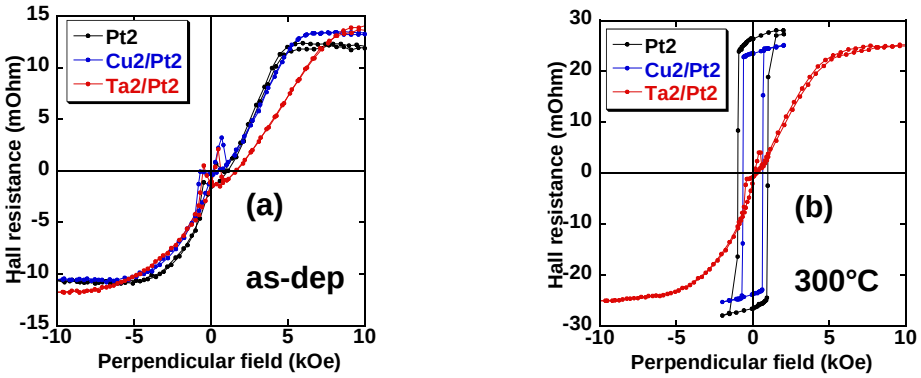

Figure I-21: Hall hysteresis loops for Ta3/Pt20/Co2.2/Mg1.0NatOx/X structures with X= Pt, Cu/Pt or Ta/Pt in (a) The as-deposited state and (b) After annealing at 300°C.

The second possible explanation is based on the fact that Pt, Cu and Ta have different crystalline structures. Pt and Cu are both fcc, but with a very different lattice parameter. On the contrary, Ta (bcc) is usually considered as amorphous in very thin films. One can thus imagine that structural constraints imposed by the capping material could modify the crystallization of the MgO layer, hence modifying the anisotropy properties of the Co/MgO interface.

I-5. Growth of magnetic layers on oxides

Up to now we considered Pt/Co/Oxide trilayers. Reverse Oxide/Co/Pt stackings are expected to give less out-of-plane anisotropy because of the more difficult growth of a metal on an oxide layer [Jan_06, Man_07, Bed_07, Fen_09]. In this part, we present results on such Co and CoFeB-based structures, which could lead to the realization of full perpendicular magnetic tunnel junctions. We will first look at the growth of different magnetic materials (Co, CoFe, CoFeB, NiFe) onto thermally oxidized Si substrates. Then we will present the anisotropy properties of Co layers grown on different oxides, namely thermal SiO_2, naturally or plasma-oxidized Al, and MgO oxide obtained either by natural oxidation of metallic Mg or by deposition from an MgO target.

I-5.1 Growth of magnetic materials on thermally oxidized SiO_2

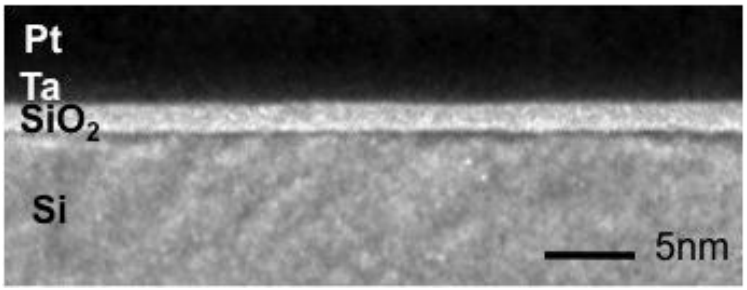

Figure I-22: TEM cross section of a Si/SiO_2/Ta/Pt structure.

We first present results concerning the growth of different magnetic materials (MM) layers on thermally oxidized SiO_2 (500nm thick) with a very low surface roughness, of the order of 0.2 to 0.3 nm (rms) as the natural silicon oxide which can be observed on the microscopy cross-section shown in **Figure I-22**. This allows to eliminate any possible influence of oxide roughness on the growth of magnetic materials and to choose the magnetic material which gives highest PMA when it grows on oxide.

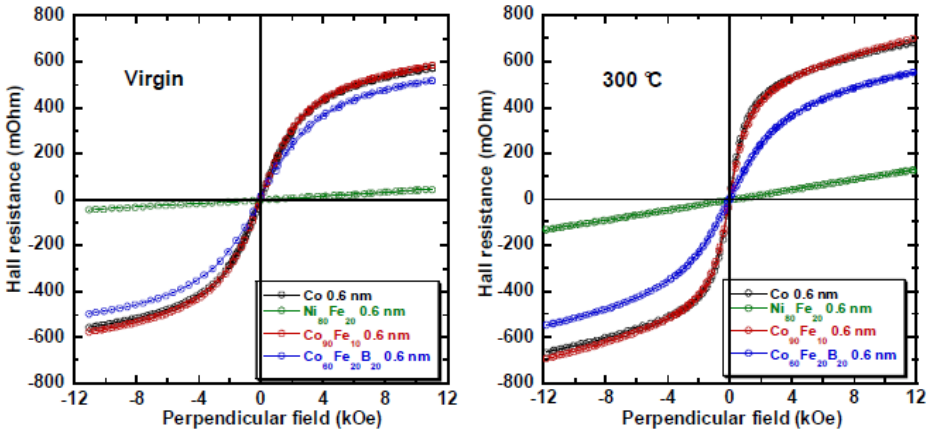

Figure I-23: Variation of the Hall resistance as a function of perpendicular magnetic field in SiO_2/MM0.6/Pt3 structures in the as-deposited state (left) and after annealing at 300°C (right). MM stands for Co (black), $Ni_{80}Fe_{20}$ (green), $Co_{90}Fe_{10}$ (red) and $Co_{60}Fe_{20}B_{20}$ (blue).

We will investigate the growth of different magnetic materials: Co, $Co_{90}Fe_{10}$, amorphous $Co_{60}Fe_{20}B_{20}$ and Permalloy ($Ni_{80}Fe_{20}$) on SiO_2, with thicknesses of 0.6 and 1.5 nm. Hall hysteresis loops of different SiO_2/MM/Pt3 structures with a magnetic thickness of 0.6 nm are presented in **Figure I-23** before and after annealing at 300°C. In as-deposited state all magnetic layers exhibit a superparamagnetic behaviour (no clear saturation of the magnetization). Permalloy does not give any magnetic signal.

Annealing at 300°C visibly improves the magnetic structure for the samples with Co and CoFe. The corresponding Hall curves present a lower saturation field, indicating the presence of a PMA contribution.

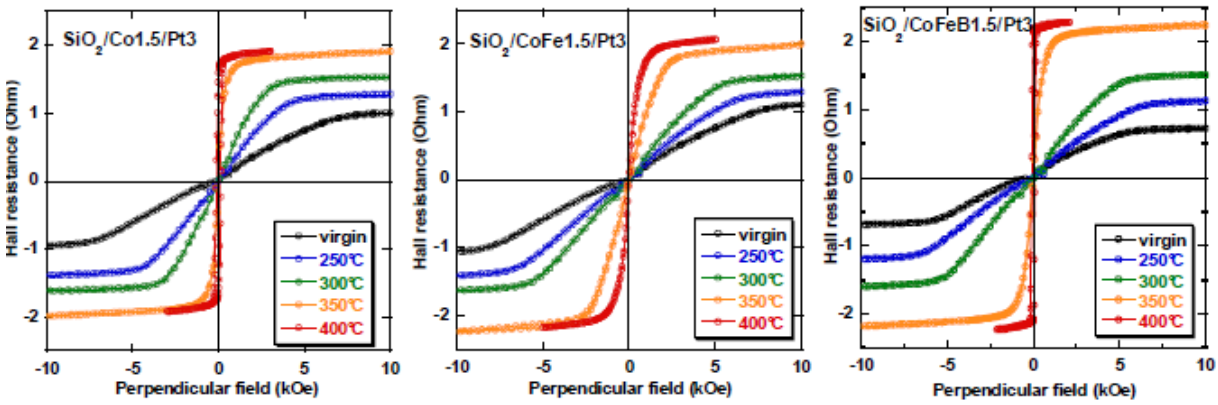

Figure I-24: Variation of the Hall resistance as a function of perpendicular magnetic field in SiO_2/MM1.5/Pt3 structures for different annealing temperatures. MM stands for Co (left), $Co_{90}Fe_{10}$ (middle) and $Co_{60}Fe_{20}B_{20}$ (right).

On the contrary, EHE loops for samples with thicker (1.5 nm) magnetic layers show a clear ferromagnetic behaviour (**Figure I-24**), with a well defined saturation field even in the virgin state. Annealing leads to a progressive increase of the perpendicular anisotropy in all samples. After annealing at 400°C, Co and CoFeB samples exhibit 100% remanence, whereas the magnetization of the CoFe sample is still in plane, although with a greatly reduced saturation field.

I-5.2 Growth of Co on different oxides

We will now focus on the perpendicular anisotropy properties of Co layers grown on different oxides.

I-5.2.A Growth of Co on thermally oxidized SiO_2

We first present the perpendicular anisotropy properties of Co layers grown on SiO_2. **Figure I-25** shows the variation of the Hall resistance as a function of the perpendicular applied field for a Co layer deposited on thermally oxidized SiO_2, with a thickness of 0.6nm (**left**) and 1.5 nm (**right**). As it was shown in the preceding Section (**I-5.1**) all curves exhibit a superparamagnetic behaviour when the Co thickness is 0.6 nm, with a zero remanent magnetization and no clear saturation at high field whatever annealing temperature. This behaviour is in agreement with the results from the literature [Mor_95, Cai_01] for discontinuous (island-like) growth, and contrasts with the case of standard Pt/Co/Pt trilayers with equivalent cobalt thickness, which give perfectly square hysteresis loops and anisotropy fields of a few kOe [Met_07].

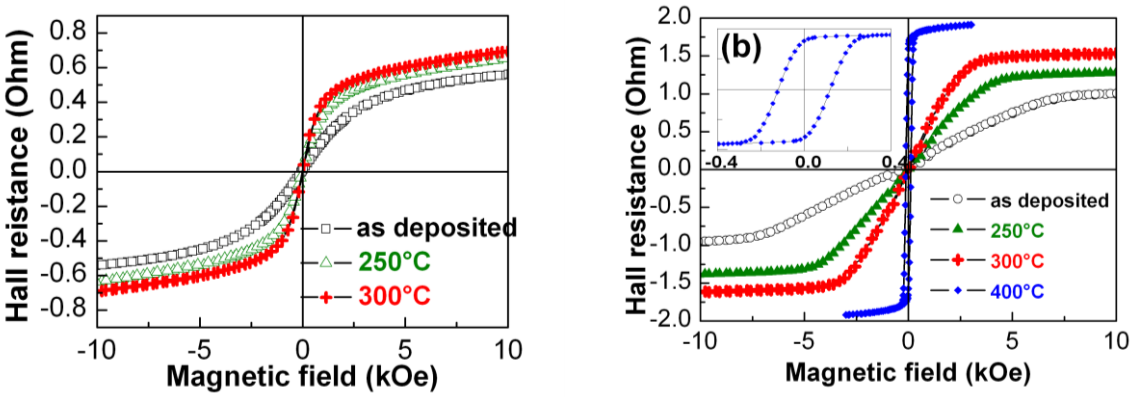

Figure I-25: Hall resistance as a function of perpendicular applied field for SiO_2/Co/Pt structures after different annealing treatments for a cobalt thickness of 0.6nm (left) and 1.5nm (right). The inset in the right figure is a zoom of the curve measured after annealing at 400°C.

A clear ferromagnetic behaviour is observed for Co layers 1.5 nm thick (linear variation of the Hall resistance, well defined saturation field). Before annealing, the magnetization lies in-plane with an anisotropy field of about -8 kOe (with the usual sign convention of negative anisotropy fields for in-plane magnetization). Assuming a M_S value close to pure Co (1400 emu/cm^3), this field is much smaller than the Co demagnetizing field (about -18 kOe), indicating an already significant PMA contribution. This contribution increases steadily with increasing annealing temperature, and 100% remanence is obtained after annealing at 400°C. Although a smaller PMA is obtained in the virgin state compared to Pt/Co1.5/Pt structures (H_{an}= -8kOe compared to -2.5 kOe), larger values are obtained after 400°C annealing (H_{an}= +0.5 kOe compared to -0.7 kOe). This implies that, despite a degraded growth of Co on oxide, the Oxide/Co interface brings much more perpendicular anisotropy than the Pt/Co one after annealing, and probably limits Pt/Co intermixing [Rod_09].

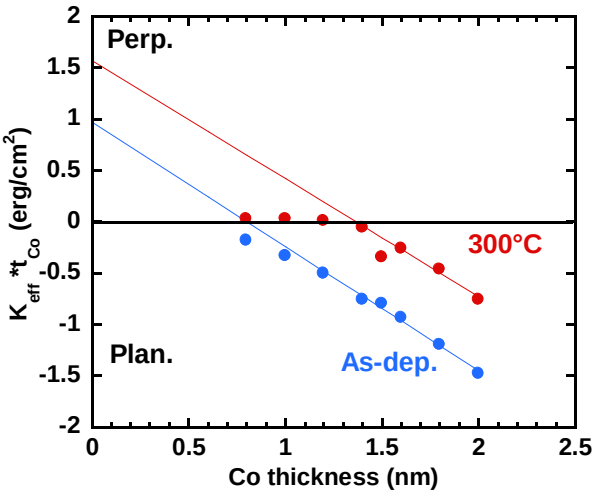

Figure I-26: Plots of K_{Eff}*t_{Co} as a function of Co thickness before and after annealing at 300°C in SiO2/Cox/Pt3 structures. Lines are fits to Equation I.1.

The critical layer thickness was determined for Co layers in SiO_2/Co/Pt structures from the variation of the anisotropy field as a function of thickness. **Figure I-26** shows the variation of K_{Eff}*t as a function of Co thickness before and after annealing at 300°C. The critical thickness increases with annealing (from 0.8 nm in the virgin state to 1.4 nm after 400°C annealing). This is mainly due to an increase of the interface anisotropy, without so much change in the volume contribution. The deviation from linear behaviour after annealing at 300°C at small Co

thicknesses can be tentatively attributed to Pt/Co intermixing at high annealing temperatures, leading to a progressive PMA decrease.

I-5.2.B Growth of Co on different oxides prepared by sputtering

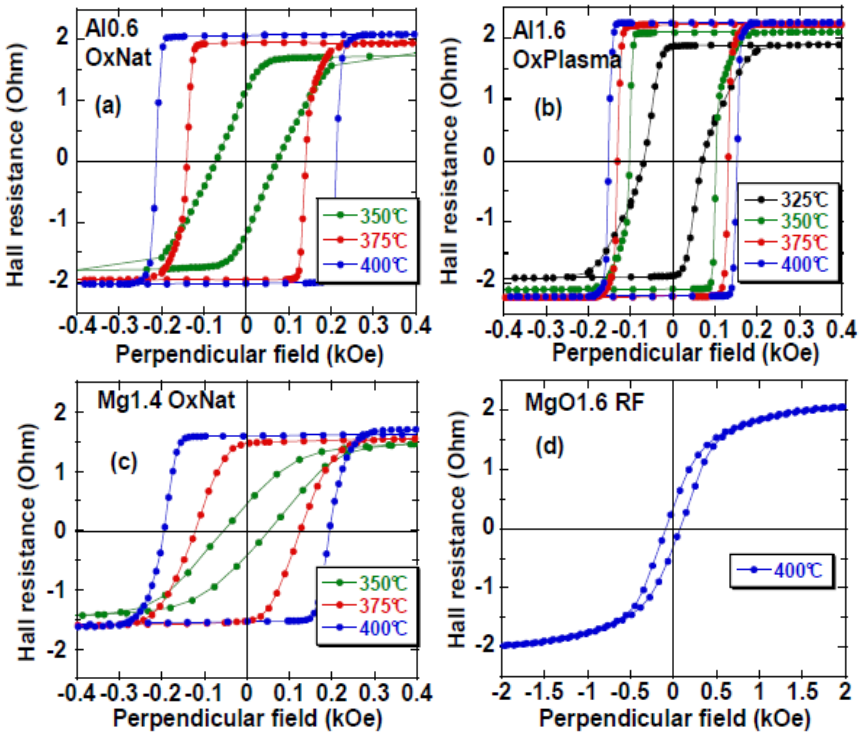

Figure I-27: Variation of the Hall resistance as a function of perpendicular magnetic field in Ox/Co1.5/Pt3 structures for different annealing temperatures. Ox stands for (a) Natural Al, (b) Plasma Al, (c) Natural Mg oxidations and (d) RF MgO deposition.

We now present results concerning the growth of 1.5 nm thick Co layers on different oxides, namely naturally oxidized Al, plasma oxidized Al and MgO prepared by either natural oxidation of Mg metal or by RF deposition from an MgO target.

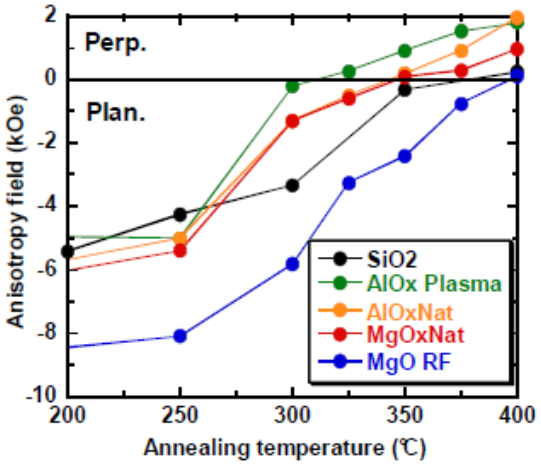

Figure I-28: Variation of the anisotropy field with annealing temperature in different Ox/Co1.5/Pt3 structures.

The magnetization lies in-plane for all samples in the as-deposited state. However, as can be seen in **Figure I-27**, the perpendicular magnetic anisotropy increases systematically with

annealing temperature and magnetization is out-of-plane after annealing at 325°C (plasma oxidized Al), 350°C (natural oxidation of Mg and Al) or 400°C (RF deposition of MgO). **Figure I-28** shows the variation of the anisotropy field as a function of annealing temperature for these different oxides. The largest anisotropy values are obtained for Co deposited onto plasma oxidized Al, probably because of a more uniform (homogeneous) oxidation compared to natural oxidation, which mainly proceeds through the grain boundaries. Except for the (possibly oxygen-deficient) RF-sputtered MgO oxide, a larger PMA is obtained for these oxides compared to SiO_2. The anisotropy seems to scale with the enthalpy of formation of the different oxides (see Ellingham's diagrams in **Appendix 2**), as already noticed in previous investigations **[Rod_09]**, and results from hybridization of Co and O orbitals at the interface **[Yan_11]**.

The variation of the effective anisotropy times Co thickness as a function of Co thickness is presented in **Figure I-29a** for samples grown on MgORF oxide. The interface anisotropy increase with annealing temperature as was the case for the growth on SiO_2 substrates presented before. One also observes a slight increase of the volume contribution. The same deviation from the linear behaviour is observed for the highest (350 and 400°C) annealing temperatures. **Figure I-29b** shows that the increase of the interface anisotropy (together with the slight increase of the volume one) with annealing leads to a strong enhancement of the critical Co thickness (from 0.7 nm before annealing to 1.6 nm after annealing at 400°C). The critical thickness at 300°C is lower than for SiO_2 (1.1 nm after 300°C annealing compared to 1.4 nm) since MgO RF brings lower PMA.

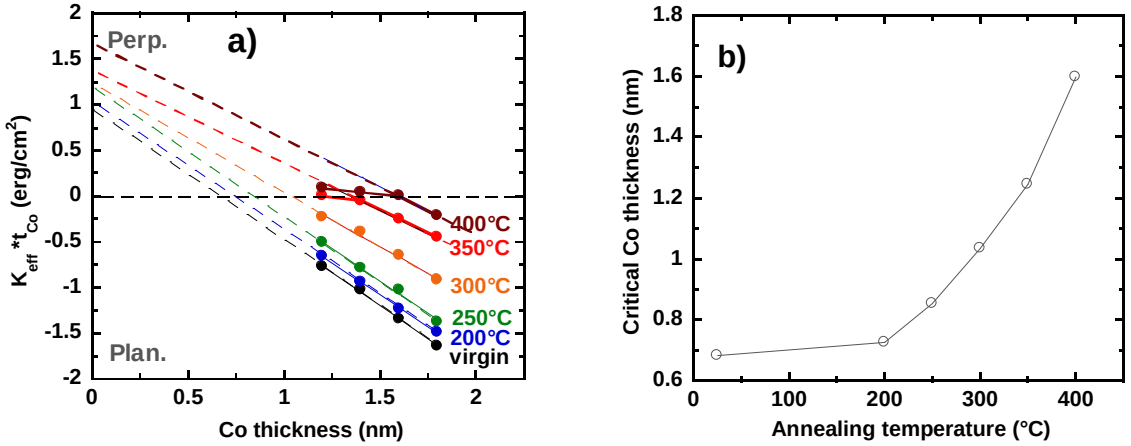

Figure I-29: (a) Plots of $K_{Eff}*t_{Co}$ as a function of Co thickness after annealing in MgO1.6RF/Co/Pt3 structures. Lines are fits to Equation I-1; (b) Critical Co thickness as a function of annealing temperature.

I-5.2.C Comparison with Pt/Co/Ox and Pt/Co/Pt structures

Pt/Co/Oxide and Oxide/Co/Pt structures could appear similar, both having the same Pt/Co and Co/oxide interfaces. However different growth conditions, related to surface energies between metal/metal and metal oxide interfaces completely modify the magnetic properties of a magnetic metal deposited on either an oxide or on a metallic surface, with important consequences on the magnetic anisotropy. The critical layer thickness it is a good parameter for the comparison between top and bottom electrodes since it mainly reproduces the interfacial anisotropy variation with annealing temperature, the total volume anisotropy being more or less dominated by the demagnetizing energy.

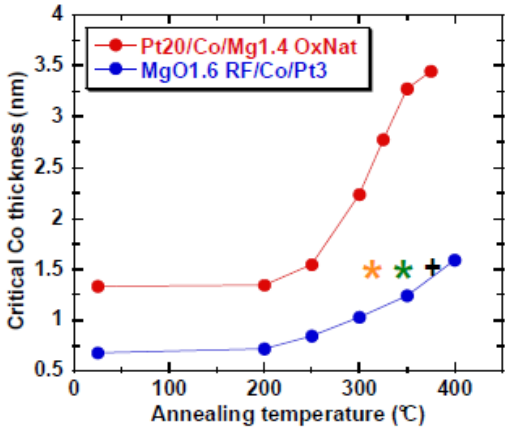

Figure I-30: Comparison of critical Co thicknesses in bottom (red) and top (blue) electrodes. A critical thickness of 1.5 nm is obtained after 310°C annealing for plasma oxidized Al (orange star), 340°C for naturally oxidized Mg (red star) and 375°C for SiO_2 (plus sign).

Figure I-30 compares the variation of the critical Co thickness with annealing temperature for both Pt/Co/MgOxnat and MgORF/Co/Pt structures. Even if both structures evolve in a similar way with annealing, Oxide/Co/Pt structures exhibit a systematically lower critical thickness than Pt/Co/Oxide ones. This difference between top and bottom electrodes can be observed even in as deposited state and is mostly related to growth problems since the oxide interface has an important contribution after annealing. Focusing on the critical thickness of 1.5 nm we can observe that the bottom electrode with MgNatOx is already perpendicular at 250°C contrary to the inverse structure which needs a much higher annealing temperature of 340°C. For the top electrodes the annealing temperature for which the critical thickness of 1.5 nm is obtained depends on the type of oxide and oxygen content (lower temperatures correspond to strongly oxidized electrodes like Al plasma oxidation and Mg natural oxidation). So the lower critical thickness for the top electrode is not only related to the difficult growth of Co on oxide but also to the oxygen concentration at the upper oxide interface. One must note that AlOx (either plasma or naturally oxidized) as well as naturally oxidized Mg deal with the deposition of a metallic layer on the SiO_2 substrate and subsequent oxidation, which is not the case for RF-deposited MgO layers.

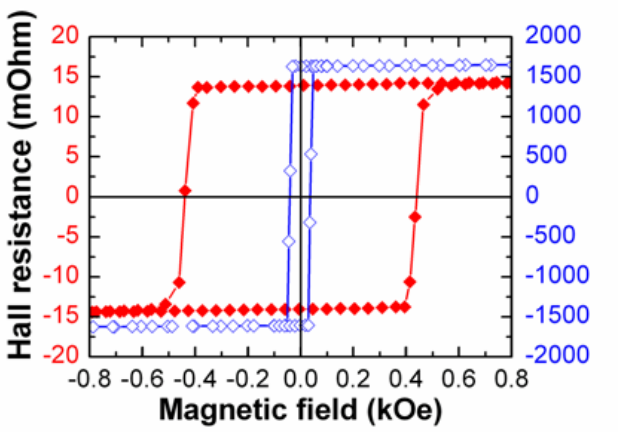

Figure I-31: Comparison between bottom Ta3/Pt20/Co0.5/CoFeB1 /MgO1.6 RF (red) and top MgO1.6 RF/CoFeB1/Pt3 (blue) electrodes after annealing at 350°C.

This difference in perpendicular anisotropy between top and bottom electrode was observed for all magnetic materials we used. **Figure I-31** compares top and bottom electrodes based on Co/CoFeB magnetic layers. Both electrodes have 100% perpendicular remanence after

annealing at 350°C. However, the top MgO/CoFeB1 electrode, despite its smaller magnetic thickness, has a much smaller coercive field than the bottom Co0.5/CoFeB1/MgO electrode.

Contrary to the interfacial anisotropy which slightly increases with annealing for the top Oxide/Co/Pt electrode and more strongly for the bottom Pt/Co/Oxide one (**Figure I-32a**), the volume anisotropy has different variations at high annealing temperatures (**Figure I-32b**). For the bottom electrode, high annealing temperatures lead to a decrease of the volume anisotropy (from a positive to a negative value) which can be interpreted as a volume modification (slight mixing) near the Pt/Co interface. On the contrary, the volume anisotropy contribution of the top electrode increases for high annealing temperature. The explanation is related to the more difficult growth of Co on oxide than on Pt resulting in a rougher interface with Pt in the as-deposited state. This roughness is progressively reduced upon annealing.

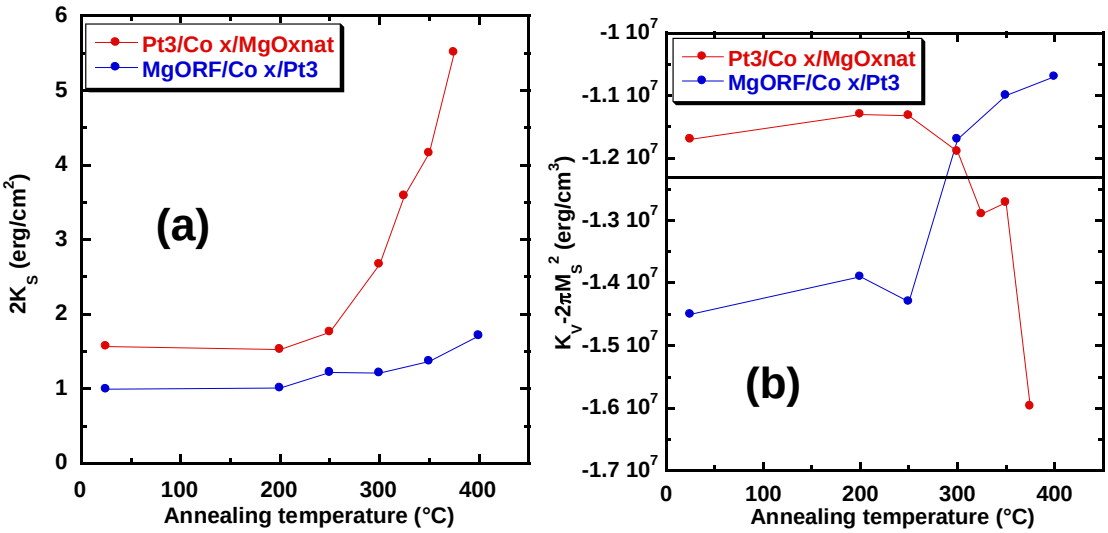

Figure I-32: (a) Interface and (b) Volume anisotropies as a function of annealing temperature in Pt20/Cox/Mg1.4 NatOx and MgO1.6RF/Cox/Pt3 structures. The horizontal line in (b) corresponds to $-2\pi M_S^2$, with M_S= 1400 emu/cm^3.

We now compare the contribution to PMA of bottom Pt/Co and Oxide/Co interfaces in Pt/Co/Oxide and Oxide/Co/Pt structures. In the case of Pt3/Co1.5/Pt3 structures, **Figure I-33** shows that their anisotropy increases slightly with annealing temperature but is still in-plane even after annealing at 400°C. This means that, according to the anisotropy variations with annealing and magnetic thickness presented in this Chapter, the oxide/Co interface brings more perpendicular anisotropy to the Co layer after annealing than the Pt/Co interface. The positive influence of the Co/oxide interface on the Pt/Co one in terms of thermal stability is inferred from the comparison between anisotropy properties of Pt/Co/Pt and Pt/Co/Oxide structures (see **Section I-4**).

For high annealing temperatures the anisotropy then comes from the Co-oxide interface, high temperature assisting oxygen diffusion and formation of Co-O bonds. This hypothesis is supported by X-ray reflectivity measurements on Pt/Co/AlOx layers that show a direct correspondence between maximum perpendicular magnetic anisotropy and onset of Co oxide formation **[Rod_09, Fet_09]**. This is also supported by X-ray spectroscopy measurements **[Man_07, Man_08b]**. We think that hybridization at the Co/oxide interface is the main origin of perpendicular anisotropy. In the case of Co/Oxide interfaces, the 3d orbitals of cobalt hybridizes with the 2p orbitals of oxygen. This hybridization lowers the Co-O binding energy, perpendicularly to the interface. As a consequence, these orbitals possess a lower energy than those lying in-plane, creating a strong perpendicular magnetic anisotropy despite the relatively

weak spin-orbit coupling. Experimental evidence for the PMA origin related to Co-O bond formation will be presented in **ChapterII-5**.

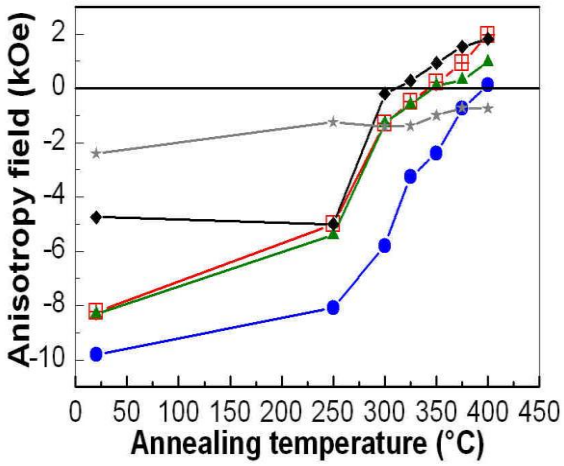

Figure I-33: Variation of the anisotropy field with annealing temperature in different Oxide/Co1.5/Pt3 structures and comparison with Pt3/Co1.5/Pt3 (gray stars).

I-6. Conclusions

In this Chapter we presented possible origins of the perpendicular anisotropy induced at magnetic metal/oxide interface, through hybridization of orbitals between oxygen and the magnetic metal. We also presented our first experimental results on PMA properties of bottom Pt/magnetic metal/oxide and top oxide/magnetic metal/Pt electrodes.

The perpendicular anisotropy of bottom Pt/Co/MgO electrodes greatly increases with annealing, the critical Co thickness going from 1.3 nm in the as-deposited up to almost 3.5 nm after annealing at 375°C. Large differences are observed between Co and CoFeB electrodes, the latter exhibiting a non-monotonous variation with annealing. RF deposition of MgO appears very dependent on the sputtering conditions, as shown by the large difference of PMA properties between both sputtering machines used. The Pt buffer thickness and the nature of the capping layer also influence the anisotropy properties of these bottom electrodes.

The anisotropy of top oxide/Co/Pt electrodes is much smaller, whatever the oxide considered, with a maximum critical thickness of about 1.6 nm after annealing at 400°C. This seems to be related to a much difficult growth of the magnetic layer on oxide than on Pt, as will be confirmed in the next **Chapter**. Interface and volume contributions to the perpendicular anisotropy vary differently for both electrodes. While the increase of anisotropy upon annealing in bottom electrodes is mainly due to the interfacial contribution, that of the top electrodes mainly comes from an increase of the volume contribution.

I-7. References

[Ber_70] L. Berger, *Side-jump mechanism for the Hall effect of ferromagnets*, **Phys. Rev. B** **2** (1970) 4559.

[Bed_07] S. Bedanta, T. Eimüller, W. Kleemann, J. Rhensius, F. Stromberg, E. Amaladass, S. Cardoso and P.P. Freitas, *Overcoming the dipolar disorder in dense CoFe nanoparticle ensembles: Superferromagnetism,* **Phys. Rev. Lett.** **98** (2007) 176601.

[Bro_89] F.J.A. den Broeder, D. Kuiper, H.C. Donkersloot and W.A. Hoving, *Comparison of the magnetic anisotropy of [001] and [111] oriented Co/Pd multilayers,* **Appl. Phys. A** **49** (1989) 507.

[Bro_91] F.J.A. den Broeder, W. Hoving and P.J.H. Bloemen, *Magnetic anisotropy of multilayers,* **J. Magn. Magn. Mater.** **93** (1991) 562.

[Bru_88] P. Bruno, *Magnetic surface anisotropy of cobalt and surface roughness effects within Néel's model,* **J. Phys. F: Met. Phys.** **18** (1988) 1291.

[Bru_89] P. Bruno, *Tight-binding approach to the orbital magnetic moment and magneto-crystalline anisotropy of transition-metal monolayers,* **Phys. Rev. B** **39** (1989) 865.

[Cai_01] J.-W. Cai, S. Okamoto, O. Kitakami and Y. Shimada, *Large coercivity and surface anisotropy in MgO/Co multilayer films,* **Phys. Rev. B** **63** (2001) 104418.

[Car_08] B. Carvello, C. Ducruet, B. Rodmacq, S. Auffret, E. Gautier, G. Gaudin and B. Dieny, *Sizable room-temperature magnetoresistance in cobalt based magnetic tunnel junctions with out-of-plane anisotropy,* **Appl. Phys. Lett.** **92** (2008) 102508.

[Cho_10] G.-M. Choi, B.-C. Min and K.-H. Shin, *FePdB layer for perpendicular magnetic tunnel junctions*, **Appl. Phys. Lett.** **97** (2010) 202503.

[Daa_90] G.H.O. Daalderop, P.J. Kelly and M.F.H. Schuurmans, *First-principles calculation of the magnetocrystalline anisotropy energy of iron, cobalt, and nickel,* **Phys. Rev. B** **41** (1990) 11919.

[Daa_94] G.H.O. Daalderop, *Magnetic anisotropy from first principles*, in "Ultrathin Magnetic Structures I", Springer Verlag, J.A.C. Bland and B.Heinrich Eds, Berlin, New York (1994).

[Dah_08] Y. Dahmane, S. Auffret, U. Ebels, B. Rodmacq and B. Dieny, *Perpendicular magnetic anisotropy at Co/Oxide interfaces,* **IEEE Trans. Magn.** **44** (2008) 2868.

[End_10] M. Endo, S. Kanai, S. Ikeda, F. Matsukura and H. Ohno, *Electric-field effects on thickness dependent magnetic anisotropy of sputtered MgO/$Co_{40}Fe_{40}B_{20}$/Ta structures,* **Appl. Phys. Lett.** **96** (2010) 212503.

[Fen_09] G. Feng, S. van Dijken and J.M.D. Coey, *MgO-based double barrier magnetic tunnel junctions with thin free layers*, **J. Appl. Phys.** **105** (2009) 07C926.

[Fet_09] F. Fettar, H. Garad, L. Ortega, A.Y. Ramos, B. Zawilski, P. Plaindoux, S. Auffret, B. Rodmacq and B. Dieny, *Investigation of metallic/oxide interfaces in Pt/Co/AlOx trilayers by hard X-ray reflectivity,* **IEEE Trans. Magn.** **45** (2009) 3905.

[Fow_10] C. Fowley, N. Decorde, K. Oguz, K. Rode, H. Kurt and J.M.D. Coey, *Perpendicular magnetic anisotropy in CoFeB/Pd bilayers,* **IEEE Trans. Magn.** **46** (2010) 2116.

[Fow_11] C. Fowley, K. Rode, K. Oguz, H. Kurt and J.M.D. Coey, *Electric field induced changes in the coercivity of a thin-film ferromagnet*, **J. Phys. D: Appl. Phys.** **44** (2011) 305001.

[Gay_86] J.G. Gay and R. Richter, *Spin anisotropy of ferromagnetic films,* **Phys. Rev. Lett.** **56** (1986) 2728.

[Gra_68] U. Gradmann and J. Müller, *Flat ferromagnetic epitaxial 48Ni/52Fe(111) films of few atomic layers*, **Phys. Stat. Sol.** **27** (1968) 313.

[Ike_10] S. Ikeda, K. Miura, H. Yamamoto, K. Mizunuma, H.D. Gan, M. Endo, S. Kanai, J. Hayakawa, F. Matsukura and H. Ohno, *A perpendicular-anisotropy CoFeB–MgO magnetic tunnel junction,* **Nature Mater.** **9** (2010) 721.

[Jan_06] Y. Jang, C. Nam, J.Y. Kim, B.K. Cho, Y.J. Cho and T.W. Kim, *Magnetic field sensing scheme using CoFeB/MgO/CoFeB tunneling junction with superparamagnetic CoFeB layer,* **Appl. Phys. Lett.** **89** (2006) 163119.

[Joh_96] M.T. Johnson, P.J.H. Bloemen, F.J.A. den Broeder and J.J. de Vries, *Magnetic anisotropy in metallic multilayers,* **Rep. Prog. Phys.** **59** (1996) 1409.

[Jun_10a] J.H. Jung, S.H. Lim and S.R. Lee, *Strong perpendicular magnetic anisotropy in thick CoFeB films sandwiched by Pd and MgO layers,* **Appl. Phys. Lett.** **96** (2010) 042503.

[Jun_10b] J.H. Jung, S.H. Lim and S.R. Lee, *Strong perpendicular magnetic anisotropy in an MgO/CoFeB/Pd unit structure with a thick CoFeB layer*, **J. Appl. Phys.** **108** (2010) 113902.

[Lan_01] S. Landis, *Réseaux de plots magnétiques sub-microniques réalisés à partir de substrats prégravés,* **PhD Thesis, Grenoble University** (2001).

[Man_06] S. Mangin, D. Ravelosona, J.A. Katine, M.J. Carey, B.D. Terris and E.E. Fullerton, *Current-induced magnetization reversal in nanopillars with perpendicular anisotropy,* **Nature Mater.** **5** (2006) 210.

[Man_07] A. Manchon, *Magnétorésistance et transfert de spin dans les jonctions tunnel magnétiques,* **PhD Thesis, Grenoble University** (2007).

[Man_08a] A. Manchon, C. Ducruet, L. Lombard, S. Auffret, B. Rodmacq, B. Dieny, S. Pizzini, J. Vogel, V. Uhlir, M. Hochstrasser and G. Panaccione, *Analysis of oxygen induced anisotropy crossover in Pt/Co/MOx trilayers,* **J. Appl. Phys.** **104** (2008) 043914.

[Man_08b] A. Manchon, S. Pizzini, J. Vogel, V. Uhlir, L. Lombard, C. Ducruet, S. Auffret, B. Rodmacq, B. Dieny, M. Hochstrasser and G. Panaccione, *X-ray analysis of oxygen-induced perpendicular magnetic anisotropy in Pt/Co/AlOx trilayers,* **J. Magn. Magn. Mater.** **320** (2008) 1889.

[Met_07] P.J. Metaxas, J.-P. Jamet, A. Mougin, M. Cormier, J. Ferré, V. Baltz, B. Rodmacq, B. Dieny and R.L. Stamps, *Creep and flow regimes of magnetic domain-wall motion in ultrathin Pt/Co/Pt films with perpendicular anisotropy,* **Phys. Rev. Lett.** **99** (2007) 217208.

[Mir_10] I.M. Miron, G. Gaudin, S. Auffret, B. Rodmacq, A. Schuhl, S. Pizzini, J. Vogel and P. Gambardella, *Current-driven spin torque induced by the Rashba effect in a ferromagnetic metal layer,* **Nature Mater.** **9** (2010) 230.

[Mon_02] S. Monso, B. Rodmacq, S. Auffret, G. Casali, F. Fettar, B. Gilles, B. Dieny and P. Boyer, *Crossover from in-plane to perpendicular anisotropy in Pt/CoFe/AlO_x sandwiches as a function of Al oxidation: A very accurate control of the oxidation of tunnel barriers,* **Appl. Phys. Lett.** **80** (2002) 4157.

[Mor_95] C. Morawe and H. Zabel, *Structure and thermal stability of sputtered metal/oxide multilayers: The case of Co/Al_2O_3,* **J. Appl. Phys.** **77** (1995) 1969.

[Nak_98] N. Nakajima, T. Koide, T. Shidara, H. Miyauchi, H. Fukutani, A. Fujimori, K. Iio, T. Katayama, M. Nývlt and Y. Suzuki, *Perpendicular magnetic anisotropy caused by interfacial hybridization via enhanced orbital moment in Co/Pt multilayers: Magnetic circular X-ray dichroism study,* **Phys. Rev. Lett.** **81** (1998) 5229.

[Née_54] L. Néel, *Anisotropie magnétique superficielle et surstructures d'orientation*, **J. Phys. Rad.** **15** (1954) 225.

[Nis_09] L.E. Nistor, B. Rodmacq, S. Auffret and B. Dieny, *Pt/Co/oxide and oxide/Co/Pt electrodes for perpendicular magnetic tunnel junctions,* **Appl. Phys. Lett.** **94** (2009) 012512.

[Nis_10] L.E. Nistor, B. Rodmacq, C. Ducruet, C. Portemont, I.L. Prejbeanu and B. Dieny, *Correlation between perpendicular anisotropy and magnetoresistance in magnetic tunnel junctions,* **IEEE Trans. Magn.** **46** (2010) 1412.

[Rod_03] B. Rodmacq, S. Auffret, B. Dieny, S. Monso and P. Boyer, *Crossovers from in-plane to perpendicular anisotropy in magnetic tunnel junctions as a function of the barrier degree of oxidation,* **J. Appl. Phys.** **93** (2003) 7513.

[Rod_09] B. Rodmacq, A. Manchon, C. Ducruet, S. Auffret and B. Dieny, *Influence of thermal annealing on the perpendicular magnetic anisotropy of Pt/Co/AlOx trilayers,* **Phys. Rev. B** **79** (2009) 024423.

[Smi_55] J. Smit, *The spontaneous Hall effect in ferromagnetics*, **Physica** **21** (1955) 877.

[Tan_91] S.L. Tang, P.F. Carcia, D. Coulman and A.J. McGhie, *Scanning tunneling microscopy of Pt/Co multilayers on Pt buffer layers,* **Appl. Phys. Lett.** **59** (1991) 22.

[Tho_56] W. Thomson, *On the electro-dynamic qualities of metals: Effects of magnetization on the electric conductivity of nickel and of iron*, Proc. Roy. Soc. Lond. **8** (1856–1857) 546.

[Wan_93] D.S. Wang, R. Wu and A.J. Freeman, *Magnetocrystalline anisotropy of Co-Pd interfaces,* **Phys. Rev. B 48** (1993) 15886.

[Wei_07] M. Weisheit, S. Faehler, A. Marty, Y. Souche, C. Poinsignon and D. Givord, *Electric field-induced modification of magnetism in thin-film ferromagnets*, **Science 315** (2007) 349.

[Wel_94] D. Weller, Y. Wu, J. Stöhr, M.G. Samant, B.D. Hermsmeier and C. Chappert, *Orbital magnetic moments of Co in multilayers with perpendicular magnetic anisotropy,* **Phys. Rev. B 49** (1994) 12888.

[Yam_11] M. Yamanouchi, R. Koizumi, S. Ikeda, H. Sato, K. Mizunuma, K. Miura, H.D. Gan, F. Matsukura and H. Ohno, *Dependence of magnetic anisotropy on MgO thickness and buffer layer in $Co_{20}Fe_{60}B_{20}$-MgO structure*, **J. Appl. Phys. 109** (2011) 07C712.

[Yan_11] H.X. Yang, M. Chshiev, B. Dieny, J.H. Lee, A. Manchon and K.H. Shin, *First-principles investigation of the very large perpendicular magnetic anisotropy at Fe/MgO and Co/MgO interfaces*, **Phys. Rev. B 84** (2011) 054401.

[Yoo_05] I. Yoo, D.K. Kim and Y.K. Kim, *Switching characteristics of submicrometer magnetic tunnel junction devices with perpendicular anisotropy,* **J. Appl. Phys. 97** (2005) 10C919.

Chapter II

ANISOTROPY AND TRANSPORT PROPERTIES OF PERPENDICULAR MAGNETIC TUNNEL JUNCTIONS

Chapter II

ANISOTROPY AND TRANSPORT PROPERTIES OF PERPENDICULAR MAGNETIC TUNNEL JUNCTIONS

Magnetic tunnel junctions (MTJ) with perpendicularly magnetized electrodes are gaining more and more interest, since they are considered to possess great advantages over conventional planar MTJ's (better stability against thermal fluctuations, potentially lower write current densities). However, the main two classes of perpendicular magnetic electrodes currently under study suffer from serious drawbacks: those based on Pt/Co or Pd/Co multilayers consist of very thin (less than 1 nm) magnetic layers, and thus are not expected to lead to a full polarization of the electrons, which is at the basis of magnetoresistance effects. On the other hand, those based on Co or Fe layers exchanged coupled to (Rare Earth-Transition Metals) alloys suffer from a great chemical reactivity which makes them difficult to handle in industry. In addition, these latter structures have a poor thermal stability, and thus it is difficult to use them as magnetic electrodes in MgO-based tunnel junctions for which high temperature annealing is required (good crystallization of the MgO barrier and of the CoFeB electrodes) for obtaining large magnetoresistance effects.

The aim of the first **Chapter** was to introduce a new class of materials, Oxide/Cobalt/Platinum trilayers, for which perpendicular magnetization can be stabilized for rather large Co thicknesses (1.5 to 2.0 nm) after annealing at temperatures of about 350°C to 400°C. We also previously prepared inverse structures (Platinum/Cobalt/Oxide trilayers), in which similar heat treatments led to a critical Co thickness (above which the magnetization of the Co layer falls back in-plane) larger than 3.0 nm.

One should thus be able to prepare perpendicular Co/Oxide/Co stackings with very good PMA properties after annealing at or above 350°C. These structures possess some of required properties for high-performance perpendicular junctions, namely rather thick magnetic electrodes and very good thermal stability. However, we will see later that the crystallographic structure itself (bcc or fcc) plays a key role in the TMR of this type of MTJ. That's the reason why we also considered Pt/Co/CoFeB electrodes, hoping that the MgO barrier could impose its texture to the CoFeB layer upon its crystallization after annealing. But the anisotropy in these structures was lower so a Pt/Co multilayer was introduced in order to keep overall strong anisotropy. However, later experiments on planar MTJ with Pt buffer and also literature reports showed that the texture of the buffer (Pt, Pd) could dominate over the influence of the MgO barrier and induce (111) texture of the magnetic electrode, leading to a strong decrease of the transport properties.

It is not so straightforward to simply stack the top electrode onto the bottom one. The main problem arises from stray fields created by the magnetically softest layer when it reverses its magnetization direction. These stray fields emanating from the small inverse growing domains can amount to some hundreds of Oe, depending on the thickness of the magnetic layers, and act as a supplementary applied field. The difference in coercive fields between the soft and hard layers must thus be larger than the stray field of the softest one, in order to stabilize the intermediate antiparallel magnetic configuration. This limits the maximum thickness of the bottom electrode, whose anisotropy, and thus coercive field, decreases with increasing thickness.

Other problems can arise from the influence of roughness of the bottom magnetic electrode on the growth of the top one (in the previous **Chapter**, we only considered top electrodes grown on very flat SiO_2 substrates).

Finally, as we will see below, strong magnetic interactions between bottom and top electrodes can considerably modify the magnetic properties of the full stacking. This means that the optimization of such perpendicular junctions cannot be done independently for bottom and top electrodes alone, but always considering the full stacking.

II-1. Magnetic tunnel junctions

II-1.1 Origin of magnetoresistance in MgO based junctions

A ferromagnetic material can spin polarize the electron current flowing through it, producing a disequilibrium between the two Mott conductions channels.

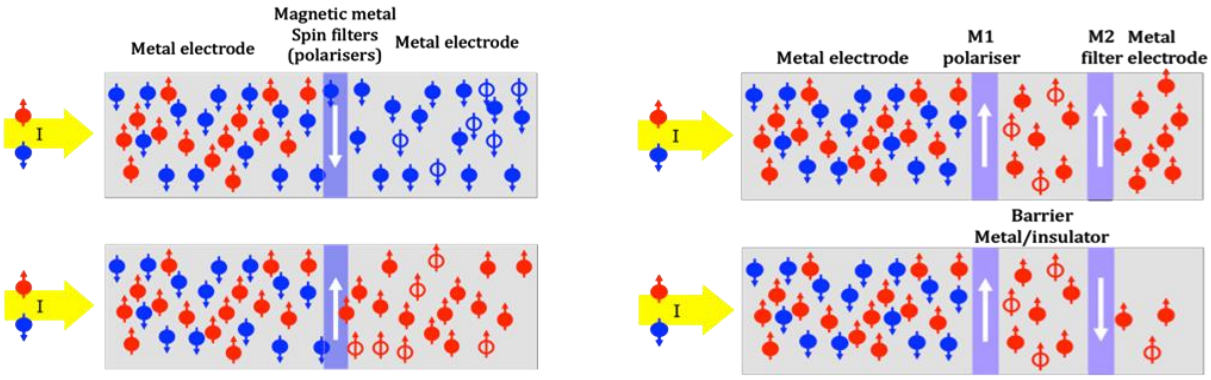

Figure II-1: (a) A ferromagnetic material, depending of its magnetization direction, will first select the electrons with spin parallel to the magnetization and will spin polarize the electron current flowing through in two up ↑ or down ↓ states; (b) System with two magnetic layers acting as polarizer (M1) and analyzer (M2).

This spin polarization is given by the following expression: $P=(j_{\uparrow}-j_{\downarrow})/(j_{\uparrow}+j_{\downarrow})$. As a function of the magnetic material the current can be totally spin polarized P=1, or partially polarized. But how can we detect in this case the polarization effect of the first magnetic layer, since measuring the current will not bring us any information about the spin? The answer comes from magnetic material's property of spin-filtering. In order to detect the polarisation effect of the first magnetic layer a second magnetic layer can be added in the system, separated from the first one by a metallic or insulating spacer as in **Figure II-1**. This is similar to light polarizers used in optics. Now playing with the magnetization configuration of the two magnetic layers parallel or antiparallel one can observe that there is a large difference in the resistance of the structure between the two states.

Here we will focus on the case of MTJ and we will try to better understand the phenomena responsible for the polarization in the case of tunnel transport. First spin polarization measurements were made by Tedrow et al. in 1970 in FM/Al_2O_3/Al junctions **[Mes_70, Ted_71]** and observation made for different polarizations helped to relate it to the density of states: $P(E_F) = (D^{\uparrow} - D^{\downarrow})/(D^{\uparrow} + D^{\downarrow})$. Four years later, performing measurements at low temperature on magnetic junctions based on Fe/GeOx/Co, Jullière **[Jul_75]** observed a large dependence of the resistance on the magnetic configuration of the magnetic layers. Inspired by the results obtained by Tedrow on spin polarization, he developed a model in order to explain this resistance change called TMR. Jullière's model is based on two hypotheses:
- the electron spin is conserved through the tunnelling process

- the electron probability of transition between the two magnetic layers by tunneling through the barrier is proportional to the product of the density of states of the two electrodes as shown in **Figure II-2.**

According to this the current represented by the two channels is proportional to the density of states at the Fermi level of the two electrodes. Since the electrodes are ferromagnetic

there will be a difference between the density of states of the spin up ($D^{\uparrow}$) and down ($D^{\downarrow}$) (majority or minority) electrons.

When electron states on each side of the barrier are spin-polarized (parallel or antiparallel) the electron will find more easily free states to tunnel (low resistance state) when the magnetization are parallel than when they are antiparallel (high resistance state) (**Figure II-2**). The result is a large difference in the resistance as a function of the magnetic configuration of the electrodes.

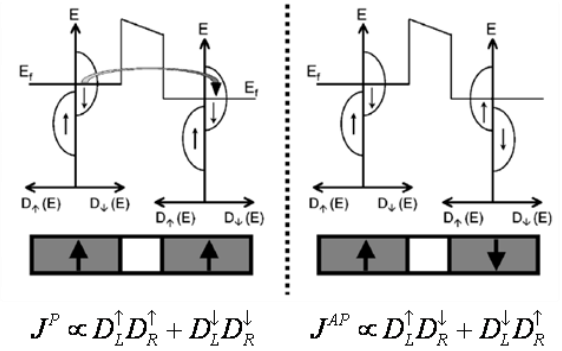

$J^{P} \propto D_L^{\uparrow} D_R^{\uparrow} + D_L^{\downarrow} D_R^{\downarrow}$ $J^{AP} \propto D_L^{\uparrow} D_R^{\downarrow} + D_L^{\downarrow} D_R^{\uparrow}$

$$P(E_F) = (D^{\uparrow} - D^{\downarrow})/(D^{\uparrow} + D^{\downarrow})$$

$$TMR = \frac{\Delta R}{R_P} = \frac{2 P_L P_R}{1 - P_L P_R}$$

P_L, P_R: polarization of the left and right layer

Figure II-2: Jullière's model for parallel and antiparallel orientations of the magnetic electrodes.

Even if this model provides a simple physical explanation of the TMR phenomenon, it is insufficient to describe all cases observed in literature, especially for crystalline insulating barriers. Its limits are reached for the prediction of the polarisation sign. This shows that there is something else that matters in the tunneling transport. Stearns **[Ste_77]** showed that the bands around Fermi level have free-electron-like character, dominating the tunneling and determining the polarization. But, what about the barrier contribution to the spin polarisation? The answer came with Slonczewski's tunnel transport theory based on free electron model **[Slo_89]** several years later. This model takes into consideration the nature of the barrier for the calculation of polarization. Since we talk about tunneling effect, which is a pure quantum effect, the electron should be considered as a wave vector. Inside the electrodes the electrons are plane waves (e^{iky}, where $k_{\uparrow(\downarrow)}$ are wave vectors of the spin up and down electrons), contrary to the barrier where electrons are evanescent waves ($e^{-q_0 y}$), where q_0 is the wave vector of the electrons in the barrier). Increasing the barrier thickness will reduce the tunneling probability of electrons.

When the barrier is thick enough so that $e^{2q_0 a} \gg 1$, the transmission probability reduces to the product between the transmission probability of both magnetic layers and the probability of presence of the electron in the barrier is: $T = T_L T_R e^{-2q_0 a}$ showing clearly the tunnel character which is translated to the conductance by using the Landauer formula (from **Figure II-3**). TMR is related to the polarization through the conductance and is fully described by the wave vectors of the electrons in the barrier q and the magnetic layers as shown by the formula below:

$$\frac{\Delta G}{G_P} = \frac{G_P - G_{AP}}{G_P} = \frac{2P^2}{1+P} \qquad \text{where} \qquad \Delta G = G_P - G_{AP} = 16 q_0^2 e^{-2q_0 a} \left[\frac{(k_{\uparrow} - k_{\downarrow})(q_0^2 - k_{\uparrow} k_{\downarrow})}{(q_0^2 + k_{\uparrow}^2)(q_0^2 + k_{\downarrow}^2)} \right]^2$$

$$P = \left(\frac{k_{\uparrow} - k_{\downarrow}}{k_{\uparrow} + k_{\downarrow}} \right) \left(\frac{q_0^2 - k_{\uparrow} k_{\downarrow}}{q_0^2 + k_{\uparrow} k_{\downarrow}} \right) \qquad \text{with} \qquad q_0 = \pm \sqrt{\frac{2m(U-E)}{\hbar^2} + k_{\parallel}^2}$$

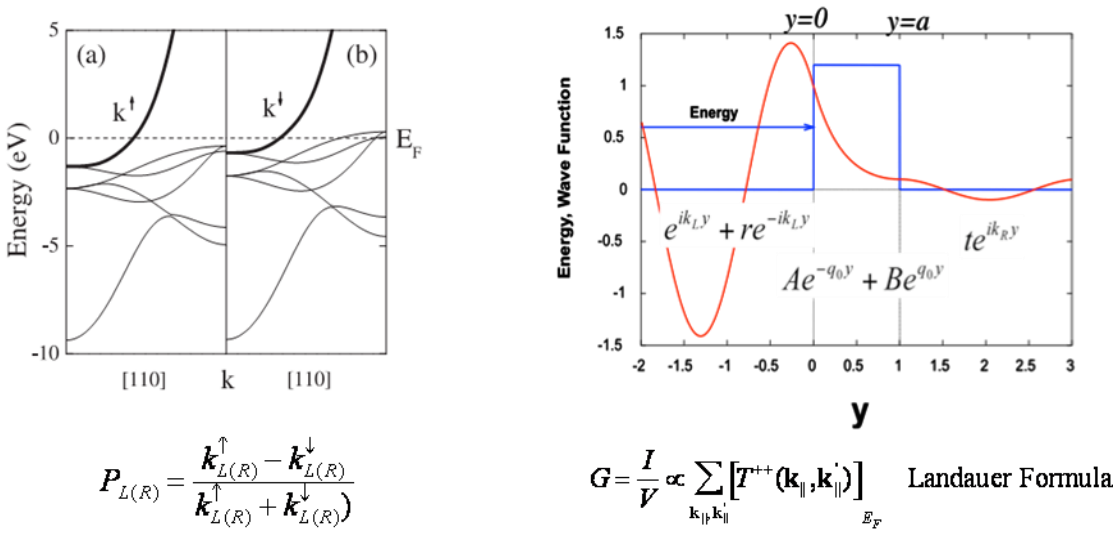

$$P_{L(R)} = \frac{k^{\uparrow}_{L(R)} - k^{\downarrow}_{L(R)}}{k^{\uparrow}_{L(R)} + k^{\downarrow}_{L(R)}}$$

$$G = \frac{I}{V} \propto \sum_{\mathbf{k}_{\parallel}\mathbf{k}'_{\parallel}} \left[T^{\uparrow\uparrow}(\mathbf{k}_{\parallel}, \mathbf{k}'_{\parallel})\right]_{E_F}$$

Figure II-3: Stearn's [Ste_77] and Sonczewski's [Slo_89] models taking into consideration the wave vectors from both electrodes and barrier in the calculation of the polarization and the TMR.

In the case of a high barrier $q_o >> k_{F\uparrow}, k_{F\downarrow}$, the polarization is reduced to $P = (k_\uparrow - k_\downarrow)/(k_\uparrow + k_\downarrow)$. Considering the assumption that the density of states is proportional to the electrons wave vector in electrodes: $D(E_F) \propto k$ one obtains the Jullière's formula for the TMR from **Figure II-2.**

At the time where a significant TMR (11.8%) was measured at room temperature in CoFe/AlOx/Co by Moodera et al. **[Moo_95]**, Slonczewski's theory of TMR was ready to explain this case, since evanescent waves in alumina have free-like character. This was the beginning for the road towards the highest TMR values, which could make possible industrial applications. All efforts consumed to obtain high TMR with AlOx barriers reached the limit of 80% **[Wei_07]**.

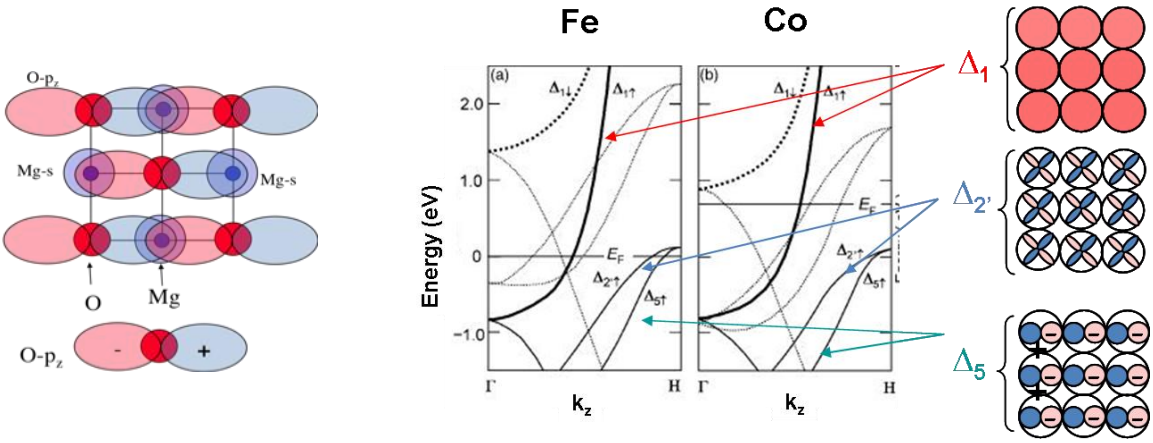

Figure II-4: (a) Δ1 band structure of MgO (2 band s-p Tight-Binding model, M. Chshiev); b) Fe and Co density of states and resulting bands at Fermi level in (001) (Γ-H) direction: majority (solid line) Δ1, Δ2', minority Δ2, Δ2', and double degenerate Δ5 bands [Yua_06].

The solution was to find another insulator material with additional spin-filtering properties. It was already there since 2001 when Butler et al. **[But_01]** predicted, using a tight binding model, that epitaxial systems based on crystalline Fe(100)/MgO(100)/Fe(100) could give 1000% TMR. The theory takes into consideration the valence bands Δ1 (as evanescent

state) in the insulator MgO (001), which comes from a linear combination of atomic orbital p_z of O and s orbital's of Mg, represented schematically in **Figure II-4**. As a consequence it should be used with magnetic electrodes materials having electrons of symmetry Δ1 for which the barrier is transparent, and through which they can pass with a low decay rate. This is the case of Fe which has 4 types of bands symmetry: Δ1, Δ2, Δ2', Δ5 arising from the crystalline bcc (001)symmetry by linear atomic orbital combinations of s, p, and d orbitals. Since Fe and MgO have the same crystallographic symmetry and the same (001) bcc texture, both will have the same electrons of symmetry Δ1.

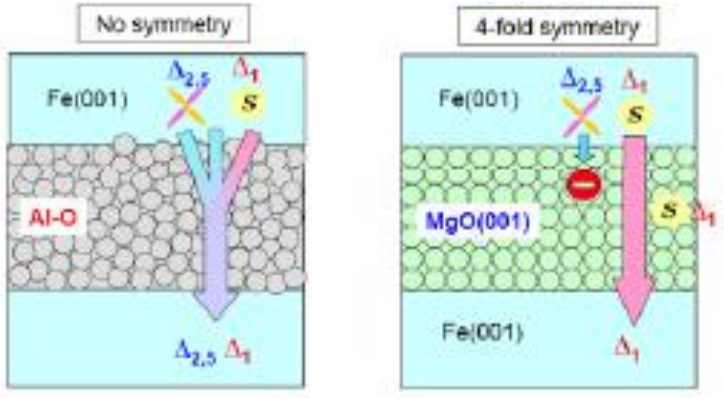

Figure II-5: Tunneling transport in amorphous AlOx and crystalline MgO barriers. Thanks to the crystalline nature of the MgO barrier the spins selectivity is increased, the crystalline symmetry acting as an additional filter to the tunnel transport [Yua_07].

It should be noted that the decay rate depends on wave function symmetry **[Zha_04]** but also on the electron spin polarizations state (up or down). Compared to an amorphous barrier, a crystalline barrier is a spin-filter as a function of the wave function symmetry as is shown in **Figure II-5.**

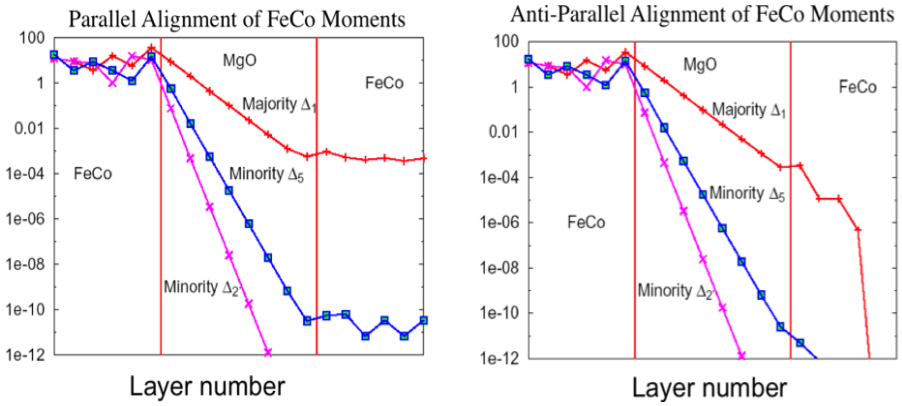

Figure II-6: Tunneling density of states on each atomic layer at Fermi level for a FeCo/MgO/FeCo junction. Left panel: parallel spin alignment, right panel: antiparallel spin alignment [Zha_04].

In order to better understand the origin of the higher TMR values obtained with MgO crystalline barrier compared to amorphous AlOx, we can look at the density of states in the FeCo/MgO system for both cases of parallel and antiparallel alignment of the magnetic layers presented in **Figure II-6**. In the case of parallel alignment we can see that electrons of Δ1 symmetry exist at Fermi level just for majority electrons, and readily enter into the MgO and decay slowly inside MgO. So bcc (001) FeCo acts as an half metal for this symmetry. Since there

is no present Δ_1 symmetry at Fermi level for the minority electrons, the conduction is dominated by Δ_5. In the antiparallel case the conduction is based on Δ_5 symmetry, since there are no Δ_1 states symmetries present at the Fermi level for minority electrons. The difference between the highly conductive parallel state (through $\Delta 1$ channel) and the almost insulating antiparallel state (through Δ_5 channel) results in a huge TMR.

Tunneling density of states at Fermi level depends strongly on symmetry of Bloch states in ferromagnetic layer. By consequence any impurities at the interface like oxygen (in the case of over-oxidized electrodes) can strongly change the density of states in the ferromagnetic layer and also affect the Bloch states having a strong impact in the decrease rate of $\Delta 1$ states as it is shown in **Figure II-7** [Yan_10].

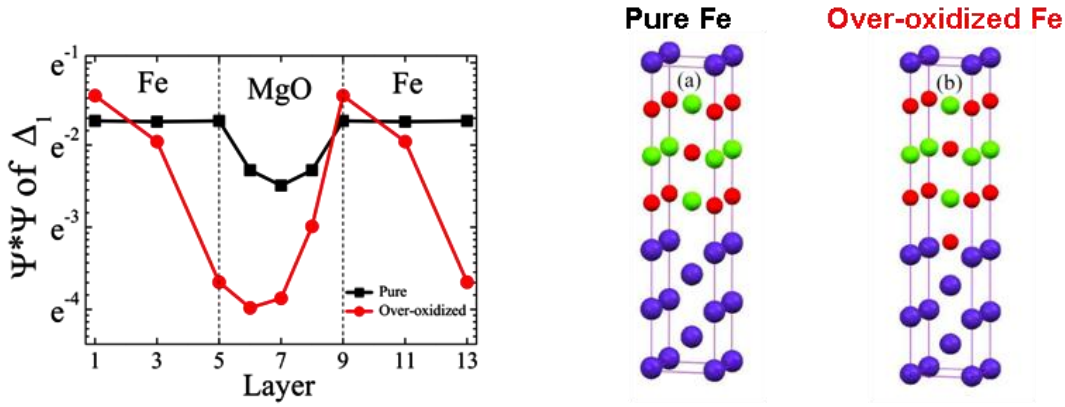

Figure II-7: Bloch state character at Γ-point at the Fermi level as a function of layer number in pure and over-oxidized Fe/MgO interfaces. Bloch states are absent at Fermi level in the under-oxidized case [Yan_10].

All this theoretical predictions initiated a large experimental effort towards large TMR values in MTJ with crystalline MgO barriers. Since there is a good epitaxial fit between the Fe and MgO $\sqrt{2}a_{Fe}/a_{MgO}$ =0.981, Fe(001)/MgO(001)/Fe(001) MTJ were fabricated having very high TMR values of 200% [Yua_04]. Another epitaxial system CoFe/MgO/CoFe also gave high TMR [Par_04]. But it is difficult to transfer the epitaxy technique to industry (deposition on 200/300 mm Si substrates). Sputtering techniques are more adapted to industrial mass production but this technique is not well adapted for obtaining the right (001) orientation of both barrier and magnetic layers. The solution to this problem was to use amorphous CoFeB electrodes, which will not influence the texture orientation of the MgO layer. The MgO bcc (001) texture improves upon annealing at 300-350°C and leads to the crystallization of the CoFeB magnetic layers with the same symmetry. This is the reason why magnetoresistance increases with annealing temperature [Hay_05, Jia_09]. As it was shown before, in order to have a high TMR the CoFeB based electrodes must have the same crystal (001) symmetry as that of the barrier since in this direction the $\Delta 1$ bands of CoFeB are half metallic and the barrier is transparent for this $\Delta 1$ channel. On the contrary, for symmetry mismatch between the barrier and the magnetic electrodes the TMR strongly decreases [Yua_00, Yua_07]. The TMR ratio was found to depend critically on both composition (higher TMR for Fe-rich alloys) and CoFeB thickness [Lee_07], and on diffusion of atomic species as Ta or Mg at MgO interfaces/volume [Ike_08].

Despite all these technological difficulties, very high TMR of 600% [Ike_08] was observed in MTJ fabricated by RF magnetron sputtering. But the inconvenient of these structures for applications is the high value of the resistance-area (RA) product of 100 Ω.μm². The new technique of spin torque switching requires low RA products (< 10 Ωμm²) in order to avoid breakdown of the insulating barrier. So a compromise must be found between a high TMR and a low enough RA product.

In conclusion the conditions necessary to obtain a large TMR in crystalline MTJ are:

- good epitaxial matching between ferromagnetic layers and crystalline barrier
- high symmetry Bloch state for one of two electron spin states in the ferromagnetic electrodes ($\Delta 1$)
- evanescent states in the insulator with the same Bloch state symmetry
- low roughness of the interfaces between magnetic layers and the barrier
- well crystallised barrier with a small quantity of defects and high affinity for oxygen
- high spin-polarization magnetic materials
- well established parallel and antiparallel magnetic states

II-1.2 Perpendicular magnetic tunnel junctions

Figure II-8 shows the number of publications on perpendicular junctions as a function of time. Interest for such structures really started in 2008 with the use of MgO barriers.

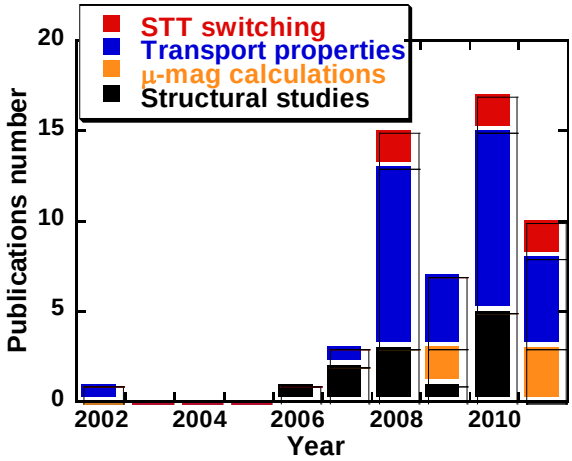

Figure II-8: Evolution with time of the number of publications on perpendicular tunnel junctions. We differentiate between structural studies, micro-magnetic calculations, transport properties and spin-transfer torque experiments.

The first report on perpendicular magnetic tunnel junctions dates back from 2002 [Nis_02]. In this publication, Nishimura et al. presented results on electrodes made of Rare Earth-Transition Metal (RE-TM) alloys exchange-coupled to a 1.0 nm thick CoFe layer, separated by an Al_2O_3 barrier. In pillars 300 nm in size, they obtained a TMR ratio of up to 55%, with RA products down to 10^3 $\Omega\mu m^2$ for 1.3 nm thick barriers. They also showed that using a ferrimagnetic TbFeCo alloy could greatly reduce the coupling field between soft and hard electrodes. At this time, RE-TM were probably the best choice, since Al_2O_3 barriers require only moderate annealing to optimize their transport properties.

One then had to wait until 2007 [Hat_07] for results about anisotropy properties of structures with an MgO barrier. The first results on TMR properties in MgO-based structures (64% TMR) appeared in 2008 [Ohm_08a], with electrodes made of RE-TM alloys exchanged-coupled to an Fe layer. The same year, Nakayama et al. presented the first results on spin transfer switching [Nak_08], in CoFeB magnetic layers exchange-coupled to RE-TM alloys. With an RA product as low as 16 $\Omega\mu m^2$, they obtained critical current densities of 5 MA/cm^2.

Since 2009, different materials have been tested, in order to induce perpendicular anisotropy in the magnetic electrodes on both sides of the MgO barrier (RE-TM alloys, CoCrPt alloys, ordered $L1_0$ alloys, (Co/Pt) and (Co/Pd) multilayers. All materials have their advantages and drawbacks. RE-TM alloys can be relatively easily fabricated, but their anisotropy properties

greatly depend on both alloy composition and annealing temperature, which makes their optimization quite difficult. Diffusion of Rare-Earth metals, as well as possible pollution of the deposition machines, can also be a problem. CoCrPt alloys generally require high temperature deposition, as is the case for ordered $L1_0$ PtFe or PtCo alloys. Co-based multilayers could appear as the best choice, since they can induced a rather strong anisotropy, even after annealing at temperatures (300-350°C) required for optimizing TMR properties of MgO barriers.

However, the main drawback of all these PMA-inducing materials resides in the fact that they generally induce a crystallographic texture (except for $L1_0$ structures) incompatible with the (001) texture of the MgO crystalline barrier. These materials are mostly fcc (111) textured, and will impose the same texture to the amorphous magnetic CoFeB electrodes upon annealing.

The great breakthrough came in 2010 **[Ike_10]** when structures based on Ta/CoFeB electrodes were proposed, very similar to their in-plane counterparts. The problem of the bcc (100) texturation of the CoFeB electrode upon crystallization is thus solved. Perpendicular anisotropy, although much smaller than in all other proposed structures, mainly arises from the CoFeB/oxide interface **[Mon_02]**. After patterning into sub-micronic pillars, two well-separated parallel and anti-parallel states are obtained, leading to both high TMR ratio (120%), low RA product (18 $\Omega\mu m^2$), and low STT switching current densities (4 MA/cm^2). **Table II-1** summarizes, as a function of year and research teams involved, the number of publications on perpendicular magnetic tunnel junctions. Literature about perpendicular electrodes alone has been reported in **Chapter I**.

Year	Ref	Team	Barrier	Hard	Soft	S/μ	TMR (%)	RA Ωμm²
2002	**Nis_02**	**Canon**	**AlOx**	**RE-TM/CoFe**	**RE-TM/CoFe**		**55**	**10^3**
2005	Yoo_05	Korea Univ.				**μ**		
2006	Che_06	SPIN, Taiwan	AlOx/MgO	RE-TM/CoFe	RE-TM/CoFe	**S**		
2007	Can_07	SPIN, Taiwan	AlOx	RE-TM	RE-TM		70	10^7
	Per_07	SP2M/Grenoble	MgO	$L1_0$	$L1_0$	**S**		
	Hat_07	Tokyo Tech.	MgO	RE-TM/Fe	RE-TM/Fe	**S**		
2008	Par_08a	Car. Mellon	AlOx	(Co/Pt)	(Co/Pt)		0.3	10^2
	Par_08b	Car. Mellon	AlOx	(Co/Pt)	(Co/Pt)		15	
	Kim_08a	Korea Univ.				**μ**		
	Lee_08	SPIN, Taiwan	MgO	(Co/Pt)	(Co/Pd)	**S**		
	Ye_08a	SPIN, Taiwan	MgO	(Co/Pt)	(Co/Pd)		32	10^4
	Ye_08b	SPIN, Taiwan	MgO	RE-TM	(Co/Pt)	**S**		
	Car_08	Spintec	AlOx	(Co/Pt)	(Co/Pt)		8	10^8
	Duc_08	Spintec	AlOx	(Co/Pt)	(Co/Pt)		8	10^8
	Kim_08b	Tohoku	MgO	$L1_0$	$L1_0$		6	
	Ohm_08a	**Tokyo Tech.**	**MgO**	**RE-TM/Fe**	**RE-TM/Fe**		**64**	**$3\ 10^4$**
	Ohm_08b	Tokyo Tech.	MgO	RE-TM/Fe	RE-TM/Fe	**S**		
	Nak_08	**Toshiba**	**MgO**	**RE-TM/CoFeB**	**RE-TM/CoFeB**		**15**	**16**
	Yos_08	Toshiba	MgO	$L1_0$	$L1_0$		105	10^4
	Kis_08	Toshiba	MgO	?	$L1_0$			
2009	Sbi_09	A*STAR				**μ**		
	Lim_09	Korea Univ.	AlOx	(Co/Pd)	(Co/Pd)		12	
	Zhu_09	Qualcomm				**μ**		
	Nis_09b	Spintec	MgO	(Co/Pt)	(Co/Pt)	**S**		
	Miz_09	Tohoku	MgO	(CoFe/Pd)/CoFeB	(CoFe/Pd)/CoFeB		67	
	Par_09	Tohoku	MgO	(CoFe/Pd)/CoFeB	(CoFe/Pd)/CoFeB		3	
	Wat_09	Tohoku	MgO	CoCrPt/CoFe	CoCrPt/CoFe		6	$2\ 10^8$
2010	Yak_10a	AIST	MgO	RE-TM/CoFeB	(Pt/Co)/CoFeB		85	4.4
	Yak_10b	AIST	MgO	RE-TM/CoFeB	(Pt/Co)/CoFeB		62	4
	Wan_10	Beijing	AlOx	(Co/Pt)	(Co/Pt)		15	$3\ 10^4$
	Wor_10	IBM	MgO	?	?		100	10
	Tad_10	MINT	MgO	(Co/Pd)/CoFeB	(Co/Pd)/CoFeB		10	
	Hei_10	Seagate				**μ**		
	Zha_10	Shanghai				**μ**		
	Ye_10	SPIN, Taiwan	MgO	RE-TM	RE-TM	**S**		
	Lee_10	SPIN, Taiwan	MgO	RE-TM/CoFeB	RE-TM/CoFeB		5	
	Ban_10	Spintec	AlOx	(Co/Pt)	(Co/Pt)		6	21
	Nis-10a	Spintec	MgO	(Co/Pt)	(Co/Pt)	**S**		
	Nis-10b	Spintec	MgO	(Co/Pt)	(Co/Pt)	**S**		
	Miz_10	Tohoku	MgO	(CoFe/Pd)/CoFeB	(CoFe/Pd)/CoFeB		91	
	Hir_10	Tohoku	MgO	$L1_0$	$L1_0$	**S**		
	Ike_10	**Tohoku**	**MgO**	**Ta/CoFeB**	**Ta/CoFeB**		**120**	**18**
	Yod_10	Toshiba	MgO	Fe alloy?	Fe alloy?		22	18
	Li_10	Yanshan Univ.	MgO	(Co/Pt)	(Co/Pt)	**S**		
2011	Wan_11	Beijing		Ta/CoFeB	Ta/CoFeB			$2\ 10^6$
	Wor_11	IBM	MgO	(Co/Pd)/CoFeB	Ta/CoFeB		46	12
	Zhu-11	Shanghai				**μ**		
	Nis_11	Spintec	MgO	RE-TM/CoFeB	Ta/CoFeB		80	18
	Miz_11a	Tohoku	MgO	(Pd/Co)/CoFeB	(Pd/Co)/CoFeB		120	$2\ 10^4$
	Miz_11b	Tohoku	MgO	(Pd/Co)/CoFeB	(Pd/Co)/CoFeB		100	

Table II-1: Publications on perpendicular magnetic tunnel junctions since 2002. RE-TM stands for Rare Earth-Transition Metal alloys, $L1_0$ for ordered alloys, (Co/Pt(Pd)) for multilayers, ? for unknown structures, S for structural studies and μ for micro-magnetic calculations. Lines in red emphasize the main breakthroughs.

II-1.3 Capres: a tool for macroscopic tunnel magnetoresistance measurements

Electrical measurements are necessary in the case of MTJ in order to determine their transport properties as a function of the magnetic configuration of the electrodes, giving the tunnel magnetoresistance TMR and resistance-area product RA, which are important parameters for MRAM applications. Standard measurement techniques, also called current perpendicular to the plane (CPP) (**Figure II-9a**), require submicron pillars fabrication with all necessary connections wires in order to pass a current perpendicular to the plane of the sample and measure the resistance between the top and bottom electrodes. But the pillars and connection fabrication require a long process with different steps as lithography, etching, metal and dielectric deposition. A disadvantage of this technique is the time and effort required to fabricate pillars and defects possibly induced during this process, leading sometimes to TMR values much smaller than the real one.

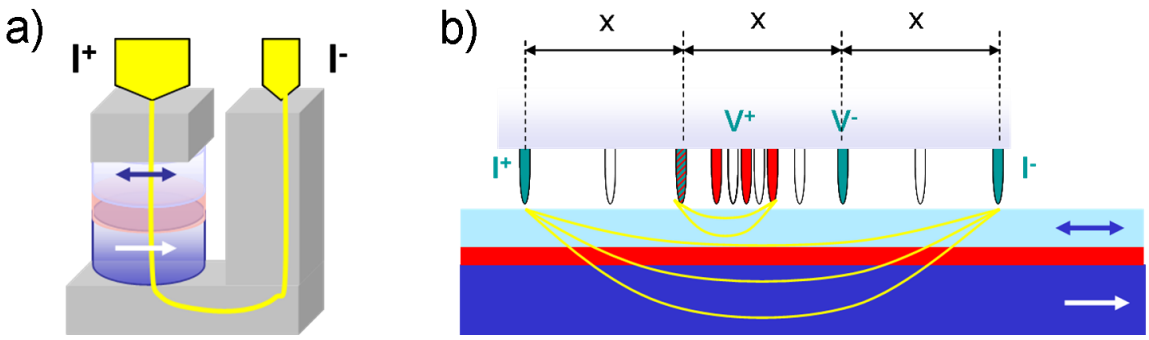

Figure II-9: Schematic representation of the two geometries of transport measurements: (a) Current perpendicular to the plane and (b) Current in plane geometry.

An alternative way to measure magnetoresistive properties is the Current In Plane tunneling (CIP) technique developed by Worledge et al. [Wor_03]. This method uses 4-point resistance measurements on the surface of an unpatterned sample, for various probe spacings. The current is injected between the two external contacts and the voltage is measured using the interior contacts, thus eliminating contact resistances (**Figure II-9b**). A multi four-point probe is used with different distances x between contacts in order to pass the current in the whole sample thickness. For low x distances the current passes mainly in the top electrode whereas for large distances the current also circulates in the bottom electrode through the barrier. Making several voltage measurements with increasing spacing between the probe points in the parallel and antiparallel configuration of the magnetizations (**Figure II-9b**), two curves of resistance vs probe distance (Rsq_{high} and Rsq_{low}) are obtained as shown in **Figure II-10a**, giving the resistance of the top electrode (R_T) for zero spacing, and the combination of top and bottom (R_B) resistances in parallel $R_T R_B/(R_T+R_B)$) for large spacing. The MR-CIP ratio is calculated as (Rsq_{high} - Rsq_{low})/ Rsq_{low} (**Figure II-9b**).

The TMR and RA values, as well as the R_T and R_B resistances of the sample, are obtained by fitting the MR-CIP data to a model considering a network of parallel and series resistances [Wor_03].

The best fitting conditions are obtained when the distance between probe points spans a range between λ and 5λ (**Figure II-10b**), where λ is a parameter related to the RA, R_T and R_B values by the following formula: $\lambda = \sqrt{\frac{RA}{R_T + R_B}}$

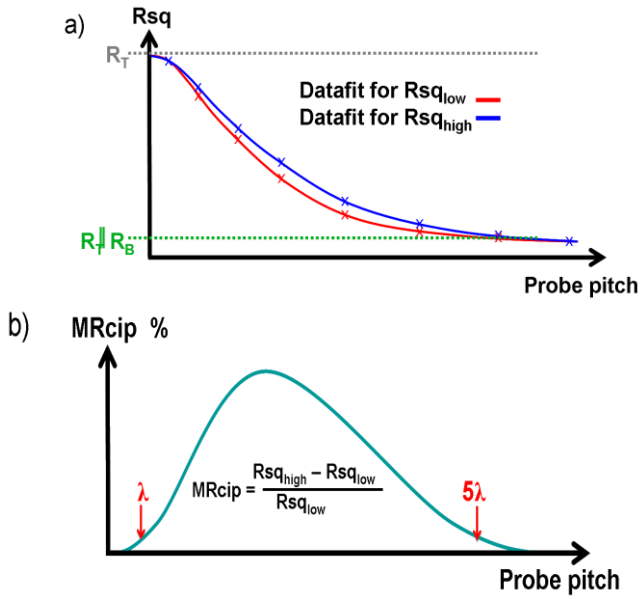

Figure II-10: (a) Resistance as a function of probe pitch in the parallel and antiparallel configurations; (b) Corresponding MR-CIP curve.

The R_T/R_B ratio must also be adjusted, since it can affect the measurements accuracy as shown in **Figure II-11**. R_T must be larger than R_B in order to force the current to penetrate into the sample and reach the bottom electrode through the barrier. A ratio of 5 is enough to have a good accuracy on the measurements.

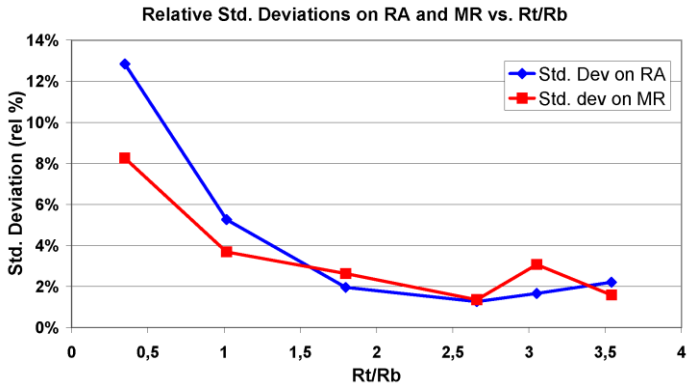

Figure II-11: Relative standard deviation on RA and TMR as a function of the R_T/R_B ratio [Cap].

If the RA product is approximately known, both the above equation and constraint on R_T/R_B allow to evaluate the R_T and R_B values needed to span at best the λ-5λ range, and both buffer and capping layers of the junction (resistivity and thickness) will be adjusted accordingly. For the measurement one will use the most appropriate set of probes available.

If the RA product is unknown, one will have to first choose an arbitrary R_B value, adjust R_T to $R_T/R_B=5$, and then make successive measurements with different probes. The shape of the corresponding successive MR-CIP curves will allow progressively optimizing electrode resistances and probe distance in order to obtain the maximum shown in **Figure II-9b**. This can imply the deposition of several samples. Moreover, such a trial and error procedure can give no result at all if, for any reason, the real magnetoresistance of the sample is zero. In that case, only the RA product of the barrier will be extracted.

The surface state of the sample is also crucial. Mechanical defects (scratches) can render the measurement impossible. Ruthenium is the best capping layer, since its surface is covered by a conductive and mechanically hard ruthenium oxide (probe should only contact the top surface, and not penetrate into the sample down to the barrier). Chemical surface contamination can also be a problem and, since all these structures must be annealed at high temperature before measurement, a bad vacuum during annealing can lead to such a contamination. A supplementary surface etching/Ru deposition can be necessary before CIP measurements.

Once all this problems are more or less solved, CIP measurement is generally performed in two steps. One first records an R(H) curve for an arbitrary distance between probes, which allows to choose the appropriate field interval (for in-plane measurements, the maximum field available is about 300 Oe). This also gives information on the magnetic properties of the sample (transition fields of both layers, coupling between layers). Then MR-CIP measurements are performed using two applied fields corresponding to the parallel and anti-parallel states of the magnetizations.

In the case of structures with perpendicular anisotropy, things are even more complicated. Due to the presence of a soft magnetic-flux closure element underneath the sample, the magnetic field (with a maximum value of 1.5 kOe) cannot be varied during MR-CIP measurements, since it would induce unwanted and dramatic mechanical deformations of the probes. R(H) curves cannot thus be performed, and the magnetic state of the system must be known in advance (VSM or Hall effect) in order to choose the two field values corresponding to the parallel and anti-parallel states. This puts a supplementary constraint since MR-CIP cannot be performed on small samples (positioning problems), while VSM or Hall measurements cannot be performed on large samples (not mentioning that Hall measurements are almost impossible when thick buffer and capping layers, imposed by the R_T and R_B values, are present).

II-2. Anisotropy properties of top and bottom electrodes in full stacking

The following study of magnetic and anisotropy properties, is mainly conducted on magnetic electrodes made of a single cobalt layer. The great advantage of using single magnetic layers for both bottom and top electrodes is that one doesn't have to suspect any deviation of the Co moments from the perpendicular direction, direct coupling between Co atoms being much stronger than for example indirect coupling through Pt in Co/Pt multilayers.

II-2.1 Increased anisotropy of the top electrode

Figure II-12 shows the Hall response of bottom, top and full Ta3/Pt20/Co1.2/MgO1.2/Co1.4/Pt3 MTJ structures after annealing at 350°C. In the full structure (**Figure II-12c**), the ratio of the amplitudes of the two transitions is slightly different from the expected one. This is due to different Hall coefficients of the layers, since magnetization measurements give the expected ratio between the two transitions.

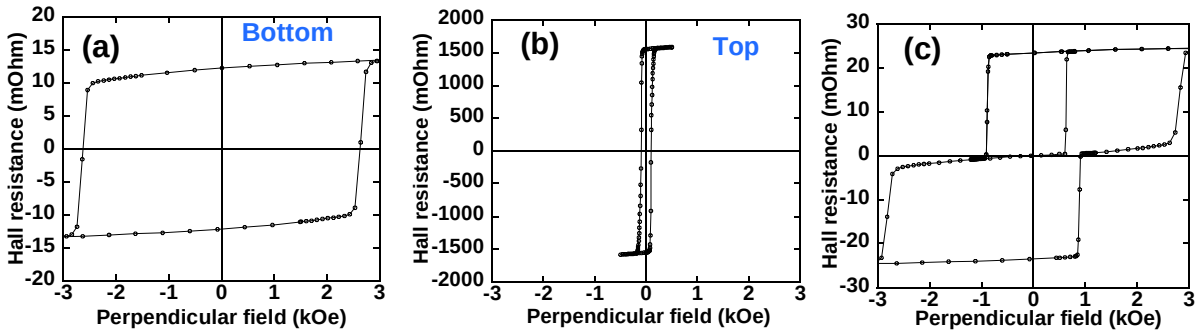

Figure II-12: (a) Bottom Ta3/Pt20/Co1.2/MgO1.2 electrode, (b) Top MgO1.2/Co1.4/Pt3 electrodes and (c) Ta3/Pt20/Co1.2/MgO1.2/Co1.4/Pt3 full junction after annealing at 350°C. The MgO barrier is obtained by natural oxidation for 600" under 160mbar.

The coercive field of the hard bottom electrode is mainly identical in both **Figure II-12a** and **c.** On the contrary, the most spectacular observation is that the coercive field of the top electrode sharply increases from 100 Oe to 750 Oe when it is deposited onto the bottom one, compared to the case where this top electrode is deposited on SiO_2. Such an effect has been observed in all structures examined, independently of the barrier considered (AlOx or MgO) and for all MgO barriers prepared under different conditions (natural Mg oxidation or RF deposition from an MgO target). By preparing specific samples, we will try now to understand this effect, which could be either of magnetic or structural origin.

Another example of such effects is shown in **Figure II-13** through in-plane measurements of a top MgO1.4/Co1.5/Pt3 alone (**a**) or deposited on top of a Ta3/Pt20/Co buffer (**b** and **c**) after annealing at 350°C. The MgO barrier is now obtained by two successive deposition/oxidation of a Mg 0.7nm thick layer. The large influence of the bottom electrode (**Figure II-12c**) can now be observed through the anisotropy field of the top electrode, which increases from about 1 kOe for the top electrode alone to more than 12 kOe when it is deposited on the bottom electrode.

Curves (**b**) and (**c**) in **Figure II-13** show the results obtained when decreasing the bottom Co layer thickness from 1.2 to only 0.3 nm. By doing that, one try to keep the same growth conditions for all layers (especially the growth of the first Mg layer on top of a Co one)

and to minimize any magnetic influence of the bottom electrode. Curve (**c**) gives practically the same value of the anisotropy field, again very much larger than for the top electrode alone.

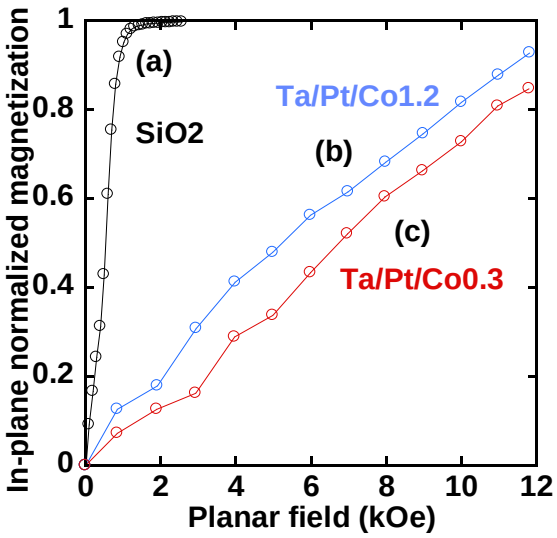

Figure II-13: Variation of the in-plane component of the magnetization in (a) SiO_2/MgO1.4/Co1.5/Pt3 and Ta3/Pt20/Co/MgO1.4/Co1.5/Pt3 structures with a bottom Co thickness of (b) 1.2 or (c) 0.3 nm after annealing at 350°C. All three structures have perpendicular magnetization, and curves are measured as a function of the in-plane applied field.

Figure II-14a shows the hysteresis loop of a bottom MgO1.4/Co2/Pt3 electrode, directly deposited on SiO_2, after annealing at 350°C. The field is applied perpendicular to the plane. Compared to **Figure II-13a**, increasing the Co thickness from 1.5 to 2.0 nm (that is above the critical thickness, **Chapter I**) decreases the anisotropy field, and now the magnetization is in-plane. The anisotropy field is about -2 kOe (with usual sign conventions).

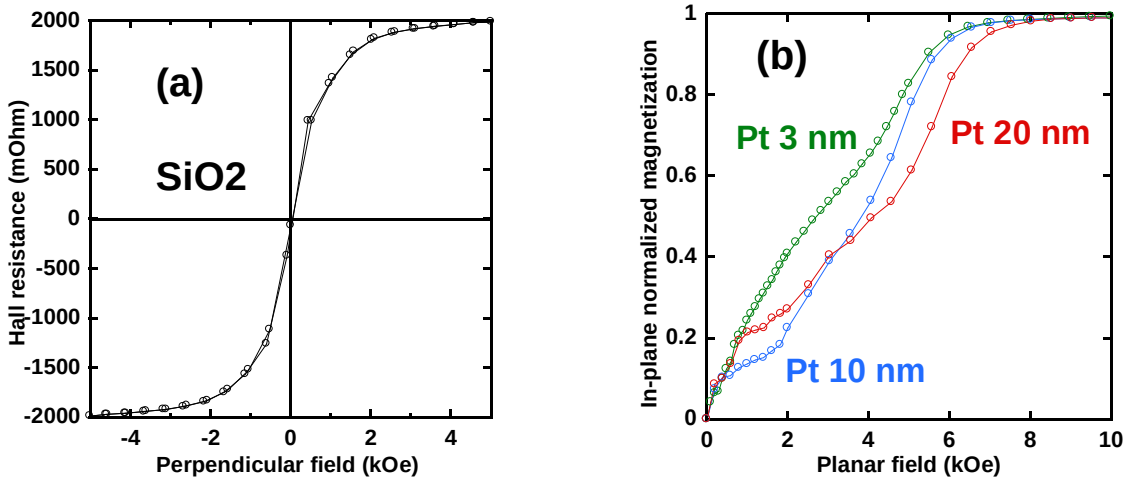

Figure II-14: Hysteresis loop of (a) A bottom SiO_2/MgO1.4/Co2/Pt3 electrode as a function of perpendicular field and of (b) A full Ta3/Pt/Co0.3/MgO1.4/Co2/Pt3 structure with varying Pt thickness as a function of planar field after annealing at 350°C.

The full structures (**Figure II-14b**) are Ta3/Pt/Co0.3/MgO1.4/Co2/Pt3 stackings annealed at 350°C. The Pt buffer layer thickness is 3, 10 or 20 nm. The idea here is to test

possible influence of Pt on the anisotropy of the top electrode, since it is known that anisotropy increases with Pt thickness (see for example **Figure II-20**). **Figure II-14b** shows that magnetization of the top electrode is now perpendicular-to-plane, and that the Pt thickness has a very limited influence on its anisotropy field, which amounts to about 6 kOe. It is also the case for the coercive field, which is constant at 0.5 kOe.

The next test is conducted on Ta3/Pt20/Cu1/Co1.2/MgO1.4/Co1.5/Pt3 structures. Inserting a Cu layer between the Pt and Co ones is another way to study the possible influence of the Pt layer, because of the interfacial nature of anisotropy. Although the anisotropy of the bottom Co1.2 nm layer greatly decreases because of the Cu insertion, no effect can be observed on the anisotropy of the top layer, which is still much larger than that of the top electrode alone.

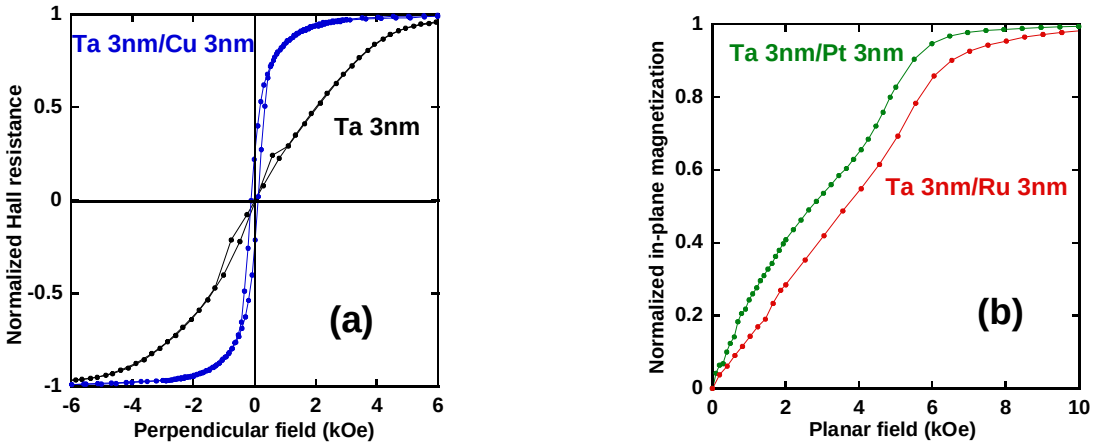

Figure II-15: Anisotropy properties of Buffer/Co0.3/MgO1.4/Co2/Pt3 structures annealed at 350°C. Buffer stands for (a) Ta3, Ta3/Cu3 and (b) Ta3/Pt3, Ta3/Ru3.

Finally, we study the influence of the nature of the buffer layer, in Buffer/Co0.3/MgO1.4/Co2/Pt3 stackings annealed at 350°C (**Figure II-15**). Buffer stands for either Ta3, Ta3/Cu3, Ta3/Pt3 or Ta3/Ru3. Structures grown on a Ta3 buffer have in-plane anisotropy, with an anisotropy field of about -5 kOe. Those grown on a Ta3/Cu3 buffer are perpendicular, but with a multi-domain state in zero applied field (**Figure II-15a**). On the contrary, those grown on a Ta3/Pt3 or Ta3/Ru3 buffer have a much stronger perpendicular anisotropy (**Figure II-15b)**, with anisotropy fields of about 6 kOe for Pt and 7 kOe for Ru. This very large influence of the underlying layers on the anisotropy properties of the top electrode means that the key parameter is the quality of growth of the Mg layer. A better growth is obtained on SiO_2 compared to Ta for instance, but much better anisotropy properties are obtained when Mg grows on Pt or Ru buffers.

II-2.2 Anisotropy properties of the top electrode in full stacking

As we said in **Chapter I**, the perpendicular anisotropy is very large for bottom Co 1.2 nm thick electrodes, especially when annealing temperature is above 300°C. One must recall that our Hall setup is limited to 17 kOe. The determination of anisotropy fields is even more difficult since, when both electrodes are perpendicular, in-plane magnetic measurements are the sum of both contributions, which makes the transformation from M_Z to M_X impossible. **Figure II-16b** gives an example of such an in-plane measurement for a Co1.2/MgO/Co1.2 structure after annealing at 275°C. From in-plane measurements (right figure), the anisotropy field of the top soft layer can be reasonably estimated, but it is not the case for the bottom hard one.

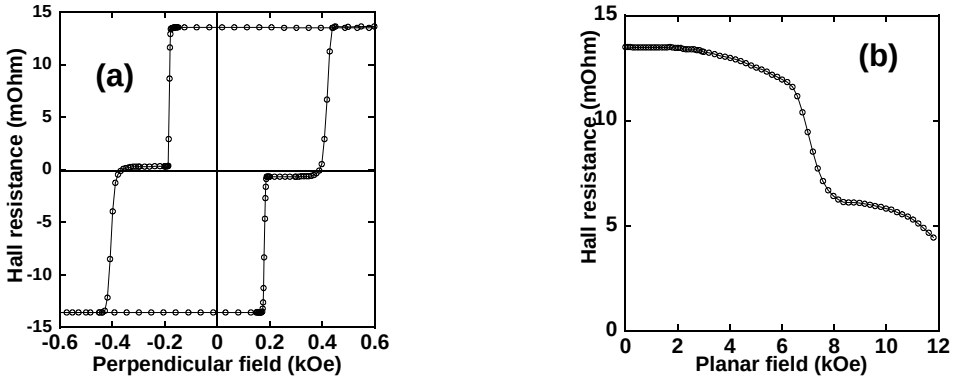

Figure II-16: Hall resistance as a function of (a) Perpendicular and (b) Planar field in a Ta3/Pt20/Co1.2/MgO1.4/Co1.2/Pt3 structure after annealing at 275°C.

We will now examine in more details the evolution of the PMA properties of the top electrodes deposited onto bottom ones, namely in Ta3/Pt20/Co1.2/MgO1.4/Cox/Pt3 structures. These properties will be compared to those of the bottom ones presented in **Chapter I**.

Figure II-17 shows the Hall hysteresis loops of these structures for different top Co thicknesses in the as-deposited state. As we mentioned in the previous section, the anisotropy of the top electrode is much larger than that of the top MgO/Co/Pt3 electrodes alone studied in **Chapter I**. As an example, the top MgO/Co0.6/Pt3 electrode gives a perfectly square hysteresis loop, whereas a superparamagnetic behaviour is observed for the same structure directly grown on SiO_2. The critical top Co thickness is slightly larger than 1.1 nm in the as-deposited state.

The evolution with annealing for similar structures with a 1.6 nm thick Co top layer is showed in **Figure II-18**. For such a Co thickness, the top electrode is perpendicular after annealing at 275°C. The increase of the anisotropy with annealing is faster for the bottom electrode. Although the total Hall amplitude progressively increases with annealing, as usually observed in such structures, the ratio of the amplitudes of both transitions does not depend so much on annealing.

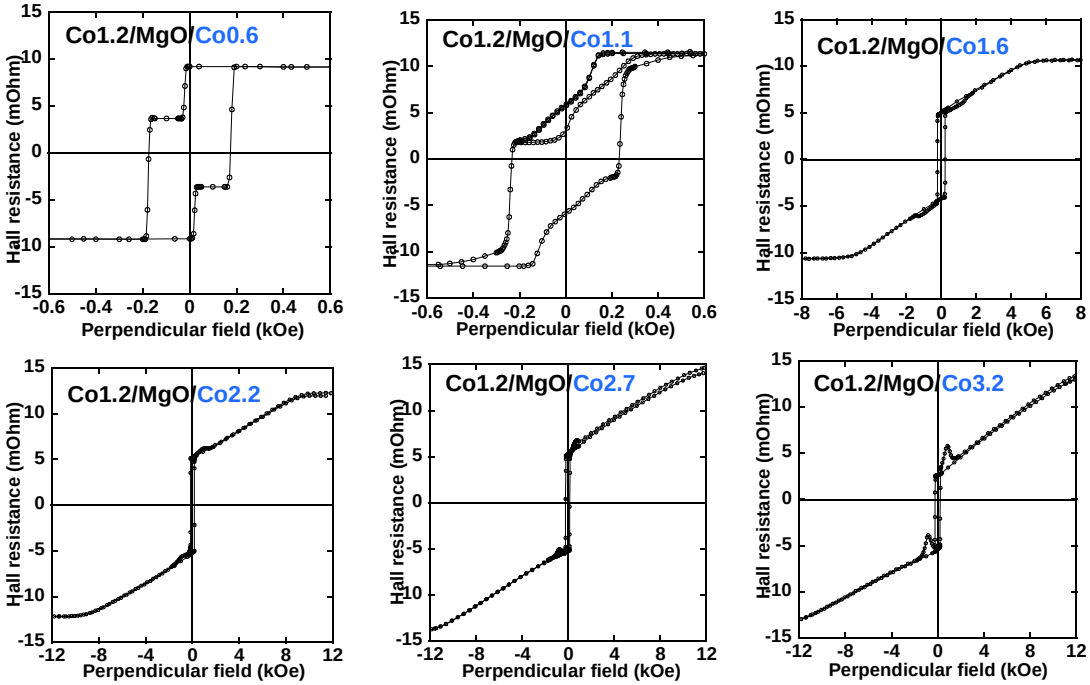

Figure II-17: Hall resistance as a function of applied magnetic field in Ta3/Pt20/Co1.2/ MgO1.4/Cox/Pt3 structures in the as-deposited state.

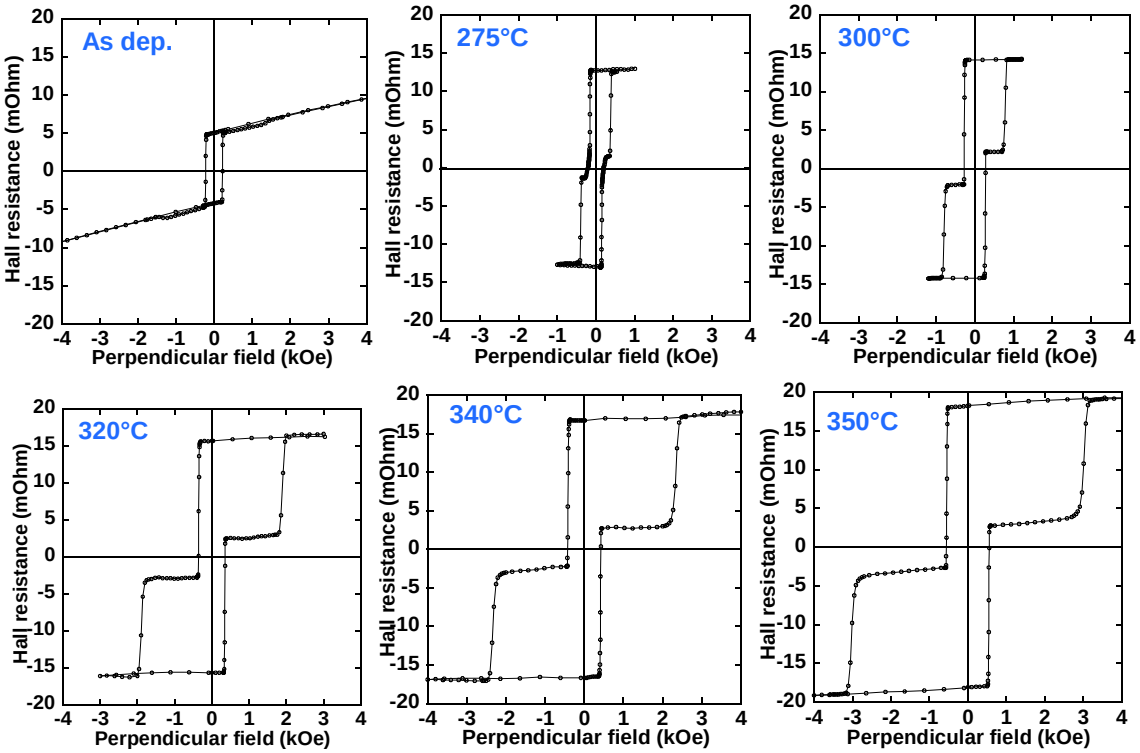

Figure II-18: Evolution with annealing of a Ta3/Pt20/Co1.2/MgO1.4/Co1.6/Pt3 structures.

Finally the variation of the anisotropy field in structures presented below as a function of top Co thickness for different annealing temperatures is summarized in **Figure II-19a.** One observes the 1/t behaviour of the anisotropy field, characteristic of the interfacial contribution to the anisotropy. **Figure II-19b** shows the anisotropy variations for the same data plotted as $K_{Eff}*t_{Co}$ as a function of t_{Co}. One can see that the critical thickness sharply increases with annealing (more than 3.2 nm after 350°C annealing), mainly because of a decrease of the volume contribution $K_V - 2\pi Ms^2$ (change of the slope of the curves).

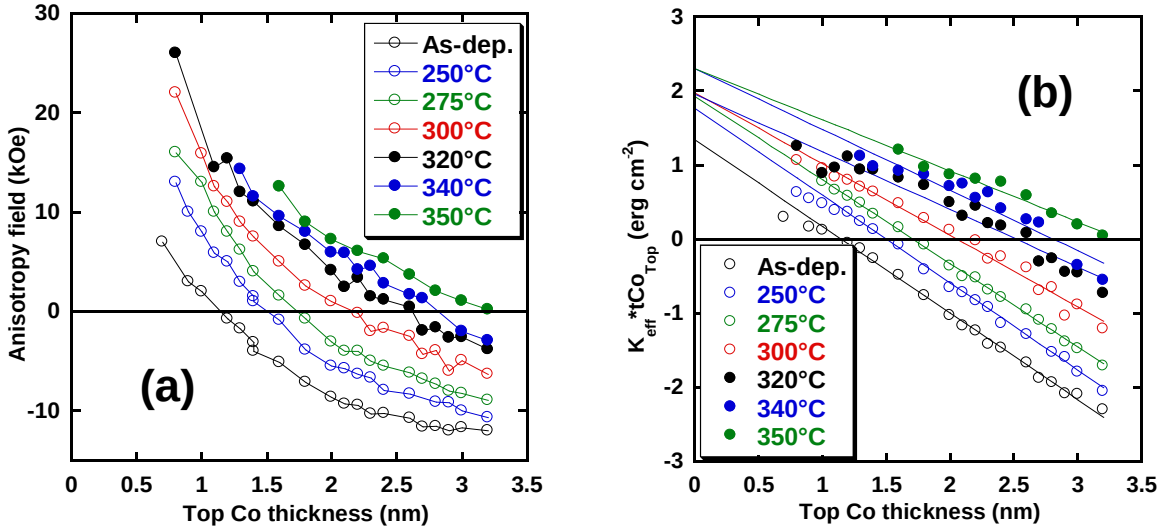

Figure II-19: (a) Anisotropy field and (b) Effective anisotropy times Co thickness in Ta3/Pt20/Co1.2/MgO1.4/Cox/Pt3 structures for different annealing temperatures.

II-2.3 Perpendicular anisotropy of the bottom electrode

Different bottom electrodes were studied in order to find the best compromise between high PMA and TMR values. Pt/Co/MgO structures bring high anisotropy but there is a mismatch between the Co (hcp or fcc) and the MgO bcc structure that reduces the TMR. A solution could be to insert a thin CoFeB layer between the Co and MgO layers keeping a large PMA at the same time. However pMTJ structures having Pt/Co/MgO electrodes are the simplest ones and more adapted for a fundamental study of the anisotropy properties as a function of the oxygen content at the interface Co/MgO and with annealing temperatures.

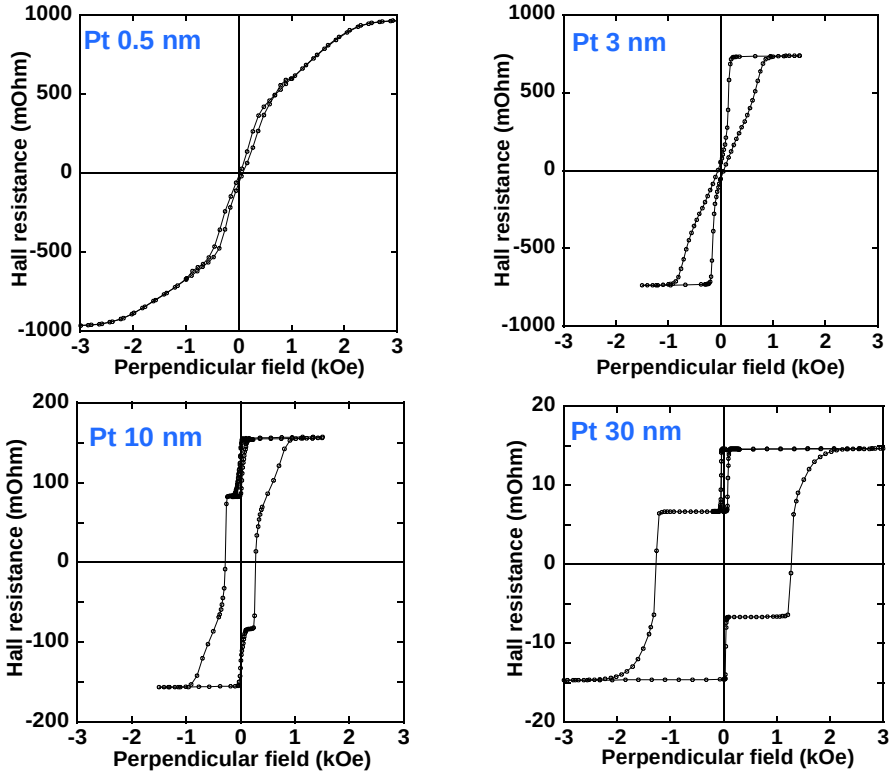

Figure II-20: Hysteresis loops of Ta3/Pt/(Co0.5Pt0.4)*5/Co0.5/CoFeB0.5/MgO2.0RF/CoFeB0.5/ Co0.5/Pt3 structures for different Pt buffer thicknesses after annealing at 325°C.

Figure II-20 shows the evolution with Pt buffer thickness of the hysteresis loops of Ta3/Pt/(Co0.5Pt0.4)*5/Co0.5/CoFeB0.5/MgO2.0/CoFeB0.5/Co0.5/Pt3 structures after annealing at 325°C. The MgO barrier was obtained by RF sputtering of a MgO target, and the bottom (Co/Pt) multilayer is intended to increase the perpendicular anisotropy of the bottom electrode, since CoFeB brings less interfacial anisotropy than pure Co, probably because of boron diffusion towards the MgO or Pt interface upon crystallization. As already noted in **Chapter I** the perpendicular anisotropy of the bottom electrode increases with increasing Pt buffer thickness. One must note that the anisotropy of the top electrode also increases with buffer thickness, as can be deduced from the evolution of its hysteresis loop for 10 and 30 nm thick Pt buffers.

The influence of the thickness of the bottom Co electrode on the anisotropy properties of full structures: Ta3/Pt20/Cox/MgO1.4/Co2/Pt3 annealed at 350°C is presented in **Figure II-21**. The coercive field of the bottom hard electrode progressively decreases as the Co thickness increases, and for a Co thickness of 2.0 nm only one transition is observed. The evolution of perpendicular anisotropy is similar to the one presented in **Chapter I** for single bottom electrodes, except that the critical Co thickness is found here between 2.5 and 2.8 nm instead of

3.4 nm. For a bottom Co thickness equal or larger to 2.0 nm, both layers switch simultaneously, and the bottom electrode magnetization falls in-plane at a thickness of 2.8 nm.

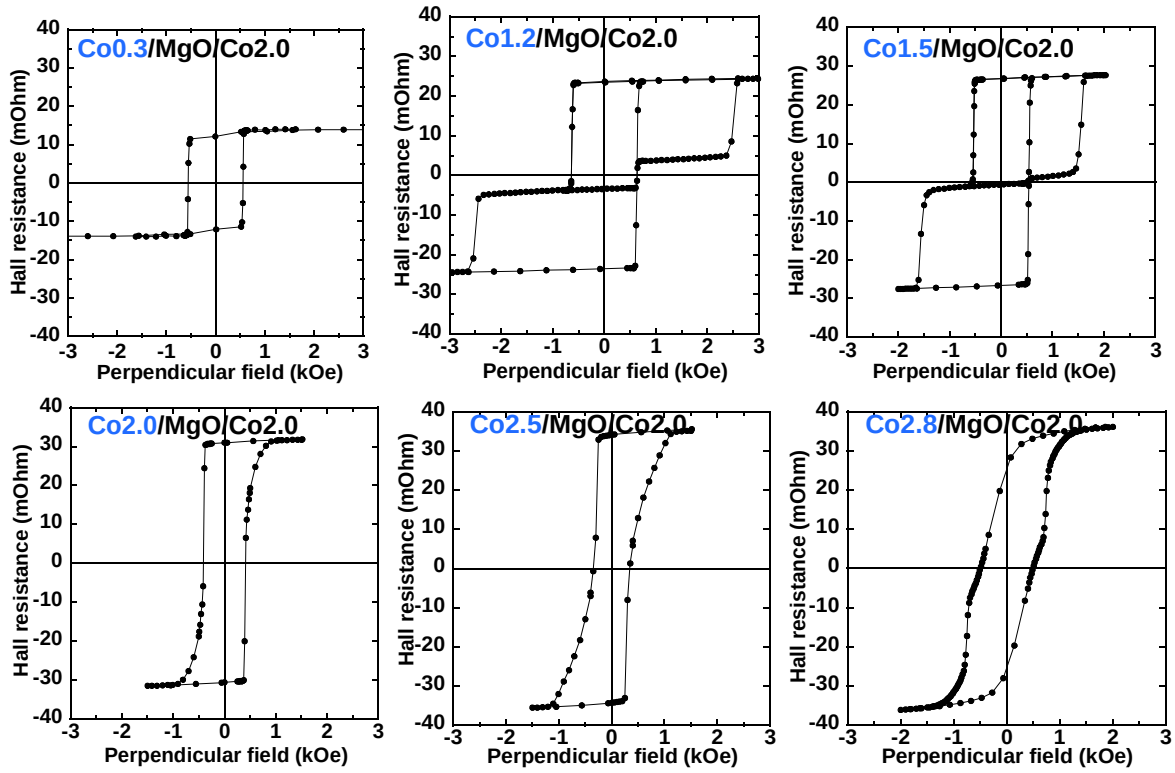

Figure II-21: Hall resistance as a function of applied magnetic field in Ta3/Pt20/Cox/MgO1.4/Co2 /Pt3 structures after annealing at 350°C.

II-2.4 Comparison between top and bottom electrodes

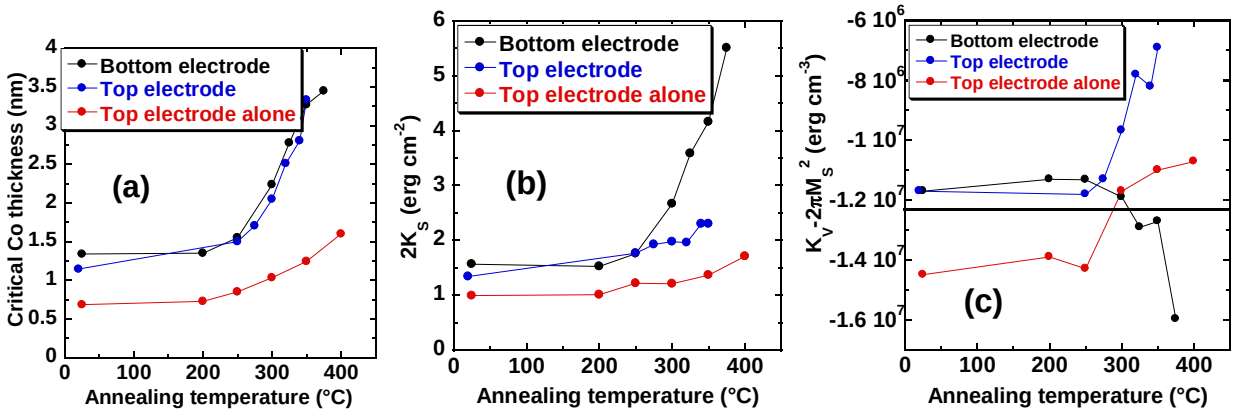

Figure II-22: Comparison between bottom (black) and top (blue) electrodes in full stacking: Ta3/Pt20/Co12/Mg14oxnat/Cox/Pt3, and top (red) electrode alone: thermal evolution of (a) The critical Co thickness, (b) The interface anisotropy energy and (c) The volume anisotropy energy. The horizontal line in (c) corresponds to $2\pi M_S^2$, assuming a magnetization of the Co layer of 1400 emu cm^{-3}.

Lets now compare the anisotropy properties of the top electrodes in full stackings to those of top and bottom ones as studied in **Chapter I**, as summarized in **Figure II-22**.

The first observation is that both bottom and top electrodes in full stackings exhibit a similar evolution of the critical thickness: from about 1.2 nm in the virgin state, the critical

thickness starts increasing after 250°C annealing, and reaches in both cases more than 3 nm after 350°C annealing. However, the thermal evolution of this critical thickness, calculated as $t_{cr}= -2K_S/(K_V-2\pi M_S^2)$, has a completely different origin for both electrodes. In bottom ones, it arises from a large increase of the average interface contribution, without so much variation of the volume one. It is the reverse in top electrodes, where the increase of critical thickness results from a modest increase in K_S but in a large increase of K_V. One can note that the top electrode alone (**Chapter I**) gives the same variation of K_S and K_V as the top electrode in full stackings, but with smaller K_S and K_V values, resulting in a much smaller critical thickness.

II-2.5 Mutual interaction between electrodes

The influence of the top Co electrode thickness on the magnetic properties of Ta3/Pt20/Co1.2/MgO1.4/Cox/Pt3 structures annealed at 350°C is showed in **Figure II-23**. The evolution of the perpendicular anisotropy is essentially similar to that observed in **Figure II-17** in the virgin state. The top Co electrode 3.2 nm thick is still perpendicular (although in a multi-domain state) after annealing at 350°C.

The striking observation on **Figure II-23** is that the coercive field of the bottom electrode strongly decreases (from 5.0 to 1.5 kOe) as the thickness of the top electrode increases. We studied such effects in more details for different annealing temperatures, as reported in **Figure II-24**.

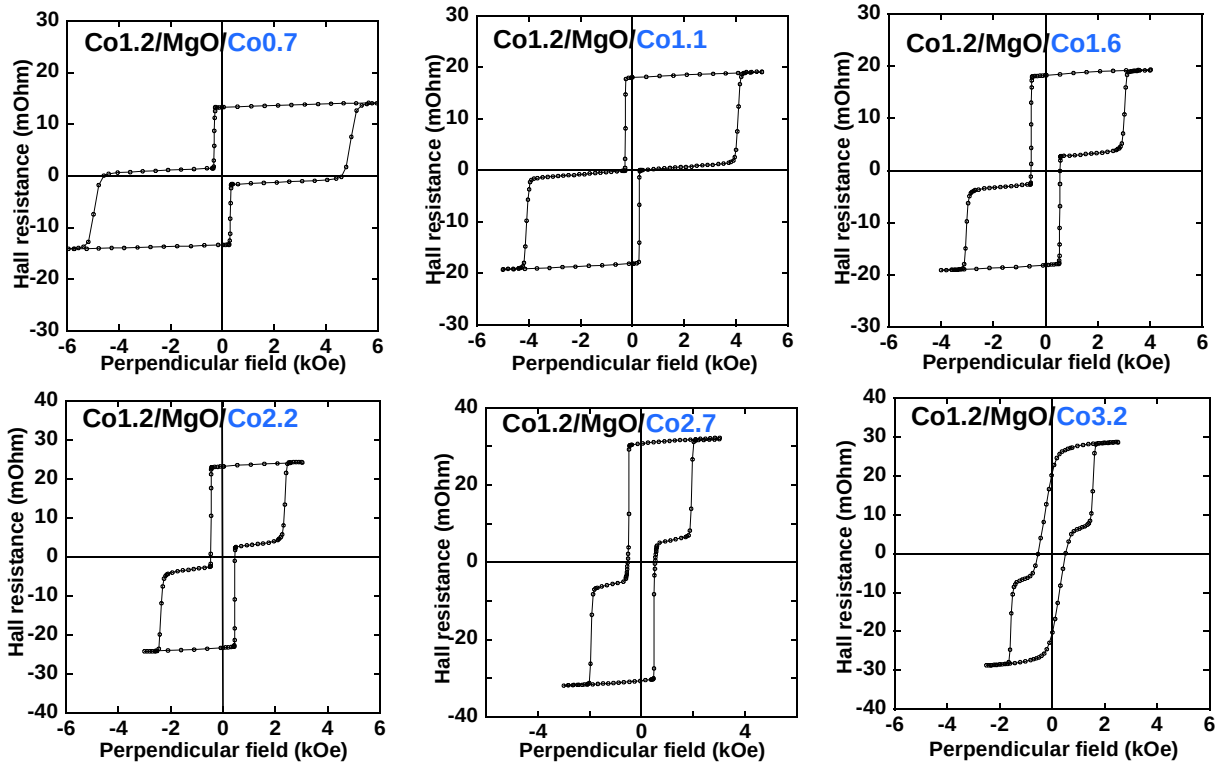

Figure II-23: Hall resistance as a function of applied magnetic field in Ta3/Pt20/Co1.2/MgO1.4/Cox/Pt3 structures after annealing at 350°C.

Figure II-24 gives the variation of the coercive field of the bottom electrode as a function of the thickness of the top one. For annealing temperatures smaller than 300°C, the bottom coercive field slightly increases with annealing, but is essentially independent of the top Co thickness. This is no more the case for higher annealing temperature, since one observes a very

sharp decrease of the coercive field of the bottom electrode when increasing top Co thickness. Unfortunately, it is not possible to tell whether the variation of the anisotropy field follows the same trend. This anisotropy field does not depend so much on the top Co thickness below 300°C annealing (as is the case for the coercive field), but increases so strongly for larger annealing temperatures (see **Chapter I**) that it becomes rapidly non-measurable with our Hall set-up (maximum field of 17 kOe).

This monotonous decrease of the coercive field can be taken into account with a simple phenomenological model assuming that some interaction field originating from the top layer artificially speeds up the transition of the bottom layer. Such a field should mainly depend on both top Co thickness (magnetization) and distance between electrodes (assuming charges concentrated at the middle of the layers). This distance is 0.6 nm (half the bottom Co thickness) plus 1.4 nm (barrier thickness) plus $t_{Co}/2$ (half of the top Co electrode thickness), that is 2.0 + $t_{Co}/2$. One thus is left with a qualitative relation:

$$Hc = c \cdot t_{Co} \cdot \exp\left(-\frac{t_{Co}+4}{2 \cdot \lambda}\right) \qquad \textbf{Equation II-1}$$

where λ is a characteristic decay length and c a constant. This dependence is represented as full lines on **Figure II-24** along with the experimental data points for annealing temperatures larger than 300°C.

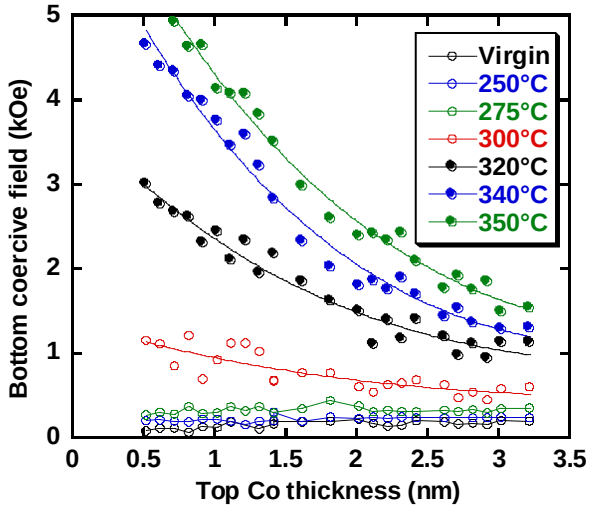

Figure II-24: Variation of the bottom coercive field as a function of the top Co thickness in Ta3/Pt20/Co1.2/MgO1.4/Co/Pt3 structures for different annealing temperatures. Curves for annealing temperatures larger or equal to 300°C are fitted to Equation II-1.

Interestingly, some universal behaviour can be obtained for high annealing temperature when coercive fields are normalized to their extrapolated value for zero Co top thickness. **Figure II-25** shows the variation of such reduced coercive field for 320, 340 and 350°C annealing, along with the corresponding fit. The common decay length λ is found to be 2.1 nm.

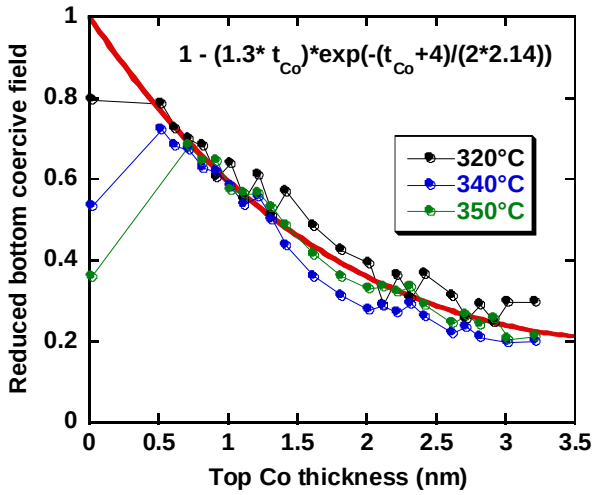

Figure II-25: Reduced bottom coercive field as a function of top Co thickness for 320, 340 and 350°C annealing. Curves can be superimposed with a common decay length of 2.1 nm.

However, things are not so clear, since **Figure II-25** also shows that the coercive field of bottom electrodes alone (ie t_{Cosup}= 0) is much smaller than its extrapolated value. This shows again that the evolution of the magnetic properties of such junctions critically depends on the detailed stacking of the layers, in particular on the nature of the last layer above the MgO barrier(Co for full stackings compared to Cu for bottom electrodes alone). Another peculiar result is that the coercive field of the top layer is also affected, and goes through a maximum around 2.0 nm for high annealing temperatures (**Figure II-26**).

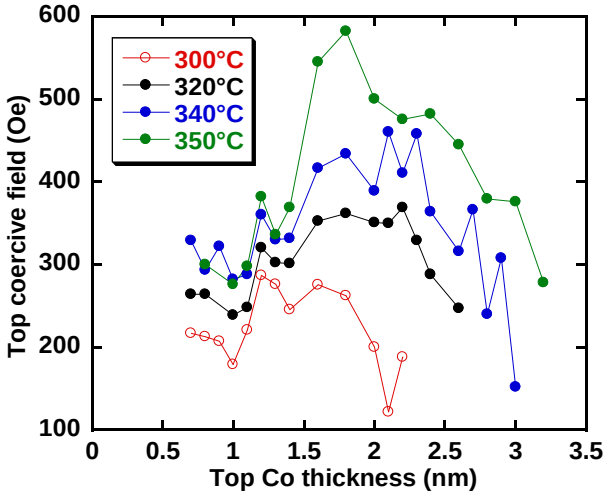

Figure II-26: Variation with annealing of the coercive field of the top Co electrode as a function of its thickness in Ta3/Pt20/Co1.2/MgO1.4/Co/Pt3 structures.

II-3. Influence of the oxidation conditions of the barrier

Very low oxygen pressures cannot be reached in our Actemium sputtering machine, such as those required now in order to prepare very thin tunnel junctions (0.8 nm) with high TMR ratio and RA values below 10 Ωμm^2. The oxidation chamber of our machine works in a static mode, the minimum attainable pressure being of the order of 100 mbar. Studies showed us that oxygen pressures between 200 and 900 mbar and oxidation times of 200 to 1200s do not change so much the PMA properties of our pMTJ, although oxidation is more aggressive than in the case of much lower pressures. According to this, influence of oxygen pressure cannot be studied in the low pressure range. A very good way to obtain a homogenous MgO barrier is the double deposition and oxidation of a thin Mg layer of 0.7 nm thick. This results in a better distribution of the oxygen content at both interfaces of the barrier.

As presented in **Chapter I**, perpendicular anisotropy in structures studied in this thesis has an important contribution from the oxide/magnetic metal interface and greatly depends on parameters like magnetic thickness and annealing temperature. This is why it is important to check the evolution of anisotropy with the oxidation conditions of the barrier (the oxygen content at the interface) in perpendicular MTJ. Systematic studies are complicated by the fact that PMA strongly varies with both magnetic thicknesses (1 kOe/0.1 nm for annealing temperatures around 300-350°C) and annealing temperatures (1 kOe/10°C).

It must also be noted that we observed quite a large evolution with time of the TMR properties of planar tunnel junctions prepared in this machine. At the beginning of our study, very low TMR ratio were obtained for planar MTJ, whereas now TMR ratio over 150% are constantly reached, and the reason for such an evolution is still unclear. On the other hand, anisotropy properties measured on samples prepared in our Plassys machine were found always much better than those obtained in the Actemium one, without any positive result concerning transport properties in the former case.

Results presented here cannot thus be taken as completely established. We will only try to show some trends about the effect of Mg thickness for constant oxidation conditions, the difference between single and double oxidation, and between RF-deposited MgO barriers in both sputtering machines.

II-3.1 Variation of the anisotropy as a function of Mg layer thickness

The oxygen content can be easily modified by varying the Mg layer thickness for constant oxidation conditions. PMA will also be affected and a systematic study is presented in the next paragraph considering the simple case of single Mg layer oxidation.

Figure II-27 shows the evolution of Ta3/Pt30/Co2/MgOx/CoFeB1.5/Co0.5/Pt3 structures after annealing at 350°C. The Mg thickness varies between 0.7 and 1.2 nm, for constant oxidation conditions (180" under 900mbar). For these oxidation conditions, small Mg thicknesses certainly lead to over-oxidation of the bottom hard magnetic electrode, which can explain both its reduced coercivity (and reduced perpendicular anisotropy, as inferred from in-plane measurements) and the slightly smaller total Hall amplitude. This results in an almost simultaneous magnetization reversal of both electrodes as can be seen for a 0.7-nm-thick MgO layer. Decreasing the applied field from positive saturation, the reversal of the soft top layer induces the nucleation of inverse “down” domains in the hardest layer. When increasing again the applied field (minor loop), these inverse domains slow down the back reversal of the soft layer towards its initially “up” configuration. The second transition on the minor loop at larger positive field, between 0.3 and 1.0 kOe, corresponds to the elimination of the above mentioned “down” domains created in the hard layer.

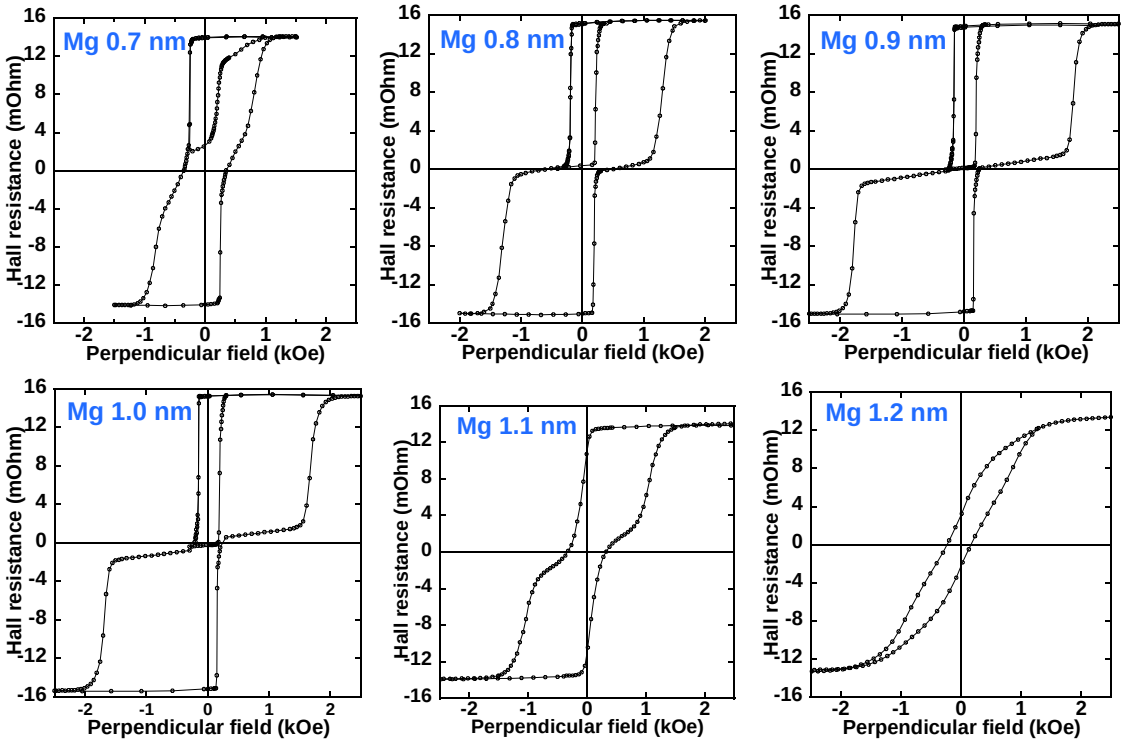

Figure II-27: Hysteresis loops of Ta3/Pt30/Co2/MgOx/CoFeB1.5/Co0.5/Pt3 structures for different Mg thicknesses after annealing at 350°C.

Two well separated magnetization reversals are obtained for Mg thicknesses between 0.8 and 1.0 nm, indicating that both magnetic layers have perpendicular anisotropy and that optimal oxidation conditions are reached in that Mg thickness range. Moreover the coercive field of the bottom hard layer goes through a maximum for Mg thickness of 0.9-1.0 nm.

More quantitative information about the anisotropy variation for the MTJ is presented in **Figure II-28a,** which shows the variation of Hall resistance as a function of in-plane magnetic field, starting from the positive remanence. The anisotropy field of the soft top layer is more or less constant for Mg layer thicknesses between 0.7 and 1.0 nm. That of the bottom layer goes through a maximum (**Figure II-28b**) between 0.9 and 1.0 nm.

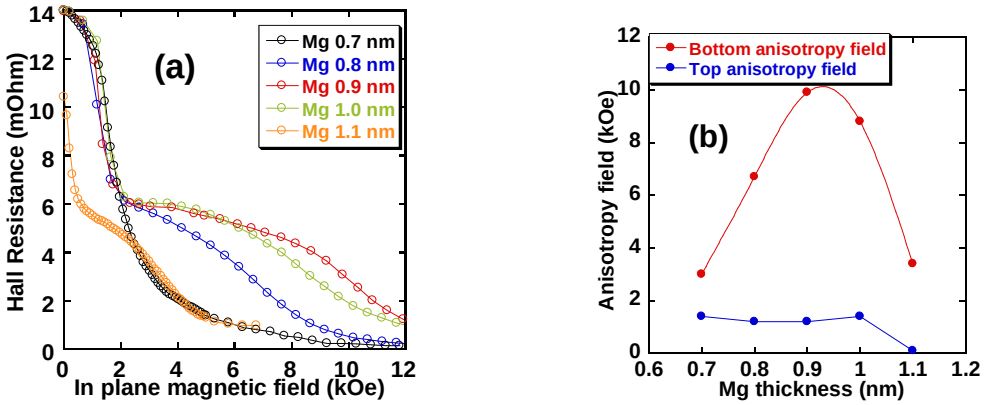

Figure II-28: (a) Hall resistance as a function of in-plane magnetic field and (b) Anisotropy field as a function of Mg thickness of bottom and top magnetic layers in Ta3/Pt30/Co2/MgOx/ CoFeB1.5/Co0.5/Pt3 structures after annealing at 350°C.

As we said in the introduction, PMA critically depends on both magnetic layer thickness, quality of the barrier and annealing conditions. To illustrate these effects, **Figure II-29** shows the hysteresis curves of four nominally identical Ta3/Pt30/Co2/MgO1/CoFeB1.5/Co0.5/Pt3 samples annealed at 350°C, prepared on a three days interval. One can see that perpendicular anisotropy varies a lot among samples. One can note that the top electrode is in this case made of a CoFeB/Co bilayer. In addition to the critical parameters cited above, a supplementary one is the influence of CoFeB crystallization and boron diffusion out of the magnetic layer. Very slight differences from sample to sample related to boron diffusion towards either MgO or Pt interfaces are expected to considerably modify interfacial anisotropy.

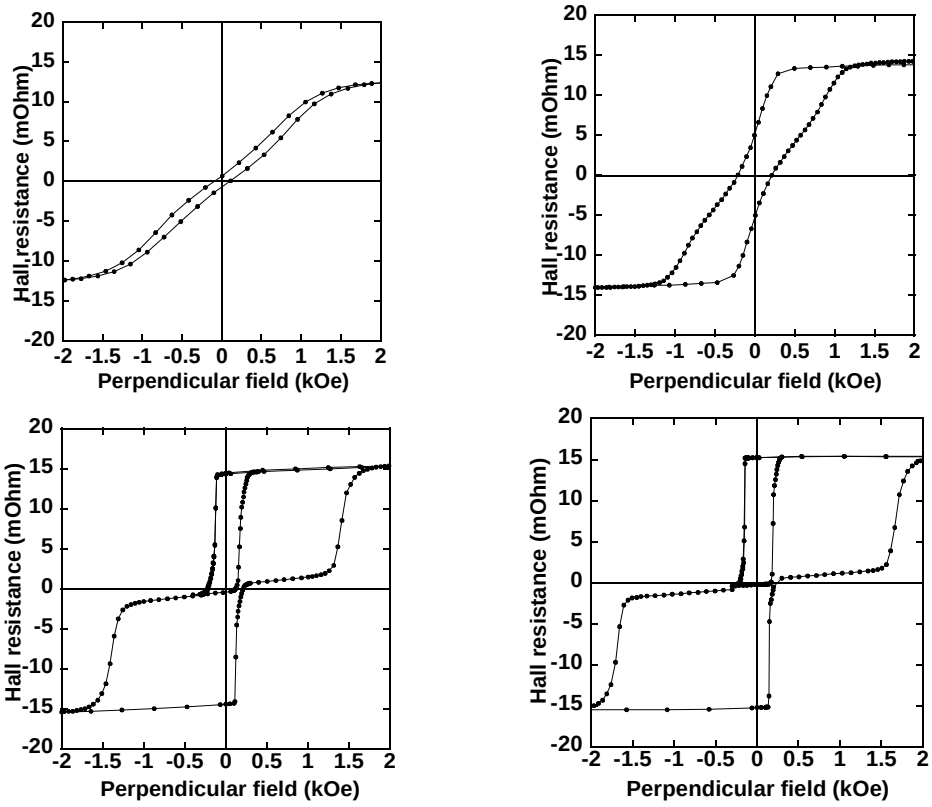

Figure II-29: Hall hysteresis curves of four nominally identical Ta3/Pt30/Co2/MgO1/CoFeB1.5/Co0.5/Pt3 structures after annealing at 350°C, deposited between February 03 and February 05 2009.

Much more stable magnetic properties were obtained when using a double deposition/oxidation of a Mg 0.7 nm thick layer. That's the reason why most of the results presented here and in the following **Chapter III** were obtained on samples prepared using such a double oxidation procedure.

II-3.2 Radio-frequency deposited MgO in two different sputtering machines

In **Chapter I** we showed that a much smaller perpendicular anisotropy is obtained when the oxide layer is prepared by RF sputtering of an MgO target. We will show here that these properties are strongly machine-dependent.

Figure II-30 shows the hysteresis loops of Ta3/Pt30/(Co0.5/Pt0.4)*5/Co.5/CoFeB0.5/ MgO/CoFeB0.5/Co0.5/Pt3 structures for different MgO thicknesses after annealing at 325°C.

These structures were prepared in our Actemium sputtering machine. Both electrodes are magnetically coupled for MgO thicknesses of 1.4 and 1.8 nm. Two transitions are observed for 2.0 nm, but the ferromagnetic coupling field is still of 420 Oe. A very thick MgO barrier of 2.4 nm is needed to decrease this coupling field to a few Oe.

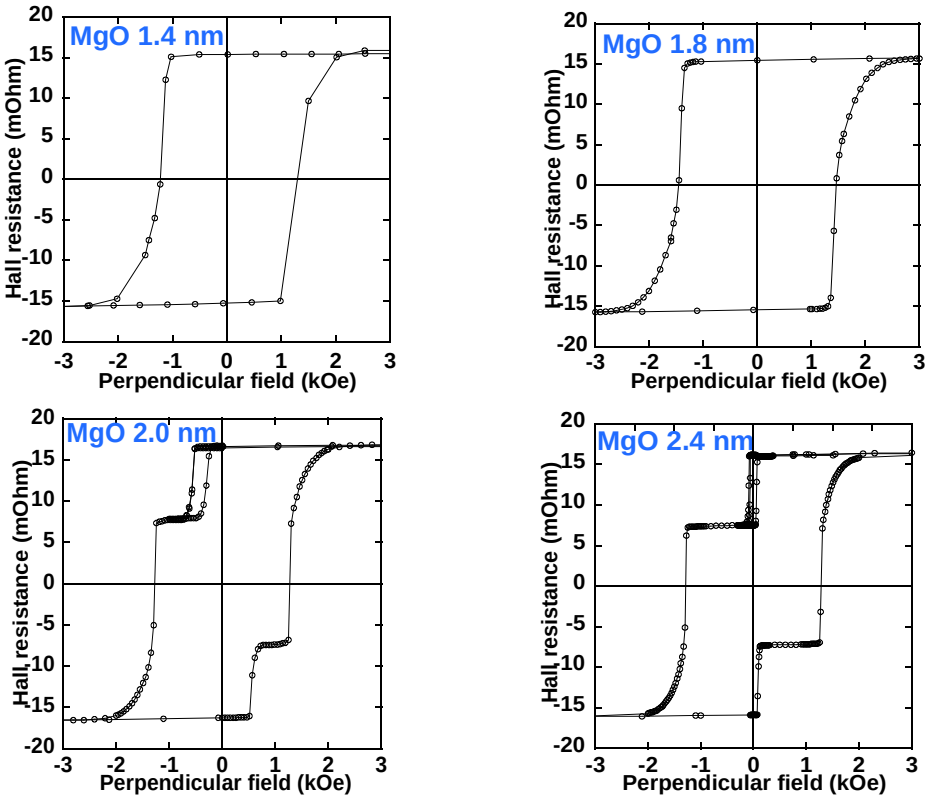

Figure II-30: Hall hysteresis curves of Ta3/Pt30/(Co0.5/Pt0.4)*5/Co0.5/CoFeB0.5 /MgORF/CoFeB0.5/ Co0.5/Pt3 structures after annealing at 325°C. Deposition was carried out in our Actemium machine.

Identical structures, annealed in the same conditions, but prepared in our Plassys machine were also investigated and results are presented in **Figure II-31**. Although electrodes are magnetically coupled at an MgO thickness of 0.6 nm, complete decoupling is now obtained for MgO thicknesses as low as 0.7 nm, with a negligible coupling field. One can also observe both an increase of the coercive field of the hard bottom layer, and an increase of the anisotropy of the soft top magnetic layer with increasing MgO thickness, its remanence increasing from almost 0 for a MgO layer 0.7 nm thick to 100% for a MgO layer 1.2 nm thick.

This different behaviour between sputtering machines is not easily understandable, since both MgO targets have the same origin. The only difference is the base pressure of both machines (almost one order of magnitude larger in the Plassys at the time the samples were prepared). This could point to some relation between vacuum quality (mainly residual water vapour) in the Plassys machine and insulating properties of the MgO barrier.

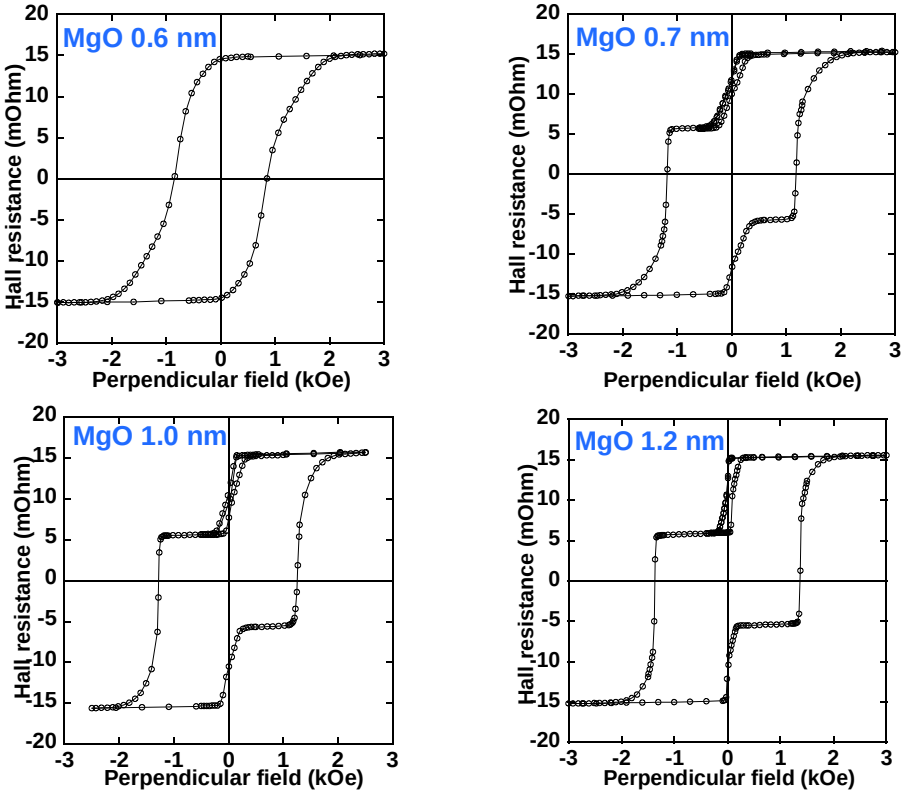

Figure II-31: Same as Figure II-30 for samples deposited in our Plassys machine.

II-4. Transport properties of perpendicular junctions

Transport properties of our p-MTJ's structures were studied using the CIP technique [Wor_03], as described in **Section II-1.3**. Although such a technique allows for a much faster and easier way of characterization compared to sub-micronic patterning, there are still some difficulties left. The first one is that the electrical resistance of top and bottom electrodes (usually made of nitrurated Cu, leading to low resistivity and low surface roughness) must be adjusted to the RA product of the MgO barrier, which is a priori unknown, since it depends on barrier nature, crystallinity and thickness, and also on the nature and thickness of magnetic electrodes. The other one is that, for perpendicularly magnetized samples, R(H) curves cannot be recorded.

II-4.1 Perpendicular junctions with high anisotropy Pt/Co/MgO electrodes

The first structures we electrically tested are depicted in **Figure II-32**, and their magnetic properties have been presented previously in this **Chapter**. Concerning transport properties, the lack of epitaxial relationship between pure Co layers [hexagonal (0001) or face-centred cubic (111) planes] and MgO barrier [(100) oriented rock-salt structure] is not expected to lead to a high tunnel magnetoresistance (TMR) amplitude. Indeed, a TMR ratio of only 10% is measured in these Pt/Co/MgO/Co/Pt structures after annealing at 350°C. Moreover, a large RA product is obtained, of the order of 300 Ωμm². Such a large value should make impossible STT switching experiments, because of a resulting too high critical voltage.

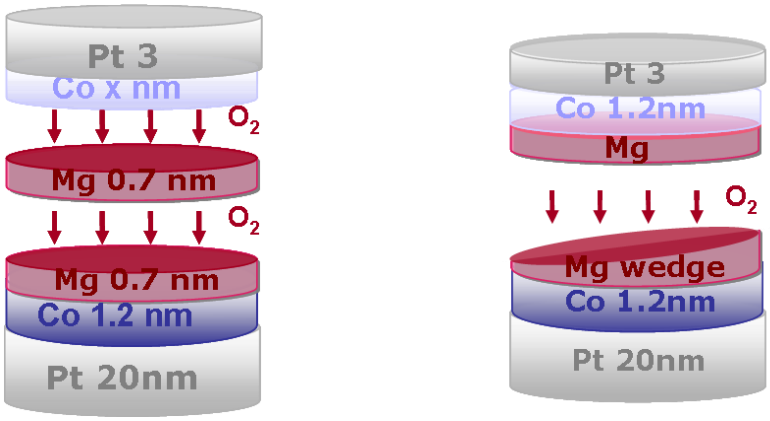

Figure II-32: Schematic Pt/Co/MgO/Co/Pt structures: (a) Successive natural oxidation of two Mg layers 0.7 nm thick; (b) Natural oxidation of a Mg wedge followed by metallic Mg deposition.

In parallel to the development of perpendicular junctions, planar ones were also optimized in our Actemium machine, and different preparation conditions of the barrier were tested, in order to decrease the RA product. The best results were obtained by depositing first a 0.9 nm Mg layer, oxidizing it and depositing on top a second Mg layer 0.5 nm thick.

We also tested these conditions in perpendicular junctions, using an Mg wedge (**Figure II-32**): the deposition of Mg is carried out off-axis, the centre of the substrate holder being offset by 100 mm from the target centre (see **Chapter I-3**). One can thus vary the Mg thickness by a factor of about 2 when using a 100 mm diameter silicon wafer. The other advantage of such a procedure is that the effect of Mg thickness is studied on a single sample, greatly reducing

instability problems mentioned above. With these deposition conditions, we obtained much smaller RA products (about 15 Ωμm²), but with a TMR still around 10%.

The effect of the Pt buffer was also tested in planar junctions with bottom Ta/Ptx/CoFeB electrodes. We also observed a strong decrease of the TMR when Pt was introduced. This means that even when pure Co is replaced by CoFeB, the negative influence of Pt structure and texture prevents from a correct crystallization of CoFeB and leads to a small TMR ratio.

II-4.2 Perpendicular junctions with low anisotropy Ta/CoFeB/MgO electrodes

II-4.2.A Magnetic properties

Platinum-free structures were recently proposed by Ohno and co-workers [Ike_10]. We also worked on such platinum-free bottom electrodes, in the framework of a Spintec-Crocus collaboration on planar junctions with low demagnetizing field (see **Section II-6**). From Ohno's work, it seems that, in macroscopic samples, the bottom Ta/CoFeB electrode is perpendicular, although with a very small coercive field (15 Oe), whereas the top electrode is in-plane. That's only after patterning into sub-micrometric pillars that both electrodes are perpendicularly magnetized.

The structures used in this study are schematically shown in **Figure II-33**. The bottom electrode consists of a Ta3/CoFeB bilayer (deposited onto a thick Cu(N) buffer for Capres measurements). Since magnetic anisotropy due to the Pt buffer layer is lost, one thus has to use this bottom electrode as the softest one, contrary to all structures studied up to now. The top electrode consists of a CoFeB layer exchange coupled to a Tb/Co multilayer, whose structure has been optimized by S. Bandiera during his thesis work [Ban_11]. The main limitation of such a multilayer is its relatively poor thermal stability (300°C).

Two series of wedged-shaped samples were prepared, the first one with a bottom CoFeB electrode of variable thickness, the other one with a constant bottom CoFeB layer thickness and a variable MgO thickness. The barrier was obtained through oxidation of a first Mg layer followed by the deposition of a second Mg layer 0.5 nm thick.

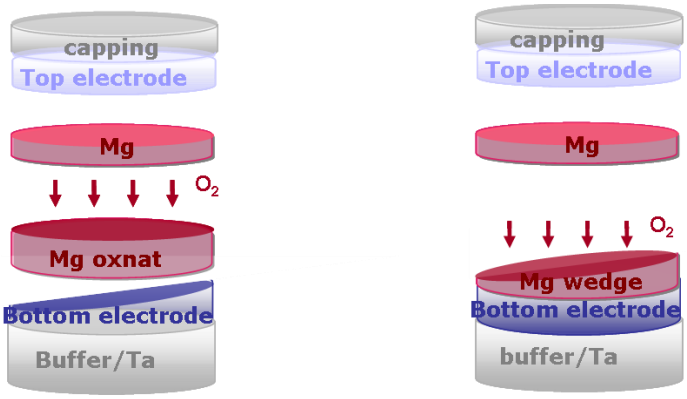

Figure II-33: Perpendicular junctions prepared with either bottom CoFeB wedge or Mg wedge.

The variation of the anisotropy properties was studied for the bottom electrode alone, with the following structure: Ta5/wedgeCoFeB1.5/MgO0.9OxNat/Mg0.5/Ta5, for which the nominal CoFeB thickness was chosen to cover a thickness range from 1.0 to 1.5 nm. The samples were annealed at 300°C and measured by VSM magnetometry along the CoFeB wedge. **Figure II-34a** shows that the absence of the Pt buffer considerably decreases the critical magnetic thickness, which is now just above 1.0 nm. A tentative fit to a straight line gives a $2K_S$ value

(averaged over both interfaces) of about 0.8 erg/cm². This is much smaller than the value obtained for bottom Pt/Co electrodes for the same annealing temperature (2.8 erg/cm²). Its difficult to discuss the value of K_V, since the magnetization of the CoFeB layer varies a lot with annealing (from about 800 to 1000 emu/cm³ in the as-deposited state to about 1400 emu/cm³ after 350°).

Figure II-34b shows a typical hysteresis loop of full structures. The coercive field of the bottom soft layer is very small, of the order of 30 Oe. That of the top hard layer is about 3.5 kOe.

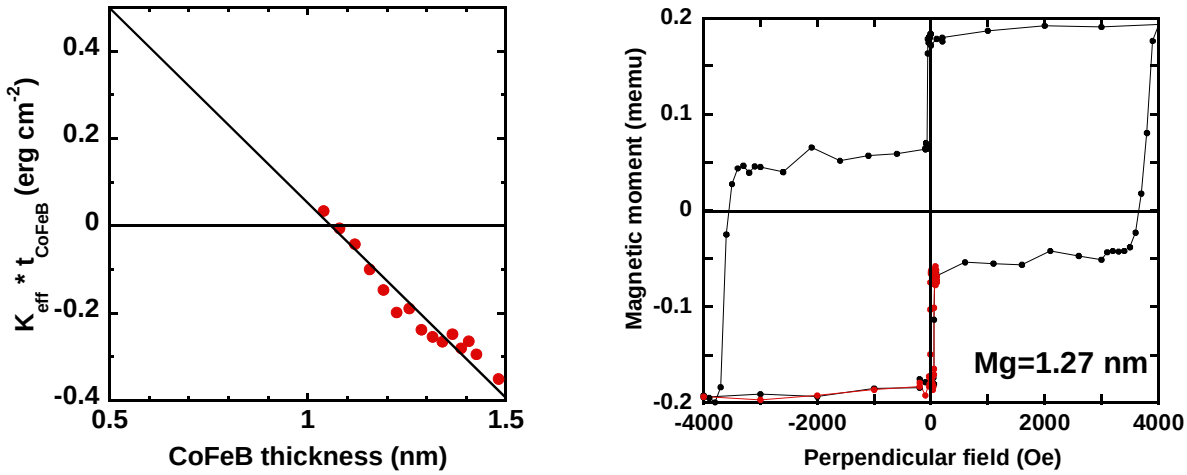

Figure II-34: (a) Variation of the effective anisotropy times CoFeB thickness as a function of CoFeB thickness in Ta5/CoFeBwedge/MgO1.4/Ta5 bottom electrodes after annealing at 300°C; (b) Hysteresis loop of a Ta/CoFeB1.0/MgO1.27/CoFeB1.6/(Tb/Co) structure after annealing at 300°C.

II-4.2.B Macroscopic transport properties

The macroscopic transport properties were measured by the Capres technique on 100 mm wafers. The CoFeB wedge was chosen to cover a thickness range of about 0.7 to 1.6 nm. Since the coercive field of the top hard layer is quite large, Capres measurements were performed under the maximum field available (+/-1.5 kOe).

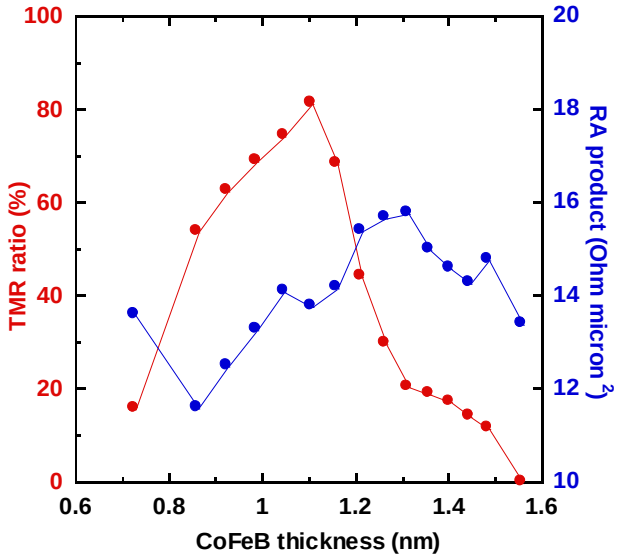

Figure II-35: Variation of TMR ratio and RA product of Ta/CoFeBx/MgO1.4/CoFeB1.6/(Tb/Co) structures as a function of bottom CoFeB thickness after annealing at 300°C.

The variations of the TMR ratio and of the RA product as a function of bottom CoFeB thickness after annealing at 300°C are shown in **Figure II-35**. The RA product is more or less independent of CoFeB thickness, with an average value of about 12 to 15 Ωμm², more favorable for STT switching experiments. The TMR ratio progressively increases with increasing CoFeB thickness, and reaches 80% for 1.1 nm. This increase is probably due to an increasing polarization of the electrons. This TMR ratio is much larger than that obtained in Pt based samples presented previously. Since the critical CoFeB thickness is only slightly larger than 1.0 nm, the maximum TMR ratio obtained for 1.1 nm means that, for that thickness, although the magnetization is back in-plane, its anisotropy field is smaller than the applied field (1.5 kOe), thus allowing to reach full parallel and anti-parallel alignments under field. For larger thicknesses, since the anisotropy field keeps increasing, it is more and more difficult to orient the magnetization direction of the soft layer out-of plane, leading to a decrease of the TMR ratio.

Figure II-36 is a map of TMR ratio and RA product on the whole 100 mm wafer. The CoFeB gradient is along the vertical diameter. The TMR and RA values are not exactly symmetrical with respect to the vertical diameter, because of geometrical misalignment in the machine.

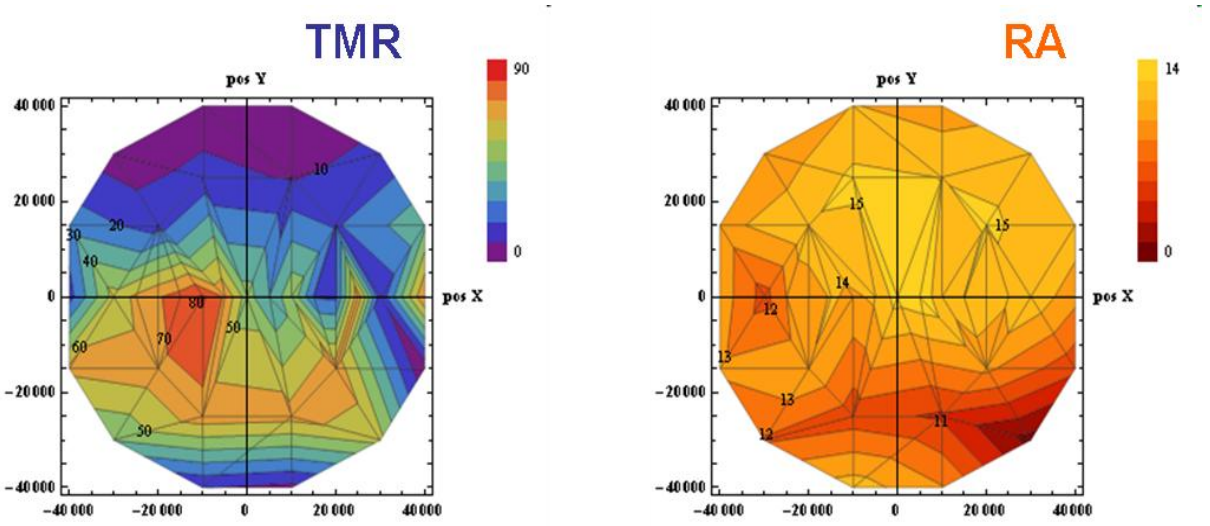

Figure II-36: Map of TMR ratio (left) and RA product (right) in Ta/CoFeBwedge/MgO1.4/ CoFeB1.6/(Tb/Co) structures after annealing at 300°C.

The TMR and RA results obtained on the MgO wedge in similar structures with a bottom CoFeB layer 1.0 nm thick, are shown in **Figure II-37**. The total Mg thickness goes from about 1.0 to 1.6 nm. The maximum TMR ratio is obtained for an Mg thickness of about 1.3 nm, whereas the RA product tends to increase with Mg thickness. This maximum of the TMR ratio is not linked to a degradation of the magnetic properties for small and large Mg thicknesses, since two well defined magnetic transitions are observed from 1.0 to 1.55 nm. It is neither due to a non-adapted choice of the applied field during the Capres measurements (1.5 kOe), since this field corresponds well to the intermediate plateau. The variation of the coercive field of the top hard layer is similar to that of the TMR ratio, indicative of a strong interplay between magnetic and transport properties.

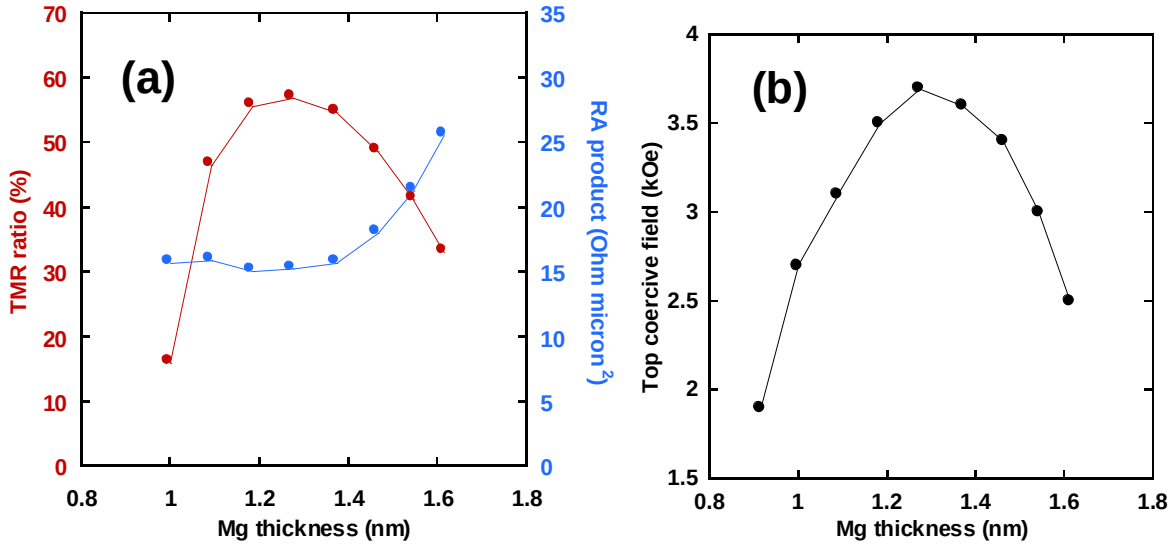

Figure II-37: Variation of (a) TMR ratio and RA product and (b) Top coercive field of Ta/CoFeB1.0 /MgO/CoFeB1.6/(Tb/Co) structures as a function of Mg thickness after annealing at 300°C.

The evolution of the TMR ratio with Mg thickness for different annealing temperatures was also investigated for the samples studied in this section and is presented in **Figure II-38**. The maximum TMR ratio is obtained for 280°C, and vanishes very rapidly for higher annealing temperatures. No magnetic measurements are available for samples annealed at 320°C, but it is probable that the poor thermal stability of the Co/Tb multilayer leads to a rapid degradation of the magnetic properties of the top electrode. As already stated above, R(H) curves cannot be recorded with the Capres tool in the perpendicular configuration. The real cause of the loss of TMR cannot thus be clearly identified.

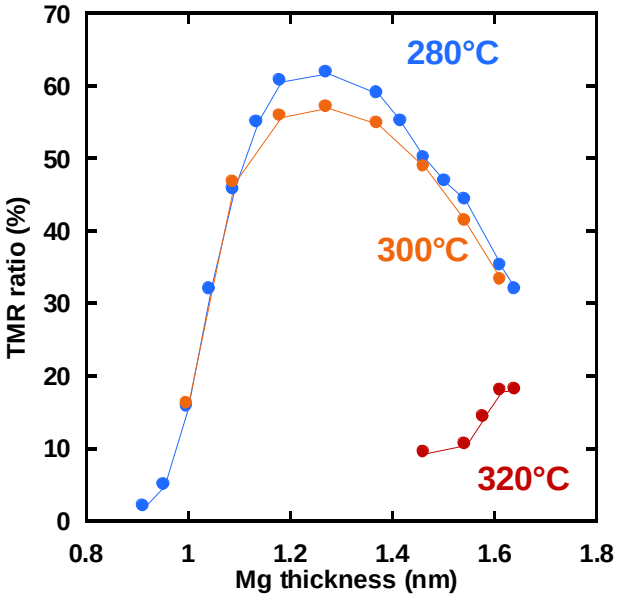

Figure II-38: Variation of the TMR ratio with MgO thickness for different annealing temperatures.

II-5. Correlation between anisotropy and magneto-resistance

Up to now, we almost independently discussed anisotropy and transport properties of perpendicular junctions. However, there is a crucial point to address: will the optimum anisotropy and transport properties (as a function of barrier thickness, oxidation conditions or annealing temperature for example) be reached at the same time? In previous sections, we showed that perpendicular anisotropy continuously increases with annealing up to at least 350 to 400°C. This parameter should thus not be a problem. On the other hand, the influence of barrier thickness and quality is not so straightforward.

Until now, only indirect information exists regarding the correlation between TMR and PMA in the case of Al oxide barriers **[Mon_02, Rod_03]**, and to our knowledge no such investigations have been conducted for MgO barriers prepared by natural oxidation. In classical spin-valves coated with a thin Al layer **[Cos_02]**, a maximum of magnetoresistance as well as a minimum in sheet resistance as a function of oxidation time of the top Al layer were observed. These features were attributed to the increase in the specular reflection at the CoFe/AlOx interface leading to a larger effective thickness of the CoFe soft layer (increasing the electrons mean free path in CoFe soft layer). The authors concluded that such a technique could be used to optimize the oxidation of the barrier, and thus the TMR response of magnetic tunnel junctions.

Although a TMR ratio of about 8% was obtained in AlOx-based tunnel junctions **[Car_08]** in which the oxidation conditions and annealing temperatures were optimized according to the PMA properties **[Rod_09]**, this does not ascertain that both maximum TMR ratio and PMA were achieved simultaneously.

The results presented here use the MgO thickness as a parameter, for constant oxidation conditions. At the time we addressed this point, no TMR results on perpendicular junctions were available **[Nis_10b]**. We will first discuss the relation between anisotropy properties and TMR ratio, comparing the anisotropy of bottom magnetic electrodes to the transport properties of in-plane tunnel junctions. Then results on perpendicular junctions will be presented.

II-5.1 Anisotropy and magnetoresistance in planar junctions

The structures studied here are unpatterned planar MgO junctions prepared in a Timaris machine (Singulus) at Crocus Technology. These are top-pinned structures of the form Ta5/free layer/Mgt/$Co_{70}Fe_{30}$2.5/Ru0.9/NiFe5/IrMn10/Ta10. Bottom Ta/Cu(N) and top Cu(N)/Ru layers are used in order to measure the transport properties by the CIPT technique using the Capres tool. The free layer consists of either $Co_{70}Fe_{30}$ or amorphous $Co_{60}Fe_{20}B_{20}$ layers 1.6 nm thick. Oxidation of the insulating barrier is performed by exposing the Mg metallic layer of variable thickness to a 1 mbar oxygen pressure during 450s. Samples are annealed under 10^{-6} mbar vacuum for 1h at 350°C.

The variation of the TMR ratio of junctions with CoFeB or CoFe free bottom electrodes is shown in **Figure II-39**. Both give a very well defined maximum for the same Mg thickness of 1.2 nm, corresponding to the optimal oxidation conditions. However, the TMR value is reduced by a factor of two when using CoFe, as a consequence of the absence of texture matching with the MgO barrier. One can also note that the width of the maximum is smaller for CoFe than for CoFeB, indicative of a larger sensitivity of the CoFe/MgO interface to over- or under-oxidation.

The anisotropy properties were studied on identical bottom electrodes grown on a Pt buffer in order to induce perpendicular anisotropy at the bottom magnetic interface and thus facilitate anisotropy measurements by Hall effect. The stacks consist of Ta3/Pt30/bottom layer1.0/Mgt/Ru5, with either $Co_{60}Fe_{20}B_{20}$ or $Co_{70}Fe_{30}$ as the bottom layer. Since there is no platinum target in the Timaris machine, SiO_2 substrates covered with the first Ta/Pt layers

deposited in our Actemium machine were transferred under clean air to the Crocus clean room, where the subsequent layers were deposited. We checked that such a procedure had no influence on the magnetic properties by depositing the complete structure in our machine with and without taking the samples out of the sputtering machine after Pt deposition. The samples were then annealed under 10^{-6} mbar vacuum for 1h at 325°C. One must note that the larger annealing temperature used for the full junctions only affects the value of the maximum TMR and not the position of its maximum as a function of Mg thickness.

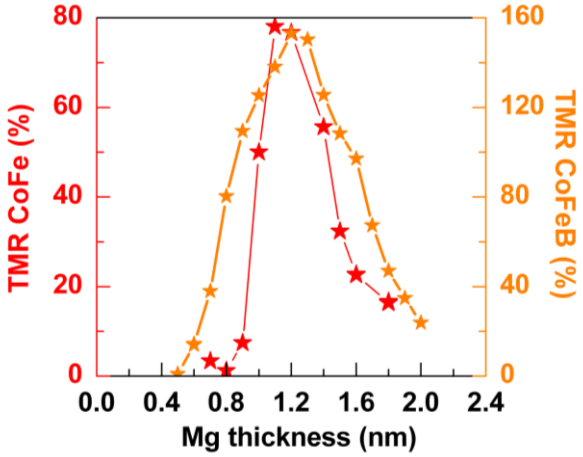

Figure II-39: TMR ratio of planar junctions as a function of Mg thickness. The free electrode is either $Co_{70}Fe_{30}$ or amorphous $Co_{60}Fe_{20}B_{20}$ 1.6 nm thick.

Let us first turn to the case of CoFe bottom electrodes. **Figure II-40** (left) presents Hall hysteresis loops measured with a perpendicular applied field for different Mg thicknesses. The magnetic remanence is smaller than 100% for Mg thicknesses of 0.6 and 1.8 nm, whereas it reaches 100% for 1.3 nm. The variation of the coercive field shows the same trend, with a maximum for a Mg thickness of 1.3 nm. Besides, a 100% increase of the Hall amplitude occurs when increasing Mg thickness from 0.6 to 1.3 nm, and a somewhat slight decrease is observed for larger Mg thicknesses. The non-monotonous variation of the perpendicular magnetic anisotropy is confirmed by anisotropy field measurements presented in **Figure II-40** (right). The anisotropy field goes through a maximum for a Mg thickness of 1.1 to 1.3 nm.

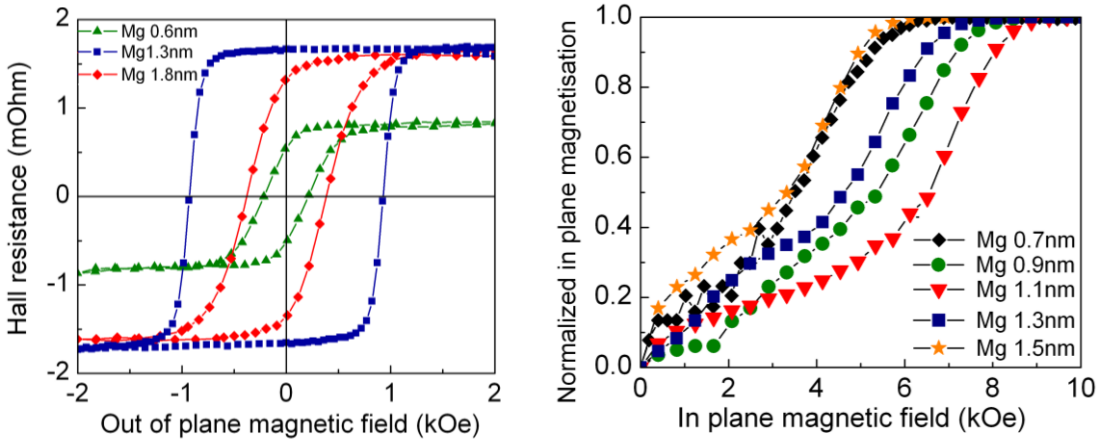

Figure II-40: Perpendicular Hall cycles (left) and normalized in-plane magnetization (right) as a function of Mg thickness in Ta3/Pt30/CoFe1.0/Mgt/Ru5 structures after annealing at 325°C.

More quantitative information is given in **Figure II-41** which presents the variation of the Hall resistance and coercive field as a function of Mg thickness for this bottom CoFe magnetic electrodes. For the present oxidation conditions, Mg thicknesses smaller than 1.2 nm lead to over-oxidation of the magnetic electrode, resulting in both reduced coercivity and decreasing Hall amplitude. For larger Mg thicknesses, remaining metallic Mg layer at the CoFe interface may cause both the small decrease of the Hall amplitude by shunting effects and also the decrease of the perpendicular anisotropy. The maximum coercive field is reached for an Mg thickness between 1.2 and 1.3 nm and can be ascribed to the optimal oxidation of the Mg barrier.

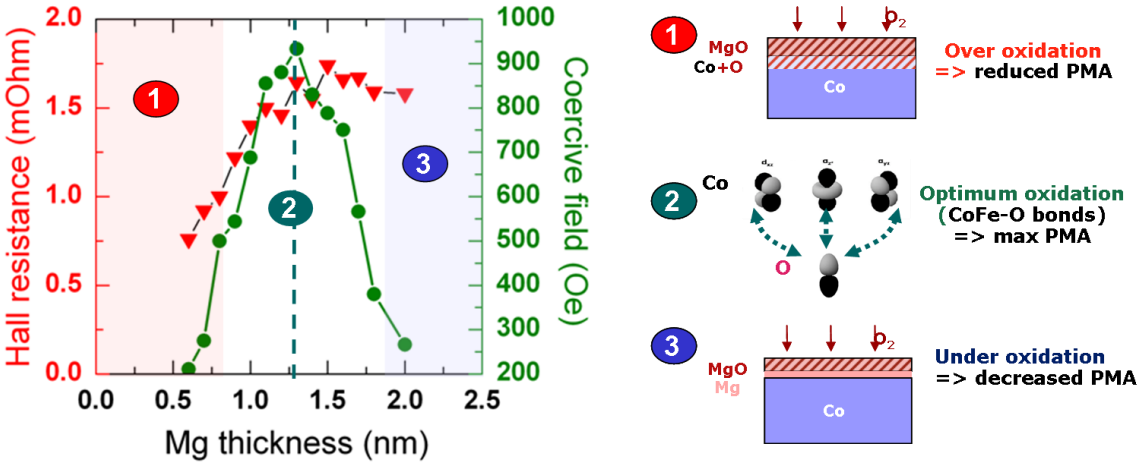

Figure II-41: Variation of the coercive field (circles) and Hall resistance (triangles) as a function of Mg thickness for Ta 3/Pt30/$Co_{70}Fe_{30}$1.0/Mgt/Ru5 bottom electrodes after annealing at 325°C.

The TMR ratio of full structures and the variation of the anisotropy field of bottom CoFe electrodes as a function of Mg thickness is presented for comparison in **Figure II-42.** One can see that both quantities give the same optimal thickness of the Mg layer, as is also the case for the coercive field of bottom electrodes. The correlation between transport and magnetic properties seems thus well established.

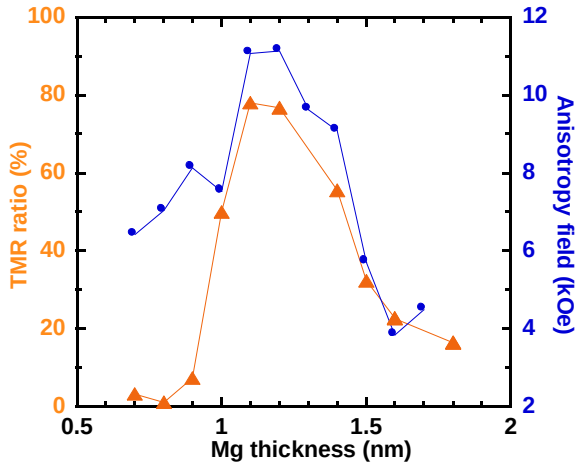

Figure II-42: Variation of the TMR ratio (triangles) of planar CoFe junctions and of the anisotropy field (circles) of CoFe bottom electrodes as a function of Mg thickness.

The same type of experiments was carried out in structures with a CoFeB bottom electrode. The influence of Mg thickness on TMR ratio of full structures and on the coercive field

of bottom CoFeB electrodes is presented in **Figure II-43**. The evolution of perpendicular magnetic anisotropy of bottom CoFeB electrodes is completely different, as can be inferred from the coercive field variation. First, coercive field value is considerably smaller (note that the field scale in **Figure II-43** is ten times enlarged as compared to that in **Figure II-41**). Second, the sensitivity of PMA to oxidation is completely lost, with an almost constant value of the coercive field whatever the Mg thickness. This could be interpreted in terms of boron diffusion towards the MgO interface **[Muk_09, You_08, Kur_10]**, leading to the disappearance of the CoFe-O interactions responsible for the interfacial perpendicular anisotropy.

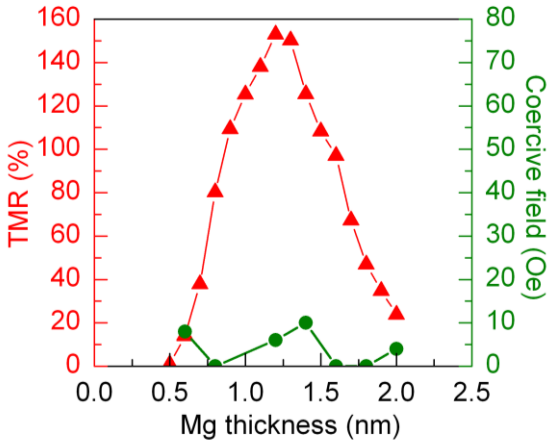

Figure II-43: Variation of the TMR ratio (triangles) of planar CoFeB junctions and of the coercive field (circles) of CoFeB bottom electrodes as a function of Mg thickness.

First principles calculations have shown the detrimental effect on TMR of the presence of boron atoms at the CoFe/MgO interface **[Bur_06]**. Experimental results are more ambiguous, since they show an increase of the TMR ratio when using CoFeB. The predicted detrimental effect of B on the TMR could be hidden by other and stronger effects like the much better growth of the MgO barrier on amorphous CoFeB than on polycrystalline CoFe **[Ike_07, Yua_05]**.

II-5.2 Anisotropy and magnetoresistance in perpendicular junctions

In **Section 2.4.1** we briefly mentioned the (poor) TMR properties of Pt/Co/MgO/Co/Pt perpendicular junctions. **Figure II-44** shows a comparison of the TMR variation in planar and perpendicular junctions as a function of Mg thickness. Both structures were obtained using an Mg wedge with the same oxidation conditions (180" under 250 mbar oxygen pressure). They only differ by their annealing temperatures, 325°C for the planar and 270°C for the perpendicular structure. A TMR ratio above 100% is obtained in the planar junctions, as compared to at most 10% in the perpendicular one.

Another difference is observed concerning the width of the TMR peak. It is less than 0.2 nm in the case of the perpendicular junction, compared to more than 0.5 nm for the planar structure. This points out the much higher sensitivity of perpendicular structures to preparation conditions.

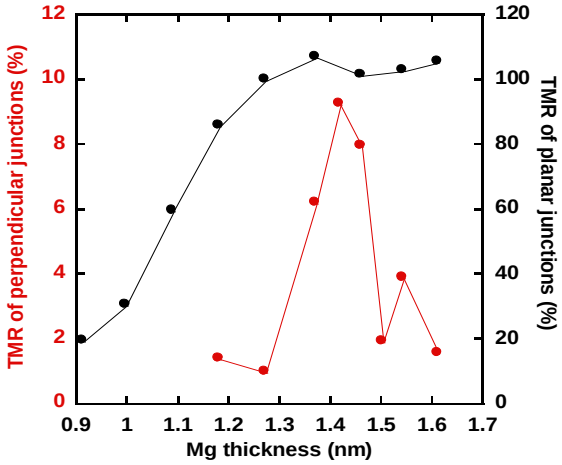

Figure II-44: TMR ratio as a function of Mg thickness for planar (black) and perpendicular (red) junctions.

Magnetic measurements were conducted on the same perpendicular junctions. **Figure II-45** shows the perpendicular loops recorded on selected samples. One must note that the positioning of the sample (a 100x10 mm rectangle) in the Capres tool is not very accurate, and one cannot guarantee the exact thickness correspondence between both measurements. However, one can observe a good agreement between transport and magnetic properties: the magnetic structure is lost for 1.18 nm (no TMR), the best magnetic structure is obtained between 1.37 and 1.46 nm (maximum TMR), and it degrades again at 1.61 nm (no more TMR). However, no TMR signal is obtained for 1.27 and 1.54 nm, whereas the intermediate plateau corresponding to the antiparallel state is still relatively well defined. This means that one needs two well defined parallel and antiparallel states in order to obtain a measureable TMR, which is quite obvious, but also that, in this bi-stable Mg thickness range, TMR ratio still critically depends on the oxidation state of the barrier, as for planar junctions.

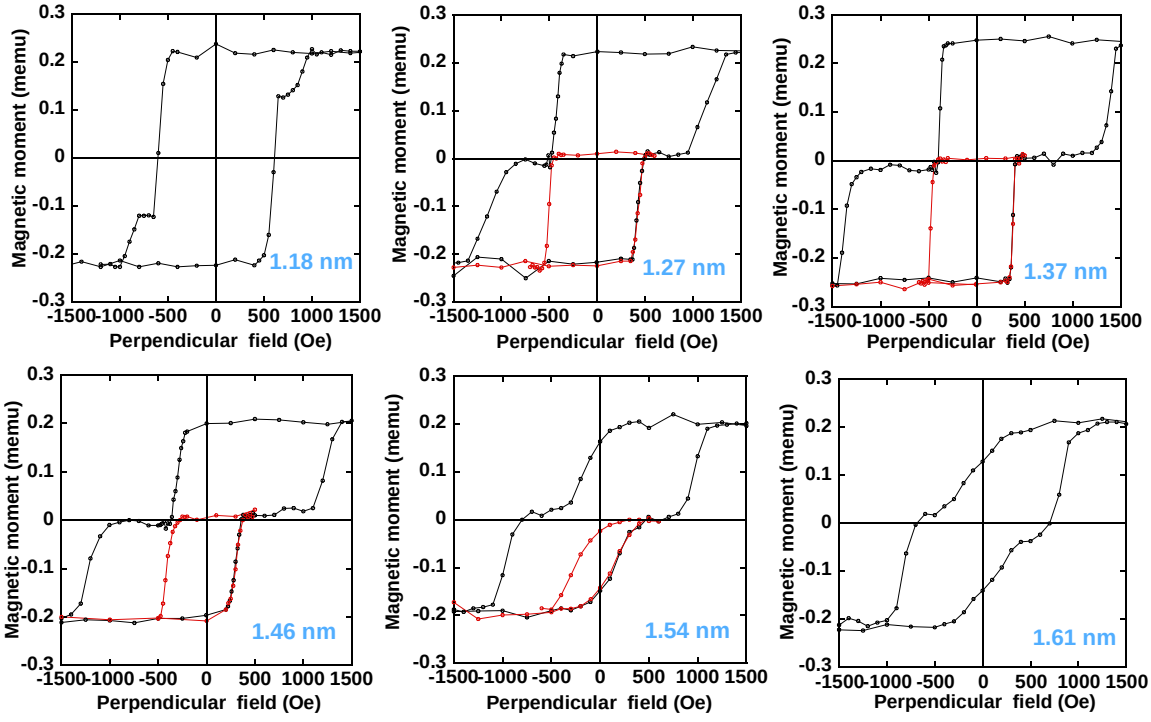

Figure II-45: Hysteresis loops of Ta3/Pt20/Co1.2/MgO/Co1.2/Pt3.0 perpendicular junctions as a function of Mg thickness after annealing at 270°C.

II-5.3 Origin of anisotropy and correlation with magneto-resistance

Results presented in the previous **Section** showed a good correlation between the variation of tunnel magnetoresistance of planar/perpendicular tunnel junctions and that of the perpendicular anisotropy of CoFe bottom electrodes or Co based pMTJ, as a function of Mg oxidation conditions for naturally oxidized barriers. In both experiments a maximum value for TMR and PMA is obtained for a Mg thickness between 1.2 and 1.4 nm. This implies that the same mechanism, namely the formation of Co(Fe)-O bonds at the interface during oxidation and the presence of a weak spin-orbit coupling, will simultaneously influence the TMR amplitude as well as the interfacial anisotropy. The presence of oxygen atoms at the magnetic metal interface with the oxide barrier (Co-O bonds) was detected by X-ray Photoemission Spectroscopy (XPS) measurements **[Man_08a, Man_08b]** and can be related experimentally to the maximum PMA. It was also shown theoretically in the case of planar Fe/MgO/Fe MTJ that the TMR is higher for the Fe-O-Mg configuration than for Fe-Mg-O one **[Zha_03]**.

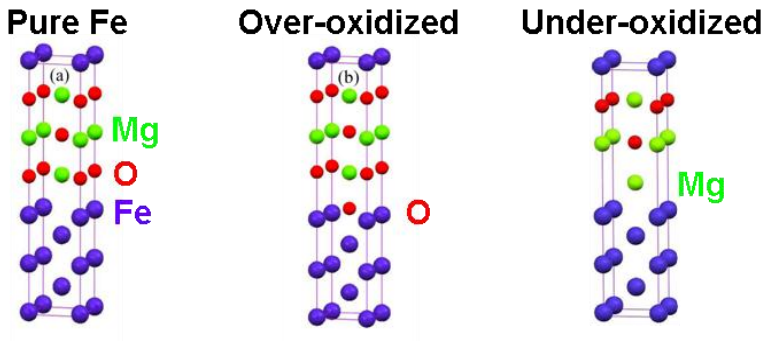

Figure II-46: Fe/MgO(100) structures: (a) Pure interface (O-terminated); (b) Over-oxidized interface (with O inserted at the interface magnetic layer); (c) Under-oxidized (Mg-terminated) interface.

To complement and better understand these experimental results, ab-initio calculations have been carried out at Spintec by M. Chshiev and co-workers **[Yan_11]** in order to study the influence of oxygen concentration along the interface on the PMA. Three cases were considered in Fe/MgO(100) structures presented in **Figure II-46**: (a) "pure" interface (O-terminated), (b) over-oxidized interface (with O inserted at the interfacial magnetic layer), and (c) under-oxidized (Mg-terminated) interface. This structure can be viewed as a model system for ferromagnetic/oxide interfaces involving bcc electrodes. The largest PMA values are obtained in the case of pure interfaces compared to over- or under-oxidized interfaces in agreement with studies presented here and in the literature **[Mon_02, Rod_03, Man_08b, Rod_09]**. The origin of the large PMA at the interface between magnetic metal and oxide is attributed to the spin-orbit induced mixing between majority Bloch state Δ1(s,pz,dz2) symmetry (resulting from hybridization between Fe-dz^2 and O-pz orbitals) and minority Bloch states Δ5(p_x,p_y,d_{xz},d_{yz}) symmetry combined with the degeneracy lift of out-of-plane 3d orbitals. Accordingly, the difference between the PMA and TMR values in the three cases investigated here can be explained looking at the impact of splitting (disappearing) of Δ1-like hybridized states at the Fermi level in the presence (absence) of additional oxygen atoms. Since the splitting of these $d_{xz,yz}$ orbitals is still relatively strong for the under-oxidized case (and larger for out-of-plane magnetization orientation compared to the in-plane one), anisotropy values are higher compared to the over-oxidized case but lower compared to the ideal Fe/MgO interfaces. Furthermore, since majority Bloch states with Δ1 symmetry for Fe and MgO are at the heart of the spin filtering phenomenon, the spin-orbit induced mixing between majority Δ1 and minority

Δ5 Bloch states can also affect the TMR. So in the case of an over-oxidized interface the Δ1 decay rate is strongly enhanced compared to the ideal one **[Yan_11, Zha_03]**. This could explain why both PMA and TMR reach a simultaneous maximum as observed experimentally, this maximum being reached for ideal oxidized interfaces.

II-6. Low effective demagnetizing field in planar magnetic tunnel junctions

The use of perpendicular anisotropy in thin films could have a strong impact in the magnetic storage industry because these structures allow for a strong increase of the efficiency of magnetic random access memories, keeping at the same time a good thermal stability of the information stored. In the case of Magnetic Tunnel Junctions problems like the size and shape limitation of planar elements with respect to the magnetization curling due to the miniaturization and discretization of magnetic media can be eliminated by using perpendicular electrodes **[Yoo_05]**. Furthermore, studies have shown that perpendicular structures may present lower critical switching currents when information is written via spin transfer (Current Induced Magnetic Switching, CIMS), since this critical current is proportional to the anisotropy field of the storage layer of the MTJ structure **[Man_06]**.

II-6.1 Previous studies

In the case of thin films with in-plane magnetization, the shape anisotropy energy which determines the value of the critical CIMS current can be reduced by adding an interface anisotropy term to the volume anisotropy one **[Joh_96]**. This interface term can even be the leading term, thus orienting spontaneously the magnetization out-of-plane below a critical magnetic thickness. This phenomenon can be used to develop various devices for spintronics applications like perpendicular MTJ's (presented in the preceding **Sections**) or planar MTJ's with reduced demagnetizing field using magnetic metal-oxide combinations.

In conventional MTJ, the demagnetizing field of the magnetic layer is $-4\pi M_S$ (-18 kOe for cobalt). It is usually the dominant contribution to the critical STT switching current linked to the in-plane anisotropy. However, the relative role of demagnetizing and anisotropy energy can be strongly modified in the presence of either volume or interfacial perpendicular anisotropy. Indeed, in that case, the demagnetizing and anisotropy terms have opposite signs, leading to an expected significant reduction in critical current density **[Ngu_05, Liu_09]**.

Low demagnetizing structures are easier to fabricate than fully perpendicular pMTJ because one just has to introduce a perpendicular anisotropy contribution to the free layer of a classical planar MTJ. Since there are different ways to obtain interfacial out-of-plane anisotropy, several research teams have proposed structures based on this concept **[Ngu_05, Liu_09, Mor_10, Ami_11, Nis_11]**.

The first low demagnetizing structure was a spin-valve one **[Liu_09]** which uses interfacial anisotropy from Co/Ni multilayers, a very versatile system in which the PMA can be tuned over a wide range by changing the thickness of each layer and/or the number of repeats. The zero-thermal-fluctuation critical current I_{c0} is reduced by a factor of 5–6 (J_{c0} = 2 10^6A/cm^2) compared to control samples with high demagnetizing energy and the same total magnetic moment, while the thermal stability is almost the same. Further reduction in critical current is expected by optimizing the spin polarization using a magnetic tunnel junction rather than a spin-valve. The same team **[Mor_10]** fabricated MgO magnetic tunnel junctions using similar Co/Ni switching layers combined with a FeCoB insertion layer to reduce the effective demagnetizing field (thanks to interface anisotropy) to 2 kOe, still keeping the tunnel magnetoresistance ratio as high as 106%. But the use of Co/Ni or Pt/Co materials is limited because of increased damping, difficulties to keep high TMR in MTJ by integrating these materials with fcc (111) texture which is incompatible with the (100) texture of the MgO barrier, and the difficulty of realizing large perpendicular anisotropy in thick free layers.

Large interfacial out-of-plane anisotropy has also been evidenced at Co/oxide interfaces [Mon_02, Rod_09, Nis_09a] and the Co(Fe)/oxide interfacial anisotropy has been shown to be able to orient the magnetization of a 1 nm thick CoFeB layer out-of-plane [Ike_10]. This makes possible to obtain a free layer with a low effective demagnetizing field in planar MTJ just by increasing the layer thickness in order to decrease the CoFeB/MgO interface anisotropy contribution. The effect of the CoFeB composition on device characteristics (anisotropy and critical thickness) was investigated in full MTJ stacks with bottom pinned $Co(80-x_1)Fe(x_1)B(20)$ and top free $Co(80-x_2)Fe(x_2)B(20)$ electrodes with x_1=20, 40, 60 and x_2=20, 60 [Ami_11]. Authors compared MTJs with a free layer thickness of 1.8 nm with standard devices and observed a 40% reduction in the average quasi-static switching current density (from 2.8 to 1.6 MA/cm^2) when the free layer was changed from a Co-rich x_1=40 and x_2=20 to a Fe-rich x_1=40 and x_2=60 composition. These authors also claim that the reduction of current density by a factor 2.4 is related to the interfacial anisotropy increase since the layer thickness is only reduced by a factor of 1.2 (from 2.03 to 1.69 nm). For a 1.8 nm free layer thickness of Fe-rich CoFeB the TMR ratio is still around 120%.

II-6.2 Low demagnetizing field in top-pinned planar junctions

We also developed planar MTJs with low demagnetizing field based on classical top pinned structures with an MgO barrier obtained by natural oxidation. The bottom CoFeB free layer has a reduced effective demagnetizing field thanks to interfacial perpendicular anisotropy from the CoFeB/MgO interface. Structures annealed at 300°C are of the form Ta3/CoFeBx/MgO1.4/CoFeB3/Ru0.9/Co2/IrMn7/Ta3 (nm) as shown in **Figure II-47**. In order to modify the interfacial PMA contribution to the effective field, the bottom layer thickness was varied by using a CoFeB wedge between 1.0 and 1.3 nm obtained by off-axis deposition from the CoFeB target. Since the PMA in Co/oxide interface is very sensitive to the oxygen content, the oxide was carefully prepared by choosing the appropriate pressure (250mbar) and time (160s) of the Mg oxidation in order to obtain the maximum PMA properties. Samples were annealed at 300°C in vacuum in order to crystallize the MgO and CoFeB electrodes and to enable the CoFe-O bond formation responsible for the PMA. Vibrating sample magnetometry (VSM) was used to extract the anisotropy field from measurements along the hard magnetization direction. The transport properties of macroscopic samples were investigated by the CIP technique.

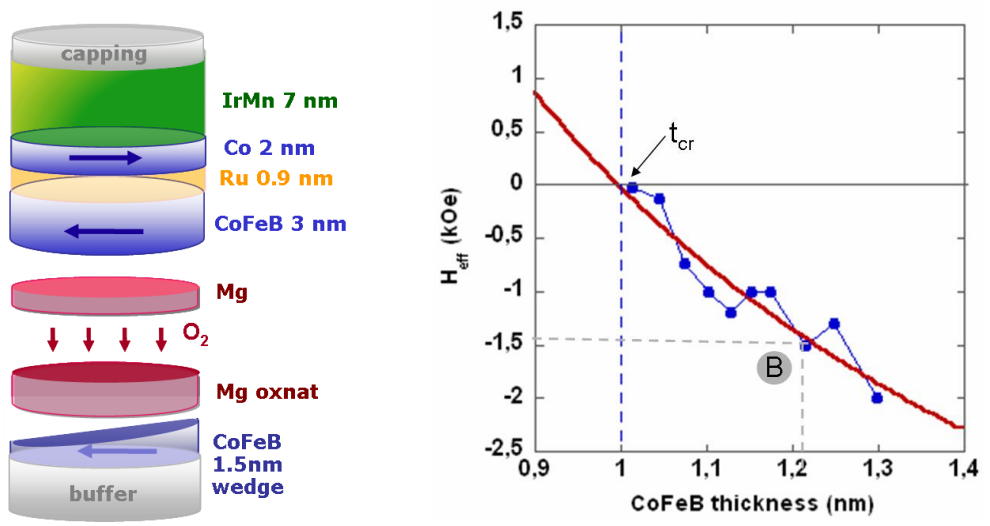

Figure II-47: Variation of the effective anisotropy field with bottom CoFeB thickness of a top-pinned planar MTJ structure with low effective demagnetizing field.

The variation of the effective anisotropy field $H_{eff}= -4\pi M_S + 2K_V/M_S + 4K_S/tM_S$ as a function of bottom CoFeB thickness is given in **Figure II-47**. The spin reorientation transition (from out-of-plane to in-plane) occurs for a CoFeB thickness of about 1 nm. H_{eff} progressively decreases with increasing CoFeB thickness because of the decreasing contribution of the interface anisotropy. The fit in **Figure II-47** gives an interfacial anisotropy 2Ks= 0.55 erg/cm^2 which is lower than values reported in the literature by Ikeda et al. (1.3 erg/cm^2) **[Ike_10]** and Amiri et al. (2.4 erg/cm^2) **[Ami_11]** probably because of the lower concentration of Fe in our CoFeB alloy, and a volume contribution $K_V - 2\pi Ms^2 = -5.5\ 10^6$ erg/cm^3. Neglecting the volume anisotropy, in agreement with the literature **[Ike_10]**, this leads to a saturation magnetization of about 950 emu/cm^3 (see **Appendix 3**). This value agrees with independent magnetization measurements, and corresponds to a demagnetizing field of about -12 kOe. By comparison, the effective field for a CoFeB thickness of 1.2 nm (point **B** in **Figure II-47**) is only -1.5 kOe. One should thus expect a reduction by a factor of about 10 of the critical switching current.

Figure II-48 shows the variation of the tunnel magnetoresistance with bottom CoFeB thickness. For large CoFeB thickness, the TMR ratio reaches 135%. It decreases with decreasing thickness below 1.2 nm because of the reduced polarization of the electrons, but is still of the order of 100% around the critical CoFeB thickness of 1.05 nm. Below this critical thickness, the TMR decreases more rapidly since the anisotropy field of the (now) perpendicular free layer progressively increases, and rapidly becomes of the order of the exchange field of the planar pinned layer (200 Oe). Thus the in-plane field needed to put the free layer in-plane is also large enough to switch the magnetization direction of the pinned layer, and the anti-parallel state cannot be reached anymore. Comparing **Figure II-47** and **Figure II-48,** one can see that, for a CoFeB thickness of about 1.2 nm, the TMR ratio is still 135% whereas the effective field is more than ten times smaller than the demagnetizing field.

Comparing our results to those of Moriyama et al **[Mor_10]**, which give an effective field of 2 kOe for a 1.1 nm CoFeB layer, our MTJ structure has thicker CoFeB layer (1.35 nm) for the same effective field, and higher TMR values (135%) due to higher spin polarization of the thicker magnetic layer. The anisotropy from the CoFeB/MgO interface is strong enough to reduce the demagnetizing field contribution without using Co/Ni multilayers and simplifying the structure, still keeping a high TMR.

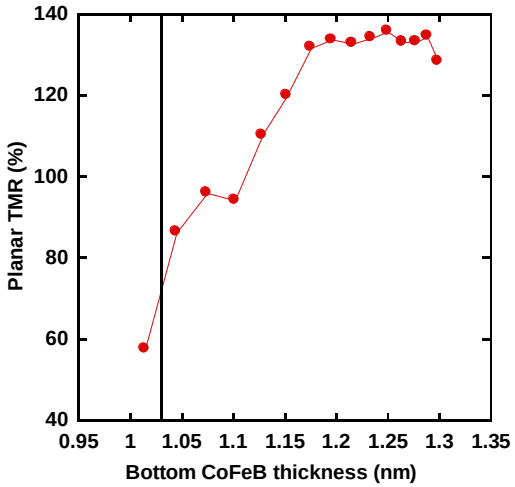

Figure II-48: Variation of the TMR ratio with bottom CoFeB thickness in planar tunnel junctions.

In conclusion, we have shown in this **Section** that, thanks to perpendicular anisotropy at the magnetic metal/oxide interface, the effective demagnetizing field of the storage layer of in-plane MgO tunnel junctions can be greatly reduced without significant decrease of the TMR ratio. Complementary magnetic measurements on these structures are reported in **Appendix 3**. STT writing experiments on submicronic memory cells based on such structures are underway.

II-7. Conclusions

In this second **Chapter** we presented results concerning the anisotropy and transport properties of magnetic tunnel junctions with perpendicular electrodes.

The most surprising observation is the increase of the anisotropy of the top electrode when it is deposited onto the bottom one. We showed that this effect has a structural origin and is related to the growth conditions of the Mg layer, which depends on the nature of the underlying layer. This large increase of the anisotropy comes from the better growth of the Mg layer on metallic materials like Pt and Ru than on Ta or SiO_2.

The anisotropy of top and bottom electrodes in pMTJ increases with annealing, as was the case for electrodes alone presented in the first **Chapter**, but have different origins for the top and bottom electrodes. For bottom electrodes the interface contribution Ks dominates, contrary to the top electrode where Kv dominates. Both bottom and top electrodes in full junctions present a critical thickness of 3.5 nm after annealing at 350°C.

Strong mutual magnetic interactions between electrodes were also observed, the coercive field of the bottom electrodes decreasing with increasing the thickness of the top electrode. For the moment with have no explanation about such an interaction.

PMA critically depends on both magnetic layer thickness and annealing conditions, but also on the quality of the barrier involving the oxygen content at the interface with the magnetic layers. This shows that perpendicular junctions are much difficult to fabricate since one needs to find the combination of stable magnetic properties and optimal PMA contribution from the magnetic metal/oxide interface.

The first structures we fabricated were based on Pt/Co/MgO trilayers showing a very high anisotropy but a low TMR of only 10%. Two different MgO oxides with the same thickness were tested giving the same TMR value but different RA values (300 $\Omega\mu m^2$ for Mg0.7+Mg0.7 natural oxidation and 15 $\Omega\mu m^2$ for Mg0.9NatOx/Mg0.5). The low TMR in these structures is mainly due to the texture mismatch between Co and MgO.

In order to improve the TMR properties a compromise should be made by eliminating the Pt buffer and replacing the bottom Co layer by CoFeB but by consequence strongly reducing the PMA of the structure. The bottom layer thus becomes the softest one, and the top layer becomes the hardest one by exchange coupling to a Co/Tb multilayer. This results in a higher TMR of 80% with a low RA product of 15 $\Omega\mu m^2$.

A direct correlation between anisotropy and transport properties was evidenced in both single electrodes and full junctions, implying that the same mechanism (the formation of CoFe-O bonds at the interface during oxidation and the presence of a weak spin-orbit coupling) leads to the TMR and PMA maxima.

According to ab-initio calculations, the difference between the PMA and TMR values in the tree cases observed experimentally (over-oxidized, under-oxidized and ideal oxidation) can be explained by the impact of splitting of Δ1-like hybridized states at the Fermi level in the presence of additional oxygen atoms. In the case of out-of-plane magnetization, the splitting of the $\mathbf{d_{xz,yz}}$ orbitals is larger for the ideal Fe/MgO interfaces, relatively strong for the under-oxidized case, and the corresponding anisotropy values are larger compared to the over-oxidized case but lower compared to the ideal Fe/MgO interface. Furthermore, in the case of over-oxidized interfaces the Δ1 decay rate is strongly enhanced compared to the ideal and under-oxidized cases: Δ1 bands are absent at the Fermi level, explaining the experimentally observed maximum TMR for the ideal oxidized barrier.

Finally, thanks to perpendicular anisotropy at the magnetic metal/oxide interface, the effective demagnetizing field of the storage layer of in-plane MgO tunnel junctions can be greatly reduced still keeping a TMR ratio as high as 135%. Macroscopic transport properties were studied in such samples. Although these samples were processed into sub-micrometric structures, we had not enough time to characterize their STT transport properties, and thus no corresponding results will be presented here.

II-8. References

[Ami_11] P.K. Amiri, Z.M. Zeng, J. Langer, H. Zhao, G. Rowlands, Y.-J. Chen, I.N. Krivorotov, J.-P. Wang, H.W. Jiang, J.A. Katine, Y. Huai, K. Galatsis and K.L. Wang, *Switching current reduction using perpendicular anisotropy in CoFeB–MgO magnetic tunnel junctions,* **Appl. Phys. Lett.** **98** (2011) 112507.

[Ban_10] S. Bandiera, R.C. Sousa, Y. Dahmane, C. Ducruet, C. Portemont, V. Baltz, S. Auffret, I.L. Prejbeanu and B. Dieny, *Comparison between synthetic antiferromagnets and single hard layers as reference layer in perpendicular magnetic tunnel junctions,* **IEEE Magn. Lett.** **1** (2010) 3000204.

[Ban_11] S. Bandiera, *Jonctions tunnel magnétiques à anisotropie perpendiculaire et écriture assistée thermiquement*, PhD Thesis, Grenoble University (2011).

[Bur_06] J.D. Burton, S.S. Jaswal, E.Y. Tsymbal, O.N. Mryasov and O.G. Heinonen, *Atomic and electronic structure of the CoFeB/MgO interface from first principles*, **Appl. Phys. Lett.** **89** (2006) 142507.

[But_01] W.H. Butler, X.-G. Zhang, T.C. Schulthess and J.M. MacLaren, *Spin-dependent tunneling conductance of Fe|MgO|Fe sandwiches,* **Phys. Rev. B** **63** (2001) 054416.

[Can_07] A. Canizo-Cabrera, C.-H. Chang, C.-C. Hsu, M.-C. Weng, C.C Chen, C.T. Chao, J.C. Wu, Y.-H. Chang and T.-H. Wu, *Perpendicular magnetic tunneling junction with double barrier layers for MRAM application,* **IEEE Trans. Magn.** **43** (2007) 914.

[Cap] **http://www.capres.com/**

[Car_08] B. Carvello, C. Ducruet, B. Rodmacq, S. Auffret, E. Gautier, G. Gaudin and B. Dieny, *Sizable room-temperature magnetoresistance in cobalt based magnetic tunnel junctions with out-of-plane anisotropy,* **Appl. Phys. Lett.** **92** (2008) 102508.

[Che_06] T.-J. Chen, A. Canizo-Cabrera, C.-H. Chang, K.-A. Liao, S.C. Li, C.-K. Hou and T.-H. Wu, *Comparison of the interfacial structure between MgO and Al–O oxidation layers for perpendicular magnetic tunnel junction,* **J. Appl. Phys.** **99** (2006) 08T313.

[Cos_02] V. Da Costa, A. Iovan, K. Ounadjela, W. Allen, J.F. Gregg and B. Dieny, *Spin-polarized electronic reflections at metal–oxide interfaces*, **J. Magn. Magn. Mater.** **240** (2002) 140.

[Duc_08] C. Ducruet, B. Carvello, B. Rodmacq, S. Auffret, G. Gaudin and B. Dieny, *Magnetoresistance in Co/Pt based magnetic tunnel junctions with out-of-plane magnetization,* **J. Appl. Phys.** **103** (2008) 07A918.

[Hat_07] T. Hatori, H. Ohmori, M. Tada and S. Nakagawa, *MTJ elements with MgO barrier using RE-TM amorphous layers for perpendicular MRAM,* **IEEE Trans. Magn.** **43** (2007) 2331.

[Hay_05] J. Hayakawa, S. Ikeda, F. Matsukura, H. Takahashi and H. Ohno, *Dependence of giant tunnel magnetoresistance of sputtered CoFeB/MgO/CoFeB magnetic tunnel junctions on MgO barrier thickness and annealing temperature*, **Jap. J. Appl. Phys.** **44** (2005) L587.

[Hei_10] O.G. Heinonen and D.V. Dimitrov, *Switching-current reduction in perpendicular-anisotropy spin torque magnetic tunnel junctions,* **J. Appl. Phys.** **108** (2010) 014305.

[Hir_10] T. Hiratsuka, G. Kim, Y. Sakuraba T. Kubota, K. Kodama, N. Inami, H. Naganuma, M. Oogane, T. Nakamura, K. Takanashi and Y. Ando, *Fabrication of perpendicularly magnetized magnetic tunnel junctions with $L1_0$-CoPt/Co_2MnSi hybrid electrode,* **J. Appl. Phys.** **107** (2010) 09C714.

[Ike_07] S. Ikeda, J. Hayakawa, Y.M. Lee, F. Matsukura and H. Ohno, *Dependence of tunnel magnetoresistance on ferromagnetic electrode materials in MgO-barrier magnetic tunnel junctions*, **J. Magn. Magn. Mater.** **310** (2007) 1937.

[Ike_08] S. Ikeda, J. Hayakawa, Y. Ashizawa, Y.M. Lee, K. Miura, H. Hasegawa, M. Tsunoda, F. Matsukura and H. Ohno, *Tunnel magnetoresistance of 604% at 300 K by suppression of Ta diffusion in CoFeB/MgO/CoFeB pseudo-spin-valves annealed at high temperature*, **Appl. Phys. Lett.** **93** (2008) 082508.

[Ike_10] S. Ikeda, K. Miura, H. Yamamoto, K. Mizunuma, H.D. Gan, M. Endo, S. Kanai, J. Hayakawa, F. Matsukura and H. Ohno, *A perpendicular-anisotropy CoFeB–MgO magnetic tunnel junction,* **Nature Mater.** **9** (2010) 721.

[Jia_09] L. Jiang, H. Naganuma, M. Oogane and Y. Ando, *Large tunnel magnetoresistance of 1056% at room temperature in MgO based double barrier magnetic tunnel junction*, **Appl. Phys. Expr.** **2** (2009) 083002; *Retracted article,* **Appl. Phys. Expr.** **4** (2011) 019201.

[Joh_96] M.T. Johnson, P.J.H. Bloemen, F.J.A. den Broeder and J.J. de Vries, *Magnetic anisotropy in metallic multilayers,* **Rep. Prog. Phys.** **59** (1996) 1409.

[Jul_75] M. Jullière, *Tunneling between ferromagnetic films*, **Phys. Lett.** **54A** (1975) 225.

[Kim_08a] G. Kim, Y. Sakuraba, M. Oogane, Y. Ando and T. Miyazaki, *Tunneling magnetoresistance of magnetic tunnel junctions using perpendicular magnetization $L1_0$-CoPt electrodes,* **Appl. Phys. Lett.** **92** (2008) 172502.

[Kim_08b] W. Kim, T.D. Lee and K.-J. Lee, *Current-induced flip-flop of magnetization in magnetic tunnel junction with perpendicular magnetic layers and polarization-enhancement layers,* **Appl. Phys. Lett.** **93** (2008) 232506.

[Kis_08] T. Kishi, H. Yoda, T. Kai, T. Nagase, E. Kitagawa, M. Yoshikawa, K. Nishiyama, T. Daibou, M. Nagamine, M. Amano, S. Takahashi, M. Nakayama, N. Shimomura, H. Aikawa, S. Ikegawa, S. Yuasa, K. Yakushiji, H. Kubota, A. Fukushima, M. Oogane, T. Miyazaki and K. Ando, *Lower-current and fast switching of a perpendicular TMR for high speed and high density spin-transfer-torque MRAM*, **Int. Electron Devices Meeting** Tech. Digest (2008) 1.

[Kur_10] H. Kurt, K. Rode, K. Oguz, M. Boese, C.C. Faulkner and J.M.D. Coey, *Boron diffusion in magnetic tunnel junctions with MgO (001) barriers and CoFeB electrodes,* **Appl. Phys. Lett.** **96** (2010) 262501.

[Lee_07] Y.M. Lee, J. Hayakawa, S. Ikeda, F. Matsukura and H. Ohno, *Effect of electrode composition on the tunnel magnetoresistance of pseudo-spin-valve magnetic tunnel junction with a MgO tunnel barrier,* **Appl. Phys. Lett.** **90** (2007) 212507.

[Lee_08] C.-M. Lee, J.-M. Lee, L.-X. Ye, S.-Y. Wang, Y.-R. Wang and T.-H. Wu, *Effects of MgO barrier thickness on magnetic anisotropy energy constant in perpendicular magnetic tunnel junctions of $(Co/Pd)_n/MgO/(Co/Pt)_n$,* **IEEE Trans. Magn.** **44** (2008) 2558.

[Lee_10] C.-M. Lee, L.-X. Ye, T.-H. Hsieh, C.-Y. Huang and T.-H. Wu, *Magnetic properties of TbFeCo-based perpendicular magnetic tunnel junctions,* **J. Appl. Phys.** **107** (2010) 09C712.

[Li_10] L. Li, F. Zhang, N. Wang, Y.F. Lv, X.Y. Han and J.J. Zhang, *Interlayer exchange coupling and its temperature dependence in $[Pt/Co]_4/MgO/[Co/Pt]_2$ perpendicular magnetic tunnel junctions,* **J. Appl. Phys.** **108** (2010) 073908.

[Lim_09] D. Lim, K. Kim, S. Kim, W.Y. Jeung and S.-R. Lee, *Study on exchange-biased perpendicular magnetic tunnel junction based on Pd/Co multilayers,* **IEEE Trans. Magn.** **45** (2009) 2407.

[Liu_09] L. Liu, T. Moriyama, D.C. Ralph, and R.A. Buhrman, *Reduction of the spin-torque critical current by partially cancelling the free layer demagnetization field*, **Appl. Phys. Lett.** **94** (2009) 122508.

[Man_06] S. Mangin, D. Ravelosona, J.A. Katine, M.J. Carey, B.D. Terris and E.E. Fullerton, *Current-induced magnetization reversal in nanopillars with perpendicular anisotropy,* **Nature Mater.** **5** (2006) 210.

[Man_08a] A. Manchon, C. Ducruet, L. Lombard, S. Auffret, B. Rodmacq, B. Dieny, S. Pizzini, J. Vogel, V. Uhlir, M. Hochstrasser and G. Panaccione, *Analysis of oxygen induced anisotropy crossover in Pt/Co/MOx trilayers,* **J. Appl. Phys.** **104** (2008) 043914.

[Man_08b] A. Manchon, S. Pizzini, J. Vogel, V. Uhlir, L. Lombard, C. Ducruet, S. Auffret, B. Rodmacq, B. Dieny, M. Hochstrasser and G. Panaccione, *X-ray analysis of oxygen-induced perpendicular magnetic anisotropy in Pt/Co/AlOx trilayers,* **J. Magn. Magn. Mater.** **320** (2008) 1889.

[Mes_70] R. Meservey, P.M. Tedrow and P. Fulde, *Magnetic field splitting of quasiparticle states in superconducting aluminium films*, **Phys. Rev. Lett.** **25** (1970) 1270.

[Miz_09] K. Mizunuma, S. Ikeda, J.H. Park, H. Yamamoto, H. Gan, K. Miura, H. Hasegawa, J. Hayakawa, F. Matsukura and H. Ohno, *MgO barrier-perpendicular magnetic tunnel*

junctions with CoFe/Pd multilayers and ferromagnetic insertion layers, **Appl. Phys. Lett.** **95** (2009) 232516.

[Miz_10] K. Mizunuma, S. Ikeda, H. Yamamoto, H.D. Gan, K. Miura, H. Hasegawa, J. Hayakawa, K. Ito, F. Matsukura and H. Ohno, *CoFeB inserted perpendicular magnetic tunnel junctions with CoFe/Pd multilayers for high tunnel magnetoresistance ratio,* **Jap. J. Appl. Phys.** **49** (2010) 04DM04.

[Miz_11a] K. Mizunuma, S. Ikeda, H. Sato, M. Yamanouchi, H.-D. Gan, K. Miura, H. Yamamoto, J. Hayakawa, F. Matsukura and H. Ohno, *Tunnel magnetoresistance properties and annealing stability in perpendicular anisotropy MgO-based magnetic tunnel junctions with different stack structures*, **J. Appl. Phys.** **109** (2011) 07C711.

[Miz_11b] K. Mizunuma, M. Yamanouchi, S. Ikeda, H. Sato, H. Yamamoto, H.-D. Gan, K. Miura, J. Hayakawa, F. Matsukura and H. Ohno, *Pd layer thickness dependence of tunnel magnetoresistance properties in CoFeB/MgO-based magnetic tunnel junctions with perpendicular anisotropy CoFe/Pd multilayers*, **Appl. Phys. Expr.** **4** (2011) 023002.

[Mon_02] S. Monso, B. Rodmacq, S. Auffret, G. Casali, F. Fettar, B. Gilles, B. Dieny and P. Boyer, *Crossover from in-plane to perpendicular anisotropy in Pt/CoFe/AlO_x sandwiches as a function of Al oxidation: A very accurate control of the oxidation of tunnel barriers,* **Appl. Phys. Lett.** **80** (2002) 4157.

[Moo_95] J.S. Moodera, L.R Kinder, T.M. Wong and R. Meservey, *Large magnetoresistance at room temperature in ferromagnetic thin film tunnel junctions*, **Phys. Rev. Lett.** **74** (1995) 3273.

[Mor_10] T. Moriyama, T.J. Gudmundsen, P.Y. Huang, L. Liu, D.A. Muller, D.C. Ralph and R.A. Buhrman, *Tunnel magnetoresistance and spin torque switching in MgO-based magnetic tunnel junctions with a Co/Ni multilayer electrode*, **Appl. Phys. Lett.** **97** (2010) 072513.

[Muk_09] S.S. Mukherjee, D. Mac Mahon, F. Bai, C.-L. Lee and S.K. Kurinec, *Study of boron diffusion in MgO in CoFeB/MgO film stacks using parallel electron energy loss spectroscopy*, **Appl. Phys. Lett.** **94** (2009) 082110.

[Nak_08] M. Nakayama, T. Kai, N. Shimomura, M. Amano, E. Kitagawa, T. Nagase, M. Yoshikawa, T. Kishi, S. Ikegawa and H. Yoda., *Spin transfer switching in TbCoFe/CoFeB/MgO/CoFeB/TbCoFe magnetic tunnel junctions with perpendicular magnetic anisotropy,* **J. Appl. Phys.** **103** (2008) 07A710.

[Nis_02] N. Nishimura, T. Hirai, A. Koganei, T. Ikeda, K. Okano, Y. Sekiguchi and Y. Osada, *Magnetic tunnel junction device with perpendicular magnetization films for high-density magnetic random access memory,* **J. Appl. Phys.** **91** (2002) 5246.

[Ngu_05] P. Nguyen and Y. Huai, *Spin transfer magnetic element with free layers having high perpendicular anisotropy and in-plane equilibrium magnetization,* **US 2005189574 (A1)**.

[Nis_09a] L.E. Nistor, B. Rodmacq, S. Auffret and B. Dieny, *Pt/Co/oxide and oxide/Co/Pt electrodes for perpendicular magnetic tunnel junctions,* **Appl. Phys. Lett.** **94** (2009) 012512.

[Nis_09b] L.E. Nistor, B. Rodmacq, S. Auffret, A. Schuhl and B. Dieny, *Antiferromagnetic coupling in sputtered MgO tunnel junctions with perpendicular magnetic anisotropy,* **IEEE Trans. Magn.** **45** (2009) 3472.

[Nis_10a] L.E. Nistor, B. Rodmacq, S. Auffret, A. Schuhl, M. Chshiev and B. Dieny, *Oscillatory interlayer exchange coupling in MgO tunnel junctions with perpendicular magnetic anisotropy,* **Phys. Rev. B** **81** (2010) 220407 (R).

[Nis_10b] L.E. Nistor, B. Rodmacq, C. Ducruet, C. Portemont, I.L. Prejbeanu and B. Dieny, *Correlation between perpendicular anisotropy and magnetoresistance in magnetic tunnel junctions,* **IEEE Trans. Magn.** **46** (2010) 1412.

[Nis_11] L.E. Nistor, B. Rodmacq, S. Auffret and B. Dieny, *Low effective demagnetizing field in magnetic tunnel junctions,* Intermag Conference, Taipei (Taiwan) Apr. 25-29 (2011).

[Ohm_08a] H. Ohmori, T. Hatori and S. Nakagawa, *Fabrication of MgO barrier for a magnetic tunnel junction in as-deposited state using amorphous RE–TM alloy*, **J. Magn. Magn. Mater.** **320** (2008) 2963.

[Ohm_08b] H. Ohmori, T. Hatori and S. Nakagawa, *Perpendicular magnetic tunnel junction with tunneling magnetoresistance ratio of 64% using MgO (100) barrier layer prepared at room temperature,* **J. Appl. Phys.** **103** (2008) 07A911.

[Par_04] S.S.P. Parkin, C. Kaiser, A. Panchula, P.M. Rice, B. Hughes, M.H Samant and S.-H. Yang, *Giant tunnelling magnetoresistance at room temperature with MgO (100) tunnel barriers,* **Nature Mater. 3** (2004) 862.

[Par_08a] J.-H. Park, C. Park, T. Jeong, M.T. Moneck, N.T. Nufer and J.-G. Zhu, *Co/Pt multilayer based magnetic tunnel junctions using perpendicular magnetic anisotropy*, **J. Appl. Phys. 103** (2008) 07A917.

[Par_08b] J.-H. Park, C. Park and J.-G. Zhu, *Interfacial oxidation enhanced perpendicular magnetic anisotropy in* low *resistance magnetic tunnel junctions composed of Co/Pt multilayer electrodes*, **IEEE Trans. Magn. 44** (2008) 2577.

[Par_09] J.-H. Park, S. Ikeda, H. Yamamoto, H. Gan, K. Mizunuma, K. Miura, H. Hasegawa, J. Hayakawa, K. Ito, F. Matsukura and H. Ohno, *Perpendicular magnetic tunnel junctions with CoFe/Pd multilayer electrodes and an MgO barrier*, **IEEE Trans. Magn. 45** (2009) 3476.

[Per_07] P. de Person, P. Warin, M. Jamet, C. Beigne and Y. Samson, *Magnetic coupling between high magnetization perpendicular electrodes in an epitaxial FePt/MgO/FePt magnetic tunnel junction*, **Phys. Rev. B 76** (2007) 184402.

[Rod_03] B. Rodmacq, S. Auffret, B. Dieny, S. Monso and P. Boyer, *Crossovers from in-plane to perpendicular anisotropy in magnetic tunnel junctions as a function of the barrier degree of oxidation,* **J. Appl. Phys. 93** (2003) 7513.

[Rod_09] B. Rodmacq, A. Manchon, C. Ducruet, S. Auffret and B. Dieny, *Influence of thermal annealing on the perpendicular magnetic anisotropy of Pt/Co/AlOx trilayers,* **Phys. Rev. B 79** (2009) 024423.

[Sbi_09] R. Sbiaa, R. Law, E.-L. Tan and T. Liew, *Spin transfer switching enhancement in perpendicular anisotropy magnetic tunnel junctions with a canted in-plane spin polarizer*, **J. Appl. Phys. 105** (2009) 013910.

[Slo_89] J.C. Slonczewski, *Conductance and exchange coupling of 2 ferromagnets separated by a tunnelling barrier*, **Phys. Rev. B 39** (1989) 6995.

[Ste_77] M.B. Stearns, *Simple explanation of tunneling spin-polarization of Fe, Co, Ni and its alloys*, **Physica B&C 91** (1977) 37.

[Tad_10] Z.R. Tadisina, A. Natarajarathinam, B.D. Clark, A.L. Highsmith, T. Mewes, S. Gupta, E. Chen and S. Wang, *Perpendicular magnetic tunnel junctions using Co-based multilayers*, **J. Appl. Phys. 107** (2010) 09C703.

[Ted_71] P.M. Tedrow and R. Meservey, *Spin-dependent tunnelling into ferromagnetic nickel*, **Phys. Rev. Lett. 26** (1971) 192.

[Wan_10] Y. Wang, W.X. Wang, H.X. Wei, B.S. Zhang, W.S. Zhan and X.F. Han, *Effect of annealing on the magnetic tunnel junction with Co/Pt perpendicular anisotropy ferromagnetic multilayers*, **J. Appl. Phys. 107** (2010) 09C711.

[Wan_11] W.X. Wang, Y. Yang, H. Naganuma, Y. Ando, R.C. Yu and X.F. Han, *The perpendicular anisotropy of Co40Fe40B20 sandwiched between Ta and MgO layers and its application in CoFeB/MgO/CoFeB tunnel junction*, **Appl. Phys. Lett. 99** (2011) 012502.

[Wat_09] D. Watanabe, S. Mizukami, M. Oogane, H. Naganuma, Y. Ando and T. Miyazaki, *Fabrication of MgO-based magnetic tunnel junctions with CoCrPt perpendicularly magnetized electrodes*, **J. Appl. Phys. 105** (2009) 07C911.

[Wei_07] H.X. Wei, Q.H. Qin, M. Ma, R. Sharif and X.F. Han, *80% tunneling magnetoresistance at room temperature for thin Al-O barrier magnetic tunnel junction with CoFeB as free and reference layers*, **J. Appl. Phys. 101** (2007) 09B501.

[Wor_03] D.C. Worledge and P.L. Trouilloud, *Magnetoresistance measurement of unpatterned magnetic tunnel junction wafers by current-in-plane tunneling*, **Appl. Phys. Lett. 83** (2003) 84.

[Wor_10] D.C. Worledge, G. Hu, P.L. Trouilloud, D.W. Abraham, S. Brown, M.C. Gaidis, J. Nowak, E.J. O'Sullivan, R.P. Robertazzi, J.Z. Sun and W.J. Gallagher, *Switching distributions and write reliability of perpendicular spin torque MRAM,* **Int. Electron Devices Meeting** Tech. Digest (2010) 296.

[Wor_11] D.C. Worledge, G. Hu, D.W. Abraham, J.Z. Sun, P.L. Trouilloud, J. Nowak, S. Brown, M.C. Gaidis, E.J. O'Sullivan and R.P. Robertazzi, *Spin torque switching of perpendicular Ta/CoFeB/MgO-based magnetic tunnel junctions,* **Appl. Phys. Lett.** **98** (2011) 022501.

[Yak_10a] K. Yakushiji, T. Saruya, H. Kubota, A. Fukushima, T. Nagahama, S. Yuasa and K. Ando, *Ultrathin Co/Pt and Co/Pd superlattice films for MgO-based perpendicular magnetic tunnel junctions,* **Appl. Phys. Lett.** **97** (2010) 232508.

[Yak_10b] K. Yakushiji, K. Noma, T. Saruya, H. Kubota, A. Fukushima, T. Nagahama, S. Yuasa and K. Ando, *High magnetoresistance ratio and low resistance–area product in magnetic tunnel junctions with perpendicularly magnetized electrodes*, **Appl. Phys. Exp.** **3** (2010) 053003.

[Yan_10] H.X. Yang, M. Chshiev, A. Kalitsov, A. Schuhl and W.H. Butler, *Effect of structural relaxation and oxidation conditions on interlayer exchange coupling in Fe/MgO/Fe tunnel junctions*, **Appl. Phys. Lett.** **96** (2010) 262509.

[Yan_11] H.X. Yang, M. Chshiev, B. Dieny, J.H. Lee, A. Manchon and K.H. Shin, *First-principles investigation of the very large perpendicular magnetic anisotropy at Fe/MgO and Co/MgO interfaces*, **Phys. Rev. B** **84** (2011) 054401.

[Ye_08a] L.-X. Ye, C.-M. Lee, Y.-J. Chang and T.-H. Wu, *Effect of annealing and barrier thickness on MgO-based magnetic tunnel junctions with perpendicular anisotropy*, **J. Appl. Phys.** **103** (2008) 07F521.

[Ye_08b] L.-X. Ye, C.-M. Lee, J.-W. Syu, Y.-R. Wang, K.-W. Lin, Y.-H. Chang and T.-H. Wu, *Effect of annealing and barrier thickness on MgO-based Co/Pt and Co/Pd multilayered perpendicular magnetic tunnel junctions*, **IEEE Trans. Magn.** **44** (2008) 3601.

[Ye_10] L.-X. Ye, C.-M. Lee, J.-H. lLai, A. Canizo-Cabrera, W.-J. Chen and T.-H. Wu, *Magnetic properties of MgO-based RE-TM perpendicular magnetic tunnel junctions*, **J. Magn. Magn. Mat.** **322** (2010) L9.

[Yod_10] H. Yoda, T. Kishi, T. Nagase, M. Yoshikawa, K. Nishiyama, E. Kitagawa, T. Daibou, M. Amano, N. Shimomura, S. Takahashi, T. Kai, M. Nakayama, H. Aikawa, S. Ikegawa, M. Nagamine, J. Ozeki, S. Mizukami, M. Oogane, Y. Ando, S. Yuasa, K. Yakushiji, H. Kubota, Y. Suzuki, Y. Nakatani, T. Miyazaki and K. Ando, *High efficient spin transfer torque writing on perpendicular magnetic tunnel junctions for high density MRAMs*, **Curr. Appl. Phys.** **10** (2010) e87.

[Yoo_05] I. Yoo, D.K. Kim and Y.K. Kim, *Switching characteristics of submicrometer magnetic tunnel junction devices with perpendicular anisotropy,* **J. Appl. Phys.** **97** (2005) 10C919.

[Yos_08] M. Yoshikawa, E. Kitagawa, T. Nagase, T. Daibou, M. Nagamine, K. Nishiyama, T. Kishi and H. Yoda, *Tunnel magnetoresistance over 100% in MgO-based magnetic tunnel junction films with perpendicular magnetic $L1_0$-FePt electrodes*, **IEEE Trans. Magn.** **44** (2008) 2573.

[You_08] C.Y. You, T. Ohkubo, Y.K. Takahashi and K. Hono, *Boron segregation in crystallized MgO/amorphous-$Co_{40}Fe_{40}B_{20}$ thin films*, **J. Appl. Phys.** **104** (2008) 033517.

[Yua_00] S. Yuasa, T. Sato, E. Tamura, Y. Suzuki, H. Yamamori, K. Ando and T. Katayama, *Magnetic tunnel junctions with single-crystal electrodes: A crystal anisotropy of tunnel magneto-resistance*, **Europhys. Lett.** **52** (2000) 344.

[Yua_04] S. Yuasa, T. Nagahama, A. Fukushima, Y. Suzuki and K. Ando, *Giant room-temperature magnetoresistance in single-crystal Fe/MgO/Fe magnetic tunnel junctions,* **Nature Mater.** **3** (2004) 868.

[Yua_05] S. Yuasa, Y. Suzuki, T. Katayama and K. Ando, *Characterization of growth and crystallization processes in CoFeB/MgO/CoFeB magnetic tunnel junction structure by reflective high-energy electron diffraction*, **Appl. Phys. Lett.** **87** (2005) 242503.

[Yua_06] S. Yuasa, A. Fukushima, H. Kubota, Y. Suzuki and K. Ando, *Giant tunneling magnetoresistance up to 410% at room temperature in fully epitaxial Co/MgO/Co magnetic tunnel junctions with bcc Co(001) electrodes,* **Appl. Phys. Lett.** **89** (2006) 042505.

[Yua_07] S. Yuasa and D.D. Djayaprawira, *Giant tunnel magnetoresistance in magnetic tunnel junctions with a crystalline MgO(001) barrier*, **J. Phys. D: Appl. Phys.** **40** (2007) R337.

[Zha_03] X.-G. Zhang, W.H. Butler and A. Bandyopadhyay, *Effects of the iron-oxide layer in Fe-FeO-MgO-Fe tunneling junctions*, **Phys. Rev. B** **68** (2003) 092402.

[Zha_04] X.-G. Zhang and W.H. Butler, *Large magnetoresistance in bcc Co/MgO/Co and FeCo/MgO/FeCo tunnel junctions*, **Phys. Rev. B** **70** (2004) 172407.

[Zha_10] Z. Zhang, Y. Qiu, Q.Y. Jin and Y. Liu, *Micromagnetic study of fieldlike spin torque effect on the magnetization switching in tunnel junctions with perpendicular anisotropy,* **Appl. Phys. Lett.** **97** (2010) 172501.

[Zhu_09] X. Zhua and S.H. Kang, *Inherent spin transfer torque driven switching current fluctuations in magnetic element with in-plane magnetization and comparison to perpendicular design*, **J. Appl. Phys.** **106** (2009) 113906.

[Zhu_11] W. Zhu, Y. Liu and C.-G. Duan, *Modeling of the spin-transfer torque switching in FePt/MgO-based perpendicular magnetic tunnel junctions: A combined ab initio and micromagnetic simulation study*, **Appl. Phys. Lett.** **99** (2011) 032508.

Chapter III

INDIRECT EXCHANGE COUPLING IN PERPENDICULAR MAGNETIC TUNNEL JUNCTIONS

Chapter III

INDIRECT EXCHANGE COUPLING IN PERPENDICULAR MAGNETIC TUNNEL JUNCTIONS

More than twenty years ago, the discoveries of antiferromagnetic (AF) exchange coupling between Fe layers through a Cr spacer **[Grü_86]** and of giant magnetoresistance in magnetic multilayered structures **[Bai_88]** opened the way to important technological developments in the field of spintronics **[Die_91, Fer_01, Wol_01]**. These discoveries triggered numerous experimental and theoretical investigations **[Fer_94]**. In particular, the oscillatory character of exchange coupling as a function of the spacer and ferromagnetic (FM) layer thicknesses in metallic sandwiched structures was observed **[Par_90, Par_91, Blo_94]**.

Before the intense development of MgO-based junctions motivated by their transport properties **[Yua_06, Ike_08]**, fundamental aspects have been addressed, like electronic band matching at interfaces **[But_01, Mat_01]** and indirect exchange coupling (**IEC**) **[Fau_02, Kat_06, Yan_07, Wu_08]** through the insulating barrier, leading to antiferromagnetic coupling for small barrier thicknesses. Experimental studies conducted on fully epitaxial Fe/MgO/Fe MTJ structures **[Fau_02, Kat_06]** as well as in Fe/MgO/γ-Fe_2O_3 **[Yan_07]** and Fe_3O_4/MgO/Fe_3O_4 **[Wu_08]** ones addressed the variation of indirect exchange coupling as a function of both barrier thickness and measurement temperature. This AF coupling strongly increases in amplitude as the MgO thickness is reduced down to a critical thickness below which pinholes formation takes place, leading to direct ferromagnetic coupling between magnetic electrodes. The AF coupling amplitude was observed to increase as a function of measurement temperature. The results were found in qualitative agreement with earlier theories by Slonczewski and Bruno **[Slo_95, Bru_95]**. Furthermore, studies on Fe/MgO/γ-Fe2O3 structures **[Yan_07]** suggested that the coupling strength not only depends on the spacer material but also on the ferromagnetic material and its electronic state.

Concerning in-plane epitaxial tunnel junctions, AF IEC has been ascribed, through *ab-initio* calculations, to either oxygen vacancies in the MgO barrier **[Kat_06]** or oxidation of the magnetic electrodes **[Wu_08]**. More recent theoretical investigations based on first-principles calculations in Fe/MgO/Fe structures **[Yan_11]** showed the impact of structural relaxation and oxidation conditions on the nature of IEC in MTJs. IEC is found to be antiferromagnetic for relaxed structures in agreement with experiments. Furthermore, it was shown that the oxygen concentration at the Fe/MgO interface plays a critical role in the IEC strength: vacancy strongly enhances the AF IEC while additional oxygen, on the contrary, weakens the AF IEC and may even change its sign to ferromagnetic.

All these theoretical studies on the IEC should be taken with care in the case of sputtered MTJ. Things are more complicated since these structures are far from being perfect in terms of layers crystallinity and interface roughness, contrary to the case of epitaxial structures.

On another hand, there is a growing interest in magnetic tunnel junctions with perpendicular magnetic anisotropy (PMA), as we showed in the preceding **Chapter**. These structures are known for their larger thermal stability and better efficiency for spin transfer torque switching, as has been demonstrated in perpendicular spin-valves **[Man_06]**. However, there exist very few basic studies on indirect coupling in these structures. Using an insulating NiO spacer separating two (Co/Pt) multilayers, Liu and Adenwalla **[Liu_03]** observed an increase in indirect coupling as a function of measurement temperature, as predicted by Bruno **[Bru_95]**. At the same

time, they observed an oscillatory variation of the coupling with spacer thickness, which they tentatively attributed to the antiferromagnetic structure of the NiO spacer.

In general all these studies on planar and perpendicular MTJ suggest that the behavior of the tunneling electrons at the interface is quite important for IEC. However, no experimental information exists in literature about IEC through an insulator in MgO-based junctions comprising electrodes with out-of-plane anisotropy. Since it has been recently predicted **[Mor_04]** that roughness induced Néel dipolar coupling **[Née_62]** in perpendicularly magnetized structures could turn from ferromagnetic to antiferromagnetic when increasing PMA it is interesting to investigate how the PMA will affect the IEC in pMTJ.

We present in this Chapter evidence for antiferromagnetic coupling in non-epitaxial perpendicular MgO-based tunnel junctions prepared by dc sputtering. This coupling is studied as a function of annealing treatments, measurement temperature, and also as a function of the thickness of both barrier and magnetic electrodes **[Nis_09b, Nis_10]**. A correlation is observed between the IEC amplitude and the perpendicular interfacial anisotropy at the barrier/electrode interface. Furthermore, an oscillatory variation of AF coupling as a function of the magnetic electrode thickness is reported, in agreement with Bruno's predictions **[Bru_93]**.

III-1. Indirect exchange coupling: theoretical models and experimental determination

In the literature there are different possible interpretations of the coupling between two magnetic layers separated by an insulator. A first approach is based on the behavior of the tunneling electrons represented by the Slonczewski's spin-current model and Bruno's indirect exchange coupling model. The second concerns the influence dipolar coupling induced by interface roughness (Néel orange peel coupling) and its recent extension to the case of perpendicular anisotropy. The different approaches are presented in the following sections.

III-1.1 Slonczewski's and Bruno's models

IEC can be interpreted either in terms of the spin torque exerted by one ferromagnetic layer on the other one [Slo_95], or in terms of density of states in the spacer induced by the ferromagnet [Bru_95]. First phenomenological explanations for the indirect coupling across an insulator (at T=0) were presented by Slonczewski in the framework of spin-current model (V=0, no current flowing trough the barrier and no energy dissipation). The so-called "conservative exchange coupling" is associated with the spin information transport across the insulating barrier by spin-polarized s electrons and their interaction with more localized d electrons resulting in perpendicular field like torque (produced by the rotation of the magnetization from one ferromagnetic layer relative to another).

For an insulating spacer, theory predicts a non-oscillatory exponential decrease of IEC with increasing barrier thickness, reflecting the tunnelling mechanism of the coupling [Sti_05]. According to Slonczewski's model [Slo_95], IEC changes sign and becomes antiferromagnetic for a relatively low potential barrier.

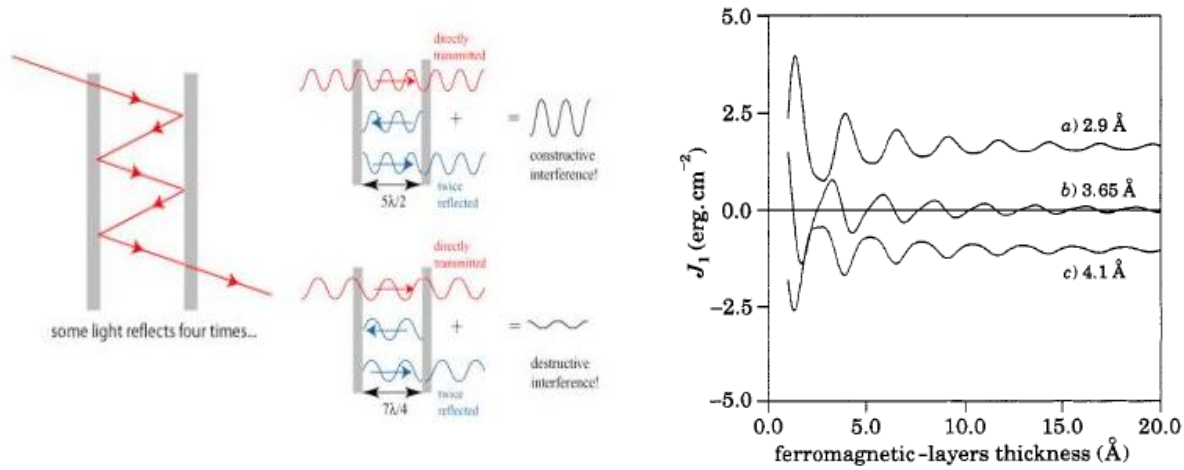

Figure III-1: (a) Thin films acting as Fabry Perot cavities; (b) Resonator model: coupling oscillations in the ferromagnetic layer as a function of its thickness for different paramagnetic spacer thicknesses (from [Bru_93]).

Bruno proposed a general approach to the interlayer coupling offering at the same time a deep physical insight of the phenomenon and a simple technique to obtain analytical results. In this approach the interlayer coupling is ascribed to quantum interferences of electron waves in the ferromagnetic layer due to (spin-dependent) reflections at the magnetic metal/spacer interfaces [Bru_93, Bru_95]. This can be simply explained by analogy to the finite layers with an optical

Fabry-Perot cavity. Adding a ferromagnetic layer to a spacer will modify its electronic structure at the interface resulting in the reflection of the electrons at the spacer/ferromagnet interface.

Figure III-1a presents the case of a two ferromagnetic films separated by a spacer (limited spacer thickness). In this case multiple reflections will take place in the spacer at both interfaces with the ferromagnetic layers. But in reality ferromagnetic layers are also limited and have interfaces with metals, so reflections will be expected also at the magnetic layer/metal interface. As a consequence the quantum interferences approach was first used to explain the oscillatory behaviour of coupling as a function of ferromagnetic layers thickness obtained by Barnas et al. **[Bar_92]** with a free electron model.

In the limit of large spacer thickness D and ferromagnet layers of finite thickness L, an analytical expression of the coupling was obtained, describing the coupling oscillation as a function of the magnetic thickness with a period given by $k_{\downarrow}$ (Fermi wave vector of minority spin electrons in the ferromagnet) and an amplitude decreasing as L^2. For small magnetic layer thicknesses (finite layers), multiple reflections take place, producing a decrease of the coupling when the thickness increases, since by analogy with optics the reflection coefficients are proportional to the layer thickness.

$$J_1 = \frac{1}{4\pi^2}\frac{\hbar^2}{2m}\mathrm{Im}\left\{\frac{r_{\infty}^{\downarrow 2}}{2}\exp[2ik_F D]\left[\frac{k_F^2}{D^2} - 2(1-r_{\infty}^{\downarrow 2})\left(\frac{D}{k_F}+\frac{L}{k_F^{\downarrow}}\right)^{-2}\exp[2ik_F^{\downarrow} L]\right]\right\} \quad \textbf{(Equation III-1)}$$

The oscillatory behaviour of IEC as a function of the ferromagnetic layers thickness is to be expected in general for insulating or metallic spacers as it can be observed in **Equation III-1** by the presence of the exponential layer thickness term. Bruno presented only the case of the variation of the coupling with magnetic layers separated by a metallic spacer, presented in **Figure III-1b**. One can observe that coupling oscillates around different energy values (positive, negative or zero) depending on the metallic spacer thickness D. Bruno also used this resonator model to explain the variation of coupling with the metallic/insulator spacer thickness and to predict its variation with temperature.

Electron states in the spacer can be propagative Bloch states (as in bulk metallic spacers) and also evanescent waves (insulator) because of the finite thickness of the spacer. Considering the complex Fermi surface **[Bru_95]**, the quantum interference approach allows treating metal and insulator spacers in a unified manner. Both electron states contribute to the coupling giving different behaviours: propagative states (metal spacer) give rise to oscillatory contributions, while evanescent states (insulator) yield exponentially decreasing contribution (see **Figure III-2**). This can be described mathematically by considering the electrodes space vector k_F as a real quantity for metals and imaginary for insulator, which will change the exp(2ikD) term contribution in the above **Equation III-1**.

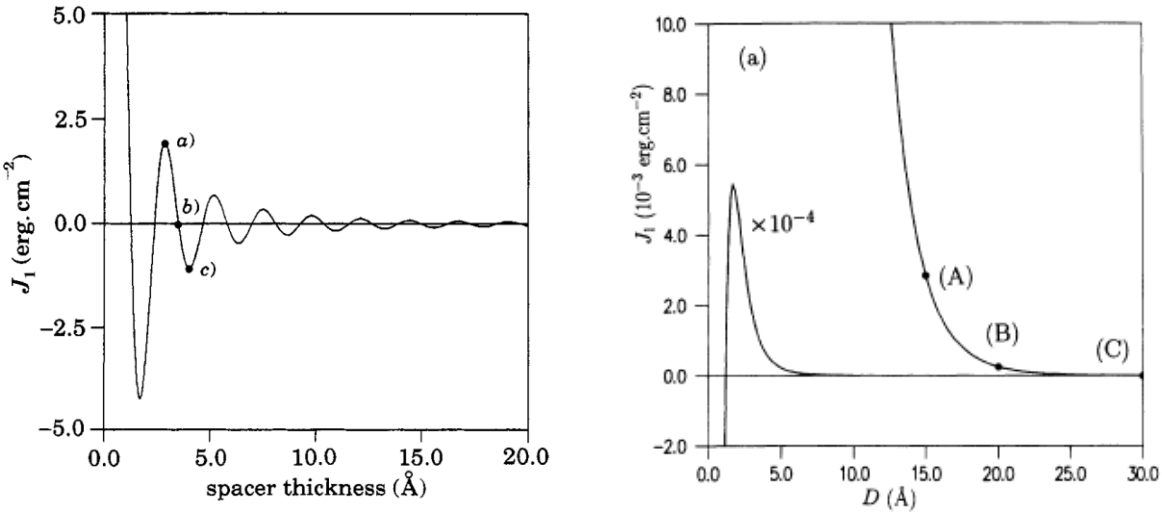

Figure III-2: Bruno's model [Bru_93, Bru_95] describing the variation of the coupling with (a) A metal spacer and (b) An insulating spacer.

Furthermore in the case of an insulating spacer at T=0K Bruno's model reduces to Slonczewski's results: the coupling strength exponentially decreases with increasing the layer thickness showing the transport character of the barrier represented in **Figure III-2**. In this case the change of sign in the coupling for low insulator thickness is explained by including contributions from states well above the Fermi level. For large spacer thicknesses the most important contribution to the coupling arises from the neighborhood of the Fermi level and it depends on the Fermi wave vector for majority-spin (minority spin) electrons in the ferromagnet. According to Bruno's model the coupling sign depends on the wave vectors of spin up (k↑) and spin down (k↓) electrons in the ferromagnet and in the insulating layer (k) as follows: when $ki^2<k\uparrow k\downarrow$ an antiferromagnetic coupling is expected, in the other case $ki^2>k\uparrow k\downarrow$ a ferromagnetic coupling is expected.

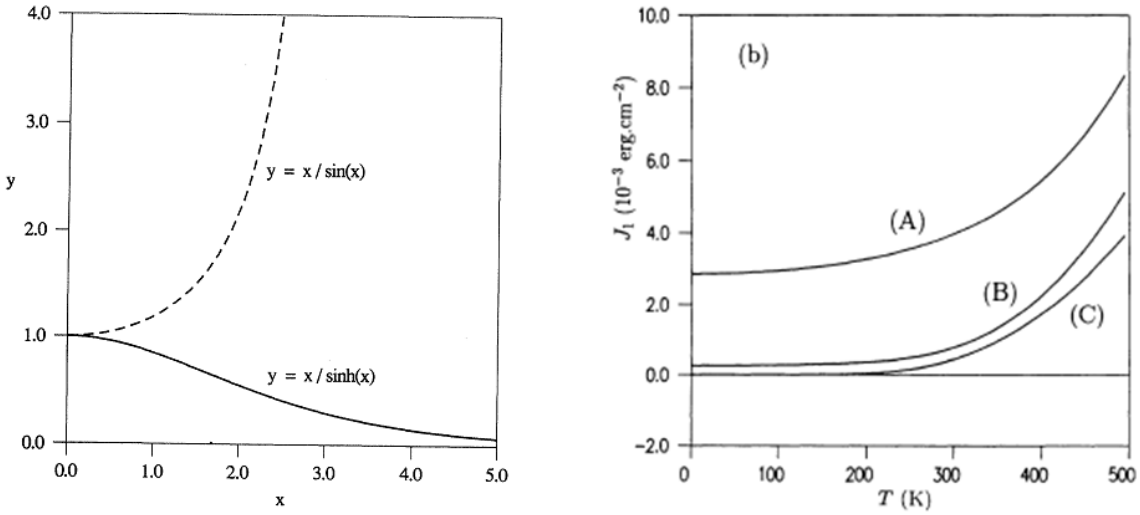

Figure III-3: Temperature variation of the coupling for a metallic spacer (left) and an insulating layer for three different thicknesses (right) [Bru_93, Bru_95].

Bruno's theoretical model **[Bru_95]** predicts that changes in the electronic density of states of the barrier have a crucial importance for the strength of IEC, which can be also influenced by the presence of impurities or defects in the barrier **[Zhu_05]**.

Concerning the thermal variation of the coupling, Bruno's model is the first one giving a plausible explanation for experimental observations, in the framework of quantum interferences. Despite the unified treatment the temperature dependence of coupling has different variations for a metallic compared to an insulating spacer. For a metallic spacer the coupling decreases contrary to the case of an insulator spacer for which the coupling strongly increases with temperature as in shown in **Figure III-3**. In the case of a metal k_F is broadened by increasing the temperature $\Delta k_F = k_B T\ m/\hbar^2 k_F$ which produces a blurring of the coupling oscillation for $D >> k_F^{-1}$. In the case of an insulator the electron energy increases with $k_B T$ above Fermi level, resulting in a thermally assisted coupling. Bruno's model describes very well the coupling variation for metallic barrier at any temperature, but for an insulator spacer the theory is valid only at low temperature with a limit given by $T = \hbar^2 k_F / 2 k_B\ m\ D$.

III-1.2 Néel's model and its extension to perpendicular magnetization

In order to explain experimental observations of coupling between two magnetic thin layers separated by a non magnetic one, Néel introduced the magnetostatic coupling due to the surface topography of the layers **[Née_62]**, also called orange peel coupling. Interfacial roughness is commonly observed in thin films grown by sputtering. If roughness is present at the top surface of a magnetic film M_1 (**Figure III-4**), the growth of a non magnetic layer NM on top of M_1 will more or less reproduce this roughness. This will also be the case for the second magnetic layer M_2 grown on NM. The roughness at both bottom and top NM interfaces will thus be correlated. Since the in-plane magnetization of layers M_1 and M_2 cannot follow the undulation of the surface because of strong exchange coupling, dipoles charges will appear at both interfaces. These charges from the M_1/NM and NM/M_2 interfaces interact through the spacer favoring a parallel alignment (ferromagnetic) between magnetizations of M_1 and M_2 layers. An antiparallel alignment is not energetically favorable due to the presence of these dipole charges. The coupling energy is given by **[Koo_99]**:

$$J \propto \frac{\pi^2 \cdot h \cdot M_1 \cdot M_2}{\lambda \cdot \sqrt{2}} \cdot \exp\left(-\frac{2\pi\sqrt{2} \cdot t}{\lambda}\right) \qquad \textbf{Equation III-2}$$

where M_1 and M_2 are magnetizations, t the thickness of the spacer and h and λ the amplitude and wavelength of the correlated roughness.

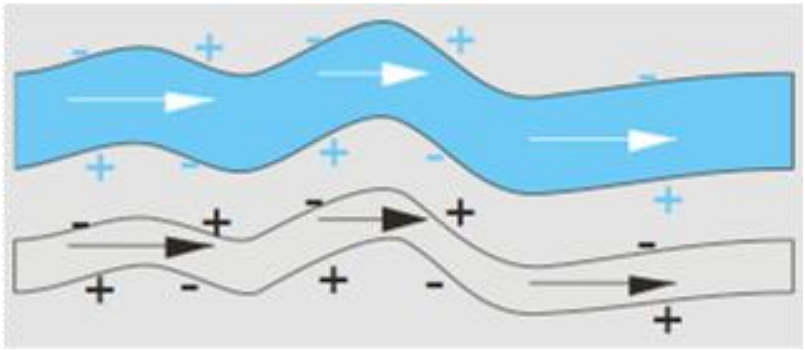

Figure III-4: Schematic representation of two magnetic layers separated by a spacer with correlated roughness in the case of in plane magnetizations.

Extension of Neel's model to perpendicularly magnetized systems was presented by Moritz et al **[Mor_04]**. In the presence of roughness, for low anisotropy energies, the magnetization of the two magnetic layers, because of strong exchange coupling, will prefer to stay uniformly parallel to the z-axis (perpendicular to the average interface plane) (**Figure III-5a**) in order to minimize the surface charges. Parallel alignment is favoured in this case, since the charge densities are opposite

in the parallel magnetic configuration. On the other hand, in the case of a system with strong anisotropy, the magnetization tends to be locally always perpendicular to the interface (**Figure III-5b**) resulting in the appearance of an in-plane contribution (projection effect) and in volume charges which are responsible for the antiferromagnetic coupling.

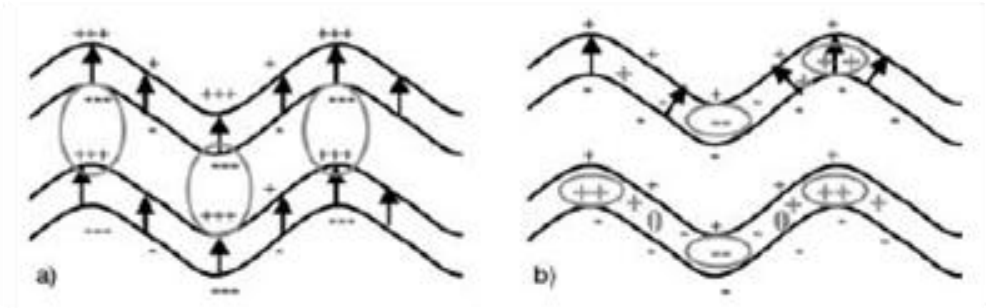

Figure III-5: Schematic representation of the magnetization in the case of (a) Low anisotropy, the average magnetization being parallel to the *z*-axis; (b) Large anisotropy, the magnetization locally follows the normal to the interface [Mor_04].

The dependence of this coupling on the strength of the uniaxial perpendicular anisotropy is presented in **Figure III-6**. For low values of the anisotropy energy, the coupling is ferromagnetic. For larger anisotropy, the coupling favours an antiparallel alignment of the magnetizations. The transition occurs for an anisotropy energy of about 1.3 10^6 J/m^3 (13 Merg/cm^3), which in the case of cobalt, corresponds to an anisotropy field of a few kOe.

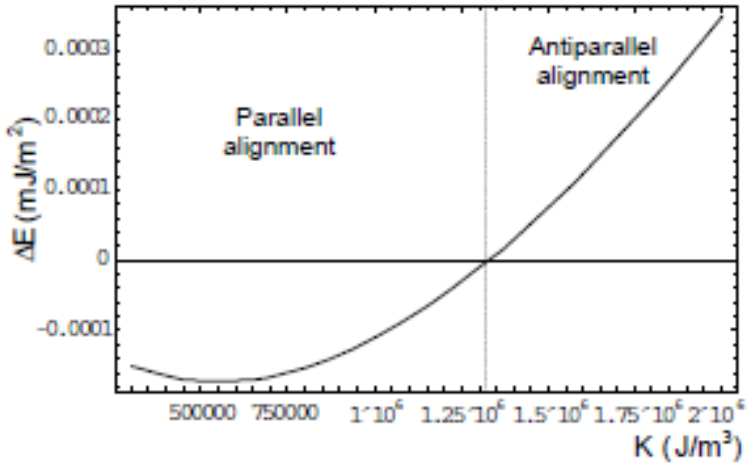

Figure III-6: Variation of the coupling energy with the anisotropy energy [Mor_04].

III-1.3 Experimental determination

In order to measure an eventual shift of the hysteresis loop, one has first to be sure of the correct calibration of the experimental set-up. In our VSM and Hall effect set-ups, the field calibration is obtained through the response of a Hall sensor. The zero of this Hall sensor is further checked by measuring the hysteresis loop of a single 50 nm thick $Ni_{80}Fe_{20}$ (permalloy) film, with a coercive field of a few Oe. The accuracy on eventual loop shifts is estimated to about 5 Oe.

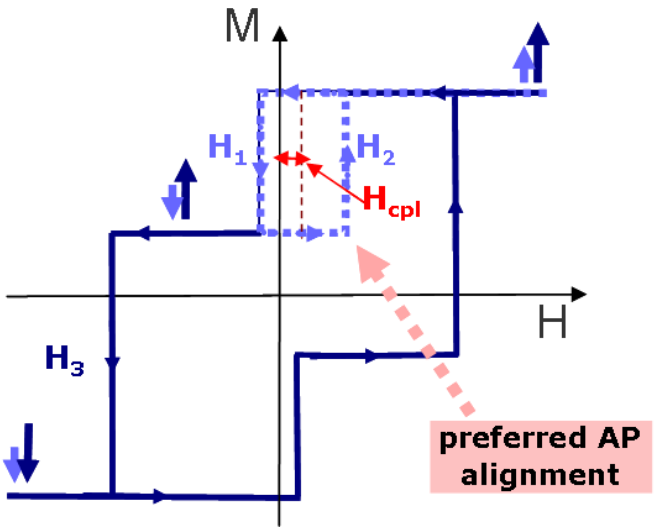

Figure III-7: Hysteresis loop for a perpendicular MTJ in out-of-plane applied field. Coming from positive saturation, the shift of the minor hysteresis loop towards positive fields indicates a preferred antiparallel alignment of the magnetizations.

The sign and amplitude of the magnetic coupling between both magnetic electrodes are determined from minor hysteresis loops (**Figure III-7**) (reversing only the magnetization of the softest layer). All minor loops are recorded with the same frequency (0.2 Hz) and field steps (5 Oe). Starting from the positive saturated state (↑↑, parallel configuration) the shift of the minor hysteresis loop towards positive field indicates a preferred antiparallel (↑↓) alignment of the magnetizations of both layers. By convention, the coupling field will be taken negative in this case. VSM and SQUID measurements can be carried out to extract absolute values of the magnetizations of both top M_{ST} and bottom M_{SB} magnetic layers with corresponding t_T and t_B thicknesses. The coupling energy is calculated by the following formula:

$$J_{cpl} = \frac{H_{cpl} \cdot M_{sT} \cdot t_T \cdot M_{sB} \cdot t_B}{M_{sT} \cdot t_T + M_{sB} \cdot t_B}$$ **Equation III-3**

III-2. Indirect exchange coupling in perpendicular junctions

Magnetic characterization of pMTJ presented in **Chapter II** sometimes showed minor hysteresis loops. However no mention was made about interlayer coupling between electrodes.

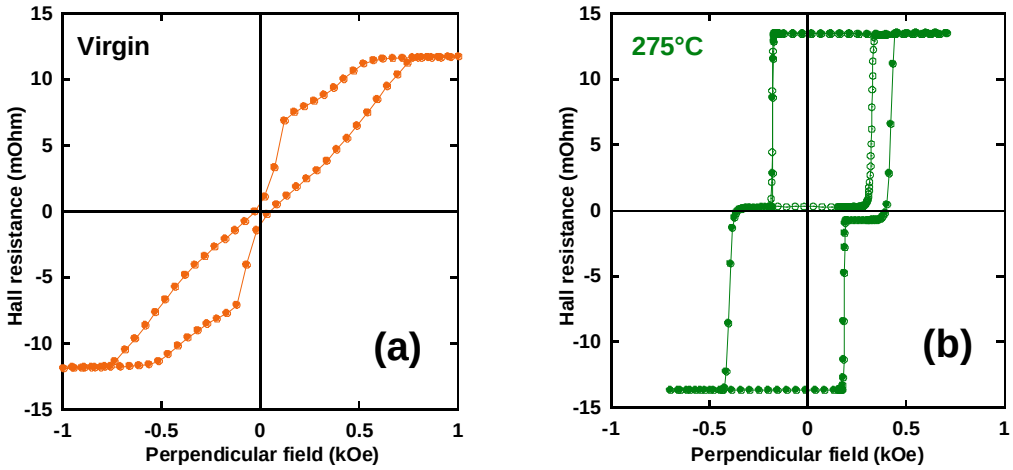

Figure III-8: Hall hysteresis loops for a Pt/Co1.2/MgO1.3/Co1.2/Pt structure (a) Before and (b) After annealing at 275°C.

Figure III-8 presents the Hall hysteresis loops for a Pt/Co1.2/MgO1.3/Co1.2/Pt structure before and after annealing at 275°C. In the as-deposited state (**Figure III-8a**), only the bottom electrode magnetization is out-of-plane, since it grows on a thick Pt buffer, thus favoring a strong interfacial perpendicular magnetic anisotropy. The top in-plane magnetized electrode saturates in a field of about -0.7 kOe, much smaller than its demagnetizing field value $4\pi Ms$ (about -18 kOe for Co), indicating a rather strong perpendicular contribution. After annealing at 275°C (**Figure III-8b**), both electrodes exhibit 100% perpendicular remanence. One can clearly observe a shift of the minor hysteresis loop of the soft layer towards positive field values, indicating a preferred antiparallel alignment of the magnetizations. Thanks to this antiferromagnetic coupling, the two magnetic transitions are clearly observed, although the coercive fields of both electrodes are very close to each other. The coupling field amounts to -68 Oe, corresponding to a coupling energy of about -4.8 10^{-3} erg/cm^2, assuming a Co magnetization of 1400 emu/cm^3.

One can note that in previous studies of epitaxial structures with in-plane magnetization [Fau_02, Yan_07], the coupling always turned ferromagnetic for MgO thicknesses larger than 0.8-0.9 nm. In our case, AF coupling is observed for a much thicker (1.3 nm) MgO layer.

III-2.1 Domains nucleation in the hard magnetic layer

A possible explanation of the observed preferred antiparallel configuration between hard and soft layers is domain replication in the hard layer, through magnetostatic interactions, as observed in (Pt/Co)/Pt/(Pt/Co) structures [Rod_06]. Even if magnetostatic coupling through stray fields are negligible in uniformly magnetized macroscopic samples, it is no more the case when the magnetic layers are in a multidomain state, or when the lateral size of the sample is reduced.

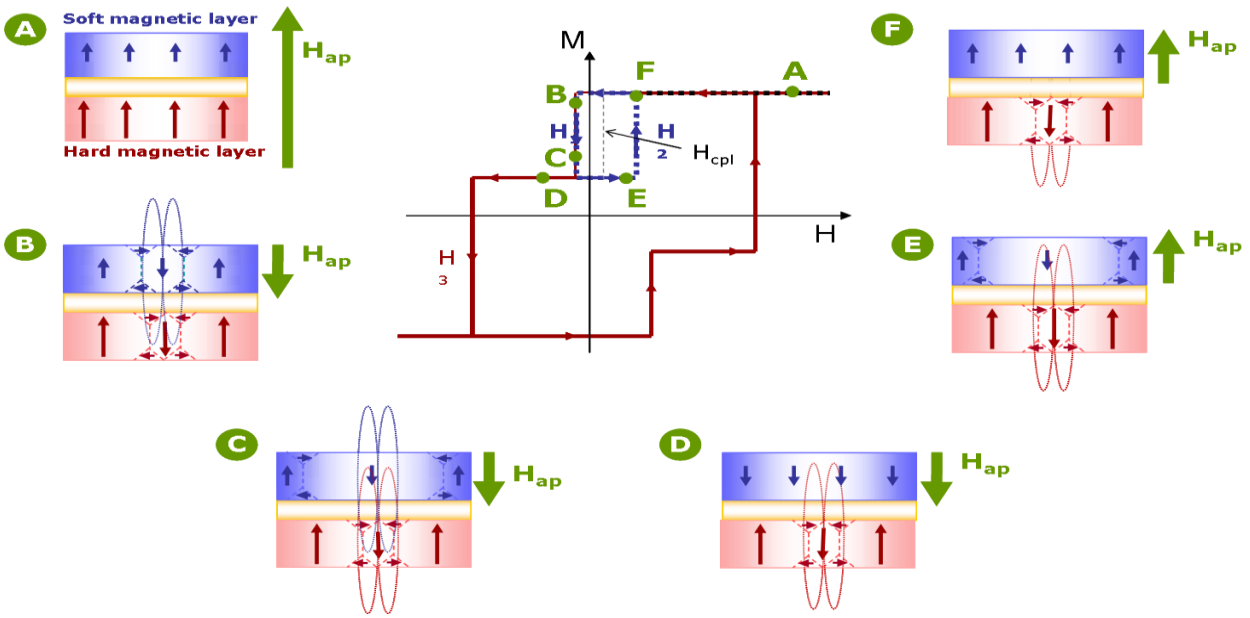

Figure III-9: Domain replication in the hard magnetic layer during switching of the soft magnetic one.

The hypothesis of domain replication is illustrated in **Figure III-9**. After saturation of the two layers in a positive applied field (**A**), the soft layer is switched by applying a field in the opposite direction. It must be noted that the switching process in these junctions is a nucleation/propagation one. When the soft layer begins to switch, the small first inverse domains will create strong stray fields which can induce replicated domains in the hard layer (**B**). If the anisotropy of the hard layer is strong enough, these domains will be stable during the complete reversal of the soft layer (**C** and **D**). When the magnetic field is now applied in the positive direction (in order to complete the minor loop of the soft layer), stray fields from the hard layer will act as a negative bias field. This will delay the back reversal of the soft layer towards positive saturation (**E**). The resulting loop shift will be some sort of antiferromagnetic coupling between soft and hard layers.

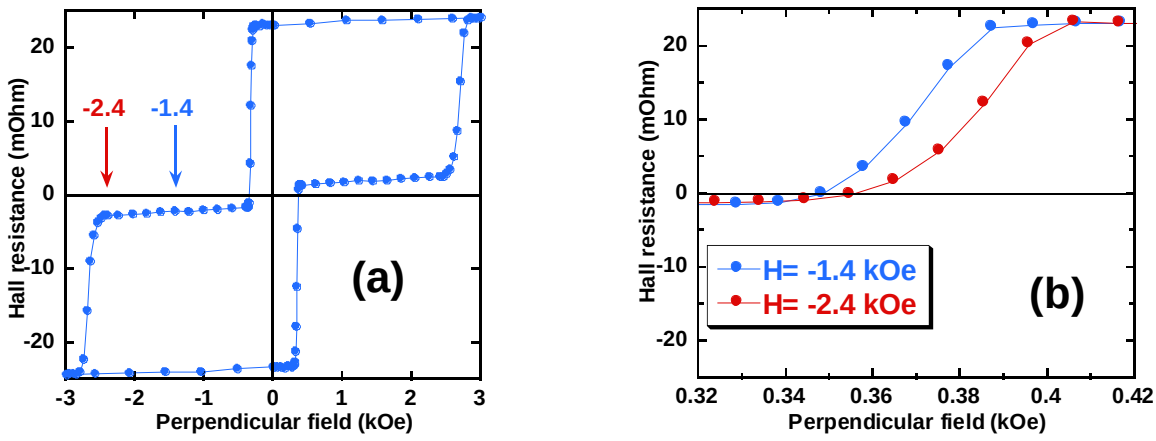

Figure III-10: (a) Major loop of a Ta3/Pt20/Co1.2/MgO1.4/Co1.5/Pt3 structure annealed at 350°C; (b) Back switching of the soft layer after application of a negative field of -1.4 kOe (blue) or -2.4 kOe (red) to switch its magnetization from parallel to antiparallel state relative to the hard layer.

This effect can be experimentally observed when the negative field used to switch the magnetization of the soft layer from "up" to "down" approaches the nucleation field of the hard layer. An example is given in **Figure III-10** for a Ta3/Pt20/Co1.2/MgO1.4/Co1.5/Pt3 sample

annealed at 350°C. **Figure III-10a** shows the major loop, and **Figure III-10b** shows the back "down-up" switching of the soft layer after having switched it from "up" to "down" in a field of -1.4 (middle of the anti-parallel plateau) or -2.4 kOe (close to the nucleation field of the hard layer). The "up-down" coercive field of the soft layer is 0.325 kOe, whereas the reverse "down-up" coercive field increases from 0.369 to 0.385 kOe. The "total" antiferromagnetic coupling field thus goes from -22 to -30 Oe. One can also note that the signal level is identical for both curves. The magnetization state of the hard layer is practically unchanged, the proportion of "down" domains created in the hard layer being extremely small.

In order to test this hypothesis of domain replication at the origin of the observed hysteresis loop shift, we tried to switch the soft layer by rotation of the magnetization instead of nucleation. To do that, one can rotate the sample under a fixed perpendicular applied field: the magnetization of the soft layer will follow the field direction during rotation, whereas the magnetization of the hard layer will keep its original direction with respect to the sample normal. The condition which must be fulfilled in order to perform this experiment is that the in-plane saturation field of the soft layer must be smaller than both the out-of-plane coercive field and in-plane saturation field of the hard layer.

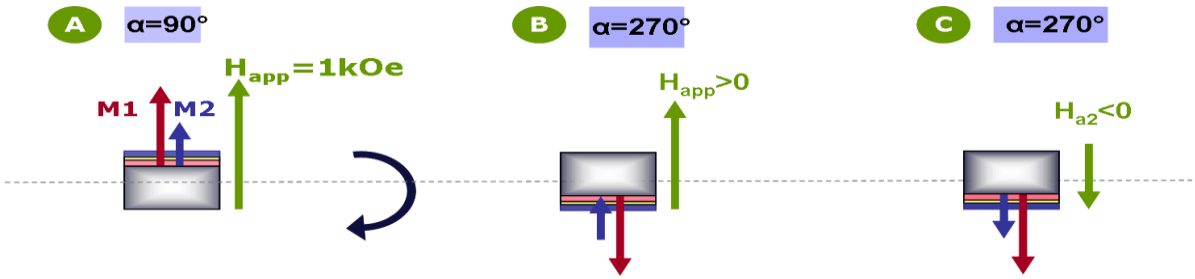

Figure III-11: Schematic representation of coherent rotation of the soft magnetic layer.

A schematic representation of the experiment is showed in **Figure III-11**. In (**A**) both layers are "up" saturated under a large positive field. The (still positive) field amplitude is then reduced to a value larger than the anisotropy of the soft layer but much lower than that of the hard one. Then (**B**), the field being kept constant, the sample is rotated from the 90° to the 270° direction with respect to the sample normal. The magnetization of the soft layer will thus keep parallel to the applied field ("up") whereas that of the hard layer will follow the sample rotation and become "down". This corresponds to a rotation of the soft layer from the parallel state to the antiparallel one. At this point, since the hard magnetization is now "down" with respect to the applied field, this applied field is decreased to negative values in order to switch back the soft layer to the parallel state (**C**). This back-switching is then compared to that obtained when measuring the minor loop in a conventional way.

Figure III-12 shows the out-of-plane and in-plane magnetization curves of a MTJ with an MgO RF-sputtered barrier. The bottom hard electrode is a Co/CoFeB layer deposited onto a Co/Pt multilayer, and the top soft one is a CoFeB/Co bilayer. The sample is annealed at 325°C, and the antiferromagnetic coupling field is -40 Oe. (**1**) and (**2**) on **Figure III-12a** denote P to AP and AP to P successive orientations of magnetic layers. The field chosen for the "rotation" experiment is 1 kOe. This value fulfils the above requirements. It is large enough to saturate the soft layer in-plane (**Figure III-12b**), but still smaller than the perpendicular nucleation field of the hard layer (1.3 kOe, **Figure III-12a**). In addition, it is much below the onset of in-plane rotation of the hard layer (about 4 kOe, **Figure III-12b**). During sample rotation, the soft layer will thus keep parallel to the applied field, whereas the hard one will keep parallel to the sample normal.

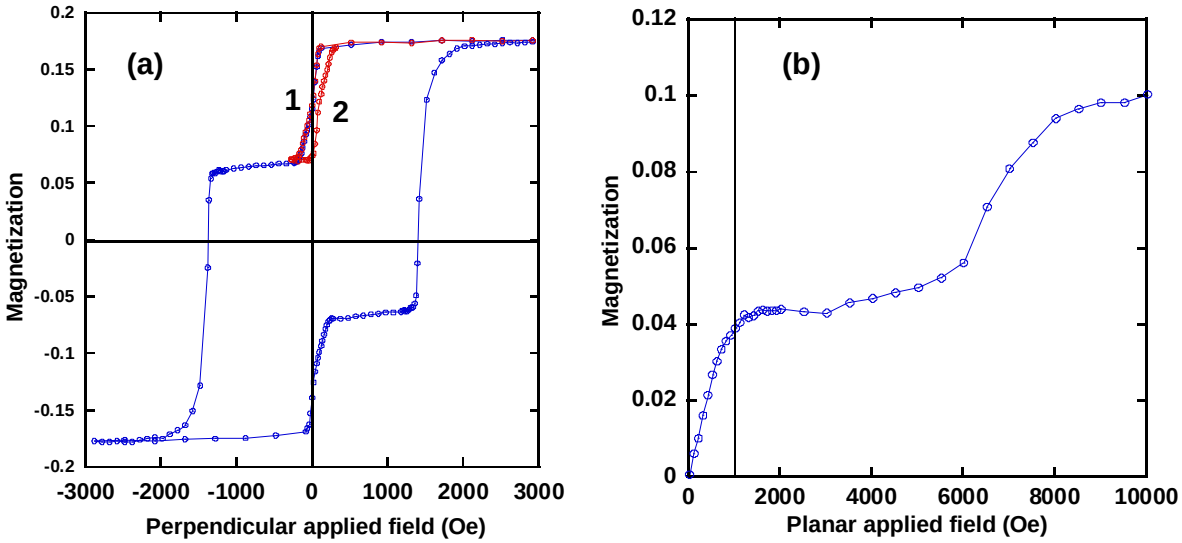

Figure III-12: (a) Out-of-plane and (b) In-plane magnetization curves of a Pt/(Co/Pt)/Co/CoFeB /MgO/CoFeB/Co/Pt structure after annealing at 325°C.

Figure III-13a gives the results of the "rotation" experiment. In (**A**), both layers are "up" saturated. In (**B**), the sample is rotated by 180°. The soft layer is still "up", and the hard layer "down". The magnetization value agrees with the evolution from (M_S+M_H) to (M_S-M_H), according to the relative amplitudes measured on **Figure III-12**. In (**C**), the soft layer switches "down" back and is again parallel to the hard layer. After a (-H → +H) and (-M → +M) transformation of curve (**3**), **Figure III-13b** shows that branches **2** and **3** of the back switching from AP to P orientation can be superimposed. This means that the shift of the minor hysteresis loop is not related to dipolar interactions due to domain formation in the hard layer when the soft layer switches.

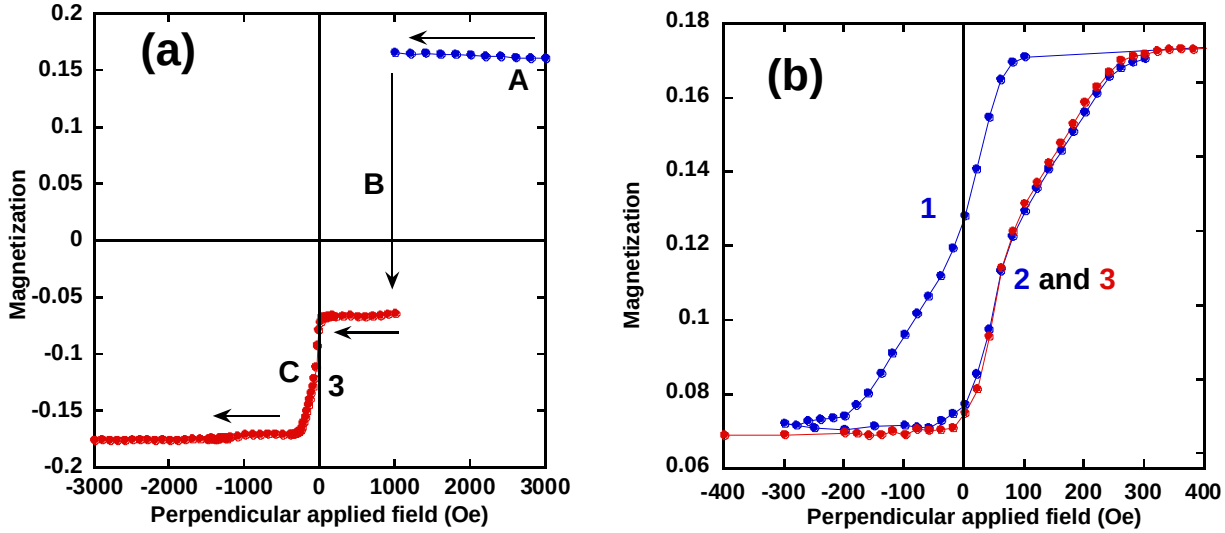

Figure III-13: (a) "Rotation" experiment: (A) both layers are "up", (B) the hard layer goes "down", while the soft layer is still "up", (C) the soft layer goes "down"; (b) Comparison with conventional switching.

III-2.2 Macrospin simulations

Figure III-14 presents Hall curves of Pt/Co1.2/MgO1.3/Co/Pt samples annealed at 250°C with a top Co thicknesses of 1.0, 1.2 and 1.4 nm. The top panel corresponds to perpendicular applied fields, whereas the bottom one corresponds to in-plane fields, starting from positive saturation. The shift of the minor loops varies a lot with top Co thickness (**see Section 3.5**): it goes from -50 Oe for 1.0 nm to -80 Oe for 1.2 nm to -40 Oe for 1.4 nm. The anisotropy field of the hard layer is more or less constant at about 9 kOe, while that of the soft layer progressively decreases with increasing thickness. However, in-plane measurements reveal a non-monotonous decrease of the M_Z component for a top Co thickness of 1.2 nm, with a local minimum for about 4 kOe. For this Co thickness, the coupling field is maximum. The same anomaly, although less pronounced, is observed for the Co thickness of 1.4 nm.

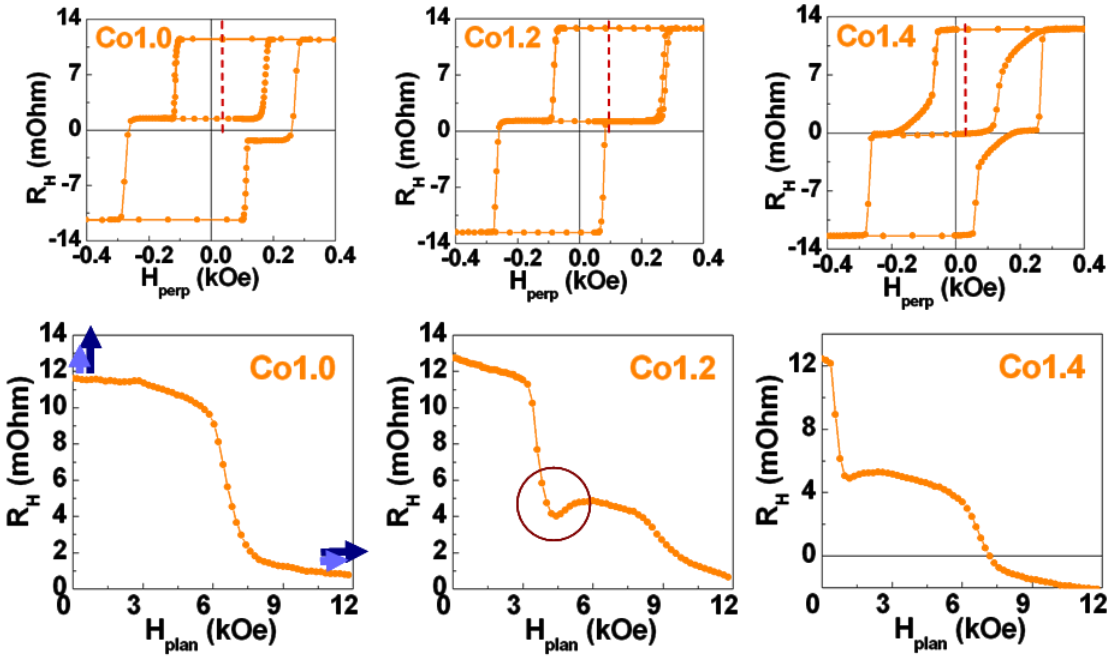

Figure III-14: Hall hysteresis loops for Co1.2/MgO1.3/Cox structures after annealing at 250°C. Upper curves correspond to perpendicular applied field for different top Co thicknesses. Bottom curves correspond to the decrease of the Mz component for in-plane fields, starting from positive saturation.

Confirmation is obtained from micromagnetic simulations using a simple model of two coupled macrospins presented in **Figure III-15** [Bud_01]. One can see that for given anisotropy values of the top and bottom layers (K_{top}=5 10^6 J/m^3, K_{bottom}=9 10^6 J/m^3), different antiferromagnetic coupling strengths (low -10^{-5}, medium -10^{-3} strong -10^{-2} J/m^2) produce different responses of the magnetization of the soft layer to the in-plane applied field. For a strong and medium coupling value we have the same anomaly as observed experimentally. The smallest coupling of 10^{-5} J/m^2 does not affect the layer switching. These simulations confirm that the anomalies in planar measurements come from antiferromagnetic interaction between the magnetizations of the two layers through the oxide spacer.

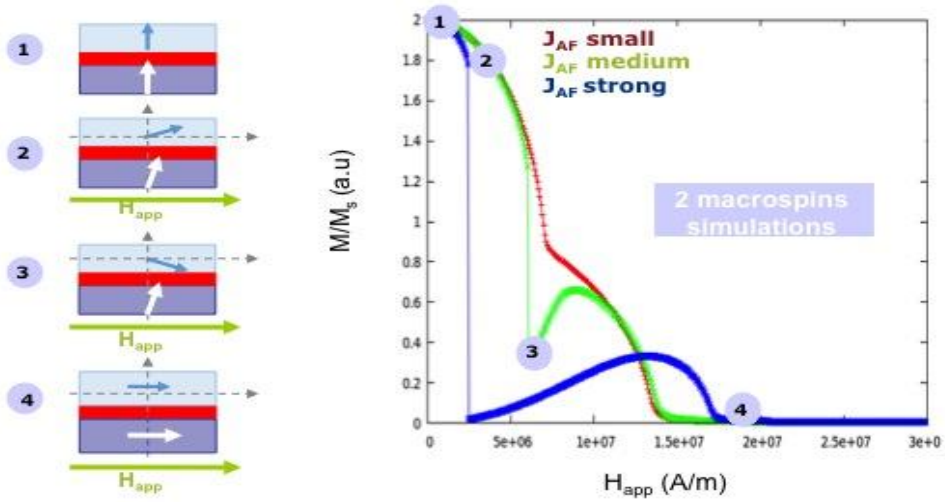

Figure III-15: Micromagnetic simulations using a simplified model of two coupled macrospins representing in plane variation of the magnetization in structures with different coupling energies.

III-3. Variation of the antiferromagnetic coupling

Experimentally AF coupling was first observed in epitaxial MTJ's by Faure-Vincent et al [Fau_02] for very thin MgO barriers (less than 0.8 nm) and was explained in terms of the conservative exchange coupling of the Slonczewski's spin current model [Slo_95]. When the MgO thickness increases, the strength of the coupling decreases and its sign changes from antiferromagnetic to ferromagnetic. For large thicknesses the ferromagnetic coupling is attributed to the dipolar coupling (Néel's coupling) induced by the roughness of the barrier.

It is hard to imagine that our sputtered samples could present a smaller interfacial roughness than samples prepared by Molecular Beam Epitaxy (MBE). The negative sign of the coupling observed in our samples with out of plane anisotropy for rather large MgO thicknesses could thus be tentatively explained by considering the model of dipolar coupling extended to perpendicular magnetization [Mor_04].

In order to see which model can better account for our experimental results, we will study in this **Section** the evolution of coupling with different parameters: barrier thickness, measurement temperature, barrier oxidation conditions and annealing temperature. Although results obtained for low barrier thickness could agree with IEC theories, it seems that interface roughness is the main contribution to AF coupling.

III-3.1 Variation with MgO thickness for RF-deposited barriers

We will first investigate the variation of the indirect coupling as a function of the MgO barrier thickness in perpendicular magnetic tunnel junctions with the following structure: Ta/Pt/(Co0.5/Pt0.4)x5/Co0.5/CoFeB1/MgO/CoFeB1/Co0.5/Pt with a MgO thickness varying from 0.6 to 1.4 nm. In order to ease the comparison with results of the literature, the barrier is prepared by RF sputtering from an MgO target, and not by natural oxidation of an Mg layer, since this latter technique could lead to a simultaneous variation of thickness and oxygen content of the barrier.

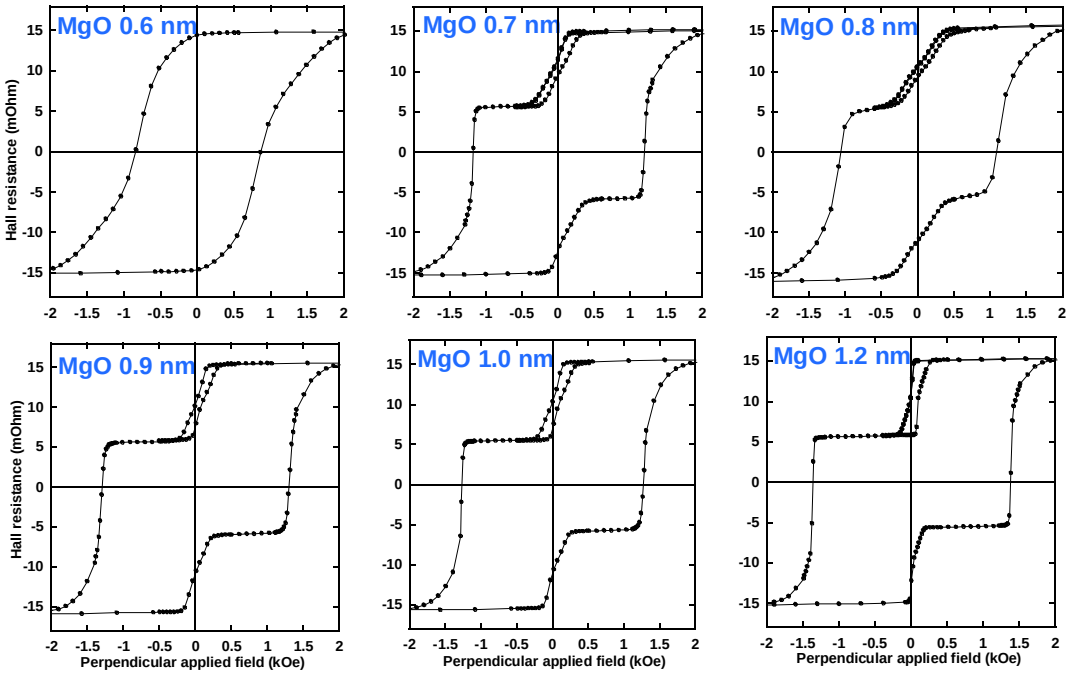

Figure III-16: Hall hysteresis loops as a function of perpendicular field for various MgO thicknesses after annealing at 325°C.

Figure III-16 presents Hall hysteresis loops measured with an out-of plane field for different MgO thicknesses after annealing at 325°C. For such an annealing temperature, both electrodes are out-of-plane. For a barrier thickness of 0.6 nm, we observe only one transition, probably because of direct ferromagnetic coupling between electrodes through pinholes. Above 0.7 nm the two transitions are recovered. Coupling turns from ferromagnetic to antiferromagnetic between 0.7 and 0.8 nm. One can also note on **Figure III-16** that the nucleation field of the soft layer progressively increases with decreasing MgO thickness, but decreases again at 0.7 nm.

The variations with MgO thickness of the coupling field between electrodes and nucleation field of the soft layer are shown in **Figure III-17.** The variation of the coupling field shows the same tendency as that observed in epitaxial junctions [Fau_02, Kat_06] (**Figure III-18**). The amplitude of the antiferromagnetic coupling increases with decreasing barrier thickness, down to a limit where direct ferromagnetic coupling dominates. The same evolution is observed for different annealing temperatures (**Figure III-17b**). A similar cut-off below 1 nm was observed in perpendicularly magnetized structures obtained by a sputtering technique [Liu_03]. The value of this cut-off is much smaller in epitaxial junctions (0.5 to 0.6 nm) because of the much better growth quality of these structures.

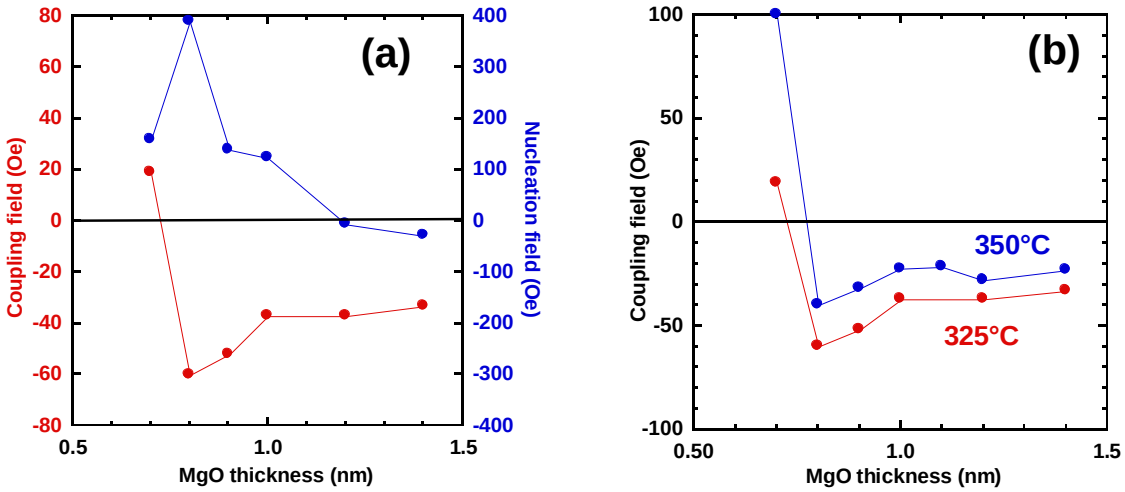

Figure III-17: (a) Variation of the coupling and nucleation fields as a function of MgO thickness after annealing at 325°C; (b) Variation of the coupling field for two annealing temperatures.

A noticeable difference between **Figure III-17** and **Figure III-18** is that, for epitaxial junctions, coupling turns ferromagnetic at about 0.8 to 0.9 nm. This is attributed to dominant roughness-induced coupling. In our case, coupling is still antiferromagnetic (however with decreasing amplitude) up to the largest MgO thickness investigated (1.4 nm). Since our structures certainly present larger interface roughness (as the larger low-thickness cut-off shows), one must admit that interfacial roughness leads to antiferromagnetic coupling in our structures, in agreement with the results of the extension of Néel's model to perpendicular structures [Mor_04]. The applicability of this model will be discussed later on. Since the number of our experimental points is quite limited in the low MgO thickness range, it is hard as this stage to differentiate between IEC models ($1/D^2$ e^{-2kD} dependency, where D is the barrier thickness) and Néel's model (e^{-kD} dependency).

By increasing the annealing temperature (**Figure III-17b**), the variation of coupling with MgO thickness shows the same tendency, although the amplitude of AF coupling is progressively reduced. This aspect will be developed in the next sections.

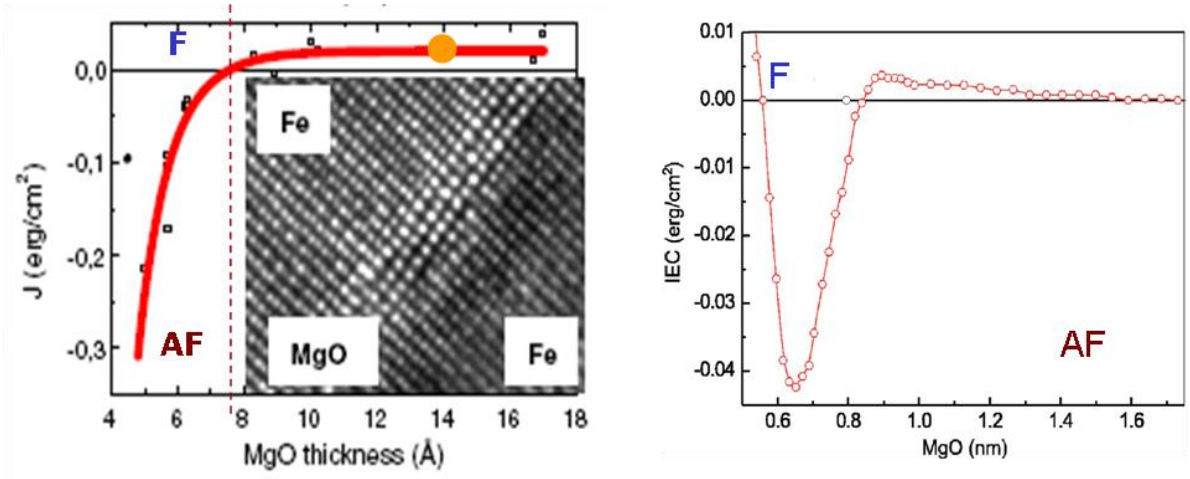

Figure III-18: Variation of the coupling energy with MgO thickness in planar epitaxial MTJ [Fau-02, Kat_06].

Turning now to the evolution of the nucleation field of the soft layer **(Figure III-17a**), two explanations can be put forward. The first possibility is a progressive modification of the anisotropy of the soft layer because of a progressive modification of the top MgO interface. However, one should in this case expect a monotonous variation, which is not the case. The second possibility is that, as the MgO thickness decreases, the coupling increases. Thus, for a constant thickness interval Δt, the corresponding width of the coupling field distribution ΔH will increase, which could explain the progressive slanting of the hysteresis loop.

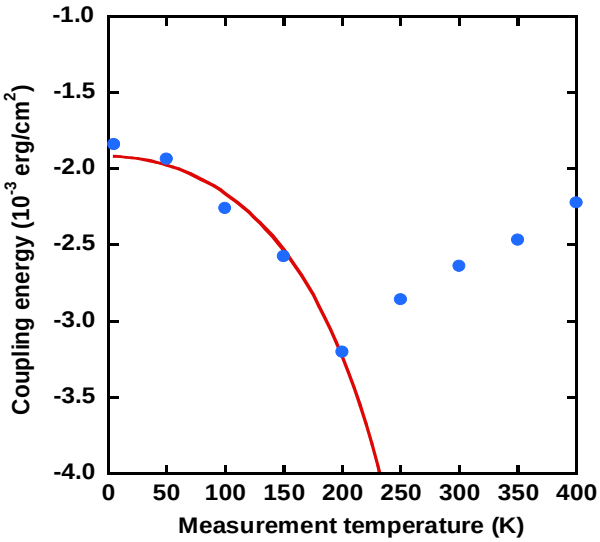

Figure III-19: Thermal variation of the magnetic coupling in Ta/Pt/(Co0.5/Pt0.4)5/Co0.5/CoFeB1/ MgORF1.4 /CoFeB1/Co0.5/Pt structures annealed at 325°C.

A way to compare both IEC and Néel' models is to look at the variation of coupling with measurement temperature. Bruno's theory predicts an increase of coupling amplitude with increasing temperature, whereas one expects a reverse behavior for Néel's theory since the coupling energy depends on the magnetizations of the magnetic layers. Such an investigation was carried out by SQUID magnetometry on samples with the following structure: Ta/Pt/(Co0.5/Pt0.4)/Co0.5/CoFeB1/MgORF1.4/CoFeB1/Co0.5/Pt annealed at 325°C. The choice of one particular structure and of annealing temperature is quite critical, since the low temperature variation of the coercive field can be very different for both magnetic layers, sometimes leading to a

simultaneous reversal of both magnetizations, although these transitions were well separated at room temperature.

Figure III-19 shows the variation of coupling energy with measurement temperature. At low temperature, the coupling strength increases with measurement temperature as predicted by Bruno for an insulating spacer **[Bru_95]**. This is linked to a smaller contribution of the states below the Fermi level at low temperatures and it is also called thermally induced exchange coupling. Fitting our data for temperatures lower than 200K with Bruno's formula:

$$J(T) = J(0) \cdot \frac{a \cdot T}{\sin(a \cdot T)}, \text{ where } a = \frac{2\pi \cdot k_B \cdot t \cdot m_e}{\hbar^2 \cdot k_F} \qquad \textbf{Equation III-4}$$

we can extract the Fermi wave vector of the barrier k_F= 0.7nm^{-1} and the 0K corresponding coupling energy J(0)= -1.9 10^{-3} erg/cm^2.

However, Bruno's model has some limitations for the description of the coupling energy variation with temperature. There is a limited temperature range in which the assumptions made for the calculation of the above equation are valid. It is given by:

$$T < \frac{\hbar^2 \cdot k_F}{2\pi \cdot k_B \cdot t \cdot m_e} \qquad \textbf{Equation III-5}$$

Calculating this temperature for our sample (k_F=0.7 nm^{-1} and t_{MgO}= 1.3 nm) leads to T=230K. One can see on **Figure III-19** that the behaviour of the coupling energy changes above this temperature, and qualitatively follows the thermal variation of the magnetization. This could be the sign of a dominant Néel type of coupling in the high temperature region.

III-3.2 Variation with annealing temperature

We previously showed that annealing greatly modifies the anisotropy properties of our samples. We will now look at the influence of annealing on the interlayer coupling properties.

Figure III-20 shows the evolution with annealing temperature of the Hall hysteresis loops of a Pt30/Co1.2/MgO1.0/Co1.0/Pt3 structure **[Nis_09b]** with an MgO barrier prepared by natural oxidation of 1 nm thick Mg layer. Arrows on **Figure III-20c** indicate the way the magnetic field is swept during the recording of a minor cycle (from positive saturation of both layers to intermediate antiparallel configuration and back to positive saturation).

In the as-deposited state (**Figure III-20a**), only the bottom electrode exhibits perpendicular anisotropy. After annealing at 250° C (**Figure III-20b**), both magnetizations are out-of-plane. Although their coercive fields are nearly identical (250 Oe), two transitions can be observed, thanks to the antiferromagnetic coupling between both magnetic layers, which amounts here to about -60 Oe. Further increasing annealing temperature (**Figure III-20c** and **d**) leads to a progressive decrease of the antiferromagnetic coupling srength.

The variation of the coupling field as a function of annealing temperature is presented in **Figure III-21** for an MgO barrier prepared by either natural oxidation or RF sputtering. The coupling amplitude progressively decreases with annealing temperature for both barriers. The smaller amplitude of variation for the RF-deposited barrier can be explained by thicker magnetic electrodes (assuming similar coupling energies).

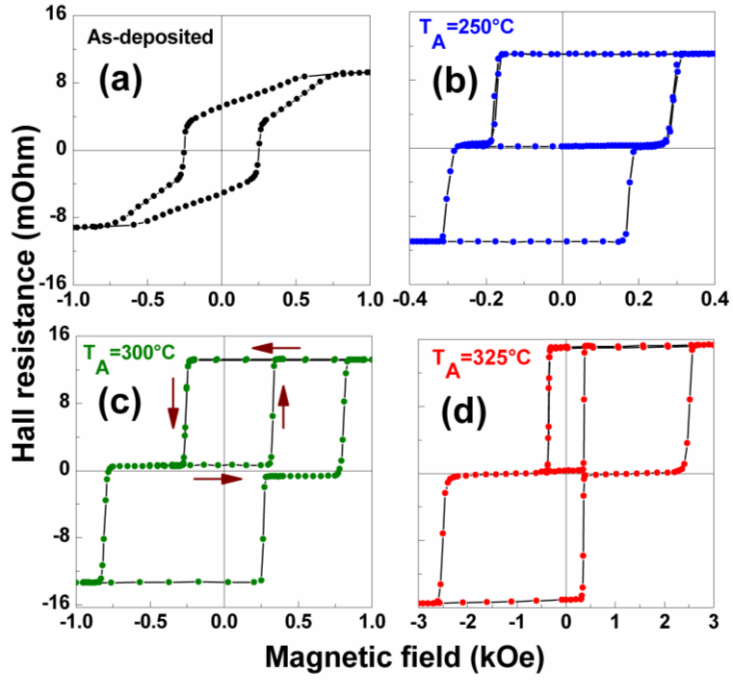

Figure III-20: Hall hysteresis loops of a Pt30/Co1.2/MgO1.0/Co1.0/Pt3 structure after annealing at different temperatures.

Assuming that annealing leads to an improvement of the quality of the MgO barrier and of its interfaces, results of **Figure III-21** are in agreement with literature **[Kat_06, Yan_07],** which relates antiferromagnetic coupling to the presence of oxygen vacancies in the insulating barrier or at the MgO interfaces. These results also agree with other interpretations **[Wu_08]** which link antiferromagnetic coupling to some oxidation of the magnetic electrodes. Annealing would thus lead to both homogenization of the oxygen concentration in the Mg layer and de-oxidation of the magnetic electrodes, both effects resulting in a decreasing antiferromagnetic coupling strength with increasing annealing temperature.

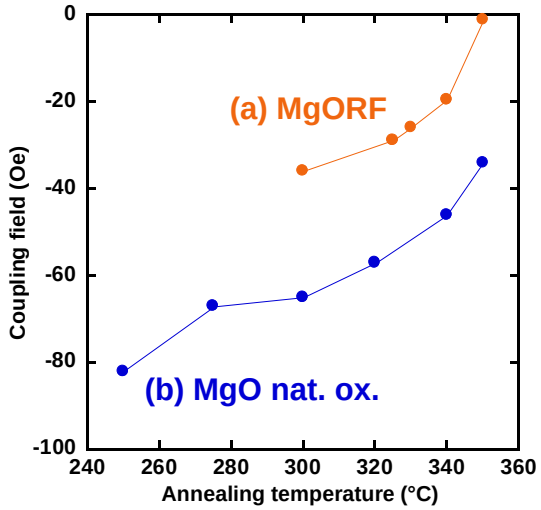

Figure III-21: Variation of the coupling field with annealing temperature in two structures with a MgO barrier prepared by either (a) RF deposition or (b) Natural oxidation.

Finally, this decreasing AF coupling with increasing anisotropy upon annealing seems to contradict the extended Néel's model of Moritz **[Mor_04]** since larger anisotropy should lead to larger AF coupling. However, any decrease of the roughness amplitude will strongly reduce the coupling field which varies as h^2, where h is the amplitude roughness. This decreased roughness would thus be the leading mechanism in our case.

III-3.3 Variation with Mg layer thickness for natural oxidation

It was already shown in previous Chapters that increasing annealing temperature leads to an increase of the perpendicular magnetic anisotropy (PMA) due to electrodes de-oxidation and Co-O bond formation. Here we try to show that this phenomenon has also consequences on the coupling strength. The AF coupling strength seems to be related to the chemical roughness due to oxygen concentration at the interface between the magnetic layers and the MgO. Another way to check this hypothesis is to vary the oxide concentration in the magnetic electrodes by using an oxide prepared by deposition and natural oxidation of the Mg layer under the same oxidation condition (900mbar and 180s).

Figure III-22 presents the evolution with MgO thickness of hysteresis loops in Pt/Co2.0/MgO/CoFeB1.5/Co0.5/Pt structures after annealing at 350°C. The thickness of the MgO barrier varies between 0.7 and 1.2 nm. For the present oxidation conditions (900 mbar oxygen pressure during 180s), small Mg thicknesses certainly lead to over-oxidation of the bottom hard magnetic electrode, which can explain both its reduced coercivity (and reduced perpendicular anisotropy, as inferred from in-plane measurements) and the slightly smaller total Hall amplitude. This results in an almost simultaneous magnetization reversal of both electrodes as can be seen in **Figure III-22a** for a 0.7 nm thick MgO layer. Decreasing the applied field from positive saturation, the reversal of the soft top layer induces the nucleation of inverse "down" domains in the hardest layer. When increasing again the applied field (minor loop), these inverse domains slow down the back reversal of the soft layer towards its initially "up" configuration. The second transition on the minor loop at larger positive field, between 0.3 and 1.0 kOe, corresponds to the elimination of the above mentioned "down" domains created in the hard layer.

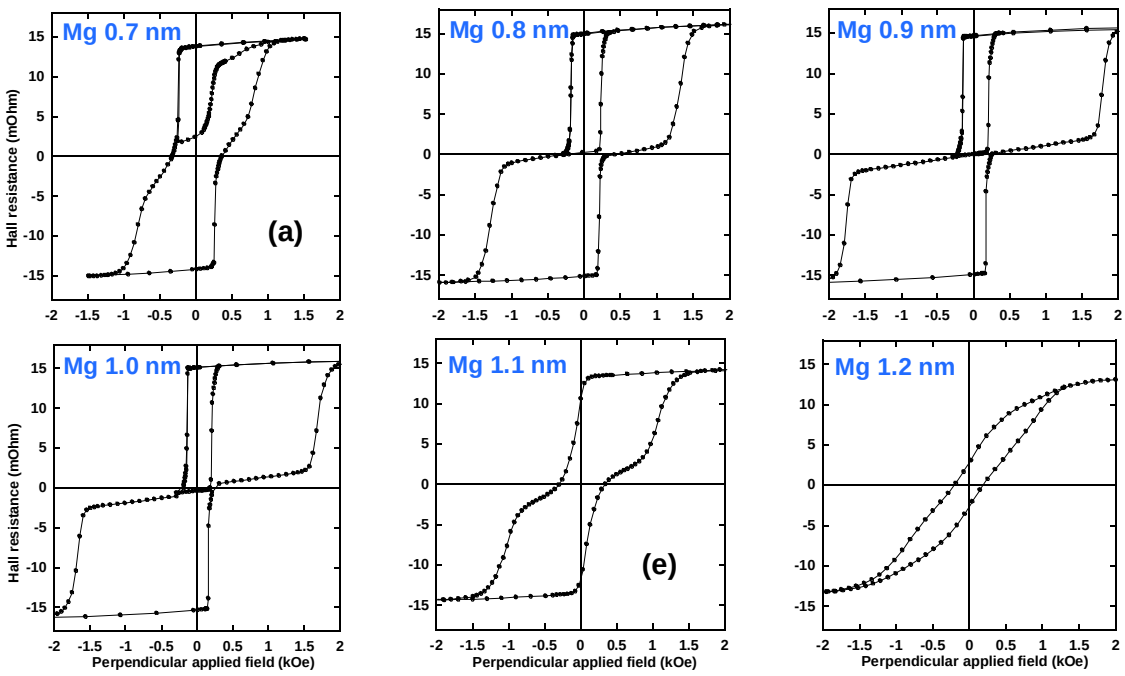

Figure III-22: Hall hysteresis loops of Pt/Co2.0/MgOx/CoFeB1.5/Co0.5/Pt structures after annealing at 350°C. The barrier is prepared by natural oxidation of a Mg layer with varying thickness.

Increasing the Mg thickness from 0.7 to 1 nm leads to a decrease of the coercive field of the soft layer, which can be related to a decreasing perpendicular magnetic anisotropy due to some progressive under-oxidation of the barrier, as observed in Pt/Co/Oxide trilayers [Rod_09]. Two well separated magnetization reversals are obtained for Mg thicknesses between 0.8 and 1.0 nm,

indicating that optimal oxidation conditions are reached in that Mg thickness range. For those samples, minor hysteresis loops show that both magnetic electrodes are antiferromagnetically coupled through the MgO barrier. For 1.1 nm thick MgO barriers (**Figure III-22e**), one again observes an overlapping magnetization reversal of both electrodes. Nucleation field changes sign for this thickness due to the combined ferromagnetic coupling of the electrodes through the under-oxidized barrier and decrease of the coercivity of the soft layer.

The influence of barrier thickness on interlayer coupling field for a Ta3/Pt30/Co1.2/MgO/Co1.2/Pt3 structure annealed at two temperatures is presented **Figure III-23**. The Mg thickness variation is obtained using the "wedge" technique presented in **Chapter I-3**. Coupling can be determined for barrier thicknesses between 1.05 and 1.5 nm, which means that the magnetic transitions of the two Co layers are well separated on this thickness range. The difference with the corresponding range observed in **Figure III-22** (from 0.8 to 1.1 nm) can have different origins: different oxidation conditions, drift in the Mg sputtering rate, or negative effect of boron diffusion on the perpendicular anisotropy (**See Chapter II**). **Figure III-23** shows that the magnitude of the antiferromagnetic coupling continuously decreases with increasing Mg thickness for both annealing temperatures. This confirms that AF coupling is linked to over-oxidation of the barrier. Increasing Mg thickness and/or annealing temperature lead to a decrease of the amplitude of AF coupling.

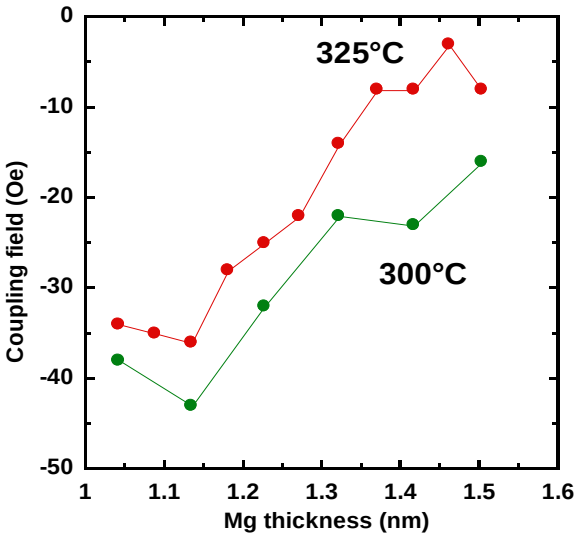

Figure III-23: Variation of the coupling field with MgO barrier thickness (natural oxidation) for two annealing temperatures.

III-3.4 Structures with low perpendicular or in-plane anisotropy

The coupling was also investigated in structures presenting low perpendicular anisotropy or in plane anisotropy.

First we will discuss the case of the low anisotropy structures of the form Ta5/CoFeB1/MgO/CoFeB1.6/TbCo/Pt2 for which results concerning the coupling are shown in **Figure III-24**. The varying Mg thickness is also obtained with the "wedge" technique. The anisotropy and transport properties of these structures have been studied in **Chapter 2**. **Figure III-24** shows that the coupling is now ferromagnetic whatever Mg thickness. However, the coupling amplitude also decreases with increasing thickness, as was the case in **Figure III-23**. Since these structures exhibit much lower anisotropy than those grown on thick Pt buffers, these results also agree with the extended Néel's model **[Mor_04]**, which predicts ferromagnetic coupling in the case of weak perpendicular anisotropy.

Another evidence for the link between perpendicular anisotropy and antiferromagnetic

coupling comes from the study of MgO junctions with in-plane magnetized electrodes. **Figure III-25a** shows the magnetization curve of a planar junction with an MgO barrier obtained by natural oxidation. Its composition is Ta3/Pt3/Co2.5/MgO1.4/Co2.5/IrMn7/Pt3. We tried to keep the same structure as that of perpendicular junctions, in order to get rid of any difference in the growth condition of the different layers. Compared to the above studied structures with perpendicular magnetic anisotropy, the smaller thickness of the Pt buffer layer, along with the larger thickness of the Co electrodes, lead to a decrease of the strength of the effective perpendicular magnetic anisotropy. As a result, the demagnetizing field now dominates over the interface anisotropy, thus leading to in-plane magnetized electrodes. For these structures, and contrary to the same junctions with out-of-plane electrodes and strong anisotropy, one observes now a classical dipolar ferromagnetic coupling between magnetic electrodes, which amounts to about 13 Oe. Ferromagnetic coupling is also observed for CoFeB magnetic electrodes and/or RF-sputtered MgO barriers in these samples with in-plane magnetic anisotropy.

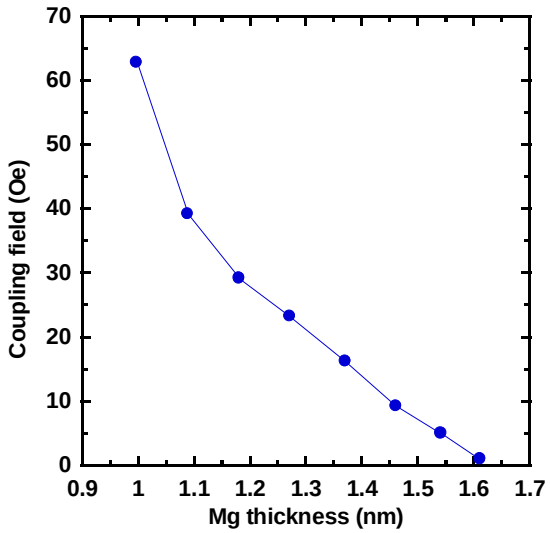

Figure III-24: Variation of the coupling field with Mg thickness (natural oxidation) of a perpendicular junction with low anisotropy after annealing at 300°C.

Figure III-25b gives another example of a more classical planar junction with a free CoFeB bottom electrode and a synthetic top-pinned electrode after annealing at 340°C. Both TMR ratio and coupling field have been measured by the CIP technique on a Mg wedge with constant oxidation conditions (**Chapter II-1.3**).

As observed in perpendicular junctions (**Chapter II-4.2**), the TMR ratio decreases with decreasing Mg thickness as a consequence of the progressive oxidation of the bottom CoFeB electrode. The coupling field is initially negative at large Mg thickness, but one cannot exclude an offset of the zero field due to calibration (no Hall sensor is installed on the Capres tool). Anyway, coupling turns ferromagnetic and its amplitude increases with decreasing Mg thickness, as was the case for junctions with low anisotropy (**Figure III-24**), and contrary to the case of perpendicular junctions with strong anisotropy (**Figure III-23**).

For small Mg thicknesses, the amplitude of the coupling field is smaller for in-plane junctions (**Figure III-25b**) than for perpendicular ones (**Figure III-24**). Three main factors can be at the origin of such a difference. First, the free bottom electrode is much thicker for the in-plane junction, leading to smaller coupling fields if one assumes comparable coupling energies. Second, the top-pinned electrode of the in-plane junction is a CoFeB/Ru/Co SAF (synthetic anti-ferromagnet) structure, the Co layer being exchange-coupled to the IrMn layer. The magnetic flux thus closes preferentially into the SAF, and has less influence on the free layer. Third, the in-plane

junction has been annealed at higher temperature (340°C compared to 300°C). The SAF structure of the in-plane junction limits Mn diffusion towards the active part (CoFeB layer), and allows for higher annealing temperatures.

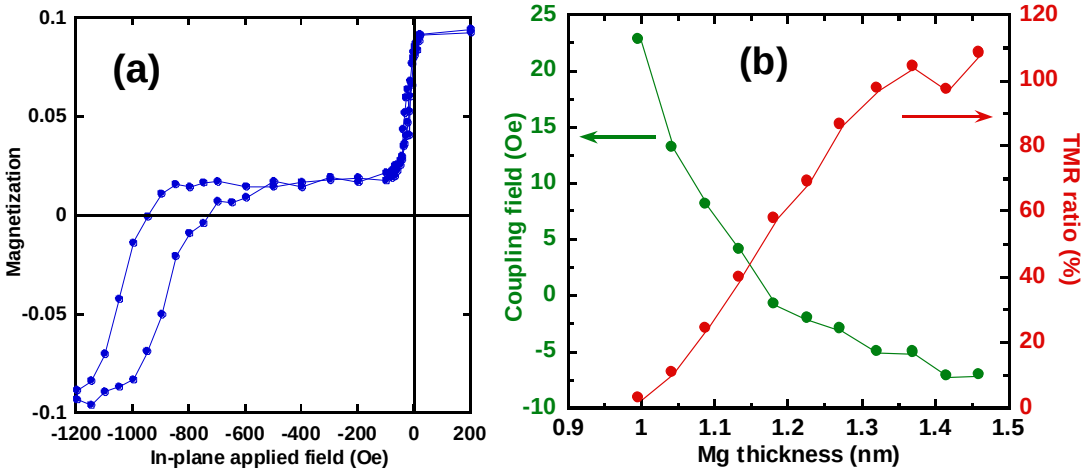

Figure III-25: (a) In-plane hysteresis loop of a Ta3/Pt3/Co2.5/MgO1.4/Co2.5/IrMn7/Pt3 planar junction after annealing at 300°C; (b) Variation of the coupling field and TMR ratio with Mg thickness in a planar Ta3/CoFeB4/MgO1.4/CoFeB3/Ru0.9/Co2/IrMn7/Ru junction annealed at 340°C.

III-4. Origin of the sign of interlayer coupling and of its variation

The main variations of the indirect coupling we presented in the preceding sections (as a function of annealing temperature and MgO barrier thickness) in perpendicular junctions with high and low perpendicular anisotropy, as well as in in-plane junctions, are gathered in **Figure III-26**.

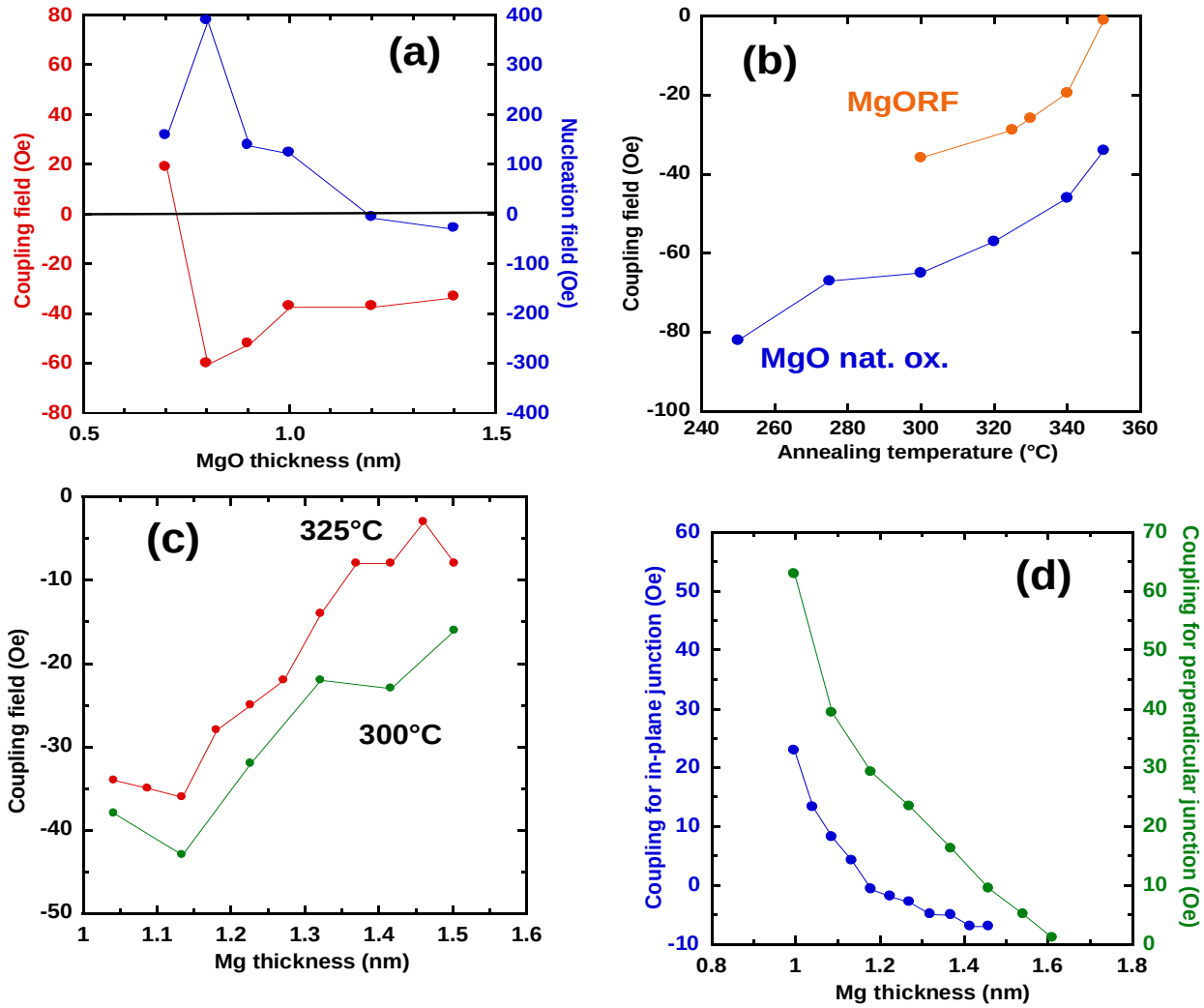

Figure III-26: Summary of the evolution of coupling field with (a) MgO RF thickness, (b) Annealing temperature, (c) and (d) Mg thickness (natural oxidation) for (c) Strong and (d) Weak perpendicular or in-plane anisotropies.

In our structures the variation of indirect coupling with MgO layer thickness (MgO RF deposition) presented in **Figure III-26a** is similar to the one observed in the literature [Fau_02, Kat_06], and agrees with Slonczewski's and Bruno's theories [Slo_95, Bru_95] for small MgO thicknesses. However, the coupling energies are much lower in our case (10^{-3} erg/cm^2 compared to 10^{-1} erg/cm^2) since in our sputtered samples coupling turns ferromagnetic for larger MgO thickness than for epitaxial samples, as consequence of a lower quality of the growth of MgO layers by sputtering than by epitaxy. Furthermore, according to the literature [Fau_02, Kat_06], for MgO layers as thick as 1.4 nm, one should expect a ferromagnetic Néel type dominant coupling contribution [Née_62]. However, in our case coupling is still antiferromagnetic for these large MgO thicknesses. This is qualitatively in agreement with Moritz model [Mor_04] which considers both effects of a strong out-of-plane anisotropy and interfacial roughness, leading to antiferromagnetic coupling **(Figure III-5**).

In sputtered perpendicular junctions with strong anisotropy, it is difficult to decide which model is more adapted, since coupling is always antiferromagnetic whatever MgO thickness, not mentioning the reduced MgO thickness range on which data points can be fitted to both IEC or Néel's theories. The variation of coupling with measurement temperature agrees with IEC models at low for temperature, whereas a Néel type behavior is observed at higher temperatures. Since all our studies of indirect coupling as a function of MgO layer thickness and annealing temperature were done at room temperature the main contribution should be Néel's type, and we will try to interpret our results in the framework of this model.

Increasing annealing temperature leads to an increase of the anisotropy, but to a decrease of the antiferromagnetic coupling (**Figure III-26b**), contrary to expectations from Néel's extended model [Mor_04]. One should thus invoke another mechanism, which could be a decrease of interfacial chemical roughness as annealing temperature increases. This mechanism would be the dominant one, and mask the predicted evolution of coupling with anisotropy (which considers constant roughness).

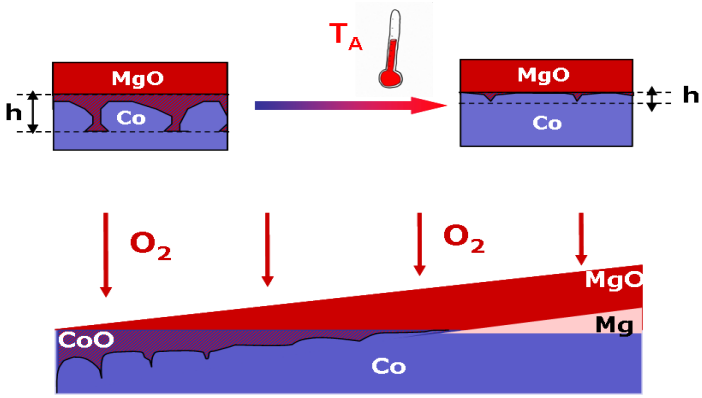

Figure III-27: Schematic representation of oxygen distribution as a function of (a) annealing temperature and (b) Mg thickness for natural oxidation.

Previous experimental studies on CoFeB-based in-plane MgO junctions [Hin_10, Liu_11, Rea_07, Sch_07] showed that annealing leads to a decrease of the oxygen content of the magnetic electrodes. This is accompanied by a decrease of the (ferromagnetic) coupling [Fen_06, Rei_09]. These results are coherent with our observed variation of the indirect coupling with Mg thickness in systems with either strong or weak perpendicular or in-plane anisotropies (**Figure III-26c** and **d**) for constant oxidation conditions. A schematic representation of the possible oxygen distribution in the structure (bottom electrode and barrier) with variable Mg layer thickness is presented in **Figure III-27**. For small Mg thicknesses the Co layer will be oxidized through grain boundaries leading to a large chemical roughness amplitude and to a large coupling field. For larger Mg thicknesses oxidation of the Co layer will be reduced and chemical roughness will decrease, resulting in a smaller coupling field. So the chemical roughness amplitude h will depend on the Mg layer thickness, leading to a rapid ($1/h^2$) decrease of the coupling amplitude with decreasing chemical roughness [Koo_99] whatever its sign (negative for strong anisotropy and positive for weak anisotropy).

A possible way to distinguish between IEC and Néel's models would be to look at the variation of the indirect coupling with MgO thickness in these junctions with low perpendicular anisotropy. For small MgO thicknesses, a change of sign of the coupling from positive to negative would be the proof of IEC coupling. Unfortunately, MgO targets are not installed in our sputtering machines at the present time.

III-5. Coupling oscillations with top Co layer thickness

The investigation of the coupling variation with the top layer thickness was possible due to the good PMA properties of the structures based on Pt/Co/MgO trilayers (already described in **Chapter II**). The choice of Co as magnetic electrodes and natural oxidation of the Mg barrier was made in order to have an optimized perpendicular magnetic anisotropy [Nis_09a], allowing to maximize both magnetic layer thickness and annealing temperature ranges in which both electrodes are out-of-plane.

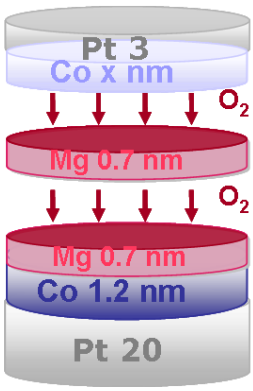

Figure III-28: Structure used in the study of coupling variation with top electrode thickness.

The structure used in this study is substrate/Ta3/Pt20/Co1.2/MgO1.3/Co/Pt3 (**Figure III-28**). The thickness of the top Co electrode varies from 0.5 to 3.2 nm. The MgO barrier is obtained through two successive deposition/oxidation steps of a metallic Mg layer 0.7 nm thick, oxidation being carried out for 10 min under 900 mbar oxygen pressure. The actual barrier thickness (1.3 nm) is estimated accounting for a 20% isotropic volume decrease of the atomic cell upon oxidation. Samples were annealed under vacuum for 30 mins up to 350°C. The 1.2 nm thick bottom Co layer grows on a thick Pt buffer. As a consequence, its magnetization is always out-of-plane and its anisotropy is larger than the one of the top Co layer for all annealing temperatures and top Co thicknesses ranges investigated.

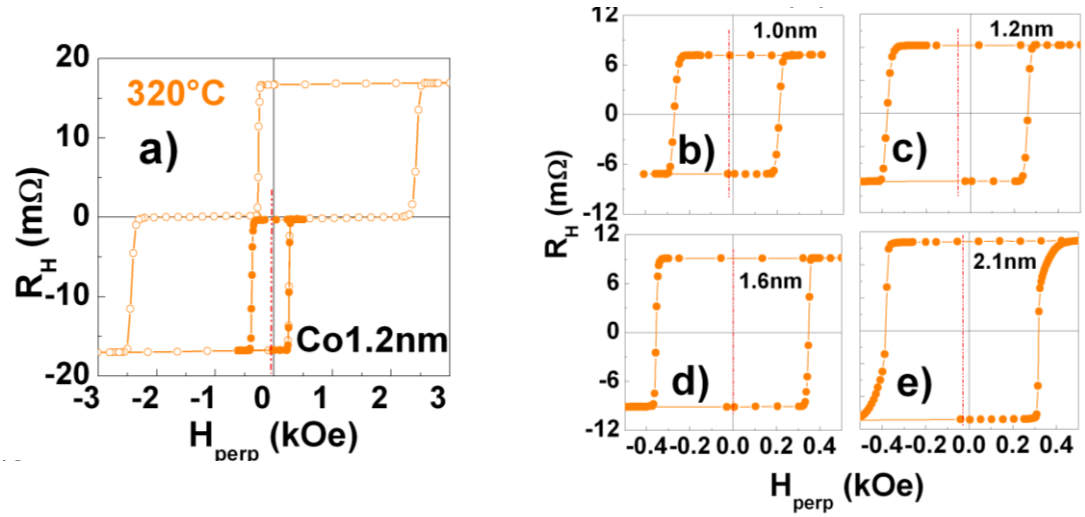

Figure III-29: Hall hysteresis loops of Pt/$Co_{1.2}$/$MgO_{1.3}$/Co/Pt structures after annealing at 320°C. Curve (a) shows both major and minor loops for t= 1.2 nm. Curves (b) to (e) show minor loops for increasing top Co thickness. The vertical line materializes the shift of the minor loop.

Figure III-29 shows the Hall hysteresis loops of these structures after annealing at 320°C. Both major and minor hysteresis loops are shown in **Figure III-29a** for a top Co thickness of 1.2 nm. The minor loop is shifted by -60 Oe (see **Figure III-29c**), indicating preferred antiferromagnetic coupling between magnetic electrodes.

Figure III-29b to **e** display minor hysteresis loops recorded for increasing top Co thickness. One can clearly observe an oscillation of the coupling field amplitude with increasing top Co layer thickness while its sign remains negative whatever Co thickness, indicating preferred antiferromagnetic coupling. The squareness of the minor loops (nucleation field/saturation field ratio) progressively varies with increasing top Co thickness above 2.0 nm, as a consequence of the corresponding decreasing perpendicular anisotropy.

A more quantitative insight is given in **Figure III-30**, which shows the variation of the coupling field as a function of top Co thickness for different annealing temperatures T_A. As a consequence of the strong PMA increase with increasing T_A **[Nis_09a]**, the critical top Co thickness (transition from out-of-plane to in-plane configuration) increases from 1.4 nm for T_A = 250°C to more than 3.0 nm for T_A = 350°C. Interlayer coupling is essentially antiferromagnetic for all ranges of top Co layer thickness and annealing temperatures investigated. The most striking feature is that coupling oscillates as a function of the top magnetic layer thickness up to at least 3 nm. Although the average coupling field strength progressively decreases with increasing T_A, period and amplitude of the oscillation are mostly independent of annealing.

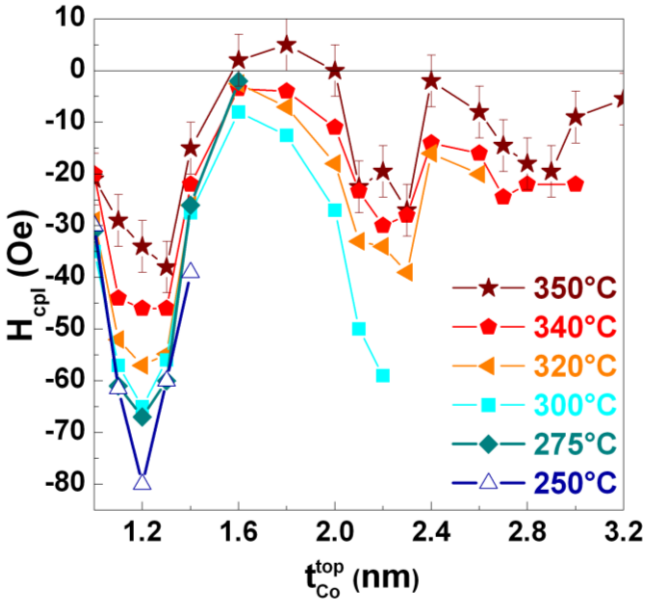

Figure III-30: Variation of the indirect coupling field with top Co thickness for different annealing temperatures. Uncertainty on coupling field (5 Oe) is only represented for T_A = 350°C.

The coupling energy is determined from the coupling field H_{cpl} using the relation:

$$J_{cpl} = \frac{H_{cpl} \cdot M_{sT} \cdot t_T \cdot M_{sB} \cdot t_B}{M_{sT} \cdot t_T + M_{sB} \cdot t_B} \qquad \textbf{Equation III-6}$$

where t and t_B (1.2 nm) represent thicknesses of the top and bottom magnetic electrodes, respectively, and M_{sT} and M_{sB} are their saturation magnetizations.

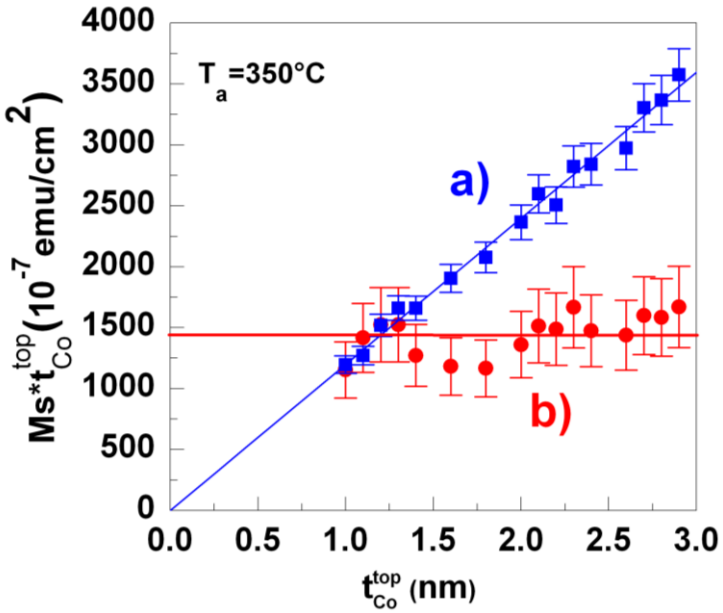

Figure III-31: Variations as a function of top Co thickness, after annealing at 350°C, of the magnetic moments of (a) Top and (b) Bottom electrodes. The blue line has a slope of 1200 emu/cm³ and zero intercept, whereas the horizontal red line corresponds to 1200 x 1.2 10^{-7} emu/cm².

Hall measurements cannot be used to extract absolute values of the magnetizations, since Hall resistance depends on both magnetization and Hall coefficient of the magnetic layers, the latter increasing substantially with annealing treatments [Rod_09]. In order to extract values of magnetizations of both bottom and top electrodes, we carried out magnetic VSM and SQUID measurements. Our analysis relies upon the hypothesis that low temperature saturation magnetization, for Co electrodes thicker than 1.0 nm, equals that of bulk cobalt, that is 1430 emu/cm³. We first carried out low temperature SQUID measurements on a Pt/$Co_{1.2}$/MgO/$Co_{1.2}$/Pt structure, and observed a 16% reduction of magnetization with temperature increasing from 5 to 300K. We thus deduce a saturation magnetization for the 1.2 nm thick magnetic electrodes of 1200 emu/cm³ at room temperature, and this value is used to calibrate our VSM measurements. The corresponding magnetization, determined from VSM measurements on the whole series of samples after annealing at 350°C, multiplied by the top magnetic thickness, is shown in **Figure III-31a** as a function of the top Co layer thickness. The expected linear variation with a slope of 1200 emu/cm³ and zero intercept is superimposed to the data points. The good agreement with experimental data (6% scatter) shows that saturation magnetization is independent of Co thickness between 1 and 3 nm. The quite small scatter of M_{sT} values, which mainly comes from experimental resolution and accuracy in the determination of sample surface, implies a rather good stability of our sputtering unit.

The same procedure is used for the bottom Co electrode, and the results (saturation magnetization multiplied by 1.2 nm) are shown in **Figure III-31b**. They reasonably agree with the horizontal line corresponding to 1430 (1200 x 1.2) 10^{-7} emu/cm². The larger scatter (20%) observed in **Figure III-31b** compared to **Figure III-31a** is related to both larger applied field and larger field interval required to switch the magnetically harder bottom layer, making the determination of its amplitude more difficult.

Based on these results, we will now assume that saturation magnetization values obtained from **Figure III-31** (1200 emu/cm³) can be used for all annealing temperatures for the determination of coupling energies according to **Equation III-6**. **Figure III-32** gives the corresponding variation of coupling energy as a function of top Co thickness. In order to make easier the analysis of the coupling oscillations on the whole range of annealing temperatures, all curves are superimposed to oscillate around zero energy, the vertical energy offset $J_{offset}(T_A)$ (included as a fitting parameter to **Equation III-7**) being given in the inset.

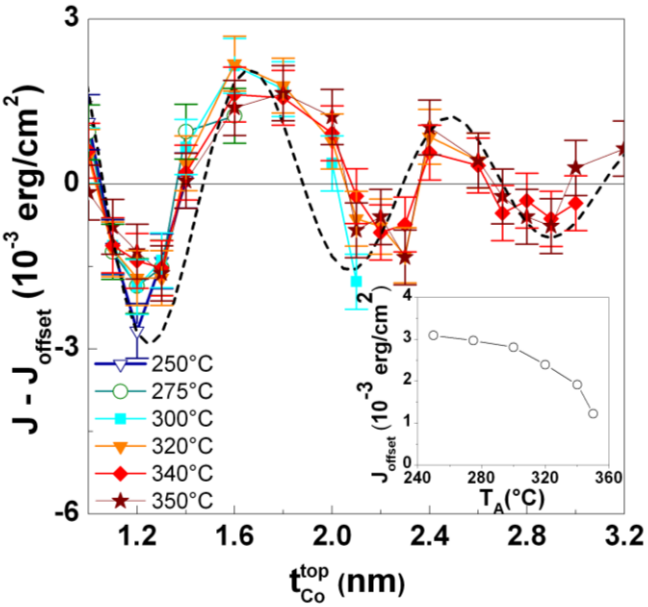

Figure III-32: Variation of the coupling energy as a function of top Co thickness, calculated from data of Figures III-30 and III-31 according to Equation III-6. Coupling energies, after allowing for a vertical offset $J_{offset}(T_A)$ given in the inset, are fitted to Equation III-7 (dotted black line).

Figure III-32 demonstrates that curves for different annealing temperatures coincide, highlighting the constant oscillation amplitude and period for all T_A used. As expected, $J_{offset}(T_A)$ progressively decreases with increasing annealing temperature. This oscillatory variation as a function of magnetic layer thickness, predicted by theory [Bru_93], has been confirmed only in the case of a metallic spacer with in-plane magnetized electrodes [Blo_94]. The rather large oscillation amplitude we observe here is certainly related to the presence of the insulating MgO barrier. This effect has been recently evidenced in MgO-capped Fe/Cr/Fe structures [Hal_09].

According to Bruno's theory [Bru_93], the oscillatory variation of the coupling as a function of magnetic layer thickness originates from Fabry-Perot-like interferences of the electron Bloch wave multiple reflections in FM layers. We apply this model to present studies and fit the corresponding J data to the following expression (see **Equation III-1**) valid in the approximation of large layer thicknesses:

$$J = \frac{A}{C^2} \cdot \sin\left(\frac{2\pi \cdot t}{\Lambda} + \Phi\right) \qquad \textbf{Equation III-7}$$

with $C = 1 + (k_F\, t)/(k_F^{\downarrow}\, D)$, and where A is a constant and t and D (1.3 nm) represent the thickness of the top magnetic electrode and barrier, respectively. Λ and Φ indicate the oscillation period and phase while $k_F^{\downarrow} = \pi/\Lambda$ is the Fermi wave vector of the spin down electrons in the ferromagnetic layer and k_F the imaginary part of the Fermi wave vector in the insulating spacer.

We should note here that despite the limitations of Bruno's model to the case of a transparent barrier, **Equation III-7** gives a reasonable agreement with experiment for both period and damping of the oscillations (with $\Lambda = 0.85$ nm, $\Phi = 0.6\pi$ and $k_F = 5$ nm^{-1}). The maximum at about 1.7 nm is clearly broader than the other ones, suggesting the possibility of additional contributions with a different period [Blo_94]. However, the Co thickness range investigated in this study (which is limited by perpendicular anisotropy properties) does not allow us to try fitting our experimental data to more than one oscillation period.

The obtained k_F value of 5 nm^{-1} represents intermediate barrier quality between ideal epitaxial MgO and amorphous Al_2O_3 cases. The oscillation period of 0.85 nm corresponds to 4.2 monolayers

(ML) for (111) fcc and (0001) hcp Co, or 4.9 ML for (001) fcc Co. However, this value for (001) fcc Co is different from that reported so far (3.5 ML) for (001) Co/Cu/Co structures **[Blo_94]**. This suggests that Co structure in our samples is closer to the case of (111) fcc crystal structure. This period leads to a wave vector $k_F^{\downarrow}$ of about 4 nm^{-1} which in this case should be the one for (111) fcc Co. Theoretical studies on exchange coupling in p-MTJs should help to clarify this point **[Yan_11]**.

III-6. Conclusions

This **Chapter** presented evidence of antiferromagnetic coupling between perpendicularly magnetized electrodes in sputtered MgO based magnetic tunnel junctions.

For RF-deposited MgO barriers, the variation of the coupling field with MgO thickness appears similar to the one observed in epitaxial planar junctions **[Fau_02, Kat_06]**. The amplitude of the antiferromagnetic coupling increases with decreasing barrier thickness, down to a limit where direct ferromagnetic coupling dominates. This cut-off happens for thicker spacers (1 nm) in the case of sputtered pMTJ, as observed by **[Liu_03],** than for epitaxial junctions (0.5-0.6 nm), because of a larger interfacial roughness. For larger MgO thickness, the coupling keeps antiferromagnetic, in agreement with Néel's model extended to perpendicular magnetization **[Mor_04]**. Two coupling contributions could co-exist in our structures, one from IEC dominating at low temperature and the other from roughness-induced coupling at higher temperature. Out-of-plane structures with low PMA and in-plane structures exhibit classical ferromagnetic Néel's coupling, confirming Moritz model. All structures show the same increase of the coupling amplitude with decreasing Mg thickness, which is attributed to over-oxidation of the magnetic electrode.

The decrease of the amplitude of antiferromagnetic coupling with increasing annealing temperature can be reconciled with Néel's theory by assuming that de-oxidation of the magnetic electrodes leads to a smaller chemical roughness of the interfaces.
We also showed that antiferromagnetic coupling oscillates as a function of magnetic thickness, as predicted by Bruno's theory **[Bru_93]** for insulating spacers. This is explained by interferences of the electron waves in the ferromagnetic layers. Although average coupling strength progressively decreases with increasing annealing temperature, the amplitude and period of the oscillations are found to be essentially independent of annealing temperature.

III-7. References

[Bai_88] M.N. Baibich, J.-M. Broto, A. Fert, F. Nguyen Van Dau, F. Petroff, P. Etienne, G. Creuzet, A. Friederich and J. Chazelas, *Giant magnetoresistance of (001)Fe/(001)Cr magnetic superlattices,* **Phys. Rev. Lett. 61** (1988) 2472.

[Bar_92] J. Barnas, *Coupling between 2 ferromagnetic-films through a nonmagnetic metallic layer*, **J. Magn. Magn. Mater. 111** (1992) L215.

[Blo_94] P.J.H. Bloemen, M.T. Johnson, M.T.H. van de Vorst, R. Coehoorn, J.J. de Vries, R. Jungblut, J. aan de Stegge, A. Reinders and W.J.M. de Jonge, *Magnetic layer thickness dependence of the interlayer exchange coupling in (001) Co/Cu/Co*, **Phys. Rev. Lett. 72** (1994) 764.

[Bru_93] P. Bruno, *Oscillations of interlayer exchange coupling vs. ferromagnetic-layers thickness*, **Europhys. Lett. 23** (1993) 615.

[Bru_95] P. Bruno, *Theory of interlayer magnetic coupling*, **Phys. Rev. B 52** (1995) 411.

[Bud_01] L. D. Buda, *Développement d'un code de calcul micromagnétique 2D et 3D: Application à des systèmes réels de types films, plots et fils*, **PhD Thesis, Strasbourg University** (2001).

[But_01] W.H. Butler, X.-G. Zhang, T.C. Schulthess and J.M. MacLaren, *Spin-dependent tunneling conductance of Fe|MgO|Fe sandwiches,* **Phys. Rev. B 63** (2001) 054416.

[Die_91] B. Dieny, V.S. Speriosu, S.S.P. Parkin, B.A. Gurney, D.R. Wilhoit and D. Mauri, *Giant magnetoresistive in soft ferromagnetic multilayers,* **Phys. Rev. B 43** (1991) 1297.

[Fau_02] J. Faure-Vincent, C. Tiusan, C. Bellouard, E. Popova, M. Hehn, F. Montaigne and A. Schuhl, *Interlayer magnetic coupling interactions of two ferromagnetic layers by spin polarized tunneling,* **Phys. Rev. Lett. 89** (2002) 107206.

[Fen_06] G. Feng, S. van Dijken and J.M.D. Coey, *Influence of annealing on the bias voltage dependence of tunnelling magnetoresistance in MgO double-barrier magnetic tunnel junctions with CoFeB electrodes*, **Appl. Phys. Lett. 89** (2006) 162501.

[Fer_94] A. Fert and P. Bruno, in *Ultrathin Magnetic Structures*, edited by B. Heinrich and J.A.C. Bland, Springer-Verlag, Berlin **2** (1994) 82.

[Fer_01] A. Fert, A. Barthélémy, J. Ben Youssef, J.-P. Contour, V. Cros, J.M. de Teresa, A. Hamzic, J.-M. George, G. Faini, J. Grollier, H. Jaffrès, H. Le Gall, F. Montaigne, F. Pailloux and F. Petroff, *Review of recent results on spin polarized tunneling and magnetic switching by spin injection,* **Mater. Sci. Eng. B 84** (2001) 1.

[Grü_86] P. Grünberg, R. Schreiber, Y. Pang, M.B. Brodsky and H. Sowers, *Layered magnetic structures: Evidence for antiferromagnetic coupling of Fe layers across Cr interlayers,* **Phys. Rev. Lett. 57** (1986) 2442.

[Hal_09] D. Halley, O. Bengone, S. Boukari and W. Weber, *Novel oscillation period of the interlayer exchange coupling in Fe/Cr/Fe due to MgO capping,* **Phys. Rev. Lett. 102** (2009) 027201.

[Hin_10] A.T. Hindmarch, K.J. Dempsey, D. Ciudad, E. Negusse, D.A. Arena and C.H. Marrows, *Fe diffusion, oxidation, and reduction at the CoFeB/MgO interface studied by soft x-ray absorption spectroscopy and magnetic circular dichroism*, **Appl. Phys. Lett. 96** (2010) 092501.

[Ike_08] S. Ikeda, J. Hayakawa, Y. Ashizawa, Y.M. Lee, K. Miura, H. Hasegawa, M. Tsunoda, F. Matsukura and H. Ohno, *Tunnel magnetoresistance of 604% at 300 K by suppression of Ta diffusion in CoFeB/MgO/CoFeB pseudo-spin-valves annealed at high temperature*, **Appl. Phys. Lett. 93** (2008) 082508.

[Kat_06] T. Katayama, S. Yuasa, J. Velev, M.Ye. Zhuravlev, S.S. Jaswal and E.Y. Tsymbal, *Interlayer exchange coupling in Fe/MgO/Fe magnetic tunnel junctions*, **Appl. Phys. Lett. 89** (2006) 112503.

[Koo_99] J.C.S. Kools, W. Kula, D. Mauri and T. Lin, *Effect of finite magnetic film thickness on Néel coupling in spin valves*, **J. Appl. Phys. 85** (1999) 4466.

[Liu_03] Z.Y. Liu and S. Adenwalla, *Oscillatory interlayer exchange coupling and its temperature dependence in $[Pt/Co]_3/NiO/[Co/Pt]_3$ multilayers with perpendicular anisotropy*, **Phys. Rev. Lett. 91** (2003) 037207.

[Liu_11] Y. Liu, A.N. Chiaramonti, D.K. Schreiber, H. Yang, S.S.P. Parkin, O.G. Heinonen and A.K. Petford-Long, *Effect of annealing and applied bias on barrier shape in CoFe/MgO/CoFe tunnel junctions*, **Phys. Rev. B 83** (2011) 165413.

[Man_06] S. Mangin, D. Ravelosona, J.A. Katine, M.J. Carey, B.D. Terris and E.E. Fullerton, *Current-induced magnetization reversal in nanopillars with perpendicular anisotropy,* **Nature Mater. 5** (2006) 210.

[Mat_01] J. Mathon and A. Umerski, *Theory of tunneling magnetoresistance of an epitaxial Fe/MgO/Fe(001) junction,* **Phys. Rev. B 63** (2001) 220403 (R).

[Mor_04] J. Moritz, F. Garcia, J.-C. Toussaint, B. Dieny and J.-P. Nozières, *Orange peel coupling in multilayers with perpendicular magnetic anisotropy: Application to (Co/Pt)-based exchange-biased spin-valves*, **Europhys. Lett. 65** (2004) 123.

[Née_62] L. Néel, *Sur un nouveau mode de couplage entre les aimantations de deux couches minces ferromagnétiques*, **C. R. Hebd. Séances Acad. Sci. 255** (1962) 1676.

[Nis_09a] L.E. Nistor, B. Rodmacq, S. Auffret and B. Dieny, *Pt/Co/oxide and oxide/Co/Pt electrodes for perpendicular magnetic tunnel junctions,* **Appl. Phys. Lett. 94** (2009) 012512.

[Nis_09b] L.E. Nistor, B. Rodmacq, S. Auffret, A. Schuhl and B. Dieny, *Antiferromagnetic coupling in sputtered MgO tunnel junctions with perpendicular magnetic anisotropy,* **IEEE Trans. Magn. 45** (2009) 3472.

[Nis_10] L.E. Nistor, B. Rodmacq, S. Auffret, A. Schuhl, M. Chshiev and B. Dieny, *Oscillatory interlayer exchange coupling in MgO tunnel junctions with perpendicular magnetic anisotropy,* **Phys. Rev. B 81** (2010) 220407 (R).

[Par_90] S.S.P. Parkin, N. More and K.P. Roche, *Oscillations in exchange coupling and magnetoresistance in metallic superlattice structures: Co/Ru, Co/Cr, and Fe/Cr,* **Phys. Rev. Lett. 64** (1990) 2304.

[Par_91] S.S.P. Parkin, *Systematic variation of the strength and oscillation period of indirect magnetic exchange coupling through the 3d, 4d, and 5d transition metals*, **Phys. Rev. Lett. 67** (1991) 3598.

[Rea_07] J.C. Read, P.G. Mather and R.A. Buhrman, *X-ray photoemission study of CoFeB/MgO thin film bilayers*, **Appl. Phys. Lett. 90** (2007) 132503.

[Rei_09] A. Reinartz, J. Schmalhorst and G. Reiss, *Influence of annealing temperature and thickness of a CoFeB middle layer on the tunnel magnetoresistance of MgO based double barrier magnetic tunnel junctions*, **J. Appl. Phys. 105** (2009) 014510.

[Rod_06] B. Rodmacq, V. Baltz and B. Dieny, *Macroscopic probing of domain configurations in interacting bilayers with perpendicular magnetic anisotropy,* **Phys. Rev. B 73** (2006) 092405.

[Rod_09] B. Rodmacq, A. Manchon, C. Ducruet, S. Auffret and B. Dieny, *Influence of thermal annealing on the perpendicular magnetic anisotropy of Pt/Co/AlOx trilayers,* **Phys. Rev. B 79** (2009) 024423.

[Sch_07] J. Schmalhorst, A. Thomas, G. Reiss, X. Kou and E. Arenholz, *Influence of chemical and magnetic interface properties of Co-Fe-B/MgO/ Co-Fe-B tunnel junctions on the annealing temperature dependence of the magnetoresistance*, **J. Appl. Phys. 102** (2007) 053907.

[Slo_95] J.C. Slonczewski, *Overview of interlayer exchange theory*, **J. Magn. Magn. Mater. 150** (1995) 13.

[Sti_05] M.D. Stiles, B. Heinrich and J.A.C. Bland, Eds., *Interlayer exchange coupling*, in "Ultrathin Magnetic Structures III: Fundamentals of Nanomagnetism", 3rd ed., Berlin, Germany: Springer (2005) 99.

[Wol_01] S.A. Wolf, D.D. Awschalom, R.A. Buhrman, J.M. Daughton, S. von Molnár, M.L. Roukes, A.Y. Chtchelkanova and D.M. Treger, *Spintronics: A spin-based electronics vision for the future,* **Science 294** (2001) 1488.

[Wu_08] H.-C. Wu, S.K. Arora, O.N. Mryasov and I.V. Shvets, *Antiferromagnetic interlayer exchange coupling between Fe_3O_4 layers across a nonmagnetic MgO dielectric layer,* **Appl. Phys. Lett. 92** (2008) 182502.

[Yan_07] H. Yanagihara, Y. Toyoda and E. Kita, *Antiferromagnetic interlayer coupling through a thin MgO layer in γ-Fe_2O_3/MgO/Fe(001) multilayers,* **J. Appl. Phys. 101** (2007) 09D101.

[Yan_10] H.X. Yang, M. Chshiev, A. Kalitsov, A. Schuhl and W.H. Butler, *Effect of structural relaxation and oxidation conditions on interlayer exchange coupling in Fe/MgO/Fe tunnel junctions*, **Appl. Phys. Lett.** **96** (2010) 262509.

[Yan_11] H.X. Yang, M. Chshiev, B. Dieny, J.H. Lee, A. Manchon and K.H. Shin, *First-principles investigation of the very large perpendicular magnetic anisotropy at Fe/MgO and Co/MgO interfaces*, **Phys. Rev. B** **84** (2011) 054401.

[Yua_06] S. Yuasa, A. Fukushima, H. Kubota, Y. Suzuki and K. Ando, *Giant tunneling magnetoresistance up to 410% at room temperature in fully epitaxial Co/MgO/Co magnetic tunnel junctions with bcc Co(001) electrodes,* **Appl. Phys. Lett.** **89** (2006) 042505.

[Zhu_05] M.Ye. Zhuravlev, E.Y. Tsymbal and A.V. Vedyayev, *Impurity-assisted interlayer exchange coupling across a tunnel barrier*, **Phys. Rev. Lett.** **94** (2005) 026806.

Chapter IV

SPIN TRANSFER TORQUE SWITCHING IN PERPENDICULAR MAGNETIC TUNNEL JUNCTIONS

Chapter IV

SPIN TRANSFER TORQUE SWITCHING IN PERPENDICULAR MAGNETIC TUNNEL JUNCTIONS

Magnetic tunnel junctions (MTJ's) are very promising for memories applications because they can be easily used for storing the information even when no current is applied. In MTJ the coding of information depends on the relative direction of the magnetization of the two magnetic layers on each side of the insulating barrier, leading to tunnel magnetoresistance effects (TMR). There are different ways of writing the information (switching the storage layer magnetization) in MTJ: with an applied field or a thermally assisted applied field. More recently, thanks to theoretical works on spin transfer torque (STT) phenomenon of Berger and Slonczewski **[Ber_96, Slo_96]** and the developpement of nanofabrication techniques, another switching technique was proposed for MRAM, called spin transfer torque switching.

In STT writing, a polarized electrical current exerts a torque on the magnetization of the storage magnetic layer, and can switch its direction for a large enough current density. This last switching technique can bring interesting advantages over other ones making possible the memory cell size reduction by suppressing the supplementary conductive line used in the case of field assisted switching. Since the current passes through the cells being written the field selection errors of the conventional field writing MRAM can be avoided.

The first experimental demonstration of spin-transfer torque switching in a nanomagnet was presented in metallic spin valve with critical switching densities > 10^7-10^8 A/cm^2, too high for practical applications **[Kat_00]**. Since the Oersted field (created by the polarized current passing through the MTJ) can mask STT effects, the lateral dimensions of the sample must decrease below 500 nm. Furthermore the energy consumption by spin-transfer torque is proportional to the size of the MTJ cell. Lower cell sizes will demand lower critical currents, but the problem for classical MRAM is the loss of data retention when the size is reduced. Perpendicular MTJ don't have this problem so STT-MTAM cells of the size of a transistor can be envisaged (30 nm). But the main problem of both MTJ and pMTJ is the barrier resistivity, which should be low enough (10 Ohmμm^2) to stand critical current densities of the order of 10^7 A/cm^2 **[Ike_07]**. In addition, the maximum writing voltage must be smaller than the breakdown voltage V_B of the insulator (about 1 V).

Large switching currents require large transistor sizes for write operation. The actual challenge is to reduce the switching current in order to increase the storage density using the advantages of pMTJ.

In this **Chapter** we will present the advantages of pMTJ for STT switching and the switching characteristics of nanometric perpendicular MTJ devices fabricated at the PTA nano-fabrication platform **[Pta_07]** with the help of different users. The micro-fabrication process is detailed in Appendix 4.

IV-1. Spin Transfer Torque: theory and experiments

IV-1.1 Theoretical model

It was previously shown that the magnetic layer magnetization has a spin polarization effect on the current passing through the layer. The reverse effect also exists: the polarized current can act on the magnetization through a torque, which can induce excitation or even magnetization switching. This is the main idea of the spin torque theory elaborated by Berger and Slonczewski **[Ber_96, Slo_96]**. The key ingredient of this theory is the conservation of the angular momentum. When a spin polarized current of conduction electrons enters a magnetic layer with the magnetization (M) opposite to or non collinear with the current polarization (P), the current will be polarized towards the direction of the magnetization. During this process of polarization the electrons precess around the magnetization axis, loosing their angular momentum, which will be absorbed by the magnetization in order to conserve the spin angular momentum of the system. One can see this as a transfer of angular momentum between the magnetization and conductions electrons through a torque exerted by the electrons on the magnetization. This torque can be expressed as:

$$\vec{T}_{STT} = a_j \cdot \vec{M} \times \left(\vec{M} \times \vec{P}\right) + b_j \cdot \vec{M} \times \vec{P} \qquad \textbf{Equation IV-1}$$

The first term corresponds to the longitudinal component of the spin transfer torque with a prefactor a_j which depends on the current (I). The second term, orthogonal to the first one, is called the field-like torque term since it acts as an external field with the amplitude bj and with the direction of the polarization perpendicular to the plane (**Figure IV-1**). The planar torque, called Slonczewski's torque, is zero at zero voltage and is a non monotonic function of applied voltage. In MgO tunnel junctions, because of the tunnelling transport characteristics of the spacer (symmetry filtering), the second term is important, representing 10-30% of the first longitudinal term **[San_08, Kub_08, Dea_08]**. It must be noted that the perpendicular torque is an even function of applied voltage for symmetric MTJ (same splitting for both electrodes) **[The_06]** and an odd function of applied voltage for asymmetric MTJ **[Man_08, 0h_09]**. This perpendicular torque can explain the switching current asymmetry and can be used in asymmetrical MTJ to prevent from field back-switching phenomena.

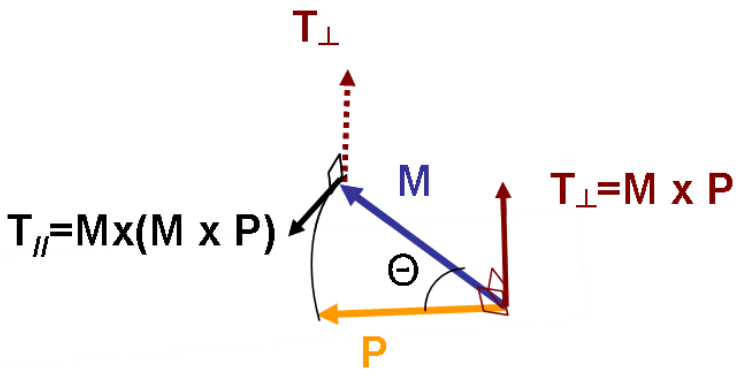

Figure IV-1: Representation of the STT torque components $T_{//}$ and $T_{\perp}$ acting on the free layer magnetization M.

Injecting a current through a magnetic material, the spin-transfer torque will modify the magnetization dynamics. One has to consider both Slonczewski's and field-like torques in the LLG equation **[Lan_35, Gil_04]** which becomes:

$$\frac{d\vec{M}}{dt} = \gamma \cdot \mu_0 \cdot \vec{M} \times \vec{H}_{eff} + \frac{\alpha}{M_s} \cdot \vec{M} \times \frac{d\vec{M}}{dt} + \vec{T}_{STT} \qquad \textbf{Equation IV-2}$$

In a magnetic material the magnetic moments feel different contributions from the dipolar and anisotropy interactions in the form of an effective magnetic field (H_{Eff}) acting as a torque $\mu_0 M \times H_{Eff}$. A misalignment between the magnetization and the effective field (due to thermal fluctuations) will result in magnetization precession around the effective field with the frequency γ (gyromagnetic ratio, depending on the electron charge and mass, $\gamma = q/2m_e$), the first term in the LLG **Equation IV-2**. This is a conservative term since in the absence of other contributions no energy dissipation occurs through the precession motion. But in real cases energy loss can also occur and damping arises due to magnetization collisions with phonons or itinerant electrons. This damping is modelled in **Equation IV-2** by the second term containing α, the damping coefficient (Gilbert damping). One can imagine the magnetization in a viscous medium, which causes the loss of the magnetization energy towards the direction of the effective field. In this case the circular precession of the magnetization will become a spiral, progressively orienting the magnetization parallel to H_{eff} (**Figure IV-2**). As a function of the current sign the spin torque term can amplify (for I<0) or attenuate (I>0) the magnetization precession. For example a negative current injected in a magnetic material will maintain the precession motion of the magnetization being opposite to the damping. Increasing the current density will increase the precession amplitude and for a critical current the magnetization will have enough energy to switch to the opposite direction, until the current helps the magnetization reaching the direction of the applied field.

Finally we can obtain the critical STT current density from the LLG equation as **[Kat_00, Sun_00, Mor_10]**:

$$J_c = \frac{2 \cdot e}{\hbar} \cdot \frac{\alpha \cdot t \cdot M_s}{\eta(\theta)} \cdot H_{eff} \qquad \textbf{Equation IV-3}$$

where e is the electron charge, ħ is the reduced Planck constant, α is the Gilbert damping coefficient, M_S and t are the saturation magnetization and thickness of the storage layer, η(θ) the spin transfer torque efficiency which depends on the relative orientation of the magnetizations (θ= 0 or π) and on the polarization P, and H_{Eff} the effective switching field.

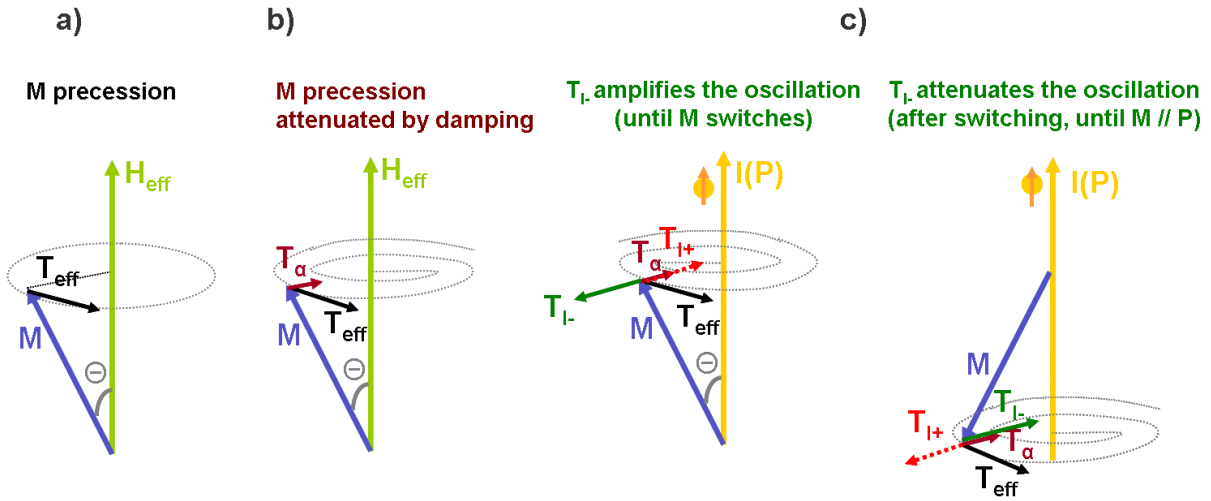

Figure IV-2: Trajectory of the magnetization in a magnetic field: (a) Without dissipation; (b) With dissipation; (c) In the presence of the spin torque terms ($T_{I+/-}$) before and after magnetization switching.

IV-1.2 Potential advantages of perpendicular magnetic tunnel junctions

According to **Equation IV-3**, the critical current for spin transfer torque reversal of the magnetization direction of the storage layer is given by:

$$I_c = \frac{2 \cdot e}{\hbar} \cdot \frac{\alpha \cdot A \cdot t \cdot M_s}{\eta(\theta)} \cdot H_{eff} \qquad \textbf{Equation IV-4}$$

where A is the area of the magnetic element.

In order to minimize I_C, one can try to maximize the spin torque efficiency term η, for example by maximizing the polarization P (P_{max}= 1) using materials with high spin polarization (CoFe alloys for instance). The parameters α, A, t and M_S are both material and technology-dependent. The area A of the magnetic cell depends on the technological process, able to go down to sub-100 nm memory points. Decreasing M_S can be done by using CoFeX alloys with different X metals (B, Si). The thickness t of the magnetic layer can be made as small as 1 nm, but this is generally accompanied by a progressive decrease of the polarization.

Concerning the damping constant α, it has been shown that even if it is quite low (0.01) for CoFeB 1.2 nm thick layers, it rapidly increases when the layers thickness is decreased when trying to enhance the PMA contribution [Ike_10]. During the fabrication process, there are evidences that surface oxides or other effects can increase the damping coefficient substantially from its value in continuous thin films [Ozh_07]. Some studies showed that switching current thresholds are lowered suggesting that the damping was reduced using a Ru layer or Ru-based composite layer deposited on the top of the storage layer [Jia_04].

Additionally, the MRAM structure must be optimized for barrier resistance and as large as possible TMR. Increasing the TMR ratio can lead to further reduction of I_C by increasing the polarization [Yod-10].

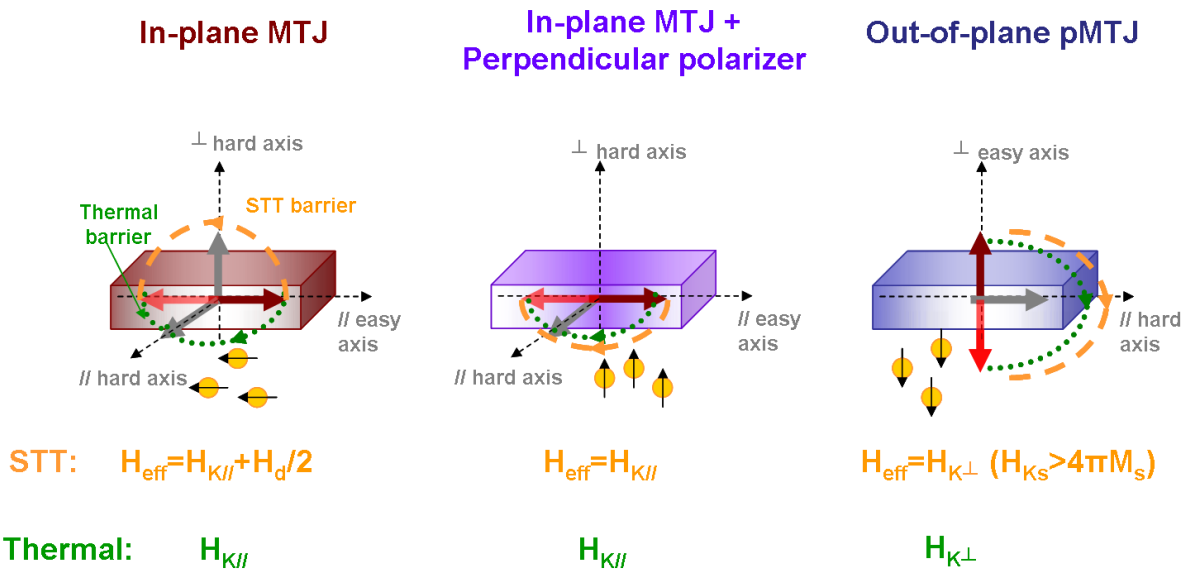

Figure IV-3: Energy barriers for STT writing and thermal stability in (a) In-plane MTJ, (b) In-plane MTJ with perpendicular polarizer and (c) Out-of-plane MTJ.

The last term in **Equation IV-4** is the effective switching field H_{Eff}. For systems with in-plane magnetization, H_{eff} can be written as:

$$H_{Eff} = H_K + \frac{H_d}{2}, \qquad \textbf{Equation IV-5}$$

where, according to our sign conventions in the preceding **Chapters**, both H_K and H_d terms are negative since they favour in-plane configuration of the magnetization. The first term H_K is the sum of intrinsic uniaxial anisotropy and shape anisotropy fields of the storage layer, dipolar field between storage and reference layers, and external applied field. The second term is the demagnetizing field of the storage layer. H_K determines the thermal energy barrier, which is mainly given by the shape of the pillars (elliptical). The total switching energy barrier is thus higher than the thermal energy barrier (**Figure IV-3a**).

A way of reducing the switching energy is to introduce a (positive) perpendicular anisotropy field $H_{K\perp}$ in the expression of H_{Eff} (**Chapter II-6**). This $H_{K\perp}$ term can be of either volume or interface origin, but usually leads to an increasing damping when materials such as Pt or Pd are used to create interface anisotropy **[Yod_10]**. The value of $H_{K\perp}$ can be chosen to almost cancel out the other terms, leading to a vanishingly small effective switching field (still keeping in mind that thermal stability must be preserved).

Another way is to use a supplementary magnetic layer with out-of-plane anisotropy, which will act as a perpendicular polarizer for the electrons **[Red_00, Hou_07, Liu_09, Pap_09, Mor_10, Ami_11, Mar_11]**. In that case the STT switching path will be in-plane, and both thermal and STT energy barriers will coincide (**Figure IV-3b**).

In magnetic junctions with out-of-plane magnetization, the effective field is given by:

$$H_{Eff} = H_{K\perp} - 4\pi M_S, \qquad \textbf{Equation IV-6}$$

where $H_{K\perp}$ is the perpendicular anisotropy field ($H_{K\perp} > 4\pi M_S$). In that case both STT and thermal energy barriers coincide (**Figure IV-3c**). The critical switching current can thus be much smaller than for in-plane magnetized electrodes. In addition, since shape anisotropy does not play anymore role in the thermal stability, magnetic cells can be made circular instead of elliptical, which makes down size scaling easier. Several papers already addressed the potential advantages of perpendicular magnetic tunnel junctions **[Hei_10, Wol_10, Yod_10]**.

In these perpendicular systems, a balance must be found between low writing energy and high enough thermal stability. The thermal stability factor Δ is expressed as:

$$\Delta = \frac{K \cdot V}{k_B \cdot T} \qquad \textbf{Equation IV-7}$$

where K is the anisotropy, V the (nucleation) volume in the storage layer, k_B the Boltzmann's constant, and T the absolute temperature. The stability of written information is given by:

$$\tau = \tau_0 \exp(\Delta) \qquad \textbf{Equation IV-8}$$

where τ is the information retention time and τ_0 a characteristic time (the inverse of the attempt rate) of the order of 10^{-9} s. Retention of information over 10 years implies a Δ value of about 40.

Comparison between performances of in-plane junctions, or between in-plane and out-of-plane ones, can thus only be done for equivalent stability factors. A figure of merit has been proposed [Kis_08], which is the ratio of the critical switching current to the stability factor, I_{C0}/Δ. However, it would be perhaps better to consider current densities J_{C0} instead of currents themselves, in order to get read of the cell area, which only depends on the quality of micro-fabrication, and not of materials performances.

Work on STT spin valves [Man_06, Tud_10] or classical STT MTJ [Liu_09, Ami_11] showed that PMA contribution should greatly reduce the required switching current by decreasing the demagnetizing field effect. Switching current densities and perpendicular anisotropy are strongly dependent on the free layer thickness as it was observed by Amiri in in-plane magnetized structures with PMA contribution [Ami_11]. Critical current densities as low as 2 MA/cm² were obtained in planar MTJ with low demagnetizing field. Fast switching, of the order of picoseconds, was observed in in-plane systems comprising an additional perpendicular polarizer [Pap_09] or with reduced demagnetizing field [Liu-09].

Requirements for industrial applications of spin torque perpendicular MRAM are the following:

- **thermal stability factor Δ > 40** for data retention times of 10 years,
- **very high TMR value**,
- **lower writing voltages U_{wr}<0.5V** to avoid breakdown in a distribution of MTJs during 10 years of operation,
- **low RA in order to have R=1000 Ohm** for sufficient read margin,
- **low diameter pillar size of around d=30nm (size of the transistor)** in order to increase the storage density.

The industrial target for switching currents densities in STT-MRAM applications is 0.5 to 1 MA/cm².

IV-1.3 Results from literature

It is difficult to find the best combination of materials meeting all the above requirements, explaining the rather small number of STT studies on perpendicular MTJ in the literature. These studies are summarized in **Table IV-1**, which gives the main characteristics of STT writing in sub-micrometric memory points. One can see that some publications do not give all information, especially about materials used. Although the first results are only three years old, performances in terms of switching current densities and thermal stability are already at the level of in-plane magnetized structures, despite the constraints imposed by perpendicular anisotropy, in terms for example of high-damping materials, limited magnetic thickness or texture matching with the MgO barrier. Rapid progress is expected as concerns TMR ratio and RA product.

Ref.	Team	Hard layer	Soft layer	TMR (%)	RA (Ωμm²)	Δ	Soft layer (nm)	J	Pulse (ns)	damping	d
Nak_08	Toshiba	RE-TM/CoFeB	RE-TM/CoFeB	15	16	107	3+1	4.8	100	-	130
Kis_08	Toshiba	?	$L1_0$	-	-	56	-	2	4	0.028	50
Hei_10	Seagate	RE-TM/CoFeB	RE-TM/CoFeB	-	-	-	3+1	2	40	0.01	70
Ike_10	Tohoku	Ta/CoFeB	Ta/$CoFe_{60}B$	120	18	43	1.2	4	100	0.01	40
Yod_10	Toshiba	Fe alloy?	Fe alloy?	22	18	32	1.5-2	0.4	5000	0.001	55
Wor_10	IBM	?	?	100	9.5	50	?	0.8	50	0.008	80
Wor_11	IBM	(Co/Pd)/CoFeB	Ta/$Co_{60}FeB$	46	12	66	0.8	2.4	50	-	80

Table IV-1: Publications on STT experiments in perpendicular magnetic tunnel junctions. RE-TM stands for Rare Earth-Transition Metal alloys, $L1_0$ for ordered alloys, (Co/Pt(Pd)) for multilayers, ? for unknown structures and - for absence of information on some parameters. Results in [Hei_10] come from micro-magnetic calculations. Δ is the thermal stability factor, J the critical switching current density (MA/cm²) and d the pillar diameter (nm).

Different materials with high PMA have been tested, in order to induce perpendicular anisotropy in the CoFeB magnetic electrodes on both sides of the MgO barrier (Rare Earth-Transition Metal alloys, ordered $L1_0$ alloys, (Co/Pt) and (Co/Pd) multilayers).

First STT experiments on pMTJ were reported on structures using RE-TM alloys for which PMA can be relatively easily obtained thanks to its bulk origin. However, the anisotropy properties of these alloys greatly depend on both alloy composition and annealing temperature, which makes their optimization quite difficult. Furthermore high annealing temperatures required to cristallize the MgO barrier can greatly affect their magnetic properties if their composition is not adapted to stand such temperatures. This can explain the low TMR measured in first STT-pMTJ experiments **[Nak_08]** which gave critical current densities of 4.8 MA/cm^2, higher than predicted for pMTJ. Authors of these first STT-pMTJ experiments claimed that the coercive field of the soft layer is strongly reduced from 1.3 kOe to 0.3kOe during the current pulse, meaning that STT switching is thermally assisted in this case.

Two years later **[Hei_10]**, a theoretical study using micromagnetic modelling examined the effect of materials properties on the switching current in pMTJ. The authors showed that using a synthetic ferromagnetic free layer (SAF) could decrease the critical current. Such a synthetic free layer should allow low critical switching currents just by tuning the interlayer exchange coupling between layers: when the softest layer of the SAF switches, it exerts a torque on hardest one resulting in a weak exchange spring effect. But this is difficult to fabricate just using Ta/CoFeB/MgO materials since in these systems the PMA comes only from the interface between CoFeB and MgO, and is just large enough to keep the magnetization of a 1 nm thick layer out-of-plane. **[Hei_10]** et al showed that the optimum material combination is CoFeB 1nm/TbFeCo 3 nm free layer, for which they estimated a critical density of 2.6 MA/cm^2 with switching times below 20 ns.

There are two problems in these systems. The first one is related to the strength of the interlayer coupling: for low coupling (4 erg/cm^2), the switching is fast but coupling is not strong enough to completely saturate the magnetization along the –z axis, resulting in a low TMR signal. The second problem is related to the nano-pillar fabrication process which can greatly affect the coupling properties of the RE-TM layers. This study brings additional explanation for the relative success of the first RE-TM pMTJ to reach critical current densities of 10^5 A/cm^2 predicted in the literature.

Ordered $L1_0$ alloys were tested by Toshiba **[Kis_08]**. Switching current densities as low as 2.5 MA/cm^2 were obtained along with a relatively low Gilbert damping constant (0.03) for the composite storage layer. The main drawback of these $L1_0$ alloys is that they generally require high temperature deposition.

Later on the advantage of perpendicular structures for reducing the current densities was clearly shown by Yoda et al. **[Yod_10]**. The efficiency of spin transfer torque writing for perpendicular MTJs with Fe-based alloys was found 4–10 times higher than in in-plane MTJs, with rather small TMR of 22–23%, but with a very small damping value of 0.001. In this case the critical current density almost reached the predicted value of 0.1 MA/cm^2.

Co-based multilayers could appear as the best choice, since they can induced a rather strong anisotropy, even after annealing at temperatures (300-350°C) required for optimizing TMR properties of MgO barriers. However, their fcc (111) texture is not compatible with the only tunnel barrier which gives high magnetoresistance, MgO, which requires a bcc (100) texture. In addition, roughness induced by these different textures contributes to a spread in magnetic properties from MTJ to MTJ.

The problem of the bcc (100) texture of the CoFeB electrode upon crystallization was solved when structures based on Ta/CoFeB electrodes were proposed in 2010 **[Ike_10]**. Perpendicular anisotropy, although much smaller than in all other proposed structures, mainly

arises from the CoFeB/oxide interface [Mon_02]. After patterning into submicronic pillars, two well-separated parallel and anti-parallel states are obtained, leading to both high TMR ratio (120%), low RA product (18 Ωμm²), and relatively low STT switching current densities (4 MA/cm²).

In 2010, IBM [Wor_10] proposed a new "unknown" material which seems perfectly suited for STT pMTJ applications: high TMR, high PMA, low damping, high enough thermal stability and very low critical current density.

IV-1.4 Experimental determination of STT characteristics

The experimental set-up used to measure the effect of a voltage pulse on the resistance of tunnel junctions (STT switching of the magnetization of the storage layer) is presented in **Figure IV-4**. Pulses of maximum 10V amplitude with a duration between 50ps and 10ns are generated by a monopolar pulse generator connected to the AC input of a bias tee to the sample measuring tip. In order to change the polarity of the pulses the tip probe must be moved by translation to the top and bottom contacts of the MTJ. In order to determine the resistance of the MTJ the tip is connected through the bias tee (DC output) to a current source in parallel with an oscilloscope which records and calculates the average of the hysteresis loops. A perpendicular magnetic field is generated by an electromagnet, homogeneous on 0.7 cm diameter located under the sample. The field frequency is 1Hz and the integration time of the recorded signal of the resistance measurement is 10 ms.

The main drawback of this set-up is the limited area of homogeneity of the perpendicular field which requires a careful repositioning of the sample when junctions spread on a 100 mm wafer are measured. Another difficulty is that the current direction in the junction is manually set since the pulse generator is monopolar. This implies a well established protocol and additional measurement time. As an example, on a given junction, 5 different pulse amplitudes and durations for both current directions mean 50 measurements (each repeated 60 times), which represent a total measurement time of 12 hours. One must recall that a 100 mm wafer comprises about 16.000 junctions. Looking only at a diameter (along a CoFeB thickness wedge for example), there are still 1.500 junctions left. Let's also note that the applied voltage must be very progressively increased, since breakdown of the junction marks the end of the measurements.

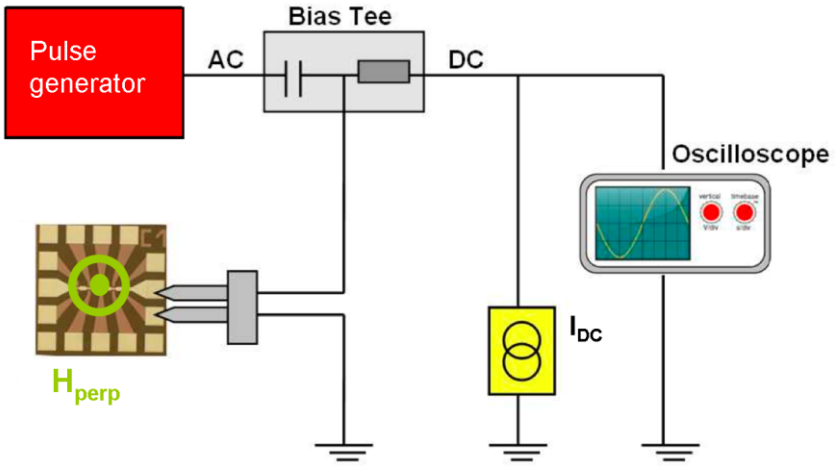

Figure IV-4: Experimental setup used to determine STT switching of tunnel junctions.

The experimental procedure is the following:

- a first R(H) hysteresis loop is recorded in order to determine the position of the two (P→AP)

and (AP→P) transitions. The hysteresis loop can be non-symmetrical with respect to zero fields because of dipolar interactions between soft and hard layers.

- for given sign, amplitude and duration of the voltage pulse, a hundred hysteresis loops are recorded, the voltage pulse being applied each time the external field equals the bias field H_0 previously determined. All hysteresis loops are then summed.

The switching probability is then determined from the shape of the resulting summation. **Figure IV-5** shows an example of such cycles. The current direction is such that in this case the antiparallel state is favoured. In **Figure IV-5a**, the cycle is symmetrical with respect to H_0, indicating that the pulse applied at H_0 was unable to switch the magnetization. In **Figure IV-5b**, for a larger pulse duration or amplitude, one observes two transitions, one at H_0 and the other one at the coercive field. This means that, among all recorded cycles, some of them led to switching at H_0. If ΔR is the total resistance variation (between parallel and anti-parallel states), and Δr the position of the intermediate plateau (with respect to the initial resistance in the parallel state), the switching probability is directly given by P= Δr/ΔR. In **Figure IV-5c**, only one transition is observed at H_0, corresponding to a 100% switching probability.

A new automatic set-up has been recently adapted to measurements in perpendicular applied field. The 100 mm wafer is displaced automatically, and all junctions are successively positioned at the centre of the magnet. Electrical contacts are then established, and R(H) curves are recorded, thus giving a map of (TMR, RA) on the whole wafer.

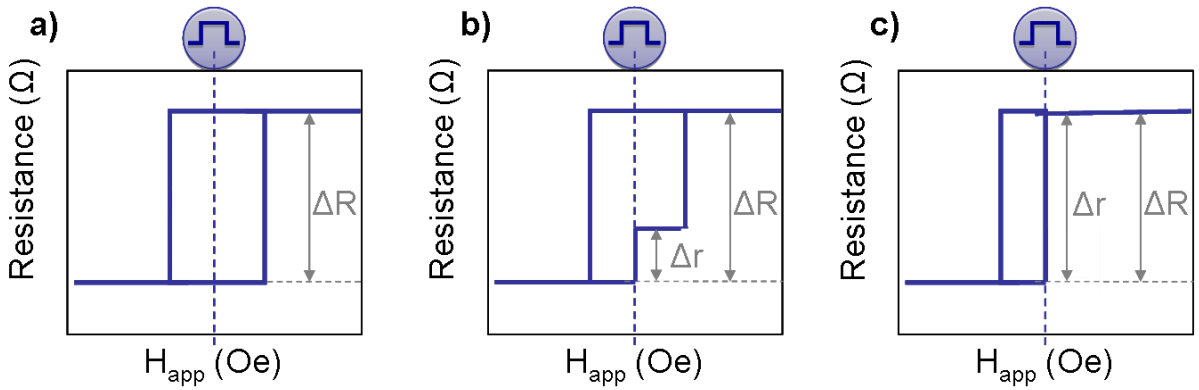

Figure IV-5: Determination of the switching probability on hysteresis loops with voltage pulses applied at the centre of the cycle.

IV-2. STT switching of CoFeB/MgO/CoFeB/(Tb/Co) based pMTJ

IV-2.1 Quasi-static TMR properties as a function of pillar size

Among perpendicular MTJ presented in Chapter II, the more appropriate for STT studies is the one comprising a bottom CoFeB free layer and a top reference CoFeB layer exchange coupled to TbCo. We choose the free layer as bottom electrode in order to maximise the anisotropy since we already showed that the growth of a perpendicular magnetic layer is more difficult on the barrier [Ike_10]. To obtain a top electrode with strong anisotropy we choose to couple the top CoFeB layer 1.6 nm thick to a material having very strong PMA as Tb/Co multilayers developed by S. Bandiera during his thesis work [Ban_11].

Two structures were fabricated in order to explore STT properties as a function of both CoFeB and Mg thicknesses. The two samples are schematically presented in **Figure IV-6**, one with a CoFeB wedge and the other with a MgO wedge/Mg composite barrier. The stack is the following for the CoFeB wedge: CuN30/Ta3/**CoFeB x**/MgOx0.9/Mg0.5/CoFeB1.6/(Tb/Co)/Ta3/Cu3/Ru7 (nm) and for the MgO wedge: CuN30/Ta3/CoFeB1/**Mg y Natox**/Mg0.5/CoFeB1.6/(Tb/Co)/Ta3/Cu3/Ru7 (nm).

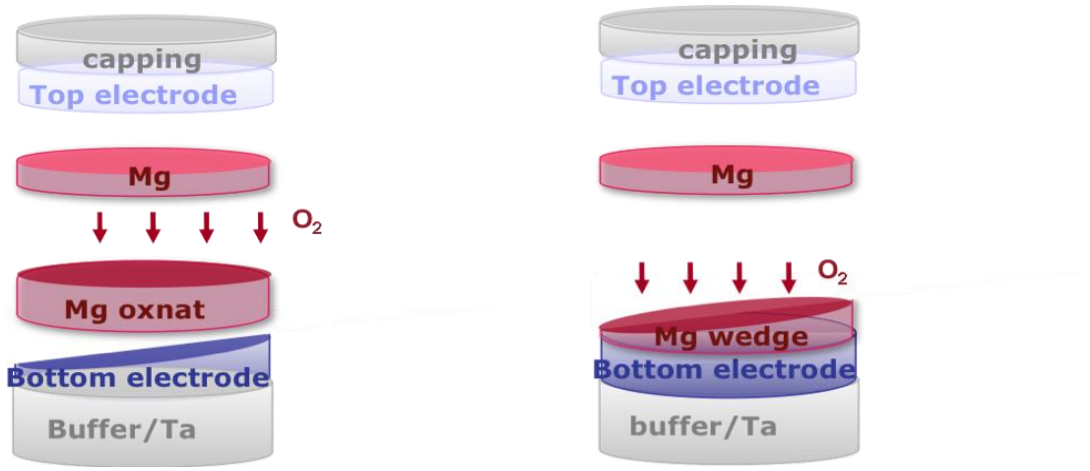

Figure IV-6: PMA structures chosen for the STT study: left structure has a wedge of the bottom CoFeB free layer and right structure has a wedge of Mg oxidized barrier.

Both sample were deposited on 100 mm wafers and annealed at 300°C. After electrical characterization by CAPRES technique (CIPT) presented in **Chapter II-1**, the samples were patterned into circular pillars with different sizes (1000 nm, 500 nm, 300 nm, 200 nm, 100 nm and 50 nm) through e-beam lithography and IBE etching technique (**Appendix 4**).

The main results presented here concern the sample with the CoFeB wedge. The other sample was prepared in order to determine optimum oxidation conditions along the Mg wedge. **Figure IV-7** gives the variation of the thickness of the (soft) bottom CoBeB thickness along the wedge as a function as the line number (L1 corresponds to the largest CoFeB thickness).

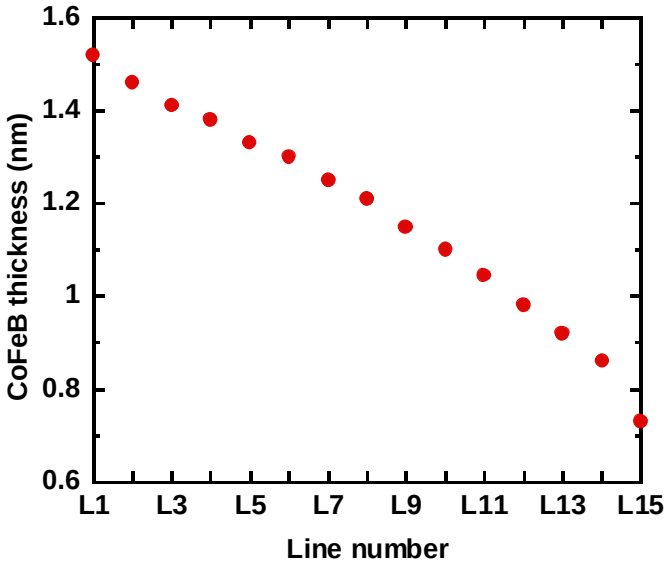

Figure IV-7: Variation of the CoFeB thickness as a function of line number along the CoFeB wedge.

The samples are first electrically characterized by quasistatic measurements of R(H) loops as a function of applied field with a DC voltage of 300 mV. The best way to verify the quality of the sample after process is to look at the TMR distribution as a function of the resistance in the parallel state (low resistance). The TMR as a function of resistance is presented in **Figure IV-8**. During the process parasitic resistances can appear, due to metallic re-depositions during IBE etching at the barrier level (Rp, parallel resistance) or remaining resin on the top of the pillars (Rs, series resistance). These parasitic resistances can be observed in the TMR distribution on the left of the TMR peak as parallel resistance for R<Rlow nominal and to the right of the TMR peak as series resistance for R>Rlow nominal.

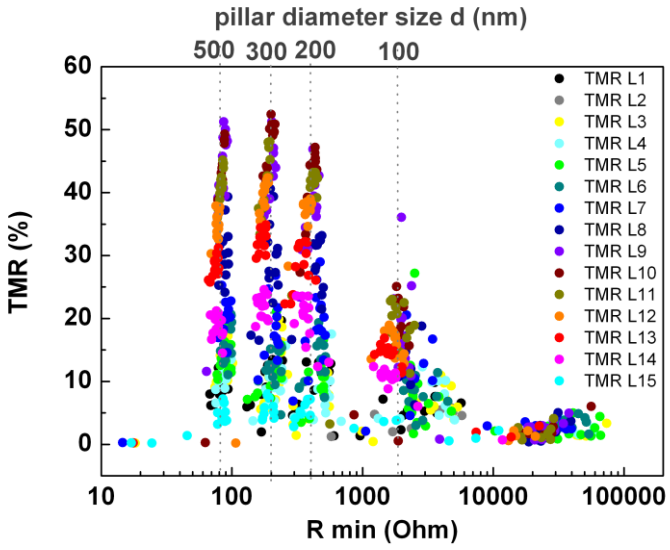

Figure IV-8: TMR distribution as a function of Rlow resistance along the CoFeB wedge for different pillar sizes (500, 300, 200, 100 nm). L1 corresponds to the largest CoFeB thickness, and junctions with 15 different CoFeB thicknesses are measured along the 100 mm diameter.

Four distributions are clearly observed with the a maximum TMR value for each peak centred around the corresponding values of the resistance expected for a RA product of 14 Ohmμm^2 (determined from macroscopic measurements) and different nominal pillar sizes of

500, 300, 200 and 100 nm. This means that parasitic resistances have a negligible contribution. In addition, the very small width of the peaks, at least for the largest pillar sizes, implies a very narrow size distribution from pillar to pillar. The TMR distribution is broader for the 100 nm pillars implying a larger size distribution or a less well defined magnetization direction of the storage layer. 50 nm pillars (corresponding to a nominal resistance of 7000 Ω) do not give any TMR signal.

Looking now at the TMR value, we can observe that, for the larger pillar sizes (500, 300, 200 nm), the maximum of the TMR is around 45-50%, that is lower than the values measured by the Capres tool on macroscopic samples (70-80%). This TMR decrease after process can be due either to the above-mentioned parasitic series resistances, or more probably to oxidation of the TbCo layer from the sides of the pillar, which could change its magnetic properties and for example decrease the coupling strength with the CoBeB top layer, leading to a slightly canted state of the reference layer.

Different colours on **Figure IV-8** correspond to different CoFeB thicknesses along the wedge (from L1 for the largest thickness to L15 for the smallest one). The TMR ratio varies with the CoFeB thickness (see **Figure IV-9**). However, the spread in the TMR values is very small for a given CoFeB thickness. The maximum TMR value does not depend so much on pillar size for 500, 300 and 200 nm diameters, but decreases by a factor of about 2 for a diameter of 100 nm.

The RA_{low} product measured on the wafer for different pillar sizes as a function of the CoFeB thickness is presented in **Figure IV-9** along with the RA measured on macroscopic sample with the Capres tool. We do not consider here the largest 500 nm pillars. They are of little interest for STT experiments because of their low resistance (around 100Ω). As it was observed before in **Figure IV-8**, the RA product of pillars with the largest diameters (300 and 200 nm) is very close to that measured before processing, around 14 Ohmμm². For the 100 nm pillars one can observe a very large spread of the RA values.

The TMR values measured on the pillars are more or less independent of pillar size for 500, 300 and 200 nm (with about half the value obtained before processing), and decreases sharply at 100nm. One can note that the overall variation of TMR as a function of CoFeB thickness (presented in **Chapter II-4.2**) is more or less the same after processing. However, quasi-static R(H) curves show that 100% perpendicular remanence is obtained up to a CoFeB thickness of 1.1 nm, as compared to 1.0 nm before processing.

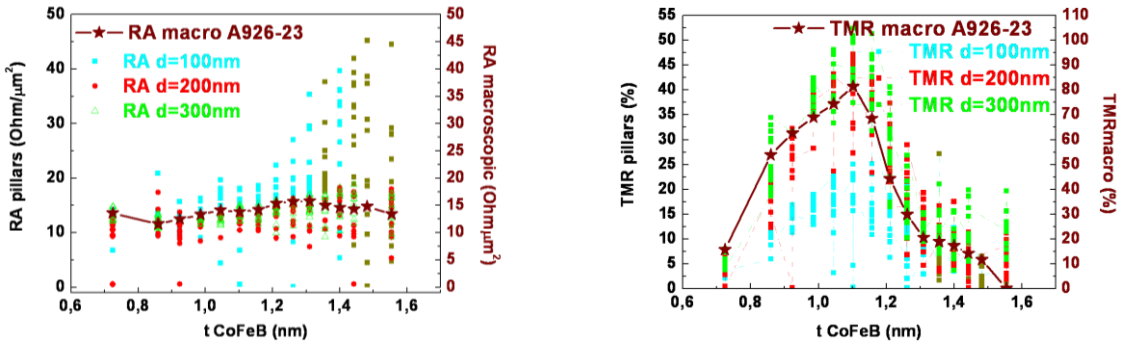

Figure IV-9: RA product (left) and TMR ratio (right) as a function of CoFeB thickness for 100, 200, 300nm pillars, and comparison with macroscopic (Capres) measurements.

Since these static measurements give encouraging results for pillars with diameters of 200 and 300 nm, we will focus on these sizes for the STT experiments presented in the next **Section**.

IV-2.2 Critical voltage and current density as a function of pillar size

Quasistatic spin-torque switching was studied following the procedure described in **Section IV-1.4**) with voltage pulses durations between 1 and 10 ns and varying amplitude. **Figure IV-10** shows that the switching probability increases with pulse length. For 10 ns, writing the parallel state requires only 400 mV. For our STT studies, choosing 10 ns long pulses is thus a good compromise, the switching speed being high (as SRAM) and the pulse voltage low enough to write information using a transistor.

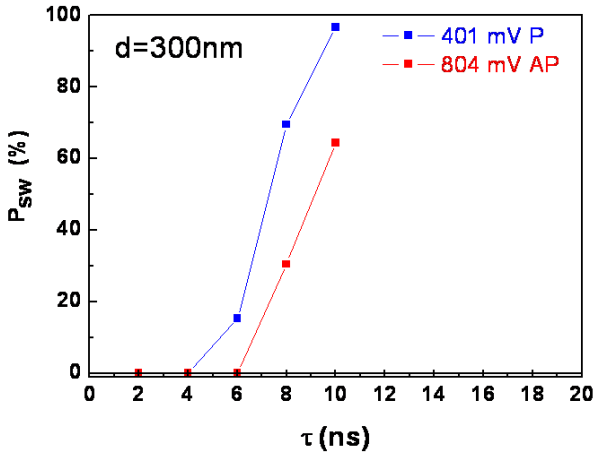

Figure IV-10: Variation of the switching probability with voltage pulse length for both current directions in 300 nm pillars on line 13 (0.92nm).

Examples of STT switching with positive and negative pulses for 200 nm pillars with two different CoFeB thicknesses are given in **Figure IV-11** and **Figure IV-12**. Every hysteresis loop is the sum of 64 measurements. One can see that the resistance level for both junctions does not evolve with time, showing that the barrier is relatively stable against repeated voltage pulses.

For both left **Figures** electrons go from the top (hard layer) to the bottom (soft layer) electrode, and in this case the parallel P state is favoured by the STT switching current. **Figures** on the right correspond to electrons going from the bottom (soft layer) to the top (hard layer) electrode, and in this case the antiparallel AP state is favoured [Kis_08].

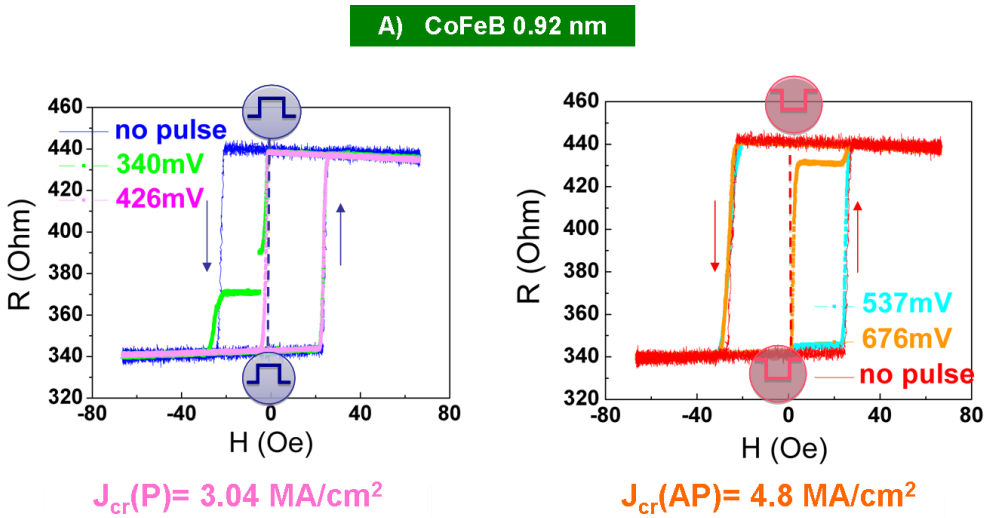

Figure IV-11: Hysteresis loops measured on a 200 nm pillar for a CoFeB thickness of 0.92nm (L13) with 10ns long pulses of different amplitudes: the P state is written on the left, and the AP state on the right.

The difference between the voltage values of AP to P and P to AP switching originates from the STT term $\eta(\theta)=P/[2(1+P^2\cos\theta)]$, the spin transfer torque efficiency, which depends on the angle between the magnetization of the free and reference layers [Slo_96, Kis_08, Sat_11].

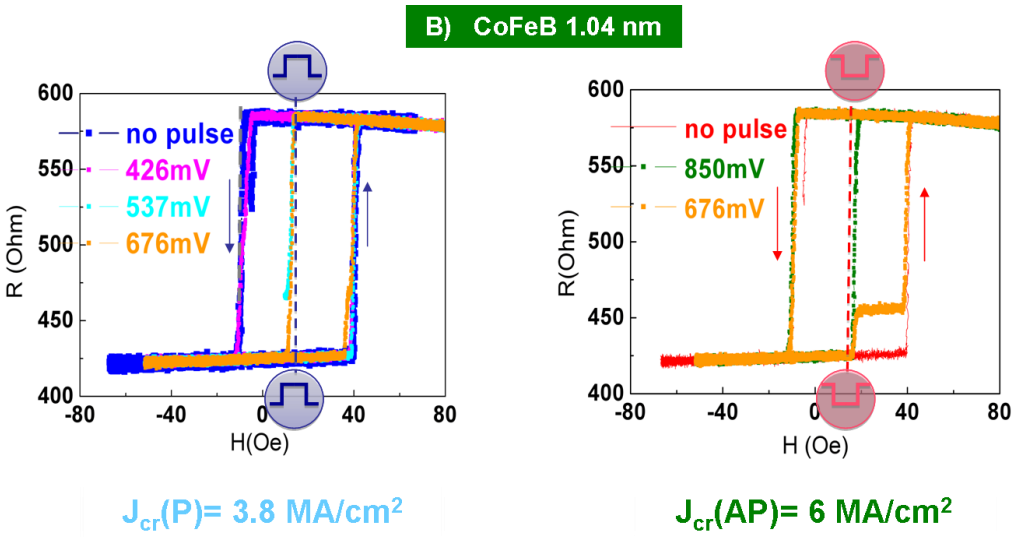

Figure IV-12: Same as in Figure IV-10 for a CoFeB thickness of 1.04 nm (L11).

For a CoFeB layer 0.92 nm thick (**Figure IV-11**), very low switching voltages of 400 mV (3.04 MA/cm²) are obtained for writing the P state and 676 mV (4.8 MA/cm²) for writing the AP state. For a 1.04 nm thick CoFeB layer (**Figure IV-12**) the P state is written with a higher voltage of 573 mV (3.8 MA/cm²). The writing voltage for the AP state also increases to 850 mV (6.0 MA/cm²).

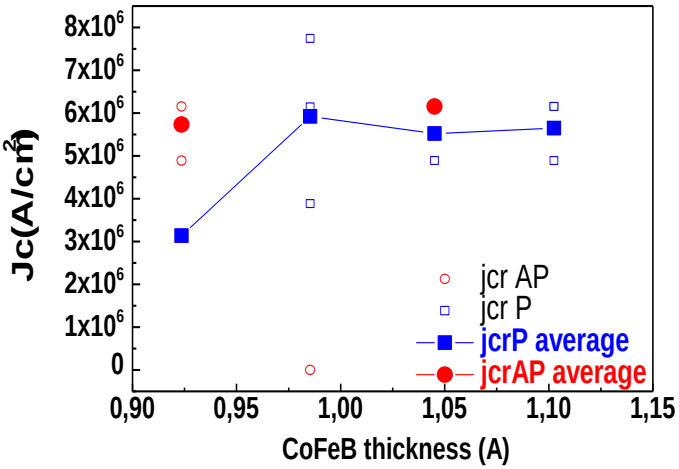

Figure IV-13: Switching current density for P (blue open squares) and AP states (red open squares) as a function of CoFeB thickness for 200nm pillar sizes and average values for the two current directions (blue and red solid symbols) calculated with the RA value measured in macroscopic samples 14Ohmμm².

These results are quite encouraging, since both magnetization states can be written with relatively short pulses and reasonably low current densities. When varying the CoFeB thickness, the current density decreases by a factor of about 1.5, whereas thickness decreases by only a factor of 1.2 (**Figure IV-13**). Since the effective anisotropy field increases with decreasing thickness, as well as the damping constant according to [Ike_10], one must consider that the decrease of the saturation magnetization (**Chapter II-6.2** and **Appendix 3**) mainly contributes

to the decrease of critical current density. This decrease of switching current density with decreasing CoFeB thickness has been observed for different CoFeB thicknesses and for different junction sizes. However not enough junctions were measured to confirm this trend.

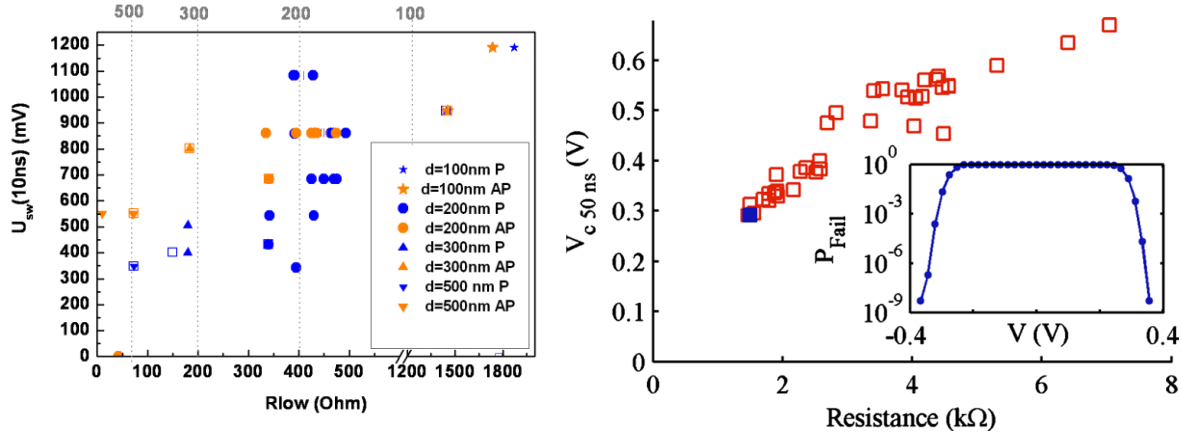

Figure IV-14: Dependence of switching voltage on the resistance of devices with different junction areas. The graph on the right is taken from [Wor_11].

The variation of the switching voltage with junction resistance is presented in **Figure IV-14**. As the size of the junctions decreases (increasing resistance), the switching voltage increases, although it should stay constant as predicted from the single domain model [Sun_00]. The same variation was observed by Worledge et al. [Wor_11] and could probably be due to problems related to the lithography process which creates edges defects. These defects are more critical for low pillar areas and can modify the switching characteristics.

On some R(H) curves (**Figure IV-15**), when the voltage pulse is applied, steps are observed on the STT induced transition from AP to P or P to AP states. These steps are the sign of successive domains depining and pinning under the influence of the STT. A domain wall state is observed only when the nucleation field is lower than the defects pinning field [Cuc_11]. At zero applied current/voltage pulse the nucleation field is higher than the pinning field. Since spin-transfer effect is essential for reducing the nucleation field it is possible to reach a situation where the nucleation field is lower than the pinning field resulting in domain wall states.

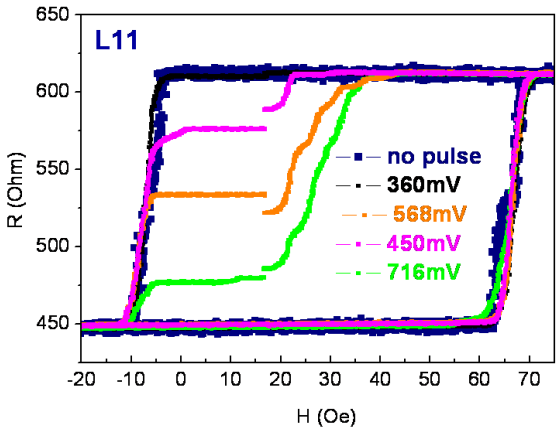

Figure IV-15: Reduction of nucleation field by STT can create a situation where the pinning field is larger, resulting in a domain wall state as observed in perpendicular spin-valves [Cuc_11].

IV-2.3 Voltage-field phase diagram

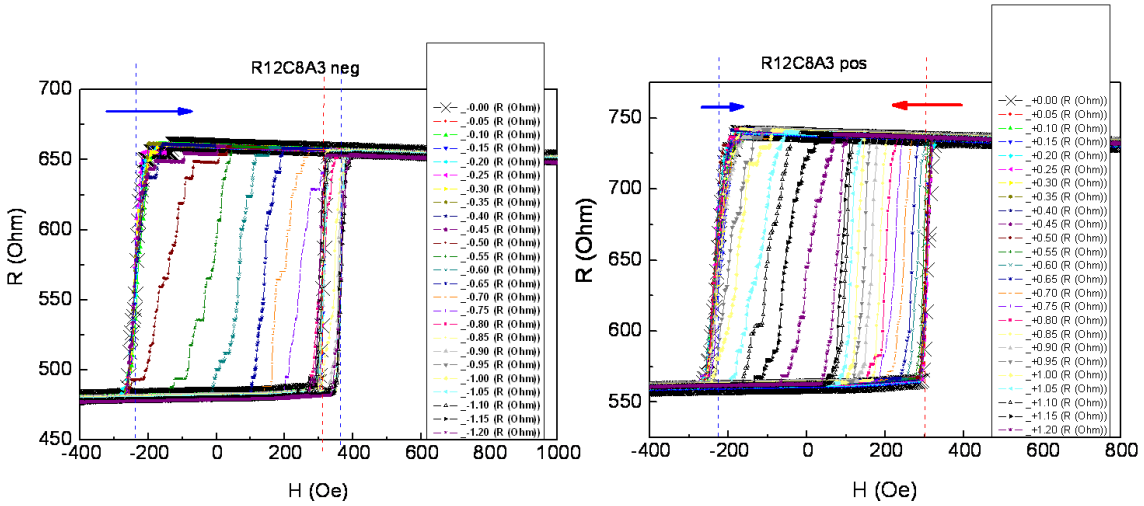

Figure IV-16: R(H) curves for different pulse amplitudes and two current directions. The voltage pulse is applied every 3 Oe all along the R(H) curve.

R(H) curves measured for a constant pulse duration (10 ns) are shown in **Figure IV-16**. In that case, the pulse is applied every 3 Oe, all along the R(H) curve for successive cycles. This procedure is repeated for increasing pulse amplitude and both current directions. These curves can be used to construct voltage-field phase diagrams as shown in **Figure IV-17** for two different pillar sizes.

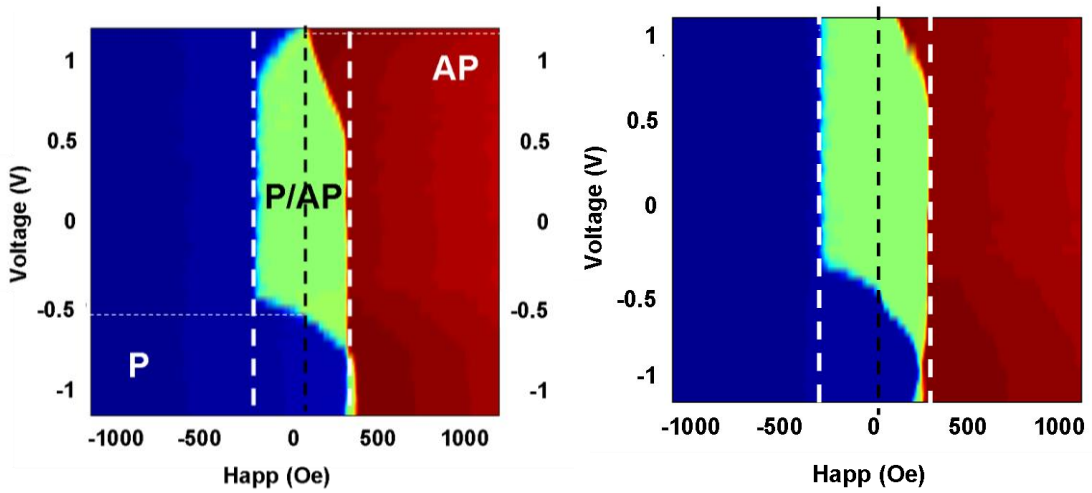

Figure IV-17: Phase diagram of quasi-static magnetic switching under applied voltage and field for a CoFeB thickness of 0.98nm (L12) and (a) 200nm pillars with 38% TMR and Rlow=476 Ohm; (b) 300nm pillars with 31%TMR and Rlow=91 Ohm. The colour code represents the resistance value: the low resistance state is represented in blue and the high resistance state in red.

Switching is here obtained under the combined actions of applied voltage and magnetic field. We can determine three regions: stable P state (low resistance state represented in blue), stable AP state (high resistance state in red), and bistable region where both parallel and antiparallel configurations exist (in green on **Figure IV-17**). White vertical lines represent the coercive field of the junction. The intercept between the vertical black line (centre of the loop) and the transition line between between bistable region and stable P or AP ones gives the critical switching voltage. From **Figure IV-17**, we obtain for both pillars critical voltages of around 450-

500 mV (3.018-3.35 MA/cm²) for writing the P state and above than 1.2 V (8.04 MA/cm²) for writing the AP state. This means that is easier to write the P state by applying negative pulses than the AP state by applying positive voltage pulses. For fields close to the coercive field the required voltage to write the P or AP states is, as expected, lower that the values obtained for pulses applied at the centre of the hysteresis loop.

One can also note that when positive pulses of large amplitude are applied in order to write the AP state, this also affects the AP-P transition. This indicates that the magnetic anisotropy of the free layer is reduced during the pulse by Joule heating effects.

IV-2.4 Stability factor determination

As we mentioned in **Section IV-1.2**, low critical current density is not the only factor determining efficiency of STT writing. Once a given P or AP state has been written, this state must be stable against thermal fluctuations for a sufficient long time. Ten years retention of information stored is usually considered. Thus, a large enough thermal stability factor Δ (Δ = $KV/k_BT \geq 40$) for a given structure is at least as important to memory applications as the low critical STT current density.

In the literature different techniques have been used to evaluate the thermal stability factor of magnetic tunnel junctions. The first one relies upon the direct determination of the anisotropy field, H_K **[Bed_10, Ami_11]**, from which Δ can be determined as $\Delta = HM_SV/2k_BT$. The second one uses STT experiments **[Hos_05, Ike_10, Lee_11, Sat_11]**, where the critical current density is measured as a function of current pulse duration. A third one consists in measuring the coercive field dependence on either applied field sweeping rate **[Nak_08, Yod_10, Wor_11]**, or applied field amplitude **[Eng_10, Sat_11]**. Although results obtained with this latter technique depend on the hypotheses made on magnetization reversal processes (domain wall motion or coherent magnetization rotation), Sato et al **[Sat_11]** showed that similar stability factors were obtained using this technique or critical STT current measurements.

The stability factor determination in the case of the sample presented here is a complex study, since one can extract a lot of information as a function of the free layer thickness and the pillar sizes. This requires statistical analysis in order to minimize problems induced by the pillar process fabrication. Only preliminary results are presented here in order to have an idea of the value of the thermal stability factor and since the time was limited we chosed the most rapid technique represented by extracting the stability factor and the anisotropy field from the coercive field dependence on the applied field amplitude at a given sweeping rate (R=35kOe/s).

In the framework of the thermal activation model the probability of switching that occurs at a magnetic field H in time τ is given by:

$$P_{sw} = 1 - \exp\left(-\frac{1}{R \cdot \tau}\right) = 1 - \exp\left(-\frac{f_o}{R} \cdot \exp\left(-\frac{E_B}{k_B \cdot T}\right)\right) \qquad \textbf{Equation IV-9}$$

where R the field sweep rate and $1/\tau = f_o \exp(-E_B/k_BT)$

The energy barrier is taken as:

$$E_B(H) = E_0 \cdot \left(1 - \frac{H}{H_K}\right)^n \Rightarrow \frac{E_B(H)}{k_B \cdot T} = \Delta \cdot \left(1 - \frac{H - H_d}{H_K}\right)^n \qquad \textbf{Equation IV-10}$$

where E_0 is the energy barrier without applied field, Δ is the stability factor (E_0/k_BT), H_d the dipolar field and H_K the anisotropy field **[Sha_94]**.

From **Equations IV-9** and **IV-10** we obtain the probability of switching as a function of applied field which was used to fit our experimental data:

$$P_{sw} = 1 - \exp\left(\frac{f_o}{R} \cdot \exp\left(-\Delta \cdot \left(1 - \frac{(H_c - H_d)}{H_K}\right)^n\right)\right) \qquad \textbf{Equation IV-11}$$

The exponent n can take values between 1 (describing domain wall regime) and 2 (describing coherent rotation regime) [Eng_10]. Since our pillars have a small size with weak pinning of the domain walls, n is higher than 1 and closest to 2. We thus take n=2 in the above **Equation IV-11**.

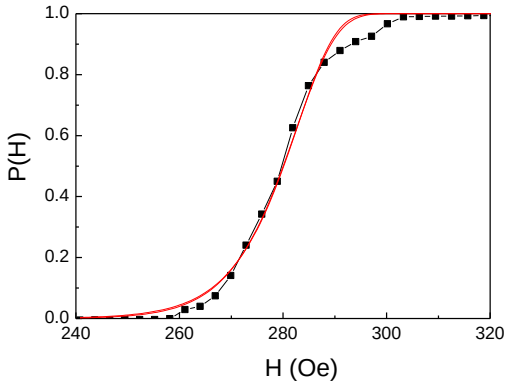

Figure IV-18: Switching probability as a function of applied field of a junction with 200 nm diameter and a CoFeB thickness of 1.1 nm.

Figure IV-18 shows an example of the switching probability (under low applied DC voltage) as a function of applied field for a 200 nm pillar with a CoFeB thickness of 1.1 nm. The experimental curve is the normalized sum of 100 successive measurements on the ascending branch of the hysteresis loop, with a field sweeping rate R of 35 kOe/s and the attempt frequency, f_0 of 10^9Hz. The zero-field offset is 252 Oe for this junction. Fitting the data to **Equation IV-11** gives a stability factor Δ of 14.7 and an anisotropy field H_K of 187 Oe.

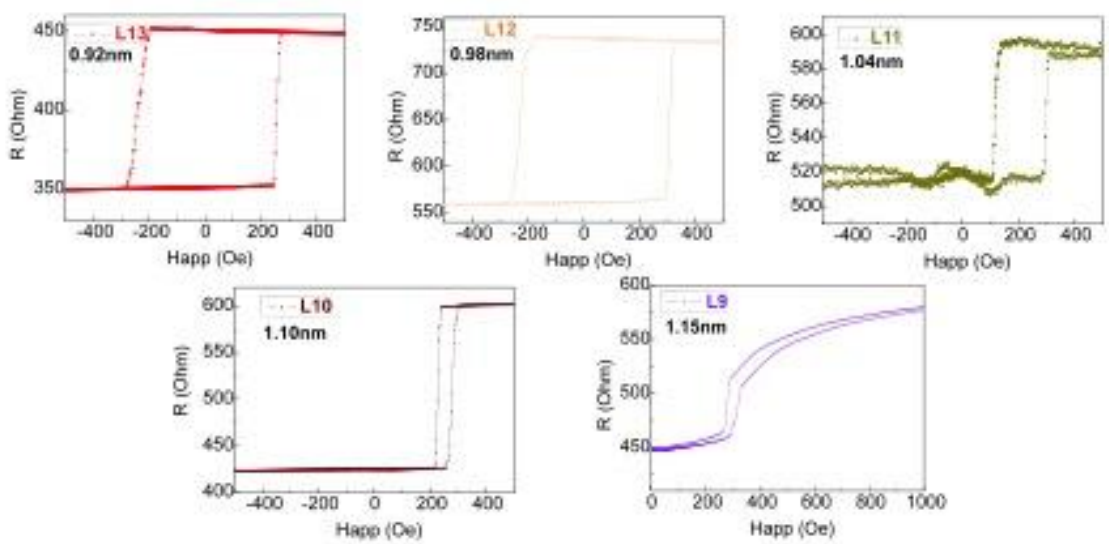

Figure IV-19: Hysteresis loops measured on 200 nm pillars with different CoFeB thicknesses.

Figure IV-19 shows examples of hysteresis loops measured with the above field sweeping rate on 200 nm pillars with different CoFeB thicknesses. One can observe a large spread of the offset fields from junction to junction. This is ascribed to different magnetic properties of the CoFeB/(Tb/Co) reference layer. One can imagine that process instabilities can lead to a different compensation of the magnetizations of the Tb and Co sub-lattices, leading to different stray fields on the soft layer from junction to junction.

Δ and H_K values for four different CoFeB thicknesses from 0.92 to 1.15 nm are presented in **Figure IV-20** for two pillar sizes (200 and 300 nm). The number of experimental points is rather limited, and only general trends can be discussed. The stability factor is comprised between 50 and 100, which is a relatively high value (we recall that a stability factor of 40 corresponds to 10 years retention of information). It decreases to about 15 for the larger CoFeB thickness. The tendency observed for the anisotropy is similar, with a progressive decrease with increasing CoFeB thickness, more or less following the variation of the coercive field (**Figure IV-19**). No significant difference is observed between both pillar sizes.

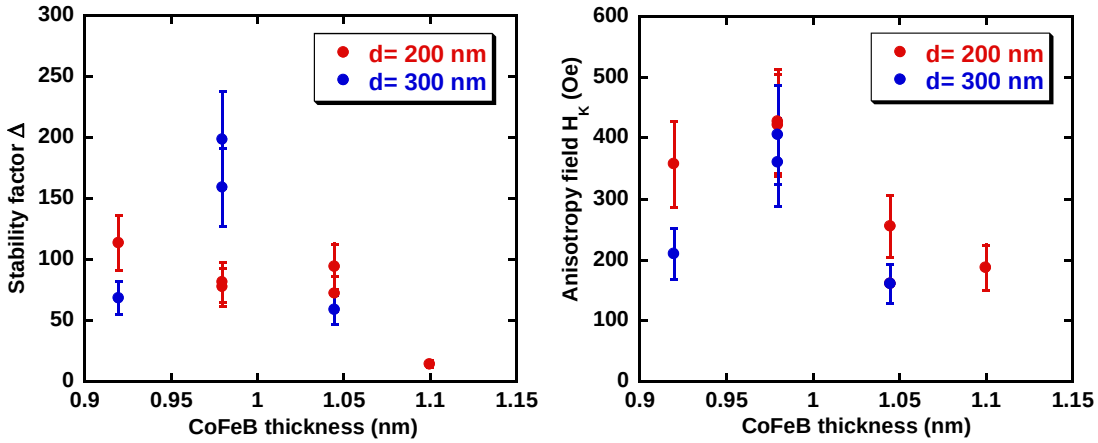

Figure IV-20: Δ (left) and H_K (right) values obtained for different CoFeB thicknesses on pillars with a diameter of 200 and 300 nm.

Finally, the nucleation volume V_N can be estimated through [Sha_94]:

$$V_N = \frac{2 \cdot E_0}{H_K \cdot M_s} = \frac{2 \cdot \Delta \cdot k_B \cdot T}{H_K \cdot M_s} \qquad \textbf{Equation IV-12}$$

where Ms is the saturation magnetization. Supposing that nucleation occurs in the whole thickness for such thin magnetic layers, a corresponding nucleation diameter d_N can be estimated as:

$$d_N = \sqrt{\frac{8 \cdot \Delta \cdot k_B \cdot T}{\pi \cdot H_K \cdot M_s \cdot t}} \qquad \textbf{Equation IV-13}$$

where t is the CoFeB thickness. Using M_S values determined previously (**Appendix 3**), **Figure IV-21** shows the variation of the nucleation diameter as a function of CoFeB thickness for both 200 and 300 nm pillars. With the same restrictions mentioned for **Figure IV-20** (reduced number of data points), the calculated nucleation diameter seems to follow the physical pillar diameter. The largest CoFeB thickness (1.1 nm) is probably too close from the critical thickness, leading to an increasing uncertainty on Δ and H_K, and thus on the nucleation diameter.

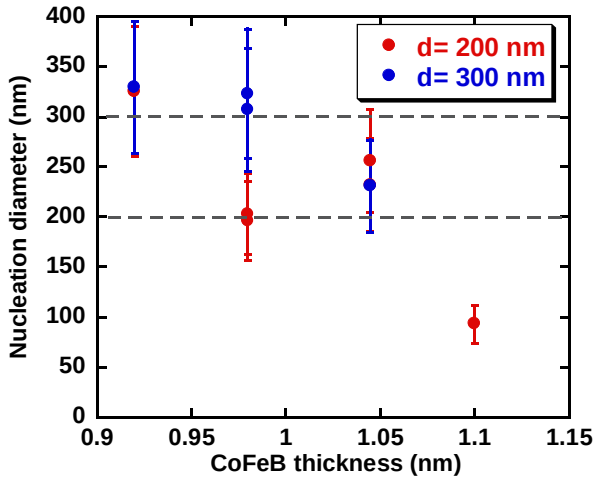

Figure IV-21: Nucleation diameter calculated from Δ and HK values shown in Figure IV-20 and using MS values given in Appendix 3.

IV-2.5 Back-tracking / back-hopping phenomena

A particular type of switching was observed, in which the magnetization of the free layer switches back to its original state against STT direction at a voltage larger than the critical switching one. This phenomenon is presented in **Figure IV-22** and occured only in some MTJ.

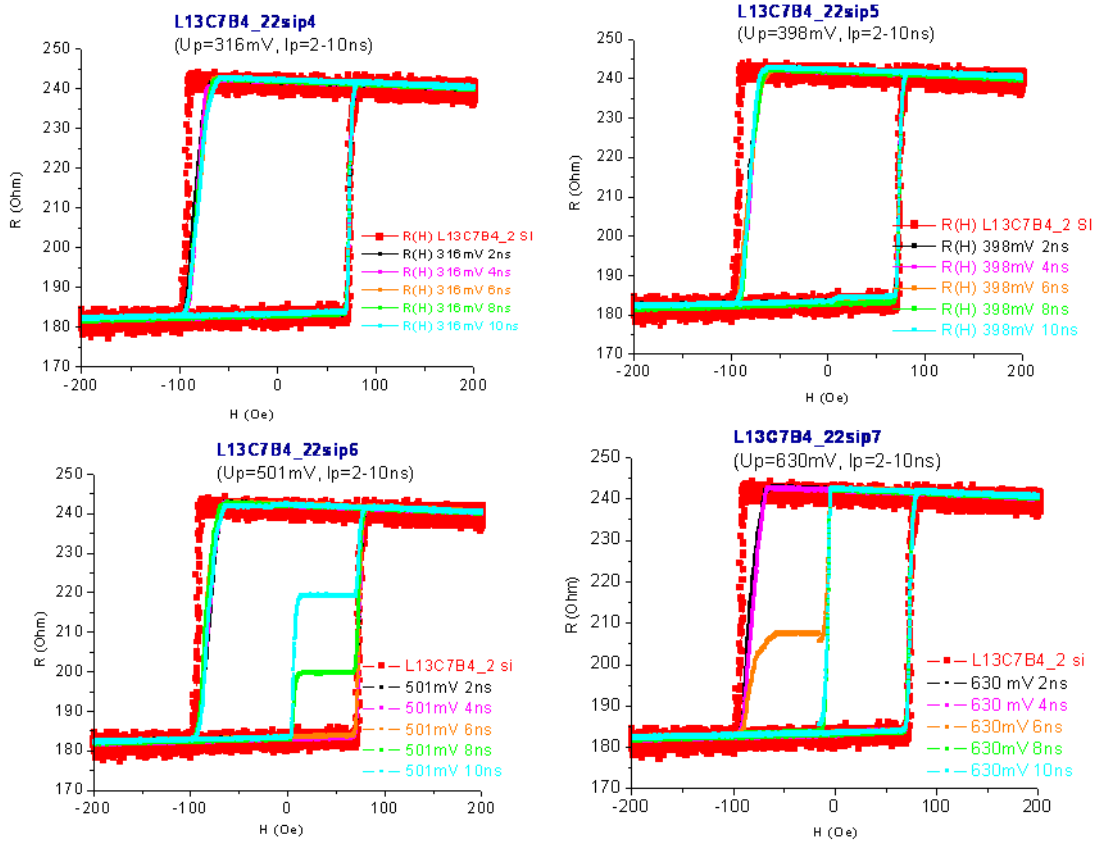

Figure IV-22: R(H) hysteresis curves showing the back-switching phenomenon for positive voltages applied to write the AP state. For a voltage higher than a critical one the STT torque writes the P state.

This phenomenon appears only for high applied voltages and can be related to a decrease of the barrier height for such voltage values because of junction heating.A bias dependent field-like torque term may also play a role. In particular the parity of the field-like torque term with respect to bias voltage and the relative magnetic orientations could be the cause of this particular type of switching **[Min_09, Oh_09]**.

IV-3. Conclusions

In this chapter we showed evidence of STT writing of a perpendicular MTJ in which the PMA of the soft layer mainly comes from the interface between the magnetic metal and oxide CoFeB/MgO.

Electrical measurements show that our nanofabrication process allows obtaining cylindrical nanopillars with 200-300 nm in diameter still keeping the RA product measured in macroscopic samples (14 Ohmμm^2). This means that no parasitic resistances have been introduced during process, and that barrier properties have been preserved. Pillars with 100 nm diameter present a larger resistance spread, and those with 50 nm diameter do not give any signal. However either processing or size reduction seem to affect the TMR properties as compared with macroscopic samples. This could come from partial oxidation of the TbCo layer, leading to weaker exchange coupling of the reference layer, or to partial canting of the magnetization of the soft layer at pillar edges. This results in a reduction of the TMR ratio from 80% in macroscopic samples to 50% in pillars. However, the critical magnetic thickness (reorientation from out-of-plane to in-plane) slightly increases after patterning, indicating an increase of perpendicular anisotropy or thermal stability.

Low switching times (10 ns) along with low switching voltages (430 mV for P writing, corresponding to current densities of 3 MA/cm^2) were obtained on 200-300 nm pillars for 0.92 nm thick CoFeB layers with a very good thermal stability factor of 50 to 100. The critical switching voltage increases (540 mV) for a CoFeB thickness of 1.04 nm for the same pulse length but remains within limits of industrial requirements. These preliminary results are very encouraging. They also indicate that increased anisotropy and damping for smaller magnetic layer thicknesses could be more than compensated by the observed decrease of the saturation magnetization.

Ref.	Team	Hard layer	Soft layer	TMR (%)	RA (Ωμm^2)	Δ	Soft layer (nm)	J	Pulse (ns)	damping	d
Nak_08	Toshiba	RE-TM/CoFeB	RE-TM/CoFeB	15	16	107	3+1	4.8	100	-	130
Kis_08	Toshiba	?	$L1_0$	-	-	56	-	2	4	0.028	50
Ike_10	Tohoku	Ta/CoFeB	Ta/$CoFe_{60}B$	120	18	43	1.2	4	100	0.01	40
Yod_10	Toshiba	Fe alloy?	Fe alloy?	22	18	32	1.5-2	0.4	5000	0.001	55
Wor_10	IBM	?	?	100	9.5	50	?	0.8	50	0.008	80
Wor_11	IBM	(Co/Pd)/CoFeB	Ta/Co_{60}FeB	46	12	66	0.8	2.4	50	-	80
Nis_11	Spintec	RE-TM/CoFeB	Ta/Co_{60}FeB	40	14	50-100	0.92	2.4	10	-	200

Table IV-2: Publications on STT experiments in perpendicular magnetic tunnel junctions. RE-TM stands for Rare Earth-Transition Metal alloys, $L1_0$ for ordered alloys, (Co/Pt(Pd)) for multilayers, ? for unknown structures and - for absence of information on some parameters. Δ is the thermal stability factor, J the critical switching current density (MA/cm^2) and d the pillar diameter (nm).

The critical switching voltage for 10 ns pulse length increases with decreasing area (increasing resistance), in disagreement with the single domain model, and is probably due to defects induced during the nanopillar fabrication process. This could also be the reason responsible for the observed large spread of the stability factor from pillars to pillar, and for unusual behaviours like back-switching phenomena. One must also note that these STT experiments were carried out at the very end of our thesis work, leaving no time to measure a large number of junctions in order to increase statistics. These results should thus be taken as preliminary ones.

The last line in **Table IV-2** compares our results to recent reports in the literature. Although progress is still needed in terms of technological process (pillars sizes) and materials quality, our results (low switching current densities, 3 MA/cm^2, along with short pulse

durations, 10 ns, and large thermal stability) place our Laboratory among the leading teams in the field of STT writing in magnetic tunnel junctions with out-of-plane anisotropy.

Finally, as we said in **Chapter II-6**, magnetic tunnel junctions with in-plane magnetized electrodes and reduced demagnetizing field were also processed into sub-micrometric pillars, but we had unfortunately no time to characterize the STT properties of these structures.

IV-4. References

[Ami_11] P.K. Amiri, Z.M. Zeng, J. Langer, H. Zhao, G. Rowlands, Y.-J. Chen, I.N. Krivorotov, J.-P. Wang, H.W. Jiang, J.A. Katine, Y. Huai, K. Galatsis and K.L. Wang, *Switching current reduction using perpendicular anisotropy in CoFeB–MgO magnetic tunnel junctions*, **Appl. Phys. Lett.** **98** (2011) 112507.

[Ban_11] S. Bandiera, *Jonctions tunnel magnétiques à anisotropie perpendiculaire et écriture assistée thermiquement*, PhD Thesis, Grenoble University (2011).

[Bed_10] D. Bedau, H. Liu, J.J. Bouzaglou, A.D. Kent, J.Z. Sun, J.A. Katine, E.E. Fullerton and S. Mangin, *Ultrafast spin-transfer switching in spin valve nanopillars with perpendicular anisotropy magnetization*, **Appl. Phys. Lett.** **96** (2010) 022514.

[Ber_96] L. Berger, *Emission of spin waves by a magnetic multilayer traversed by a current,* **Phys. Rev. B** **54** (1996) 9353.

[Cuc_11] J. Cucchiara, *Spin-transfer effects in nanopillars with perpendicular magnetization*, **PhD Thesis, Nancy University** (2011).

[Dea_08] A.M. Deac, A. Fukushima, H. Kubota, H. Maehara, Y. Suzuki, S. Yuasa, Y. Nagamine, K. Tsunekawa, D.D. Djayaprawira and N. Watanabe, *Bias-driven high-power microcrowave emission from MgO-based tunnel magnetoresistance devices*, **Nature Phys.** **4** (2008) 803.

[Eng_10] J.B.C. Engelen, M. Delalande, A.J. le Fèbre, T. Bolhuis, T. Shimatsu, N. Kikuchi, L. Abelmann and J.C. Lodder, *Thermally induced switching field distribution of a single CoPt dot in a large array*, **Nanotechnology** **21** (2010) 035703.

[Gil_04] T.L. Gilbert, *A phenomenological theory of damping in ferromagnetic materials*, **IEEE Trans. Magn.** **40** (2004) 3443.

[Hei_10] O.G. Heinonen and D.V. Dimitrov, *Switching-current reduction in perpendicular-anisotropy spin torque magnetic tunnel junctions,* **J. Appl. Phys.** **108** (2010) 014305.

[Hos_05] M. Hosomi, H. Yamagishi, T. Yamamoto, K. Bessho, Y. Higo, K. Yamane, H. Yamada, M. Shoji, H. Hachino, C. Fukumoto, H. Nagao and H. Kano, *A novel nonvolatile memory with spin torque transfer magnetization switching: Spin-RAM*, **Int. Electron Devices Meeting** Tech. Digest (2005) 459.

[Hou_07] D. Houssameddine, U. Ebels, B. Delaët, B. Rodmacq, I. Firastrau, F. Ponthenier, M. Brunet, C. Thirion, J.-P. Michel, L.D. Buda-Prejbeanu, M.-C. Cyrille, O. Redon and B. Dieny, *Spintorque oscillator using a perpendicular polarizer and a planar free layer,* **Nature Mater.** **6** (2007) 447.

[Ike_07] S. Ikeda, J. Hayakawa, Y.M. Lee, F. Matsukura, Y. Ohno, T. Hanyu and H. Ohno, *Magnetic tunnel junctions for spintronic memories and beyond*, **IEEE Trans. Elec. Dev.** **54** (2007) 991.

[Ike_10] S. Ikeda, K. Miura, H. Yamamoto, K. Mizunuma, H.D. Gan, M. Endo, S. Kanai, J. Hayakawa, F. Matsukura and H. Ohno, *A perpendicular-anisotropy CoFeB–MgO magnetic tunnel junction,* **Nature Mater.** **9** (2010) 721.

[Jia_04] Y. Jiang, T. Nozaki, S. Abe, T. Ochiai, A. Hirohata, N. Tezuka and K. Inomata, *Substantial reduction of critical current for magnetization switching in an exchange-biased spin valve*, **Nature Mater.** **3** (2004) 361.

[Kat_00] J.A. Katine, F.J. Albert, R.A. Buhrman, E.B. Myers and D.C. Ralph, *Current-driven magnetization reversal and spin-wave excitations in Co/Cu/Co pillars,* **Phys. Rev. Lett.** **84** (2000) 3149.

[Kis_08] T. Kishi, H. Yoda, T. Kai, T. Nagase, E. Kitagawa, M. Yoshikawa, K. Nishiyama, T. Daibou, M. Nagamine, M. Amano, S. Takahashi, M. Nakayama, N. Shimomura, H. Aikawa, S. Ikegawa, S. Yuasa, K. Yakushiji, H. Kubota, A. Fukushima, M. Oogane, T. Miyazaki and K. Ando, *Lower-current and fast switching of a perpendicular TMR for high speed and high density spin-transfer-torque MRAM*, **Int. Electron Devices Meeting** Tech. Digest (2008) 1.

[Kub_08] H. Kubota, A. Fukushima, K. Yakushiji, T. Nagahama, S. Yuasa, K. Ando, H. Maehara, Y. Nagamine, K. Tsunekawa, D.D. Djayaprawira, N. Watanabe and Y. Suzuki, *Quantitative measurement of voltage dependence of spin-transfer torque in MgO-based magnetic tunnel junctions*, **Nature Phys.** **4** (2008) 37.

[Lan_35] L. Landau and E. Lifshitz, *On the theory of the dispersion of magnetic permeability in ferromagnetic bodies*, Phys. Z. Sowjetunion **8** (1935) 153.

[Lee_11] J.-M. Lee, C.-M. Lee, L.-X. Ye, J.-P. Su and T.-H. Wu, *Switching properties for MgO-based magnetic tunnel junction devices driven by spin-transfer torque in the nanosecond regime*, **IEEE Trans. Magn.** **47** (2011) 629.

[Liu_09] L. Liu, T. Moriyama, D.C. Ralph, and R.A. Buhrman, *Reduction of the spin-torque critical current by partially cancelling the free layer demagnetization field*, **Appl. Phys. Lett.** **94** (2009) 122508.

[Man_06] S. Mangin, D. Ravelosona, J.A. Katine, M.J. Carey, B.D. Terris and E.E. Fullerton, *Current-induced magnetization reversal in nanopillars with perpendicular anisotropy,* **Nature Mater.** **5** (2006) 210.

[Man_08] A. Manchon, N. Ryzhanova, A. Vedyayev, M. Chshiev and B. Dieny, *Description of current-driven torques in magnetic tunnel junctions*, **J. Phys.: Cond. Matter** **20** (2008) 145208.

[Mar_11] M. Marins de Castro Souza, *Commutation precessionelle de mémoire magnétique MRAM avec polariseur à anisotropie perpendiculaire*, PhD Thesis, Grenoble University (2011).

[Min_09] T. Min, J.Z. Sun, R. Beach, D. Tang and P. Wang, *Back-hopping after spin torque transfer induced magnetization switching in magnetic tunneling junction cells,* **J. Appl. Phys.** **105** (2009) 07D126.

[Mor_10] T. Moriyama, T.J. Gudmundsen, P.Y. Huang, L. Liu, D.A. Muller, D.C. Ralph and R.A. Buhrman, *Tunnel magnetoresistance and spin torque switching in MgO-based magnetic tunnel junctions with a Co/Ni multilayer electrode*, **Appl. Phys. Lett.** **97** (2010) 072513.

[Nak_08] M. Nakayama, T. Kai, N. Shimomura, M. Amano, E. Kitagawa, T. Nagase, M. Yoshikawa, T. Kishi, S. Ikegawa and H. Yoda., *Spin transfer switching in TbCoFe/CoFeB/MgO/CoFeB/TbCoFe magnetic tunnel junctions with perpendicular magnetic anisotropy*, **J. Appl. Phys.** **103** (2008) 07A710.

[Nis_11] L.E. Nistor, B. Rodmacq, S. Auffret and B. Dieny, *Low effective demagnetizing field in magnetic tunnel junctions,* Intermag Conference, Taipei (Taiwan) Apr. 25-29 (2011).

[Oh_09] S.-C. Oh, S.-Y. Park, A. Manchon, M. Chshiev, J.-H. Han,H.-W. Lee, J.-E. Lee, K.-T. Nam, Y. Jo, Y.-C. Kong, B. Dieny and K.-J. Lee, *Bias-voltage dependence of perpendicular spin-transfer torque in asymmetric MgO-based magnetic tunnel junctions*, **Nature Phys.** **5** (2009) 898.

[Ozh_07] O. Ozhatay, K.W. Tan, P.M. Braganca, E.M. Ryan, J.C. Read, A.K. Mkhoyan, M.G. Thomas, K.V. Thadani, J.C. Sankey, J. Silcox, D.C. Ralph and R.A. Buhrman, 10th Joint MMM/Intermag Conference (2007).

[Pap_09] C. Papusoi, B. Delaët, B. Rodmacq, D. Houssameddine, J.-P. Michel, U. Ebels, R.C. Sousa, L.D. Buda-Prejbeanu and B. Dieny, *100 ps precessional spin-transfer switching of a planar magnetic random access memory cell with perpendicular spin polarizer,* **Appl. Phys. Lett.** **95** (2009) 072506.

[Pta_07] **http://www.pta-grenoble.com**

[Red_00] O. Redon, B. Dieny and B. Rodmacq, *Magnetic spin polarization and magnetization rotation device with memory and writing process using such a device*, **US Patent US6,532,164 B2**, Dec. 07 2000.

[San_08] J.C. Sankey, Y.T. Cui, J.Z. Sun, J.C. Slonczewski, R.A. Buhrman and D.C. Ralph, *Measurement of the spin-transfer-torque vector in magnetic tunnel junctions*, **Nature Phys.** **4** (2008) 67.

[Sat_11] H. Sato, M. Yamanouchi, K. Miura, S. Ikeda, H.D. Gan, K. Mizunuma, R. Koizumi, F. Matsukura and H. Ohno, *Junction size effect on switching current and thermal stability*

in CoFeB/MgO perpendicular magnetic tunnel junctions, **Appl. Phys. Lett.** **99** (2011) 042501.

[Sha_94] M.P. Sharrock, *Kinetic effects in coercivity measurements*, **J. Appl. Phys.** **76** (1994) 6413.

[Slo_96] J.C. Slonczewski, *Current-driven excitation of magnetic multilayers*, **J. Magn. Magn. Mater.** **159** (1996) L1.

[Sun_00] J.Z. Sun, *Spin-current interaction with a monodomain magnetic body: A model study*, **Phys. Rev. B** **62** (2000) 570.

[The_06] I. Theodonis, N. Kioussis, A. Kalitsov, M. Chshiev and W.H. Butler, *Anomalous bias dependence of spin torque in magnetic tunnel junctions*, **Phys. Rev. Lett.** **97** (2006) 237205.

[Tud_10] I. Tudosa, J.A. Katine, S. Mangin and E.E. Fullerton, *Perpendicular spin-torque switching with a synthetic antiferromagnetic reference layer,* **Appl. Phys. Lett.** **96** (2010) 212504.

[Wol_10] S.A. Wolf, J. Lu, M.R. Stan, E. Chen and D.M. Treger, *The promise of nanomagnetics and spintronics for future logic and universal memory,* **Proc. IEEE** **98** (2010) 2155.

[Wor_10] D.C. Worledge, G. Hu, P.L. Trouilloud, D.W. Abraham, S. Brown, M.C. Gaidis, J. Nowak, E.J. O'Sullivan, R.P. Robertazzi, J.Z. Sun and W.J. Gallagher, *Switching distributions and write reliability of perpendicular spin torque MRAM*, **Int. Electron Devices Meeting** Tech. Digest (2010) 296.

[Wor_11] D.C. Worledge, G. Hu, D.W. Abraham, J.Z. Sun, P.L. Trouilloud, J. Nowak, S. Brown, M.C. Gaidis, E.J. O'Sullivan and R.P. Robertazzi, *Spin torque switching of perpendicular Ta/CoFeB/MgO-based magnetic tunnel junctions*, **Appl. Phys. Lett.** **98** (2011) 022501.

[Yod_10] H. Yoda, T. Kishi, T. Nagase, M. Yoshikawa, K. Nishiyama, E. Kitagawa, T. Daibou, M. Amano, N. Shimomura, S. Takahashi, T. Kai, M. Nakayama, H. Aikawa, S. Ikegawa, M. Nagamine, J. Ozeki, S. Mizukami, M. Oogane, Y. Ando, S. Yuasa, K. Yakushiji, H. Kubota, Y. Suzuki, Y. Nakatani, T. Miyazaki and K. Ando, *High efficient spin transfer torque writing on perpendicular magnetic tunnel junctions for high density MRAMs*, **Curr. Appl. Phys.** **10** (2010) e87.

Conclusion

The aim of this thesis was the fabrication of magnetic tunnel junctions with perpendicularly magnetized electrodes, using perpendicular magnetic anisotropy (PMA) arising from the magnetic metal/oxide interfaces. These perpendicular junctions, according to theoretical predictions, should need less energy (current) for spin transfer torque (STT) writing applications. However, the engineering of such structures was a real challenge and a difficult task since simultaneous TMR and PMA properties impose constraints on materials being used and also limit the working window of the device. In order to reach our goal we first studied different properties of these structures, such as the origin of PMA from the metal/oxide interface, and interlayer exchange coupling phenomena.

At the time we started this study, they were only five reports in the literature on sputtered MgO-based perpendicular magnetic tunnel junctions, all consisting of RE-TM electrodes **[Che_06, Hat_07, Ohm_08, Nak_08]**, except one dealing with RE-TM hard and (Co/Pt) soft electrodes **[Ye_08b]**, but with a very limited thermal stability.

On the basis of our experience since 2002 on Pt/Co/AlOx trilayers **[Mon_02, Man_07, Rod_09]**, we thus decided to explore the anisotropy properties of Pt/Co/MgO and MgO/Co/Pt single electrodes, as well as those of Pt/Co/MgO/Co/Pt full structures. Thanks to the strong interfacial anisotropy from both Pt/Co and Co/MgO interfaces, it was possible to study the magnetic properties of these structures on a large range of Co thicknesses and annealing temperatures.

The perpendicular anisotropy of bottom Pt/Co/MgO electrodes greatly increases with annealing, the critical Co thickness going from 1.3 nm in the as-deposited state up to almost 3.5 nm after annealing at 375°C. Large differences are observed between Co and CoFeB electrodes, the latter exhibiting a non-monotonous variation of anisotropy with annealing. RF deposition of MgO appears very dependent on the sputtering conditions, as shown by the large difference of PMA properties between both sputtering machines used. The Pt buffer thickness and the nature of the capping layer also influence the anisotropy properties of these bottom electrodes.

The perpendicular anisotropy of top oxide/Co/Pt electrodes is much smaller, whatever the oxide considered, with a maximum critical thickness of about 1.6 nm after annealing at 400°C. This seems to be related to a much difficult growth of the magnetic layer on oxide than on Pt. Interface and volume contributions to the perpendicular anisotropy vary differently for both electrodes. While the increase of anisotropy upon annealing in bottom electrodes is mainly due to the interfacial contribution, that of the top electrodes mainly comes from an increase of the volume contribution. By comparison with Pt/Co/Pt structures, we can conclude that the PMA increase at high annealing temperatures mainly comes from the Co/Oxide interface in both top and bottom structures. High annealing temperature leads to oxygen diffusion and Co-O bond formation as was experimentally observed by X-ray spectroscopy measurements and by ab-initio calculations. The origin of the perpendicular anisotropy induced at magnetic metal/oxide interface is hybridization of orbitals between oxygen and magnetic metal.

The next step was to put together the top and bottom electrodes in order to fabricate perpendicular junctions and investigate their transport properties. As Pt/Co/MgO and MgO/Co/Pt structures gave the best PMA properties, they were chosen as electrodes in full junctions, although the mismatch between Co and MgO textures was expected to lead to smaller TMR signals. That's the reason why we also considered Pt/Co/CoFeB electrodes, hoping that the MgO barrier could impose its texture to the CoFeB layer upon its crystallization after annealing. However, later literature reports showed that the texture of the buffer (Pt, Pd) could dominate over the influence of the MgO barrier and induce (111) texture of the magnetic electrode, leading to a strong degradation of the transport properties.

When putting together bottom and top electrodes, the most surprising observation was the strong increase of the anisotropy of the top electrode when it is deposited onto the bottom one. We showed that this effect has a structural origin and is related to the growth conditions of the Mg layer, which depends on the nature of the underlying layer. This large increase of the anisotropy comes from the better growth of the Mg layer on metallic materials (Pt or Ru) than on Ta or SiO_2.

The perpendicular anisotropy of top and bottom electrodes in pMTJ increases with annealing, but has different origins for the top and bottom electrodes, as was the case for electrodes alone. Both bottom and top electrodes in full junctions present a critical thickness of about 3.5 nm after annealing at 350°C.

Strong mutual magnetic interactions between electrodes were also observed, the coercive field of the bottom electrodes decreasing with increasing thickness of the top electrode. For the moment we have no explanation for such an interaction.

PMA critically depends on both magnetic layer thickness and annealing conditions, but also on the quality of the barrier, as oxygen content at the interface with the magnetic layers. This shows that fabrication of perpendicular junctions is more difficult than planar ones.

First perpendicular structures were based on Pt/Co/MgO trilayers showing a very high anisotropy but a low TMR of only 10%. Two different MgO oxides with the same thickness were tested giving the same TMR value but very different RA values (300 $\Omega\mu m^2$ for Mg0.7+Mg0.7 natural oxidation and 15 $\Omega\mu m^2$ for Mg0.9NatOx/Mg0.5). The low TMR in these structures is mainly due to the structural mismatch between Co and MgO. Although these structures could not be used to investigate STT properties, they were used to evidence a direct correlation between anisotropy and transport properties in both single electrodes and full junctions, implying that the same mechanism (the formation of CoFe-O bonds at the interface during oxidation, together with the presence of weak spin-orbit coupling) leads to the TMR and PMA maxima.

According to ab-initio calculations, the difference between the PMA and TMR values in the three cases observed experimentally (over-oxididation, under-oxidation and ideal oxidation) can be explained by the impact of splitting of Δ1-like hybridized states at the Fermi level in the presence of additional oxygen atoms. In the case of out-of-plane magnetization, the splitting of the dxz,yz orbitals is larger for the ideal Fe/MgO interfaces, relatively strong for the under-oxidized case, and the corresponding anisotropy values are larger compared to the over-oxidized case but lower compared to the ideal Fe/MgO interface. Furthermore, in the case of over-oxidized interfaces the Δ1 decay rate is strongly enhanced compared to the ideal and under-oxidized cases: Δ1 bands are absent at the Fermi level, explaining the experimentally observed maximum TMR for the ideal oxidized barrier.

In these structures, we also investigated interlayer coupling through an insulator between perpendicular magnetic electrodes, and tested our results against different models.

First, RF-deposited MgO barriers allowed us to study the variation of the coupling field with MgO thickness which appeared similar to the one observed in epitaxial planar junctions **[Fau_02, Kat_06]**. The amplitude of the antiferromagnetic coupling increases with decreasing barrier thickness, down to a limit where direct ferromagnetic coupling dominates. This cut-off happens for thicker spacers (0.8 nm) in the case of sputtered pMTJ, as observed by **[Liu_03]**, than for epitaxial junctions (0.5-0.6 nm), because of a larger interfacial roughness. For larger MgO thickness, the coupling keeps antiferromagnetic, in agreement with Néel's model extended to perpendicular magnetization **[Mor_04]**. Two coupling contributions could co-exist in our structures, one from Indirect Exchange Coupling dominating at low temperature and the other from roughness-induced coupling at higher temperature. Out-of-plane structures with low PMA or in-plane magnetization exhibit classical ferromagnetic Néel's coupling, confirming Moritz model. All structures show the same increase of the coupling amplitude with decreasing Mg thickness, which is attributed to over-oxidation of the magnetic electrode.

The decrease of the amplitude of antiferromagnetic coupling with increasing annealing temperature is in agreement with Néel's theory assuming that de-oxidation of the magnetic electrodes leads to a smaller chemical roughness of the interfaces.

We also showed that the strength of the antiferromagnetic coupling oscillates as a function of magnetic thickness, as predicted by Bruno's theory **[Bru_93]** for insulating spacers. This is explained by interferences of the electron waves in the ferromagnetic layers. Although average coupling strength progressively decreases with increasing annealing temperature, the amplitude and period of the oscillations are found essentially independent of annealing temperature.

Transport properties of these Pt/Co-based perpendicular junctions could only be measured once Capres tool at Crocus Technology was equipped with a perpendicular magnetic field. At this time also we were still developing MgO barriers for in-plane junctions in our Actemium sputtering machine, and transport properties were not yet optimized (modest TMR values and rather high RA product).

In order to improve the TMR properties a compromise had to be made by eliminating the Pt buffer and replacing the bottom Co layer by CoFeB but as a consequence strongly reducing the PMA of the structure. The bottom layer thus becomes the softest one, and the top layer becomes the hardest one by exchange coupling of CoFeB to a Co/Tb multilayer. This results in a higher TMR of 80% with a low RA product of 15 $\Omega\mu m^2$.

Thanks to perpendicular anisotropy at the magnetic metal/oxide interface, the effective demagnetizing field of the storage layer of in-plane MgO tunnel junctions can be greatly reduced still keeping a TMR ratio as high as 135%. We had no time to study their STT properties after processing into sub-micrometric structures, but these experiments should be soon carried out in our Laboratory.

Electrical measurements showed that our nanofabrication process allows obtaining cylindrical nanopillars with 200-300 nm in diameter still keeping the RA product measured in macroscopic samples (14 $Ohm\mu m^2$). This means that no parasitic resistances have been introduced during process, and that barrier properties have been preserved. Pillars with 100 nm diameter present a larger resistance spread, and those with 50 nm diameter do not give any signal. Either processing or size reduction seem to affect the TMR properties as compared with macroscopic samples. This could come from partial oxidation of the TbCo layer, leading to weaker exchange coupling of the reference layer, or to partial canting of the magnetization of the soft layer at pillar edges. This results in a reduction of the TMR ratio from 80% in macroscopic samples to 50% in pillars. However, the critical magnetic thickness (reorientation from out-of-plane to in-plane) slightly increases after patterning, indicating an increase of perpendicular anisotropy or thermal stability.

Spin Transfert Torque switching experiments were conducted on such structures. Low switching times (10 ns), along with low switching voltages (430 mV for P writing, corresponding to current densities of 3 MA/cm^2), were obtained on 200-300 nm pillars for 0.86 nm thick CoFeB layers with a very good thermal stability factor of 75. The critical switching voltage increases (540 mV) for a CoFeB thickness of 1.0 nm for the same pulse length but remains within limits of industrial requirements. These preliminary results are very encouraging. They also indicate that increased anisotropy and damping for smaller magnetic layer thicknesses could be more than compensated by the observed decrease of the saturation magnetization.

The critical switching voltage for 10 ns pulse length increases with decreasing area (increasing resistance), in disagreement with the single domain model, and is probably due to defaults induced during the nanopillar fabrication process. This could also be the reason for the observed large spread of the stability factor from pillars to pillar, and for unusual behaviours like back-switching phenomena.

References

[Bru_93] P. Bruno, *Oscillations of interlayer exchange coupling vs. ferromagnetic-layers thickness*, **Europhys. Lett. 23** (1993) 615.

[Che_06] T.-J. Chen, A. Canizo-Cabrera, C.-H. Chang, K.-A. Liao, S.C. Li, C.-K. Hou and T.-H. Wu, *Comparison of the interfacial structure between MgO and Al–O oxidation layers for perpendicular magnetic tunnel junction,* **J. Appl. Phys. 99** (2006) 08T313.

[Fau_02] J. Faure-Vincent, C. Tiusan, C. Bellouard, E. Popova, M. Hehn, F. Montaigne and A. Schuhl*, Interlayer magnetic coupling interactions of two ferromagnetic layers by spin polarized tunneling,* **Phys. Rev. Lett. 89** (2002) 107206.

[Hat_07] T. Hatori, H. Ohmori, M. Tada and S. Nakagawa, *MTJ elements with MgO barrier using RE-TM amorphous layers for perpendicular MRAM,* **IEEE Trans. Magn. 43** (2007) 2331.

[Kat_06] T. Katayama, S. Yuasa, J. Velev, M.Ye. Zhuravlev, S.S. Jaswal and E.Y. Tsymbal, *Interlayer exchange coupling in Fe/MgO/Fe magnetic tunnel junctions*, **Appl. Phys. Lett. 89** (2006) 112503.

[Liu_03] Z.Y. Liu and S. Adenwalla, *Oscillatory interlayer exchange coupling and its temperature dependence in $[Pt/Co]_3/NiO/[Co/Pt]_3$ multilayers with perpendicular anisotropy,* **Phys. Rev. Lett. 91** (2003) 037207.

[Man_07] A. Manchon, *Magnétorésistance et transfert de spin dans les jonctions tunnel magnétiques,* **PhD Thesis, Grenoble University** (2007).

[Mon_02] S. Monso, B. Rodmacq, S. Auffret, G. Casali, F. Fettar, B. Gilles, B. Dieny and P. Boyer, *Crossover from in-plane to perpendicular anisotropy in Pt/CoFe/AlO_x sandwiches as a function of Al oxidation: A very accurate control of the oxidation of tunnel barriers,* **Appl. Phys. Lett. 80** (2002) 4157.

[Mor_04] J. Moritz, F. Garcia, J.-C. Toussaint, B. Dieny and J.-P. Nozières, *Orange peel coupling in multilayers with perpendicular magnetic anisotropy: Application to (Co/Pt)-based exchange-biased spin-valves*, **Europhys. Lett. 65** (2004) 123.

[Nak_08] M. Nakayama, T. Kai, N. Shimomura, M. Amano, E. Kitagawa, T. Nagase, M. Yoshikawa, T. Kishi, S. Ikegawa and H. Yoda., *Spin transfer switching in TbCoFe/CoFeB/MgO/CoFeB/TbCoFe magnetic tunnel junctions with perpendicular magnetic anisotropy,* **J. Appl. Phys. 103** (2008) 07A710.

[Ohm_08] H. Ohmori, T. Hatori and S. Nakagawa, *Fabrication of MgO barrier for a magnetic tunnel junction in as-deposited state using amorphous RE–TM alloy*, **J. Magn. Magn. Mater. 320** (2008) 2963.

[Rod_09] B. Rodmacq, A. Manchon, C. Ducruet, S. Auffret and B. Dieny, *Influence of thermal annealing on the perpendicular magnetic anisotropy of Pt/Co/AlOx trilayers,* **Phys. Rev. B 79** (2009) 024423.

[Ye_08b] L.-X. Ye, C.-M. Lee, J.-W. Syu, Y.-R. Wang, K.-W. Lin, Y.-H. Chang and T.-H. Wu, *Effect of annealing and barrier thickness on MgO-based Co/Pt and Co/Pd multilayered perpendicular magnetic tunnel junctions*, **IEEE Trans. Magn. 44** (2008) 3601.

APPENDICES

APPENDIX 1

TODAY'S RECORDING MEDIA

Characteristics. Advantages. Limits

Today's trend is a fast growth of the storage density in hard disk drives (HDD) media in which binary information is stored in a thin ferromagnetic film as alternating orientations of the local magnetization (magnetic domains) (**Figure A1-1**). Increasing the storage density is a great challenge due to all the problems that it implies: data retention, increased magnetic noise and limited write/read data speed and by consequence increased price of the product.

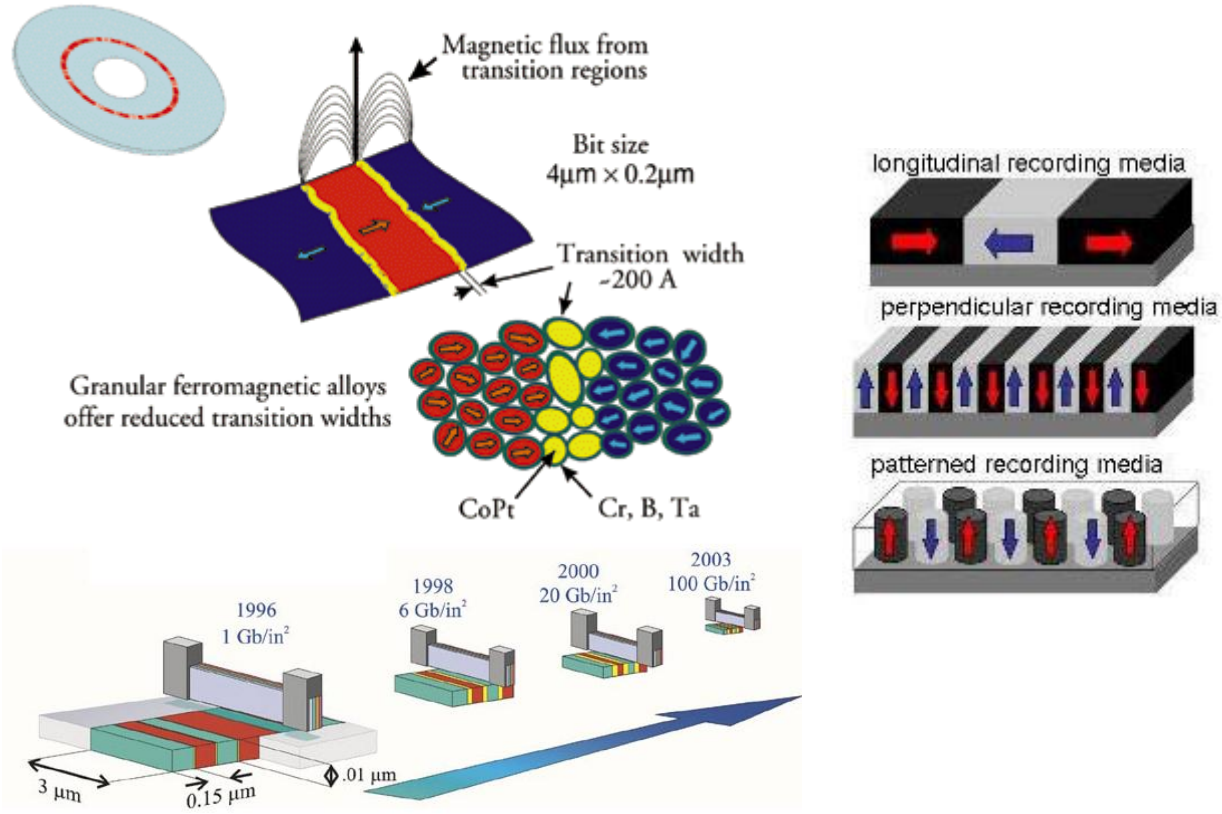

Figure A1-1: (a) HDD architecture presenting magnetic domains (bits) and the transition area. Scaling down the size of magnetic domains had the same impact in the read/write head size [Par_03]; (b) Comparison between continuous longitudinal/perpendicular and patterned-perpendicular recording media.

There is a minimum size of the magnetic domains which is imposed by their thermal stability. Actually when a ferromagnetic domain is very small, it will act like a single magnetic spin which will be submitted to thermal fluctuations. The magnetization direction can thus change randomly with time, and information is lost.

This limit is called superparamagnetic limit (< 500nm) because data retention is not possible in this case. Materials having out of plane anisotropy represent one solution to push the superparamagnetic limit to even smaller sizes. In perpendicular magnetic recording media the

magnetic bits point up or down perpendicular to the disk surface making possible to put data bits closer together and increase the area density of HDD. Perpendicular media require higher fields to set the magnetization, but once set, the magnetization is inherently more stable. The perpendicular approach was introduced in 2005 as an alternative to longitudinal recording, making possible to move beyond 500 Gbytes on 3.5" hard drives and enabling 2.5" notebook hard drives to go to 250 Gbytes.

Decreasing the domain size increases the magnetic noise from the boundary transition area between domains (domain walls). In continuous media the speed of writing/reading data is limited by the mechanical part: disk rotation and read/write head movement. The solution to noise reduction and writing/reading access speed is represented by the discrete media like Read Only Memories (ROM) and Random Access Memories (RAM).

Today the most advanced ROM memories are the Electrical Erasable Read Only Memory (most familiar FLASH) based on the floating gate transistor cell technology which brings all the advantages in terms of storage density, access speed, noise, reliability, portability and power consumption (does not require power to maintain its data). The data is stored by trapping the electrons into an additional gate (the floating gate) insulated all around by an oxide layer. Their main problem is the limited writing cycles (100 kcycles) so limited lifetime. On the other hand the access speed is also important and it is well known RAM memories are even faster than FLASH (modern StaticRAM have access times below 10ns) but these are volatile memories since they lose the data quickly when power is removed. Dynamic RAM memories seem to be more advantageous in terms of high storage density by their simpleer architecture of 1 transistor and 1 capacitor per bit compared to 6 transistors in SRAM.

[Par_03] S.S.P. Parkin, X. Jiang, C. Kaiser, A. Panchula, K. Roche and M. Samant, *Magnetically engineered spintronic sensors and memory,* **Proc. IEEE** **91** (2003) 661.

APPENDIX 2

ELLINGHAM's DIAGRAMS

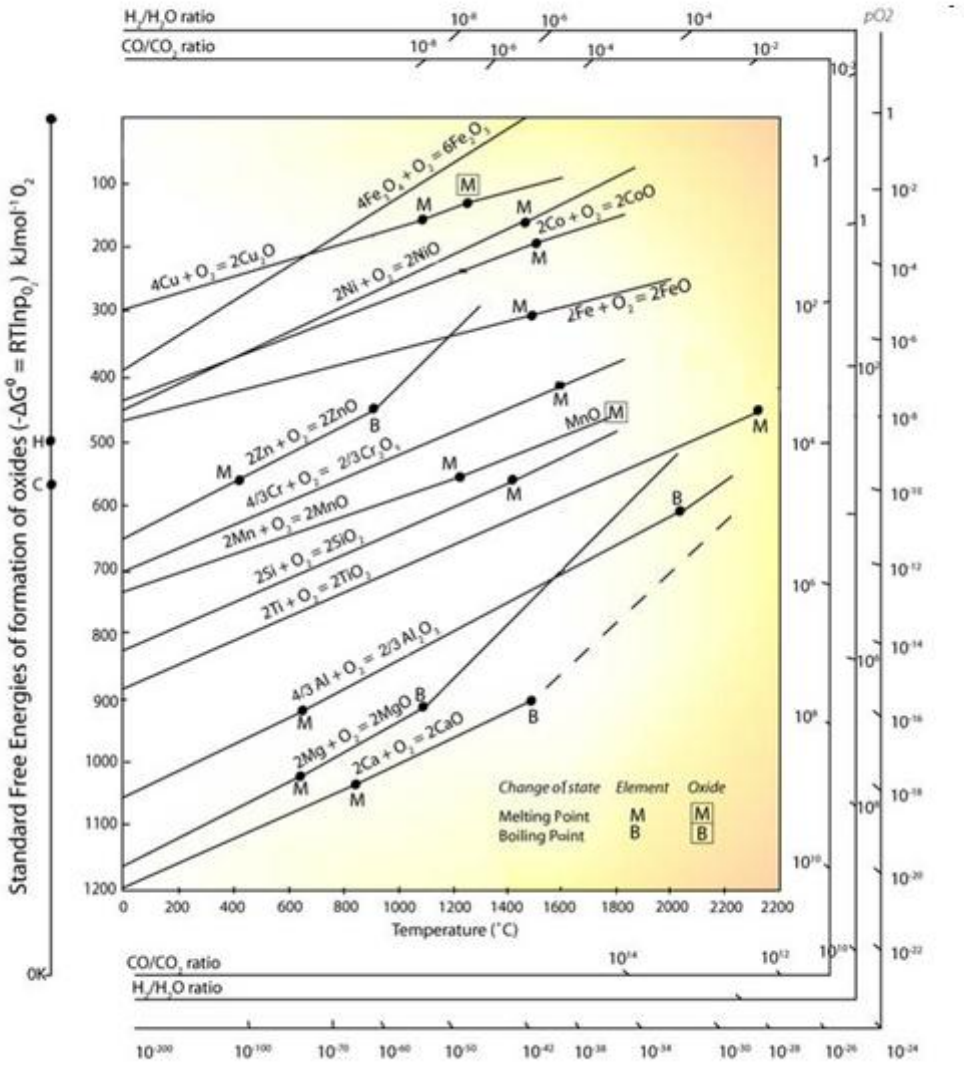

Figure A2-1: Ellingham's diagrams for oxides.

APPENDIX 3

MAGNETIC MEASUREMENTS ON IN-PLANE JUNCTIONS

In **Chapter II-6** we presented transport measurements performed on in-plane magnetic tunnel junctions where the storage layer has a reduced demagnetizing field thanks to CoFeB/MgO interfacial perpendicular anisotropy. These structures are of the form Ta3/CoFeBx/MgO1.4/CoFeB3/Ru0.9/Co2/IrMn7/Ta3 (nm).

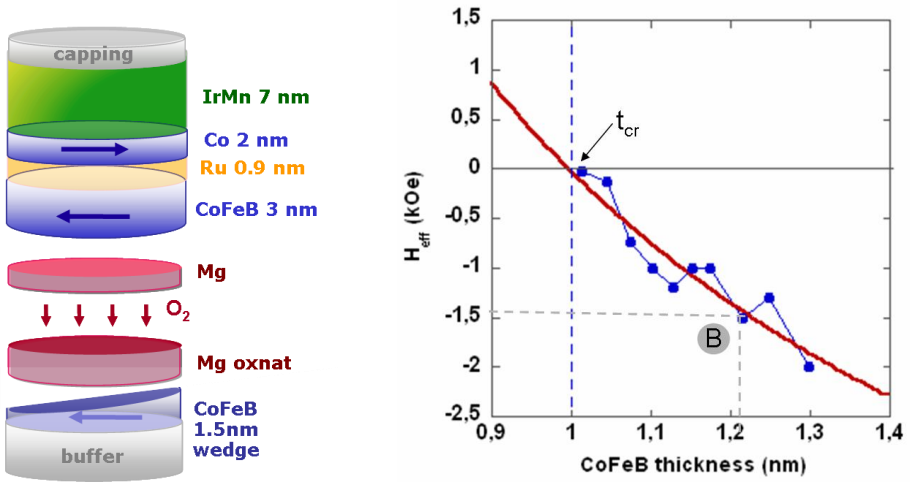

Figure A3-1: Variation of the effective anisotropy field with bottom CoFeB thickness of a top-pinned planar MTJ structure with low effective demagnetizing field.

Figure A3-1 recalls the variation of the effective anisotropy field as a function of CoFeB thickness. The transition from out-of-plane to in-plane orientation of the soft layer occurs for a CoFeB thickness of about 1 nm.

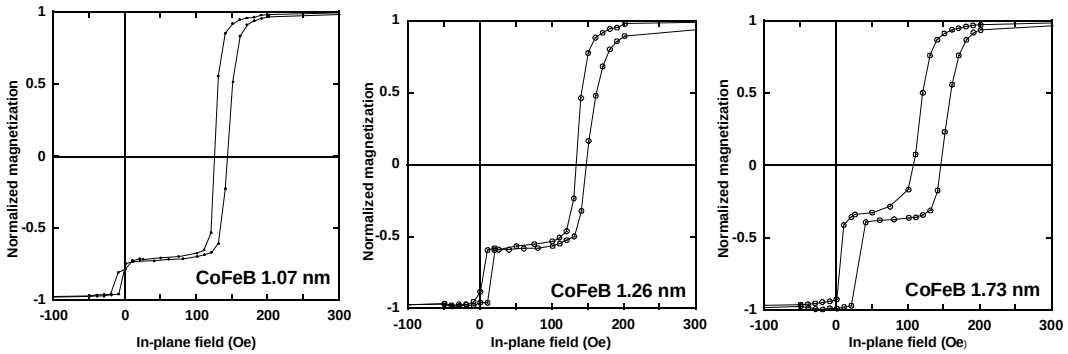

Figure A3-2: In-plane hysteresis loops for Ta3/CoFeBx/MgO1.4/CoFeB3/Ru0.9/Co2/IrMn7/Ta structures for three different thicknesses of the bottom free layer.

Figure A3-2 shows in-plane hysteresis loops of such structures for three different thicknesses of the bottom CoFeB electrode. The magnetization reversal of the top pinned layer occurs for fields of about 100 to 150 Oe. The relative amplitude of the bottom layer progressively increases with increasing thickness. In addition, the coupling between free and

pinned layer changes sign for increasing free layer thickness: it is antiferromagnetic for low thickness and turns ferromagnetic for larger thickness. The coupling sign is confirmed by transport measurements.

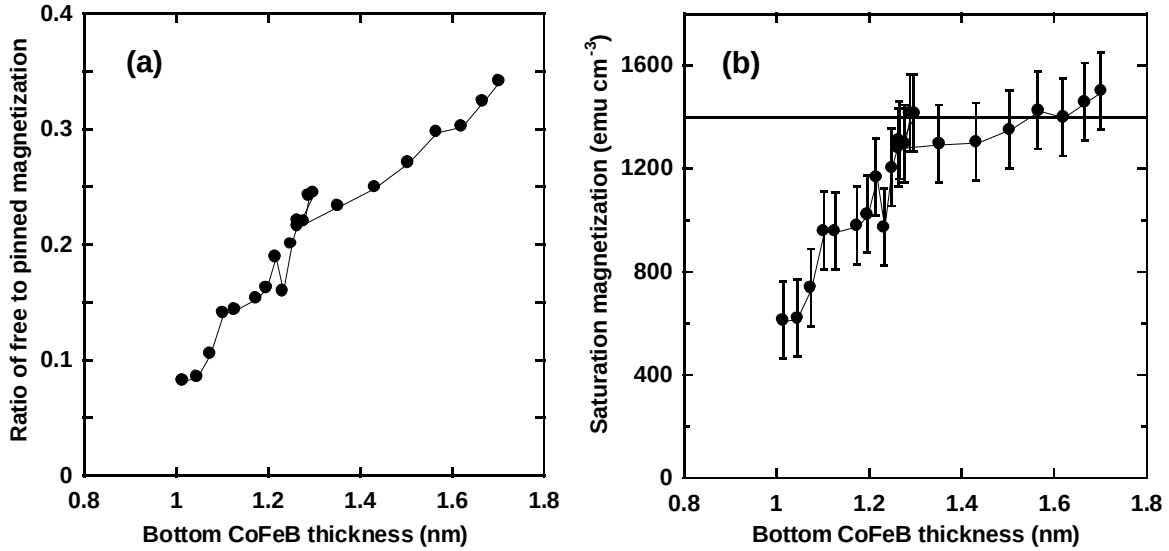

Figure A3-3: CoFeB thickness dependence of (a) The ratio of free to pinned magnetization amplitudes; (b) The saturation magnetization of the bottom free CoFeB layer.

The relative amplitude of the two magnetic transitions can be used to extract the thickness variation of the magnetization of the free layer, after correction from the effect of the angle of incidence on the real thickness of the pinned layer, since deposition is carried out on 100 mm diameter wafers, with a total 10% thickness gradient between centre and wafer edge. After these corrections, **Figure A3-3a** shows the variation of the ratio of the magnetization of both free and pinned layers as a function of the thickness of the free layer. This ratio varies linearly with thickness above 1.3 nm, indicating a constant magnetization value of the free layer. However, the slope increases for smaller thicknesses.

Assuming that both top Co and CoFeB layers have a saturation magnetization of 1400 emu/cm^3, **Figure A3-3b** gives the thickness variation of the saturation magnetization of the bottom CoFeB free layer. Above 1.3 nm, its value is more or less constant. However, it decreases rapidly with decreasing thickness, leading to a "dead layer" thickness of about 0.8 nm. Such a value agrees with recent reports in the literature [Ike_10], and with that given in **Chapter II-6-2**.

[Ike_10] S. Ikeda, K. Miura, H. Yamamoto, K. Mizunuma, H.D. Gan, M. Endo, S. Kanai, J. Hayakawa, F. Matsukura and H. Ohno, *A perpendicular-anisotropy CoFeB–MgO magnetic tunnel junction,* Nature Mater. **9** (2010) 721.

APPENDIX 4

SUB-MICROMETRIC JUNCTIONS PROCESSING AT PTA

For the nanoprocessing, the perpendicular MTJs are deposited on a thick CuN buffer layer (30nm), which will be used as the bottom electrode to pass the current for the electrical measurements. On the top of the pMTJ a thick Al/Ta mask is deposited before the process, which is used as a protection during the pillar definition.

LEVEL 1: magnetic pillars fabrication

E-beam insolation : pillar sizes definition

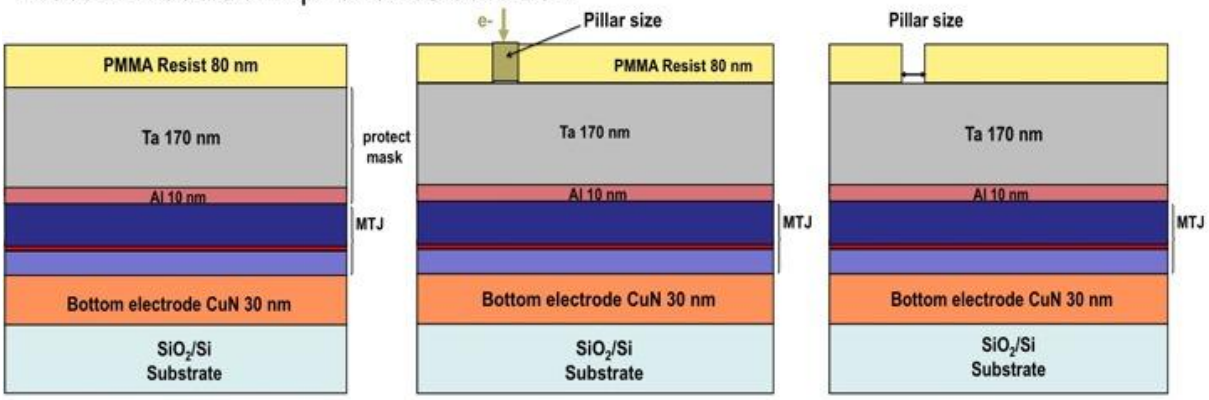

Resist deposition

Resist insolation

Resist development (exposed resist becomes soluble in a chemical developer)

Pt deposition - to protect the Ta mask at the locations where the pillars were defined during the E-beam insolation

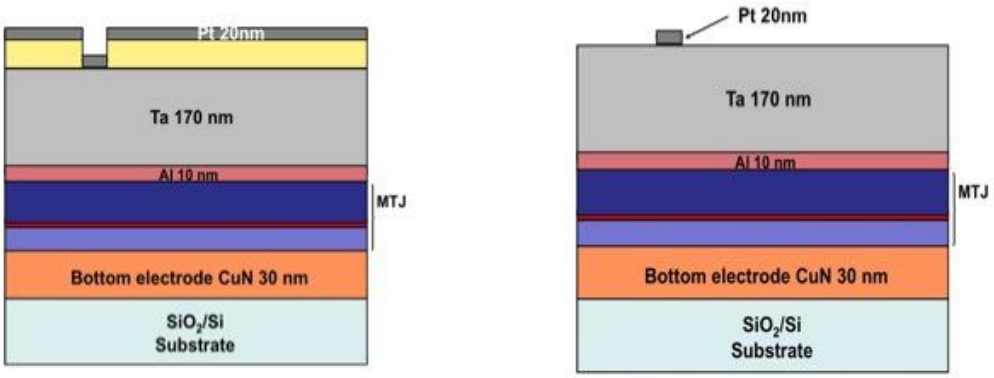

Vapor deposition of Pt layer

Lift-off => Pt pillar

Reactive Ion Etching (RIE)

= etching of the 170nm Ta layer before the MTJ pillar definition using IBE

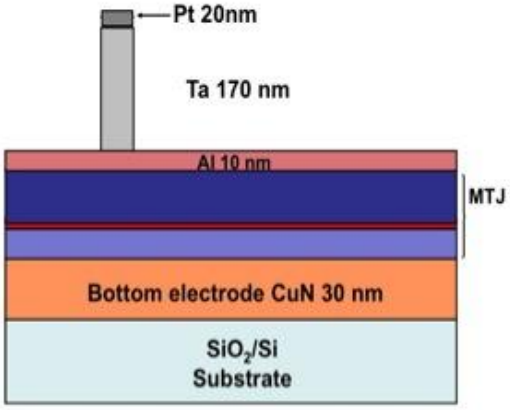

Material selective etching technique:
The SF6 plasma reacts with Ta, but not with the Pt or Al protecting layers for the MTJ

Ion Beam Etching (IBE)

= MTJ pillar definition

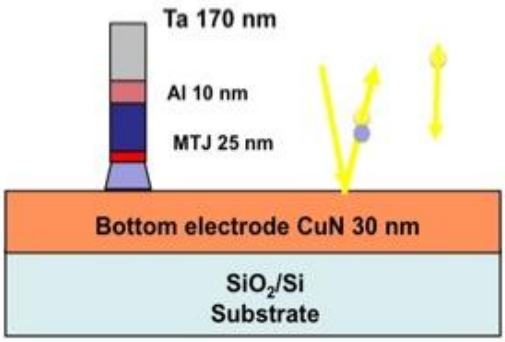

Al+MTJ etching, which is stopped in the Ta layer on top of the CuN layer

LEVEL 2: fabrication of the bottom electrode

UV lithography = bottom electrode definition

Level 2 mask for UV lithography (bottom electrode)

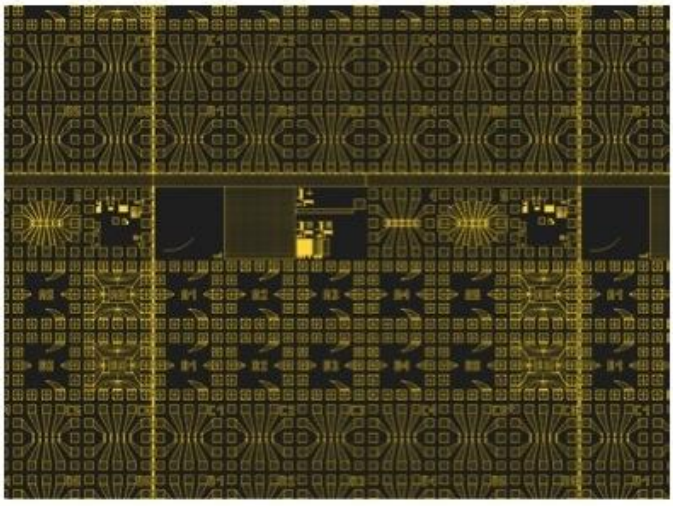

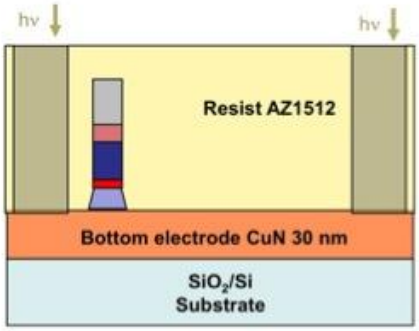

The resist is exposed to UV light and the electrodes are defined using a mask

The exposed resist is removed using a chemical developer

IBE etching = Ta/CuN etching (the resist protects the pillar during etching)

RIE etching + Lift off

- the top resist damaged by the IBE is removed by RIE, using an oxygen plasma)
-lift-off using acetone

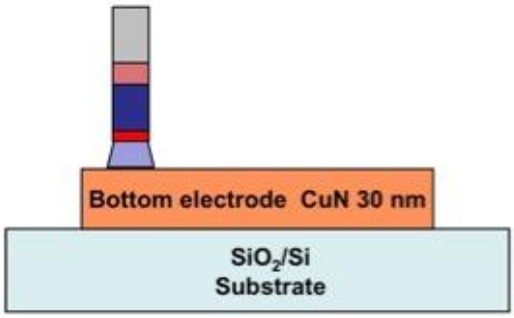

LEVEL 3: planarization and opening of the dots

UV litography = Accuflo area definition

Level 2 and 3 mask (bottom electrode + Accuflo)

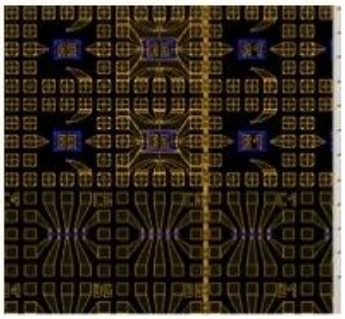

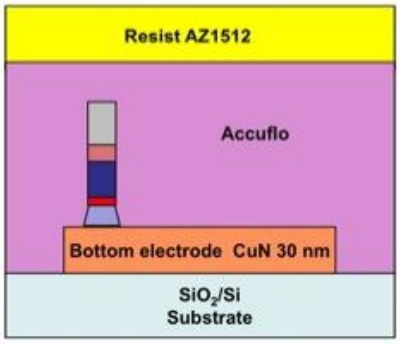

Accuflo deposition (400nm) – an insulator between the two electrodes

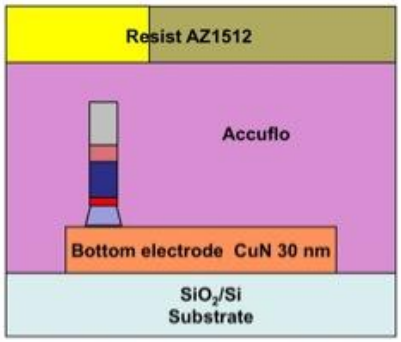

UV lithography = Accuflo definition around the pillars

Resist developing

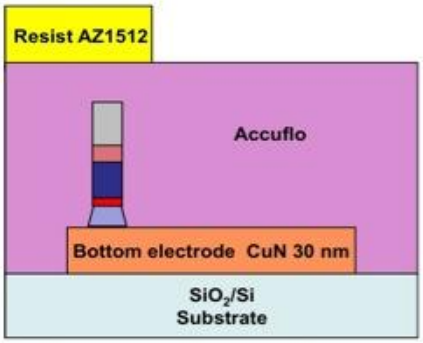

RIE = Accuflo etching using O_2 plasma (the resist has the role of a mask and protects the pillar)

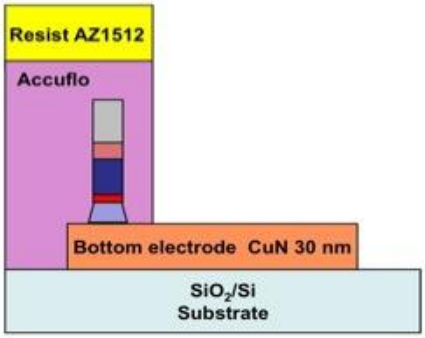

Lift-off of the resist = Accuflo definition around the pillars

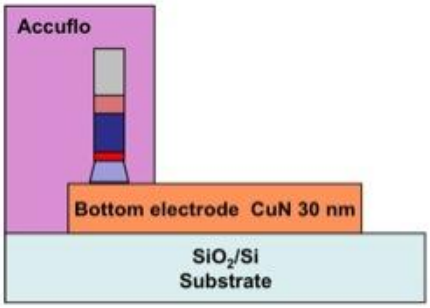

Pillar opening by RIE using an O_2 plasma (**very delicate step of nano fabrication**)

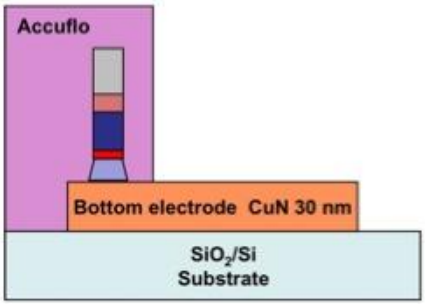

LEVEL 4: fabrication of top electrode

UV lithography = top electrode definition

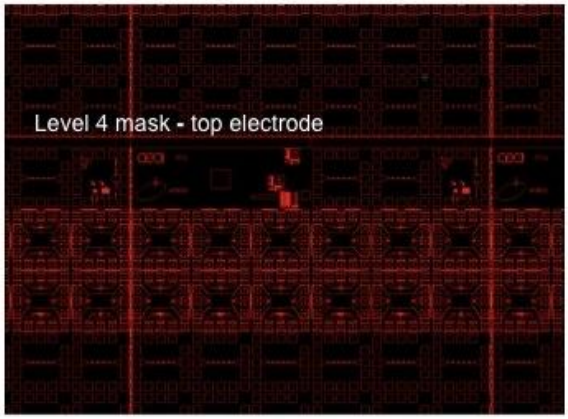

level 2 and 3 mask (bottom electrode + Accuflo)

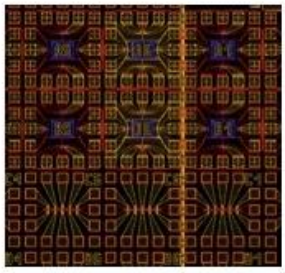

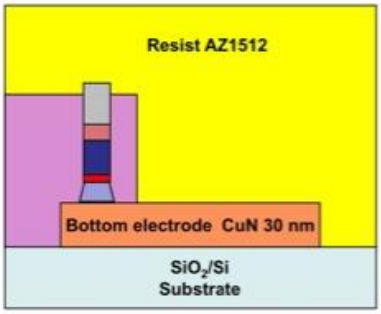

Resist deposition

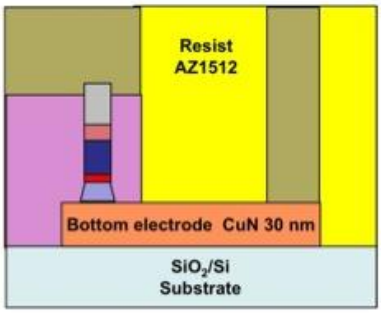

The resist is exposed to UV radiation using level 3 mask

Al deposition by evaporation = top electrode definition

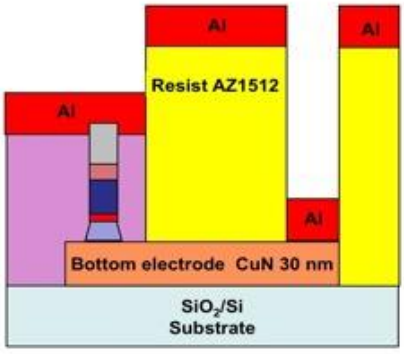

Deposition of 30 nm Al by evaporation (for a good contact during measurements)

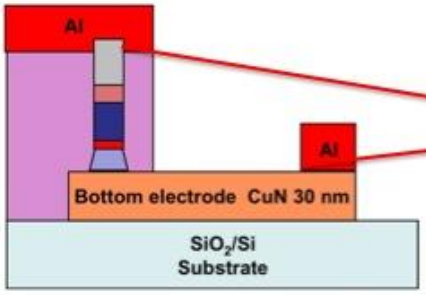

Lift-off using acetone and ultrasounds

Ready to be measured

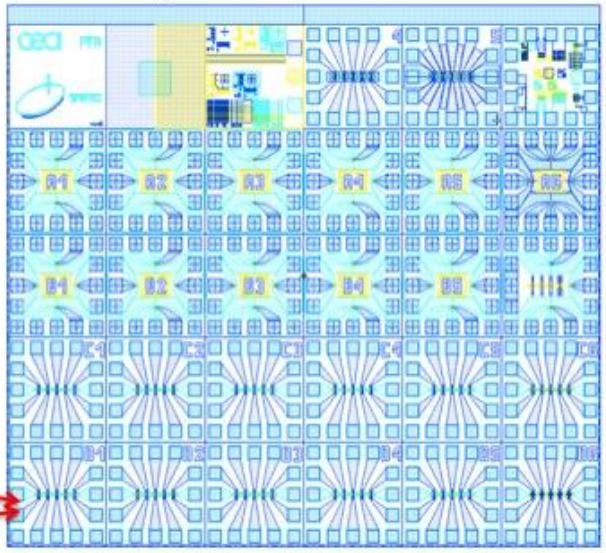

PL1 50 nm | PL2 100 nm | PL3 200 nm | PL4 300 nm | PL5 500 nm | PL6 1000 nm

APPENDIX 5

SCIENTIFIC COMMUNICATIONS

JOURNAL ARTICLES

[Gre_09] L. Grenet, M. Jamet, P. Noe, V. Calvo, J.-M. Hartmann, L.E. Nistor, B. Rodmacq, S. Auffret, P. Warin and Y. Samson, *Spin injection in silicon at zero magnetic field*, Appl. Phys. Lett. **94** (2009) 032502.

[Nis_09] L.E. Nistor, B. Rodmacq, S. Auffret and B. Dieny, *Pt/Co/oxide and oxide/Co/Pt electrodes for perpendicular magnetic tunnel junctions*, Appl. Phys. Lett. **94** (2009) 012512.

[Nis_10] L.E. Nistor, B. Rodmacq, S. Auffret, A. Schuhl, M. Chshiev and B. Dieny, *Oscillatory interlayer exchange coupling in MgO tunnel junctions with perpendicular magnetic anisotropy*, Phys. Rev. B **81** (2010) 220407 (R).

CONFERENCE PROCEEDINGS

[Nis_09] L.E. Nistor, B. Rodmacq, S. Auffret, A. Schuhl and B. Dieny, *Antiferromagnetic coupling in sputtered MgO tunnel junctions with perpendicular magnetic anisotropy*, IEEE Trans. Magn. **45** (2009) 3472.

[Nis_10] L.E. Nistor, B. Rodmacq, C. Ducruet, C. Portemont, I.L. Prejbeanu and B. Dieny, *Correlation between perpendicular anisotropy and magnetoresistance in magnetic tunnel junctions*, IEEE Trans. Magn. **46** (2010) 1412.

PERSONAL COMMUNICATIONS

[Nis_08] L.E. Nistor, B. Rodmacq, S. Auffret, A. Schuhl and B. Dieny, *Anisotropie magnétique perpendiculaire dans des structures Pt/Co/Ox et Ox/Co/Pt*, Colloque Louis Néel, La Grande Motte (France), Sep. 30-Oct. 03 2008 (**Poster**).

[Gre_09] L. Grenet, M. Jamet, P. Warin, P. Noe, V. Calvo, J.-M. Hartmann, L.E. Nistor, B. Rodmacq, S. Auffret and Y. Samson, *Spin injection in silicon at zero magnetic field*, EUROMAT 09, Glasgow (United Kingdom), Sep. 07-10 2009 (**Oral**).

[Nis_09a] L.E. Nistor, B. Rodmacq, S. Auffret, B. Dieny and C. Ducruet, *Influence of oxidation conditions of naturally oxidized MgO barriers in perpendicular magnetic tunnel junctions*, European School on Magnetism, Timisoara (Romania), Sep. 01-10 2009 (**Poster**).

[Nis_09b] L.E. Nistor, B. Rodmacq, S. Auffret, A. Schuhl and B. Dieny, *Antiferromagnetic coupling in sputtered MgO tunnel junctions with perpendicular magnetic anisotropy*, Intermag Conference, Sacramento (USA), May 04-08 2009 (**Oral**).

[Nis_09c] L.E. Nistor, B. Rodmacq, C. Ducruet, S. Auffret and B. Dieny, *Influence of oxidation conditions of naturally oxidized MgO barriers in perpendicular magnetic tunnel junctions*, International Colloquium on Magnetic Films and Surfaces, Berlin (Germany), Jul. 20-24 2009 (**Poster**).

[Nis_10a] L.E. Nistor, B. Rodmacq, S. Auffret, S. Bandiera, E. Gautier, B. Dieny, C. Portemont, C. Ducruet and L. Prejbeanu, *Taking advantage of perpendicular magnetic anisotropy in magnetic tunnel junctions*, Colloque Jacques Cartier « Nanomagnétisme et Spintronique », Grenoble (France), Nov. 24-25 2010 (**Poster**).

[Nis_10b] L.E. Nistor, B. Rodmacq, S. Auffret, M. Marins de Castro Souza, M. Chshiev, A. Schuhl and B. Dieny, *Influence of oxidation conditions on indirect coupling in perpendicular*

magnetic tunnel junctions, 55th Conference on Magnetism and Magnetic Materials, Altanta (USA), Nov. 14-18 2010 (**Oral**).

[Nis_10c] L.E. Nistor, B. Rodmacq, S. Auffret, B. Dieny, C. Ducruet, C. Portemont and I.L. Prejbeanu, *Correlation between magnetoresistance and perpendicular anisotropy in magnetic tunnel junctions*, 11th Joint MMM-Intermag Conference, Washington (USA), Jan. 18-22 2010 (**Oral**).

[Nis_10d] L.E. Nistor, B. Rodmacq, S. Auffret, A. Schuhl, M. Chshiev and B. Dieny, *Couplage indirect oscillant dans des jonctions tunnel à anisotropie perpendiculaire*, Colloque Louis Néel, Albé (France), Mar. 31-Apr. 02 2010 (**Oral**).

[Nis_10e] L.E. Nistor, B. Rodmacq, S. Auffret, A. Schuhl, M. Chshiev and B. Dieny, *Interlayer coupling in tunnel junctions with perpendicular magnetic anisotropy*, Joint European Magnetic Symposia, Krakov (Poland), Aug. 23-28 2010 (**Oral**).

[Nis_10f] L.E. Nistor, B. Rodmacq, S. Auffret, A. Schuhl, M. Chshiev and B. Dieny, *Interlayer coupling in tunnel junctions with perpendicular magnetic anisotropy*, ISAMMA, Sendai (Japan), Jul. 12-16 2010 (**Oral**).

[Nis_10g] L.E. Nistor, B. Rodmacq, C. Ducruet, C. Portemont, I.L. Prejbeanu, M. Chshiev and B. Dieny, *Direct correlation between magnetic anisotropy and tunnel magnetoresistance in magnetic tunnel junctions with MgO barrier*, RIEC International Workshop on Spintronics, Sendai (Japan), Feb. 04-05 2010 (**Invited**).

[Nis_10h] L.E. Nistor, B. Rodmacq, A. Manchon, M. Chshiev, H.X. Yang, B. Dieny, C. Ducruet, C. Portemont, L. Prejbeanu, J.H. Lee and K.H. Shin, *Perpendicular magnetic anisotropy and interlayer coupling in magnetic tunnel junctions*, International Workshop on Spintronics, KIST, Seoul (South Korea), Dec. 09 2010 (**Invited**).

[Nis_11] L.E. Nistor, B. Rodmacq, S. Auffret and B. Dieny, *Low effective demagnetizing field in magnetic tunnel junctions*, Intermag Conference, Taipei (China) Apr. 25-29 2011 (**Oral**).

[Ter_11] D. Terrade, H.X. Yang, A. Kalitsov, L.E. Nistor, M. Chshiev and B. Dieny, *Effect of occupation numbers on exchange coupling in low dimensional magnetic nanostructures*, APS March Meeting, Portland (USA), Mar. 21-25 2011 (**Oral**).

[Yan_11a] H.X. Yang, J. Lee, M. Chshiev, A. Manchon, L.E. Nistor, K. Shin and B. Dieny, *First-principles investigation of the very large perpendicular magnetic anisotropy at Fe/MgO interfaces*, Intermag Conference, Taipei (China), Apr. 25-29 2011 (**Poster).**

[Yan_11b] H.X. Yang, J.H. Lee, M. Chshiev, A. Manchon, L.E. Nistor, K.H. Shin and B. Dieny, *Nature of perpendicular magnetic anisotropy at Fe|MgO and Co|MgO interfaces from first-principles*, Recent Trends in Nanomagnetism, Spintronics and their Applications, Ordizia (Spain), Jun. 01-04 2011 (**Oral**).

PATENT

[Rod_08] **B.** Rodmacq, S. Auffret, B. Dieny and L.E. Nistor, *Three-layer magnetic element, method for the production thereof, magnetic field sensor, magnetic memory, and magnetic logic gate using such an element*, Jun. 09 2008.

APPENDIX 6

French introduction

MATERIAUX. L'AGE DE LA SPINTRONIQUE. MOTIVATION

Les **matériaux**, plus ou moins sophistiqués, sont présents dans la vie de l'homme depuis plusieurs milliers d'années. L'intelligence de l'homme, dans la nécessité d'améliorer sa condition de vie, a contribué à l'évolution des matériaux utilisés dans notre vie quotidienne (depuis les plus simples comme le bois et la pierre aux plus complexes comme le bronze et le fer). L'impact des matériaux dans l'évolution de l'homme a été si fort que nous pouvons affirmer qu'il a contribué à modeler les civilisations. Par exemple, dans le cas des Hittites (18ème siècle avant Jésus-Christ), l'amélioration de la technique de fabrication de fer de très bonne qualité en a fait l'une des civilisations les plus évoluées et puissantes de l'antiquité et l'a aidée à dominer la région méditerranéenne **[Hum_04]**. L'appréciation de l'impact des matériaux dans l'histoire de l'homme et l'évolution a été illustrée dans l'histoire en nommant chaque époque d'après le matériau utilisé:

- L'âge de la pierre - 4500 avant J-C

- L'âge du bronze - 1700 à 0

- L'âge du fer - 1500 avant J-C à 1950 après J-C

Aujourd'hui nous sommes plus orientés vers l'utilisation de matériaux fonctionnels (matériaux électroniques, matériaux pour l'optique, les matériaux pour le stockage d'hydrogène) pour des applications technologiques, mais aussi pour la recherche fondamentale, car ces matériaux sont pleins de phénomènes intéressants à comprendre et à valoriser.

Nous allons nous concentrer dans ce manuscrit sur les matériaux électroniques dans lesquels les électrons sont les premiers responsables de leurs propriétés physiques. Quelques exemples de matériaux électroniques: **les matériaux magnétiques, les métaux, les isolants**.

Le **magnétisme** est la propriété des matériaux qui répondent à un champ magnétique appliqué, et est liée au mouvement des électrons et la parité des électrons dans l'atome. Dans une image simplifiée selon Ampère et Œrsted, le mouvement des électrons (mouvement orbital autour du noyau, et mouvement de précession autour de son axe) se traduit par un courant électrique à partir duquel un champ magnétique apparaît. Mais le spin des électrons vient de la mécanique quantique combinée avec la relativité et peut être détectée par le **moment magnétique**, $m = g \mu_B s$, ou le spin moyen d'un ensemble d'électrons dans un volume donné, **l'aimantation** (M). Considérant le nombre d'électrons, la loi de Pauli pour le remplissage des niveaux d'énergie atomiques (qui permet une paire d'électrons de spins *up* et *down* sur chaque niveau d'énergie dans l'atome) et le couplage spin-orbite, on obtient le moment atomique, J. Donc dans le cas des matériaux diamagnétiques (qui n'ont pas d'électrons non appariés et des niveaux d'énergie remplis, $J = 0$) le magnétisme va résulter de l'interaction entre le champ extérieur appliqué et le mouvement des électrons dans l'atome à travers la loi de Lentz, résultant en un moment magnétique qui sera opposé au champ appliqué. Plus intéressants sont les matériaux avec un moment atomique comme les matériaux paramagnétiques et les matériaux ordonnés ferromagnétiques ou antiferromagnétiques. Dans les matériaux paramagnétiques le moment orbital non compensé (L) et moment angulaire de spin (S) se traduisent par des moments atomiques indépendants contrairement aux matériaux ferromagnétiques qui ont des moments atomiques coopératifs. C'est pourquoi la réponse à un

champ magnétique appliqué sera différente: les matériaux paramagnétiques seront uniquement ordonnés en présence d'un champ magnétique tandis que les matériaux ordonnés resteront alignés même après suppression du champ appliqué.

Les électrons sont également responsables des propriétés métalliques ou isolantes des matériaux. Dans ce cas les électrons ont le rôle de porteur de charge. Ainsi, dans une image simple, on peut distinguer de tels matériaux par la mobilité de leurs charges. Les métaux présentent une grande mobilité électronique, contrairement aux isolants.

Les techniques de fabrication peuvent changer les propriétés des matériaux. C'est pourquoi elles sont un facteur important dans l'évolution des matériaux. Un autre exemple de l'histoire: la découverte de bronze a été due à l'insertion de 10% d'étain dans le cuivre, afin de diminuer sa température de fusion, rendant plus facile l'élaboration de différents objets. Aujourd'hui, l'utilisation de matériaux magnétiques avec des métaux ou des isolants avec de nouvelles techniques de fabrication de films minces (avec des épaisseurs de couche de l'ordre de la longueur de diffusion des électrons) comme l'épitaxie par jets moléculaires ou la pulvérisation, a rendu possible la mise en évidence de nouveaux phénomènes physiques comme:
- L'anisotropie magnétique perpendiculaire interfaciale (PMA) **[Gra_68]**
- La magnétorésistance géante (GMR) **[Bai_88, Bin_89]**
- La magnétorésistance tunnel (TMR) **[Moo_95]**
- Le caractère oscillatoire du couplage d'échange RKKY **[Par_91]**.

Ces phénomènes fascinants considèrent tous le spin de l'électron, en plus de sa charge, associant magnétisme et transport électronique dans un nouveau domaine de recherche: **l'électronique de spin ou Spintronique**. Prenant en compte à la fois la charge et le spin des électrons rend la physique de ces matériaux plus complexe, mais donne un avantage supplémentaire pour les applications en offrant plus de possibilités de concevoir de nouveaux dispositifs et de réinventer l'électronique.

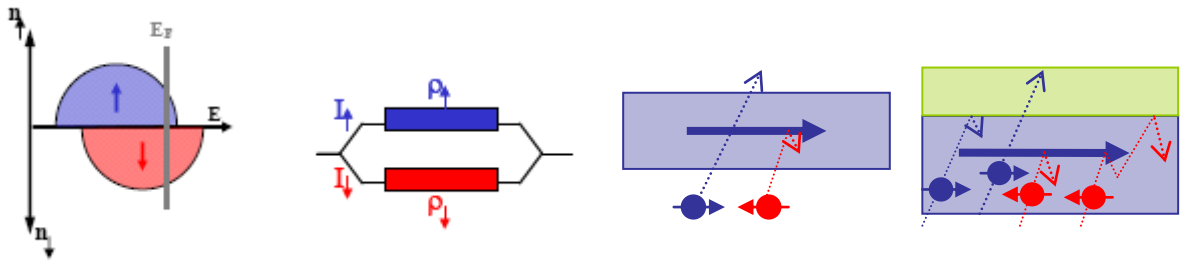

Figure 1: Briques de la Spintronique: (a) Asymétrie de spin; (b) Approximation de Mott; (c) Diffusion dépendante du spin; (d) Accumulation de spin.

La spintronique est basée sur quatre effets (voir **Figure 1**) qui, lorsque combinés, sont à l'origine de toutes les propriétés observées dans les couches minces magnétiques:
1) **L'asymétrie de spin** (électrons d): dans la densité d'états pour les électrons d localisés d'un matériau ferromagnétique, le nombre de spin (↑) d'électrons d est différent de celui de spin (↓).
2) **L'approximation de Mott**: le spin des électrons est conservé (faible probabilité d'inversion de spin après la diffusion d'électrons sur des défauts de la couche). En conséquence, deux canaux de conduction existent en parallèle pour les spin up et spin down **[Mot_36]**.
3) **La diffusion dépendante du spin** (électrons s): comme conséquence de l'asymétrie de spin, il y aura une probabilité différente de diffusion pour les électrons s de spin up et down (électrons de conduction) quand ils sont parallèles (P) ou antiparallèle (AP) à l'aimantation de la couche.
4) **L'accumulation de spin** (électrons s): les électrons s seront diffusés à l'interface magnétique/non magnétique (à cause de la différence entre les états d'équilibre et de

déséquilibre de spin). Selon l'approximation de Mott les électrons s auront de grandes longueurs de diffusion.

Parmi toutes ces propriétés de multicouches ferromagnétique-métal, la découverte de la GMR a eu le plus fort impact sur la physique fondamentale et appliquée. D'un point de vue fondamental, la GMR peut être expliquée par la **diffusion dépendante du spin** des électrons à cause de l'orientation relative des aimantations des couches magnétiques. Ainsi, lorsque les aimantations des couches sont parallèles, seuls les électrons de spin parallèle à l'aimantation peuvent passer à travers l'échantillon, car ils sont faiblement diffusés, résultant en un état de faible résistance (R_{low}). Dans le cas où les aimantations des couches sont antiparallèles, tous les électrons de spin parallèle/antiparallèle seront diffusés, résultant en un état de forte résistance (R_{high}). La variation importante de résistance entre les orientations AP et P a inspiré le nom de la GMR. Le principe schématique pour un cas simplifié de deux couches ferromagnétiques (F1 et F2) séparées par une couche non magnétique métallique (NM) est présenté dans la **Figure 2**.

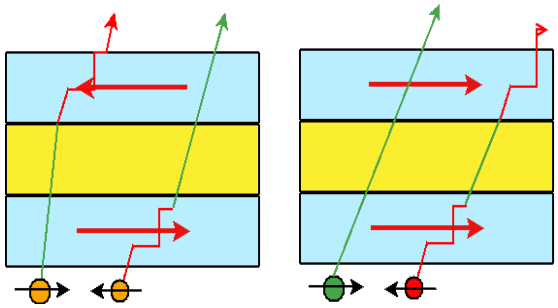

Figure 2: Explication schématique de l'effet GMR.

D'un point de vue applicatif la découverte de la GMR a offert un nouveau concept pour les dispositifs de capteur magnétique: la vanne de spin [Die_91]. Possédant une sensibilité nettement améliorée par rapport aux capteurs inductifs ou même aux capteurs à magnétorésistance anisotrope, les vannes de spin ont été rapidement intégrées dans les têtes de lecture/écriture par l'industrie des disques durs (HDD). Cela a permis une augmentation rapide de la densité surfacique d'information comme on peut l'observer dans la **Figure 3**, et a inspiré un nouveau dispositif pour les applications industrielles, la **Jonction Tunnel Magnétique.**

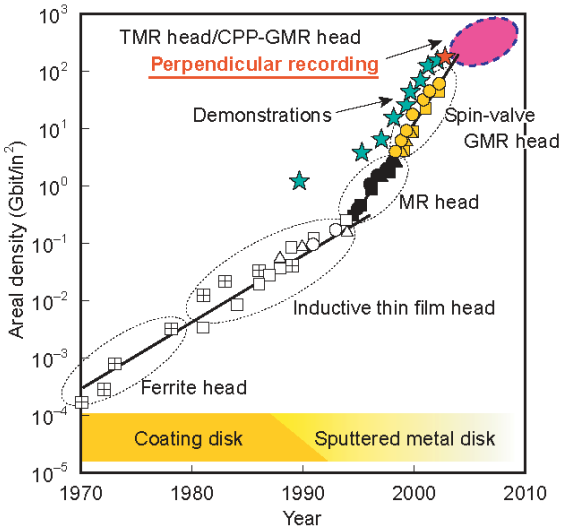

Figure 3: Technologies des têtes de lecture/écriture qui ont contribué à l'augmentation de la densité de stockage des disques durs [Fuj_06].

Les jonctions tunnel magnétiques (MTJ) sont des dispositifs spintroniques dérivés des vannes de spin en remplaçant le séparateur métallique par une couche isolante très mince (oxyde) de sorte que les électrons peuvent passer d'une couche ferromagnétique à l'autre par effet tunnel. Dans ce cas, l'effet de **filtrage en spin** est dominant par rapport à la diffusion de spin et le résultat est une variation de résistance très élevée appelée MagnétoRésistance Tunnel (TMR). C'est pourquoi les dispositifs MTJ ont un signal de sortie plus élevé que les vannes de spin, ce qui les rend très attractifs pour des applications industrielles. La différence dans les valeurs de résistance entre les configurations P et AP des couches magnétiques peut être utilisée pour un codage binaire, permettant d'imaginer de nouveaux supports d'enregistrement ou des circuits logiques.

Aujourd'hui, les ordinateurs utilisent quatre moyens de stockage des données: mémoires dynamiques à accès aléatoire (DRAM), mémoires à haute densité qui doit être constamment rafraîchies (forte consommation d'énergie); mémoires vives statiques (SRAM, utilisées dans les mémoires cache), avec lecture et écriture rapide; mémoires Flash, non volatile, mais avec un bas taux d'accès, et disques durs (HDD), qui présentent une haute densité de stockage, mais s'appuient sur des pièces mobiles, ce qui impose des limitations de taille et de vitesse.

Dans l'avenir, les besoins des consommateurs pour les supports d'enregistrement demanderont de combiner **vitesse d'accès élevée, bruit réduit, fiabilité, portabilité, non-volatilité et faible consommation d'énergie dans une puce la plus petite possible avec une densité élevée. Toutefois, on doit aussi considérer la stabilité thermique et la conservation à long terme des données** (**Annexe 1**).

La Spintronique nous donne un candidat pour cette mémoire universelle basée sur la technologie MTJ: la Mémoire Magnétique à Accès Aléatoire (**Magnetic Random Access Memory, MRAM**). Cette MRAM est attrayante pour les applications industrielles, car elle pourrait, en principe, remplacer toutes les autres sortes de mémoires. Par exemple en utilisant une mémoire MRAM dans un ordinateur, les données pourraient être chargées directement dans la mémoire de travail et de ne pas avoir à basculer entre la mémoire principale (SRAM) et le disque dur. Cela pourrait rendre possible le démarrage instantané du système et d'innover dans l'architecture informatique.

Les premières architectures MRAM utilisant des couches magnétiques minces à aimantation planaire séparées par une mince couche d'oxyde fournissent certains avantages clés: **la non-volatilité et l'endurance illimitée à la lecture/écriture** (10^{15} cycles de lecture-écriture), en plus de ceux des mémoires RAM classique (vitesse de la SRAM). L'énergie utilisée pour le fonctionnement (rétention de données pour le processus d'écriture / lecture)) est beaucoup plus petite que celle des mémoires FLASH parce que le temps requis par opération est beaucoup plus court. Mais, même si la technique d'écriture MRAM semble la plus simple en utilisant un champ appliqué afin de basculer l'aimantation de la couche libre, l'architecture requise est compliquée et nécessite beaucoup d'espace, rendant impossible d'atteindre des densités élevées. En outre, cette commutation induite par champ magnétique atteint ses limites lorsque la taille des cellules est réduite en dessous de 100 nm. Diminuer la taille des cellules va augmenter la densité de courant nécessaire pour produire le champ de commutation et également la puissance d'écriture, les erreurs de sélection pour l'écriture des cellules de mémoire va également augmenter, ainsi que l'impact des fluctuations thermiques sur la stabilité des données. Une mémoire 4Mb-MRAM a été commercialisé par Freescale Motorola (maintenant EverSpin) en 2006 **[Eve_06]** et trouve des applications dans les satellites, l'aérospatiale, l'industrie de l'automobile et des télécommunications, ou comme mémoires embarquées dans les contrôleurs ou les imprimantes.

Une mémoire MRAM stable, rapide et de haute densité est le rêve de mémoire universelle qui pourrait être utilisée dans toutes les applications et remplacer tous les supports d'enregistrement du temps présent. Mais elle exige une nouvelle technologie MRAM.

Un nouveau phénomène physique de commutation de l'aimantation, la commutation par **couple de transfert de spin** (STT) prédite par Slonczewski en 1996 **[Slo_96**, **Ber_96]** et initialement mesuré dans des vannes de spin **[Kat_00**, **Sun_02**, **Puf_03]**, donne la possibilité d'atteindre des densités de stockage des DRAM. Une architecture STT-MRAM peut être imaginée et peut apporter des avantages considérables: plus d'erreurs d'adressage puisque que seuls les piliers traversés par l'impulsion de courant seront écrits; augmentation de la densité de mémoire en supprimant la ligne d'écriture, permettant un transistor-1 MTJ par cellule comme dans la DRAM et rendant possible la réduction de la taille des cellules MTJ.

Dans le cas des nano-éléments magnétiques avec aimantation dans le plan, la limite de stabilité thermique n'est pas liée aux paramètres de commutation par courant, mais à leur forme. Dans les matériaux sans axe privilégié pour l'aimantation (sans anisotropie cristalline), une forme elliptique spécifique est nécessaire pour stabiliser l'aimantation le long du grand axe afin de minimiser l'énergie magnétostatique. Réduire la taille des cellules rend impossible de garder la forme elliptique et d'empêcher une rotation de l'aimantation à cause des fluctuations thermiques. Une solution consiste à définir la direction de l'axe d'aimantation de la couche libre en la couplant à une couche antiferromagnétique (AF). La commutation de la couche libre est réalisée par chauffage de la cellule MTJ au-dessus de la température de blocage de l'antiferromagnétique. Basé sur ce phénomène Spintec a proposé une nouvelle technique d'écriture basée sur la commutation par couple de transfert de spin assistée thermiquement (STT-TAS-MTJ) **[Pre_04**, **Oun_02**, **Noz_06**, **Her_10]**.

L'utilisation de matériaux magnétiques à aimantation perpendiculaire pourrait être une solution alternative pour maintenir l'aimantation le long d'un axe bien défini dans une MTJ et d'améliorer la résistance aux fluctuations thermiques **[Mor_06**, **Car_08**, **Yoo_05**]. Les limites de taille et contraintes de forme des éléments MTJ planaire sont éliminées en utilisant des p-MTJ. Par ailleurs des études **[Man_06**, **Nak_08]** ont montré que les structures perpendiculaires STT peuvent présenter des courants critiques de commutation inférieurs et une efficacité STT plus élevée.

Ces nouveaux éléments MTJ hors du plan sont prometteurs pour les applications industrielles et intéressants pour la physique fondamentale. Les pMTJ combinent les deux propriétés magnétiques d'anisotropie hors du plan et les propriétés de transport tunnel à travers une barrière isolante. Dans les MTJ conventionnelles les hautes performances de TMR sont données par la bonne adéquation entre la structure cristalline et la texture des électrodes et de la barrière, la qualité des interfaces, la faible rugosité de la barrière. L'anisotropie magnétique perpendiculaire (PMA) peuvent avoir des origines différentes, soit volumique (alliages hcp CoCrPt, alliages Terre Rare/ Métal de Transition, ou alliages ordonnés FePt $L1_0$, ou interfaciale (dans les multicouches Pt/Co, Pd/Co ou Co/Ni). Il a également été observé qu'une assez grande PMA peut être induite à l'interface entre les électrodes ferromagnétiques et un oxyde **[Mon_02**, **Rod_03]**. On peut profiter de cette PMA à l'interface électrode magnétique/oxyde pour fabriquer des MTJ avec aimantation hors du plan.

En conclusion les pMTJ sont très prometteuses pour augmenter la densité de stockage de l'information en conservant une bonne stabilité des données et une faible consommation électrique. Mais même si le problème de stabilité semble être résolu d'autres questions peuvent se poser:

1) Existe-t-il des techniques de nanofabrication en mesure de produire des piliers ayant la taille d'un transistor actuel (30nm)?

2) Peut-on fabriquer une électronique adaptée basée sur une cellule 1T-STT-MTJ?

Les STT-pMRAM devraient être en mesure de rivaliser avec les mémoires Flash et disques durs actuels si ces aspects techniques sont résolus à coût de production similaire. Sinon les MRAM seront utilisées dans les marchés spéciaux comme le remplacement de SRAM sauvegardées par batterie et seraient intéressantes pour les applications où la vitesse et la permanence de stockage de données sont nécessaires, éliminant ainsi l'utilisation de mémoires

combinées. Quelques exemples d'applications sont le remplacement des composants des systèmes de serveurs, les réseaux et les données de périphériques de stockage, systèmes de sécurité et imprimantes d'ordinateur. Les conséquences sont énormes compte tenu de la réduction de la taille du circuit, de la faible consommation d'énergie résultant dans une durée de vie accrue des batteries, des performances améliorant l'efficacité du transfert de données (la vitesse de démarrage de l'ordinateur). Même plus, avec les MTJ il sera possible de profiter de la dynamique de précession pour un fonctionnement à faible puissance ou pour obtenir des oscillateurs radiofréquence accordables menant à de nouveaux dispositifs RF pour l'industrie de la téléphonie mobile.

Cette thèse résume tous les efforts consentis au cours des trois dernières années, de la fabrication d'éléments pMTJ à la démonstration de faibles courants de commutation STT obtenu en utilisant l'anisotropie magnétique perpendiculaire.

L'ingénierie des pMTJ est un véritable défi et une tâche difficile parce que de bonnes propriétés de TMR et d'anisotropie perpendiculaire vont imposer des contraintes et limiter la fenêtre de travail du dispositif. Elle exige aussi une bonne compréhension des origines de la PMA et de la TMR, et une bonne maîtrise des techniques de croissance de couches minces et de caractérisation afin d'être en mesure d'optimiser les propriétés du matériau afin d'obtenir leurs meilleures propriétés dans un échantillon donné. La croissance des couches minces et leur caractérisation m'a montré la complexité physique et la richesse des structures faites de différents matériaux avec des propriétés différentes. On peut obtenir de nombreuses combinaisons de ces propriétés en utilisant des matériaux différents, en changeant l'épaisseurs des couches, en effectuant des traitements de recuit, en appliquant des champs magnétiques ou des impulsions de courant.

Nous présenterons ici les études les plus importantes et les résultats obtenus en quatre chapitres. Le **Chapitre I** sera consacré à la fabrication de matériaux ayant une contribution d'anisotropie perpendiculaire à l'interface avec un oxyde. Les deux structures métal magnétique/oxyde et oxyde/métal magnétique seront étudiées. L'origine de l'anisotropie perpendiculaire dans ces deux types de matériaux sera étudiée en faisant varier différents paramètres comme la nature du matériau magnétique, la température de recuit, les épaisseurs des couches. Le **Chapitre II** sera consacré aux structures complètes pMTJ et deux sortes de matériaux seront présentés: ceux à très forte anisotropie perpendiculaire à base de Pt/Métal Magnétique/Oxyde et ceux à faible anisotropie, comme Ta/Métal Magnétique/Oxyde. Les propriétés magnétiques et de transport des deux structures seront étudiées afin de choisir le meilleur candidat pour les applications MRAM. Une corrélation entre TMR et de la PMA a été observée et elle a contribué à confirmer l'origine de l'anisotropie perpendiculaire à l'interface métal/oxyde. Le **Chapitre III** est une étude plus fondamentale des pMTJ et concerne le couplage d'échange intercouches en présence d'anisotropie perpendiculaire. Nous présenterons une étude détaillée de l'influence sur le couplage de la température de recuit et de l'épaisseur des couches afin de comprendre son origine. Enfin, le concept de STT-pMTJ sera validé dans le **Chapitre IV**, après réalisation de jonctions tunnel magnétiques sub-microniques.

French summary

Le but de cette thèse est la fabrication et l'étude des propriétés de jonctions tunnel magnétiques à aimantation perpendiculaire qui utilisent l'anisotropie perpendiculaire présente à l'interface entre un métal magnétique et un oxyde. Ces matériaux sont prometteurs pour des applications de type mémoires magnétiques.

La découverte de l'effet de transfert de spin **[Slo_96, Ber_96]** (l'échange de moment angulaire entre les électrons et l'aimantation) a ouvert la voie vers des applications basées sur le retournement (précession) de l'aimantation à l'aide d'un courant polarisé en spin **[Sun_00]**. En théorie, dans le cas des applications mémoires, les jonctions tunnel perpendiculaires devraient nécessiter moins d'énergie (courant) pour ce type d'écriture **[Man_06]**. Mais la fabrication de telles structures représente un défi et une tâche difficile puisque l'obtention simultanée de bonnes propriétés de transport (TMR) et d'anisotropie perpendiculaire impose des contraintes sur les matériaux utilisées en limitant la fenêtre de travail, notamment en ce qui concerne l'épaisseur des couches magnétiques.

Pour atteindre cet objectif il faut d'abord comprendre mieux ces systèmes. Nous avons donc tout d'abord étudié les propriétés des différents empilements comme : l'anisotropie de l'interface métal magnétique-oxyde, le transport tunnel et le couplage entre les couches magnétiques à travers la barrière isolante.

Dans le cas des matériaux magnétiques, l'aimantation spontanée peut avoir des axes d'orientation préférentielle, et cette anisotropie peut être quantifiée par la dépendance de l'énergie magnétique en fonction de la direction de l'aimantation. Quand l'aimantation est perpendiculaire au plan des couches, on parle d'anisotropie perpendiculaire (PMA). Dans le cas des couches minces, la PMA peut avoir différentes origines: anisotropie de volume (magnétocristalline) comme dans le cas des structures hcp d'alliages CoCrPt, des alliages ou multicouches Terres Rares-Métal de Transition, ou des alliages ordonnés FePt $L1_0$, ou anisotropie d'interface/surface comme dans le cas des multicouches Pt/Co, Pd/Co, ou Co/Ni. Il a aussi été observé qu'une forte anisotropie perpendiculaire peut être induite à l'interface entre un métal magnétique et un oxyde **[Mon_02]**.

Les matériaux à anisotropie perpendiculaire ont déjà montré leurs avantages dans le cas des disques durs, permettant une forte augmentation de la densité de stockage. D'autres applications sont envisagées dans le cas des mémoires magnétiques à base de jonctions tunnel magnétiques en utilisant l'anisotropie d'interface entre un métal magnétique et un oxyde. Du point de vue fondamental ces matériaux sont intéressants et peuvent être utilisés pour étudier le déplacement de parois sous champ magnétique ou sous courant électrique, les phénomènes de transfert de spin, ou le contrôle des propriétés magnétiques par un champ électrique **[Man_06, End_10, Ike_10, Mir_10, Wei_07]**. Tous cela demande une bonne compréhension de l'origine de l'anisotropie dans ces films minces.

Dans les films minces magnétiques les interfaces ont un fort impact sur les propriétés magnétiques à cause de la réduction de l'épaisseur des couches. Dans ces couches magnétiques on a deux contributions à l'anisotropie effective, une des interfaces (Ks) et l'autre de volume (Kv) comme représenté dans la formule suivante:

$$K_{eff} = K_V - 2\pi M_s^2 + \frac{K_{s1} + K_{s2}}{t}$$

L'anisotropie de volume a deux contributions, l'anisotropie magnétocristaline et l'anisotropie de forme. L'anisotropie magnétocristalline est liée au couplage spin-orbite. Plus précisément, le moment orbital des électrons (L) est liée à la maille (structure) par l'intermédiaire des interactions avec les charges des ions dans le matériau (champs cristallin E) ce qui aura aussi un impact sur le spin des électrons (S) grâce à l'interaction spin-orbite (SO) et

l'aimantation sera alignée suivant un axe cristallin préférentiel. Par contre l'anisotropie de forme est liée à la minimisation de l'énergie magnétostatique qui force l'aimantation à rester dans le plan.

A l'interface entre deux couches ou à la surface, la symétrie cristalline est brisée et les atomes de l'interface/surface ont un environnement très différent par rapport aux atomes de volume. En considérant cet effet, Néel **[Née_54]** à prédit que l'anisotropie effective dans le cas des couches minces devrait être différente due à cette brisure de symétrie qui est responsable de l'anisotropie perpendiculaire à l'interface. La présence d'atomes lourds comme Pt (Pd, Au) à l'interface avec un matériel magnétique (Co) va induire une forte hybridation des orbitales 3d de Co et 5d de Pt **[Nak_98]** grâce au fort couplage spin-orbite et une augmentation du moment orbital de Co. Le champs cristallin va décaler les bandes 5d de Pt de spin parallèle au spin majoritaire de Co et, à cause du fort couplage spin-orbite, il apparaît un moment magnétique de Pt couplé parallèlement au moment orbital de Co. Dans le cas de la présence d'atomes à l'interface avec Co avec un couplage spin-orbite plus faible comme les oxydes, l'origine de l'anisotropie d'interface est différente. L'anisotropie à l'interface métal/oxyde vient de la formation de liaisons métal magnétique-oxygène qui produit un mélange des orbitales dxz, dyz et dz^2 de Co avec les orbitales pz de l'oxygène en présence d'un faible couplage spin-orbite qui a le rôle de séparer les niveaux des orbitales d et de mélanger les orbitales dxz et dyz.

Il a été montré dans la littérature que l'amplitude de l'anisotropie d'interface entre un métal magnétique et un oxyde dépend de l'épaisseur des couches magnétiques **[Joh_96],** de la température de recuit **[Rod_09]** et la concentration en oxygène à l'interface **[Man_08a, Man_08b]**. Les études magnétiques réalisées sur les deux structures Pt/MM/Oxyde et Oxyde/MM/Pt (MM=Co, CoFeB, CoFe, NiFe) ont aidé à confirmer la forte contribution de l'anisotropie de l'interface métal magnétique/oxyde sur l'anisotropie perpendiculaire. L'anisotropie magnétique perpendiculaire augmente de manière significative après un recuit à haute température dans les deux systèmes en comparaison avec les structures classiques Pt/Co/Pt, confirmant les résultats précédents **[Nis_09a]**. Cela montre l'importance de la température de recuit dans la formation des liaisons MM-O qui sont responsables de l'anisotropie **[Man_08a, Man_08b]**. L'avantage est une forte augmentation de l'épaisseur critique des couches magnétiques (passage de planaire à perpendiculaire) comme exemple pour l'électrode inférieure dont l'épaisseur critique augmente de 1.3nm avant recuit à 3.5nm après recuit à 375°C, ceci ouvrant la possibilité d'utiliser ces matériaux dans des jonctions tunnel à aimantation perpendiculaire. L'effet du recuit est très différent pour les deux structures et oxyde/Co/Pt: il induit une augmentation de l'anisotropie d'interface lorsque l'oxyde est déposé sur le métal alors que c'est l'anisotropie de volume qui augmente lorsque le métal est déposé sur l'oxyde. De plus on observe que lorsque la couche métallique est déposée directement sur l'oxyde, la valeur de l'anisotropie perpendiculaire est plus faible, et on obtient une épaisseur critique de seulement 1.6nm après un recuit à haute température (400°C). Ces résultats peuvent être expliqués par une mauvaise croissance d'une couche métallique sur un oxyde **[Nis_09a]**.

En variant le matériau magnétique, de grandes différences ont été observées dans ces structures. Les électrodes à base de Pt/CoFeB/MgO ont une anisotropie perpendiculaire plus faible que les structures à base de Co, et elles présentent une variation non monotone de l'anisotropie avec le recuit. Cela peut être expliqué par la cristallisation de CoFeB et la diffusion de B à l'interface avec MgO.

Des tests de différents oxydes ont aussi été faits et on a vu que la croissance d'une couche magnétique sur un oxyde dépend de la stabilité de l'oxyde (le plus stable étant MgO) **[Nis_09a]**. On a aussi testé différents types de fabrication de l'oxyde comme oxydation naturelle d'une couche métallique de Mg et dépôt radiofréquence d'une couche de MgO à partir d'une cible cristalline. Dans le cas de MgO RF l'anisotropie est plus faible.

Tous ces résultats obtenus sur des structures à base de Pt/Co/Oxyde et Oxyde/Co/Pt montrent de très bonnes propriétés d'anisotropie après des recuits à 350°C. En plus ces

structures présentent une partie des propriétés demandées pour pouvoir fabriquer des jonctions perpendiculaires: épaisseurs magnétiques assez importantes, très bonne stabilité thermique et amortissement faible (dû à la présence d'un faible couplage spin-orbite à l'interface avec l'oxyde), par opposition aux structures Pt/Co/Pt ou à base de Terres Rares.

L'étape suivante a été de mettre les électrodes ensemble pour fabriquer une jonction tunnel avec une forte anisotropie perpendiculaire. Mais ce n'est pas si évident de juste mettre les électrodes ensemble. Il faut adapter leurs propriétés pour avoir des champs coercitifs assez différents car pendant le retournement de la couche douce les champs rayonnés vont apparaître qui peuvent atteindre des centaines d'Oe en fonction de l'épaisseur des couches et agissent comme un champ supplémentaire sur le renversement de la couche dure. Donc, pour stabiliser un état intermédiaire antiparallèle, la différence entre les champs coercitifs des deux couches doit être beaucoup plus grande que les champs rayonnés par la couche douce. Cela limite l'épaisseur maximale de la couche de l'électrode inférieure (couche dure) sachant que l'anisotropie et le champ coercitif diminue avec l'augmentation de l'épaisseur.

Un résultat surprenant concerne la mise en évidence d'une anisotropie magnétique plus importante lorsque la couche douce est intégrée comme électrode supérieure. Plusieurs pistes ont été suivies pour comprendre l'origine de cet effet, comme: une possible influence magnétique de la couche inférieure de Co (en diminuant son épaisseur jusqu'à ce qu'elle ne soit plus magnétique), l'influence de l'épaisseur de la couche de croissance de Pt et l'influence de la nature des couches de croissance Ta, Ta/Pt, Ta/Ru, Ta/Cu. A la suite à ces études nous avons conclu que cet effet provenait d'une meilleure croissance de la couche métallique de Mg sur des couches métalliques comme l'électrode inférieure de Co, contrairement à la croissance directe sur l'oxyde (SiO_2) qui entraîne plus de rugosité et une plus difficile croissance. Par conséquent des épaisseurs critiques très élevées (3nm) sont obtenues pour l'électrode supérieure de Co dans une structure pMTJ à base de Pt/Co/MgO/Co/Pt, épaisseurs comparable à celles obtenues pour des électrodes inférieures.

Une interaction entre les deux couches magnétiques est aussi observée dans ces systèmes à base de Pt/Co/MgO/Co/Pt. Le champ coercitif de la couche dure (inférieure) diminue fortement lorsque l'épaisseur de la couche douce (supérieure) augmente pour différentes températures de recuit. Cela peut-être expliqué en supposant une augmentation du nombre de centres de nucléation dans la couche douce avec l'épaisseur due à une rugosité non corrélée, résultant dans des champs rayonnées de plus en plus forts sur la couche dure qui accélèrent son retournement.

Différentes structures ont été réalisées afin de choisir la mieux adaptée pour les applications mémoires MRAM. L'anisotropie est influencée par plusieurs facteurs comme les épaisseurs des deux couches magnétiques, la température de recuit et l'état d'oxydation de la barrière. Tout cela montre que les jonctions perpendiculaires sont plus difficiles à fabriquer que les jonctions planaires puisque on doit trouver les bons paramètres pour avoir des propriétés magnétiques stables et une forte anisotropie perpendiculaire.

D'abord, les structures basées sur des couches de Cobalt montrent de faibles valeurs de TMR (10%) et des produits RA élevés, malgré leur forte anisotropie perpendiculaire. Cela montre la nécessité de faire un compromis entre une forte anisotropie et une forte TMR. Notre structure à base de Pt/Co/MgO/Co/Pt présente une faible TMR à cause du manque d'accord entre la texture de l'électrode et la barrière, accord nécessaire pour augmenter l'effet de filtrage en utilisant une barrière cristalline comme MgO.

Ceci nous a conduits à essayer de fabriquer des électrodes perpendiculaires avec une couche de CoFeB amorphe entre la couche de Co et MgO en espérant que dans ce cas là, la barrière de MgO pourra imposer sa structure et texture à la couche magnétique après recuit. En essayant d'adapter le système en vue d'obtenir une plus forte TMR dans des structures de type jonctions, on a diminué l'anisotropie. Pour augmenter cette anisotropie nous avons dû introduire des multicouches Pt/Co, résultant en une électrode inférieure plus compliquée:

Pt/(Pt/Co)/Co/CoFeB/MgO. Des tests sur des jonctions planaires avec des couches de croissance de Pt ont confirmé que la structure et texture de la couche de Pt (ou Pd) peut dominer l'influence de la barrière de MgO sur la couche magnétique et induire une texture (111) incompatible avec la texture (001) de MgO, produisant une forte décroissance des propriétés de transport. La seule solution pour augmenter la TMR est d'éliminer la couche de Pt et remplacer la couche de Co par une couche de CoFeB en se limitant à une seule contribution de l'anisotropie d'interface, l'anisotropie provenant de l'interface entre le métal magnétique et l'oxyde. L'utilisation d'électrodes de CoFeB sans couche de Pt montre une augmentation de la TMR (80%) et une nette diminution du produit RA.

Finalement, nous avons montré une forte corrélation entre la valeur de la TMR et celle de l'anisotropie perpendiculaire dans des jonctions tunnels planaires et perpendiculaires basée sur une électrode inférieure de Co ou CoFeB **[Nis_10b]**. Ces résultats mettent en relief l'importance du degré d'oxydation à l'interface et ils ont encore un fois renforcé l'influence des liaisons métal magnétique/oxygène sur l'anisotropie perpendiculaire mais aussi sur les propriétés de transport, confirmant les observations théoriques qui montrent une plus forte TMR pour des structures où l'oxygène est placé entre Mg et Fe **[Zha_03]**.

Des calculs ab-inito **[Yan_11]** ont montré que la différence de PMA et TMR pour les trois cas observés expérimentalement: sous-oxydation, oxydation optimale et sur-oxydation, peut-être expliquée par l'impact sur la séparation des états hybridés Δ1 (s,pz,dz^2) au niveau Fermi en présence des atomes d'oxygène additionnels. Dans le cas d'une aimantation perpendiculaire, la séparation des orbitales dxz,yz est plus grande pour des interfaces idéales Fe/MgO et relativement forte pour le cas sur-oxydé, mais ils sont absents au niveau de Fermi pour le cas sous-oxydé. Les valeurs d'anisotropie sont plus faibles pour le cas sur-oxydé par rapport au cas d'une oxydation idéale, mais plus grande que dans le cas sous-oxydé à cause de l'absence des bandes Δ1 au niveau Fermi.

Nous avons aussi montré que, en diminuant l'épaisseur de CoFeB et en maitrisant l'oxydation de la couche métallique de Mg, on met en évidence la présence de l'anisotropie d'interface CoFeB-MgO qui peut être utilisée pour diminuer le champ démagnétisant effectif dans des jonctions planaires tout en conservant une TMR élevée

Avant le développement intense de l'étude des jonctions tunnel à base de MgO pour des applications, des problèmes fondamentaux ont été adressé comme la correspondance des bandes électronique à l'interface entre la barrière et l'électrode magnétique **[But_01, Mat_01]** et le couplage indirect entre les couches magnétiques à travers un oxyde (IEC) **[Fau_02, Kat_06, Yan_07, Wu_08]**. Des études expérimentales sur des jonctions épitaxiées de type Fe/MgO/Fe **[Fau_02, Kat_06]**, Fe/MgO/γ-Fe_2O_3 **[Yan_07]** et Fe_3O_4/MgO/Fe_3O_4 **[Wu_08]** ont montré une variation du couplage en fonction de l'épaisseur de la barrière et la température de mesure. Un couplage antiferromagnétique a été observé pour des épaisseurs très faibles de MgO jusqu'à une épaisseur critique à partir de laquelle l'apparition de trous dans la barrière conduit à un couplage ferromagnétique direct. L'amplitude du couplage antiferromagnétique augmente avec la température de mesure.

Tous ces résultats peuvent être interprétés en termes de couple de spin exercé par une couche ferromagnétique sur l'autre **[Slo_95]** ou en termes de densité d'états dans la barrière induite par le métal ferromagnétique **[Bru_95]**. Slonczewski à donné la première explication pour le couplage indirect à travers un isolant à T=0K dans un modèle de courant de spin (pour V=0, il n'y a pas de courant qui passe à travers la barrière donc pas de dissipation d'énergie). Le couplage d'échange conservatif est associé au transport de l'information de spin par les électrons s polarisés en spin à travers la barrière isolante et leur interaction avec les électrons localisés d, résultant dans un terme de couple perpendiculaire (produit par la rotation de l'aimantation d'une couche magnétique par rapport à l'autre).

Bruno a proposé une approche plus générale pour le couplage, qui offre une description physique du phénomène et une façon plus simple d'obtenir des résultats analytiques plus

proches de l'expérience. Dans cette approche le couplage d'échange est associé à des interférences quantiques des ondes électroniques dans la couche magnétique suite à des réflexions dépendantes du spin à l'interface métal magnétique/oxyde **[Bru_93, Bru_95]**. Ce modèle peut-être simplement expliqué en considérant les couches d'épaisseur finie comme des cavités optiques Fabry-Pérot. En rajoutant une couche magnétique au contact d'un oxyde on va modifier la structure électronique de l'oxyde à l'interface, résultant dans la réflexion des électrons à l'interface.

Une autre contribution au couplage peut venir de la rugosité de la barrière qui conduit à l'apparition de charges de surface dans les couches magnétiques à aimantation planaire. Une extension du modèle de couplage dipolaire de type Néel **[Née_62]** a été présentée par Moritz et al **[Mor_04].** En présence de rugosité et d'une faible anisotropie perpendiculaire, l'aimantation va préférer rester parallèle à l'axe z (perpendiculaire au plan moyen des couches) pour minimiser les charges de surface et alors un alignement parallèle des couches magnétiques est favorisé. Dans le cas ou l'anisotropie perpendiculaire est forte, l'aimantation va suivre la rugosité et sera toujours perpendiculaire localement à l'interface, conduisant à l'apparition de charges de volume et favorisant un alignement antiparallèle des aimantations.

Par contre, pour les structures perpendiculaires, il n'y a que peu d'études sur le couplage d'échange entre couches magnétiques. En utilisant un séparateur isolant de NiO qui entre deux électrodes de multicouches Co/Pt, Liu et Adenwalla **[Liu_03]** ont observé une augmentation du couplage avec la température de mesure comme prévu par Bruno **[Bru_95]**. Ils ont aussi observé que le couplage oscille en fonction de l'épaisseur de NiO, phénomène attribué à la structure antiferromagnétique de l'oxyde.

En général toutes ces études sur des jonctions planaires et perpendiculaires montrent que le comportement des électrons tunnel à l'interface entre les couches magnétiques et la barrière est très important pour le couplage indirect. Pourtant aucune information expérimentale n'existe dans la littérature sur le couplage d'échange à travers MgO dans des MTJ à anisotropie perpendiculaire. Récemment il a été montré que le couplage de type Néel induit par la rugosité dépend de la configuration magnétique des couches et peut changer de ferromagnétique à antiferromagnétique en augmentant l'anisotropie **[Mor_04]**. Par conséquent il est intéressant de voir quelle est l'origine du couplage dans des systèmes à anisotropie perpendiculaire avec une barrière de MgO.

Malgré leurs mauvaises propriétés de transport, les jonctions perpendiculaires Pt/Co/MgO/Co/Pt préparées par pulvérisation cathodique ont montré la présence d'un couplage antiferromagnétique entre les couches magnétiques de Co séparées par MgO. Grace à de très bonnes propriétés d'anisotropie dans ces systèmes, une étude détaillée du couplage a été réalisée en fonction de la température de recuit et de l'épaisseur des couches magnétiques, afin de mieux comprendre l'origine du couplage et une possible relation avec l'amplitude de l'anisotropie perpendiculaire.

Tout d'abord la possibilité d'une réplication de domaines magnétiques dans la couche dure a été exclue par des mesures de rotation cohérente de l'aimantation de la couche douce. A l'aide d'un modèle qui explique le minimum observé dans les mesures magnétiques en champs planaire, la présence d'un couplage magnétique a été validée par des simulations macrospin. Ce couplage augmente fortement lorsque l'épaisseur de la barrière diminue jusqu'à la limite d'un couplage direct ferromagnétique. Par contre, pour des grandes épaisseurs de la barrière de MgO (1.4nm), le couplage reste antiferromagnétique, contrairement aux résultats de la littérature sur des jonctions épitaxiées de Fe/MgO/Fe qui montrent un couplage ferromagnétique de type Néel **[Née_62]**. L'explication vient en considérant un couplage de type Néel (à rugosité corrélé) en fonction de l'amplitude de l'anisotropie perpendiculaire **[Mor_04].** Dans ce cas on a un couplage ferromagnétique quand l'anisotropie est faible puisque l'aimantation sera toujours perpendiculaire à la surface moyenne, donnant naissance à des charges de surface. Par contre si

l'anisotropie est forte, le couplage est antiferromagnétique et vient des charges de volume qui sont dues au fait que la direction de l'aimantation suit localement l'interface.

Une façon de vérifier la présence d'un couplage d'échange indirect comme prédit par Slonczewski et Bruno **[Slo_95, Bru_95]** est de regarder la variation de ce couplage avec la température. A basse température (aimantation constante), les mesures montrent une bonne corrélation avec le modèle de Bruno **[Bru_95].** Par contre à partir de 250K la diminution du couplage est plutôt liée à une diminution de l'aimantation et le couplage est dominé par la rugosité d'interface (couplage de type Néel). Les structures à faible anisotropie perpendiculaire ou à anisotropie planaire présentent un couplage purement ferromagnétique confirmant encore une fois l'hypothèse de corrélation entre force d'anisotropie et signe du couplage. La diminution du couplage avec la température de recuit est une indication que le couplage antiferromagnétique est lié au degré d'oxydation de la barrière et des électrodes.

Une oscillation de l'énergie de couplage en fonction de l'épaisseur de l'électrode magnétique supérieure de Co a été mise en évidence expérimentalement pour la première fois dans le cas de jonctions tunnel. Cette oscillation est en accord avec le modèle de Bruno qui décrit les couches magnétiques comme des cavités résonantes dans lesquelles ont lieu des réflexions multiples conduisant à l'interférence des fonctions d'ondes électroniques.

Finalement, des jonctions perpendiculaires à base de CoFeB-MgO ont été nano lithographiées et des mesures de commutation d'aimantation par transfert de spin sur des piliers nanométriques ont été réalisées avec de faibles courants critiques.

Les piliers de 200 à 500 nm de diamètre présentent des propriétés de transport très satisfaisantes (TMR=50%, RA= 14 Ohmμm^2), indiquant que la nanostructuration n'a pas modifié les propriétés de la barrière. Par contre pour les piliers les plus petits la dispersion de résistance et la diminution de la TMR montrent un fort impact de la nanostructuration sur les propriétés magnétiques des piliers. L'oxydation des flancs des piliers peut être à l'origine de ces effets, ayant plus d'impact pour les tailles de piliers les plus petites.

Les résultats obtenus sur des piliers de 200nm de diamètre montrent que la couche douce peut être commutée en 10ns en utilisant un faible courant polarisé (3 MA/cm^2), et que ces systèmes présentent une très bonne stabilité thermique (avec un facteur de stabilité entre 50 et 100). La tension critique de retournement pour des longueurs d'impulsion de 10ns augmente lorsque la taille des piliers diminue, contrairement aux prédictions d'un modèle macrospin. Cela est expliqué par l'existence de défauts sur les flancs des piliers introduits par la nanofabrication. Ces défauts peuvent aussi être la raison pour laquelle on observe une grande distribution des valeurs de facteur de stabilité et l'apparition de phénomènes de commutation inverse.

French conclusion

L'objectif de cette thèse a été la fabrication de jonctions tunnel magnétiques avec des électrodes perpendiculaires, en utilisant l'anisotropie magnétique perpendiculaire (PMA) aux interfaces métal magnétique/oxyde. Ces jonctions perpendiculaires, selon les prédictions théoriques, devraient avoir besoin de moins d'énergie (moins de courant) pour les applications d'écriture par couple de transfert de spin (STT). Toutefois, la fabrication de telles structures est un véritable défi et une tâche difficile car l'obtention simultanée de bonnes propriétés de TMR et de PMA impose des contraintes sur les matériaux utilisés et également limite la fenêtre de travail du dispositif. Afin d'atteindre notre but nous avons d'abord étudié les propriétés de ces différentes structures, telles que l'origine de la PMA à l'interface métal/oxyde, et les phénomènes de couplage d'échange à travers la barrière isolante.

Au moment où nous avons commencé cette étude, il n'existait que cinq rapports dans la littérature sur les jonctions tunnel magnétiques perpendiculaires à base de MgO préparées par pulvérisation, toutes constitués d'électrodes RE-TM **[Che_06, Hat_07, Ohm_08, Nak_08]**, sauf une comportant une électrode dure RE-TM et douce (Co/Pt) **[Ye_08]**, mais avec une stabilité thermique limitée.

Sur la base de notre expérience depuis 2002 sur les tricouches Pt/Co/AlOx **[Mon_02, Man_07, Rod_09],** nous avons donc décidé d'explorer les propriétés d'anisotropie d'électrodes uniques Pt/Co/MgO et MgO/Co/Pt, ainsi que celles de structures complètes Pt/Co/MgO/Co/Pt. Grâce à l'anisotropie interfaciale forte à la fois des interfaces Pt/Co et Co/MgO, il a été possible d'étudier les propriétés magnétiques de ces structures sur une large gamme d'épaisseurs de cobalt et de températures de recuit.

L'anisotropie perpendiculaire des électrodes inférieures Pt/Co/MgO augmente fortement avec le recuit, l'épaisseur critique de Co allant de 1,3 nm dans l'état brut de dépôt à presque 3,5 nm après un recuit à 375°C. De grandes différences ont été observées entre les électrodes Co et CoFeB, ces dernières présentant une variation non monotone de l'anisotropie avec le recuit. Le dépôt RF de MgO apparaît très dépendant des conditions de pulvérisation, comme indiqué par la grande différence de propriétés d'anisotropie entre les deux machines de pulvérisation utilisées. L'épaisseur de la couche tampon de Pt et la nature de la couche de couverture influencent également les propriétés d'anisotropie de ces électrodes inférieures.

L'anisotropie perpendiculaire des électrodes supérieures oxyde/Co/Pt est beaucoup plus petite, quel que soit l'oxyde considéré, avec une épaisseur critique maximale d'environ 1,6 nm après un recuit à 400°C. Cela semble être lié à une croissance beaucoup plus difficile de la couche magnétique sur l'oxyde que sur Pt. Les contributions d'interface et de volume à l'anisotropie perpendiculaire varient différemment pour les deux électrodes avec la température de recuit. Alors que l'augmentation de l'anisotropie des électrodes inférieures avec le recuit est principalement due à la contribution interfaciale, celle des électrodes supérieures provient principalement d'une augmentation de la contribution de volume. Par comparaison avec les structures Pt/Co/Pt, nous pouvons conclure que l'augmentation de l'anisotropie à des températures de recuit élevées provient principalement de l'interface Co/oxyde dans les deux structures inférieures et supérieures. Des températures de recuit élevées conduisent à la diffusion de l'oxygène et à la formation de liaisons Co-O comme cela a été observé expérimentalement par des mesures de spectroscopie des rayons X et par les calculs ab-initio. L'origine de l'anisotropie perpendiculaire induite à l'interface métal magnétique/oxyde est l'hybridation des orbitales entre l'oxygène et le métal magnétique.

L'étape suivante a consisté à assembler les électrodes inférieure et supérieure afin de fabriquer des jonctions perpendiculaires et d'étudier leurs propriétés de transport. Puisque les structures Pt/Co/MgO et MgO/Co/Pt ont donné les meilleures propriétés d'anisotropie, elles ont été choisies comme électrodes dans les jonctions complètes, bien que le désaccord de textures

entre Co et MgO était censé conduire à des signaux TMR plus petits. C'est la raison pour laquelle nous avons également considéré des électrodes Pt/Co/CoFeB, en espérant que la barrière de MgO pourrait imposer sa texture à la couche de CoFeB après sa cristallisation. Cependant, les rapports de la littérature ont montré plus tard que la texture de la couche tampon (Pt, Pd) pouvait dominer l'influence de la barrière de MgO et induire une texture (111) de l'électrode magnétique, conduisant à une forte dégradation des propriétés de transport.

Lors de la réalisation des jonctions complètes, l'observation la plus surprenante a été la forte augmentation de l'anisotropie de l'électrode supérieure quand elle est déposée sur l'électrode inférieure. Nous avons montré que cet effet a une origine structurale et est liée aux conditions de croissance de la couche de Mg, qui dépend de la nature de la couche sous-jacente. Cette forte augmentation de l'anisotropie provient de la meilleure croissance de la couche de Mg sur les matériaux métalliques (Pt ou Ru) que sur Ta ou SiO_2.

L'anisotropie perpendiculaire des électrodes inférieure et supérieure des pMTJ augmente avec le recuit, mais a des origines différentes pour les électrodes supérieure et inférieure, comme c'était le cas pour les électrodes seules. Les deux électrodes inférieure et supérieure dans les jonctions complètes présentent une épaisseur critique de l'ordre de 3,5 nm après un recuit à 350° C.

De fortes interactions magnétiques mutuelles entre les électrodes ont également été observées, le champ coercitif de l'électrode inférieure diminuant lorsque l'épaisseur de l'électrode supérieure augmente. Pour le moment nous n'avons pas d'explication pour une telle interaction.

La PMA dépend de façon critique des épaisseurs des deux couches magnétiques et des conditions de recuit, mais aussi de la qualité de la barrière, comme la teneur en oxygène à l'interface avec les couches magnétiques. Cela montre que la fabrication de jonctions perpendiculaires est plus difficile que celle des jonctions planaires.

Les premières structures perpendiculaires étaient basées sur des tricouches Pt/Co/MgO montrant une anisotropie très élevé, mais une TMR de seulement 10%. Deux oxydes MgO différents, de même épaisseur, ont été testés, donnant des valeurs de TMR similaires, mais des valeurs de RA très différentes (300 $\Omega\mu m^2$ pour Mg0,7 + Mg0,7 oxydation naturelle et 15 $\Omega\mu m^2$ pour Mg0,9OxNat/Mg0,5). La faible TMR dans ces structures est principalement due au désaccord structural entre Co et MgO. Bien que ces structures ne puissent pas être utilisées pour étudier les propriétés de STT, elles ont été utilisées pour montrer la corrélation directe entre l'anisotropie et les propriétés de transport à la fois dans les électrodes seules et dans les jonctions, ce qui implique que le même mécanisme (la formation de liaisons CoFe-O à l'interface lors de l'oxydation, et la présence d'un faible couplage spin-orbite) conduit au maximum de TMR et de PMA.

Selon des calculs ab-initio, la différence entre les valeurs de PMA et de TMR dans les trois cas observés expérimentalement (sur-oxydation, sous-oxydation et oxydation idéale) peut être expliquée par l'impact du splitting des états hybridés Δ1 au niveau de Fermi en présence d'atomes d'oxygène supplémentaires. Dans le cas de l'aimantation hors du plan, le splitting des orbitales dxz,yz est plus important pour l'interface idéale Fe/MgO, relativement fort pour le cas sous-oxydé, et les valeurs correspondantes d'anisotropie sont plus grandes par rapport au cas sur- oxydé, mais plus petites par rapport au cas de l'interface idéale Fe/MgO. En outre, dans le cas des interfaces sur-oxydées, la vitesse d'amortissement de Δ1 est fortement accrue par rapport aux cas idéal et sous-oxydé: les bandes Δ1 sont absentes au niveau de Fermi, ce qui explique le maximum de TMR observé expérimentalement pour la barrière idéalement oxydée.

Dans ces structures, nous avons également étudié le couplage intercouches à travers un isolant entre les électrodes magnétiques perpendiculaires, et testé nos résultats par rapport à différents modèles.

Tout d'abord, des barrières de MgO préparées par déposition RF nous ont permis d'étudier la variation du champ de couplage avec l'épaisseur de MgO, similaire à celle observée dans les jonctions planaires épitaxiales **[Fau_02, Kat_06].** L'amplitude du couplage antiferromagnétique augmente quand l'épaisseur de barrière diminue, jusqu'à une limite où les couplages ferromagnétiques directs dominent. Cette limite correspond à des épaisseurs de barrière plus grandes (0,8 nm), comme observé par **[Liu_03],** que pour les jonctions épitaxiales (0,5 à 0,6 nm), en raison d'une plus grande rugosité interfaciale. Pour une épaisseur de MgO plus grande, le couplage antiferromagnétique persiste, en accord avec le modèle de Néel étendu à l'aimantation perpendiculaire **[Mor_04]**. Deux contributions de couplage pourrait coexister dans nos structures, l'une de type couplage d'échange indirect dominant à basse température et l'autre dû à la rugosité à haute température. Les structures perpendiculaires à faible PMA ou à aimantation planaire montrent un couplage de Néel classique ferromagnétique, confirmant le modèle de Moritz. Toutes les structures montrent la même augmentation de l'amplitude de couplage lorsque l'épaisseur de Mg diminue, ce qui est attribué à la sur-oxydation de l'électrode magnétique.

La diminution de l'amplitude de couplage antiferromagnétique quand la température de recuit augmente est en accord avec la théorie de Néel en supposant que la désoxydation des électrodes magnétiques conduit à une diminution de la rugosité chimique des interfaces.

Nous avons également montré que la force du couplage antiferromagnétique oscille en fonction de l'épaisseur de la couche magnétique, comme prédit par la théorie de Bruno **[Bru_93]** pour des séparateurs isolants. Ceci est expliqué par les interférences des ondes électroniques dans les couches ferromagnétiques. Bien que la force moyenne du couplage diminue progressivement lorsque la température de recuit augmente, l'amplitude et la période des oscillations sont essentiellement indépendantes de la température de recuit.

Les propriétés de transport de ces jonctions perpendiculaires Pt/Co/MgO/Co/Pt ne purent être mesurées qu'une fois l'outil Capres à Crocus Technology équipé d'un champ magnétique perpendiculaire. A cette époque également nous étions encore en train de développer les barrières de MgO pour les jonctions planaires dans notre machine de pulvérisation Actemium, et les propriétés de transport n'étaient pas encore optimisées (modestes valeurs de TMR et produit RA plutôt élevé).

Afin d'améliorer les propriétés de TMR un compromis a dû être fait en éliminant la couche tampon de Pt et en remplaçant la couche Co inférieure par CoFeB, avec comme conséquence une forte réduction de PMA de la structure. La couche inférieure devient ainsi la plus douce, et la couche supérieure devient la plus dure par couplage d'échange de la couche de CoFeB à une multicouche Co/Tb. Il en résulte une TMR de 80% avec un faible produit RA de 15 $\Omega\mu m^2$.

Grâce à l'anisotropie perpendiculaire de l'interface métal magnétique/oxyde, le champ démagnétisant effectif de la couche de stockage de jonctions tunnel MgO à aimantation planaire peut être considérablement réduit en gardant une TMR élevée de 135%. Nous n'avons pas eu le temps d'étudier les propriétés STT de ces jonctions après transformation en structures sub-micrométrique, mais ces expériences devraient être bientôt réalisées dans notre laboratoire.

Les mesures électriques ont montré que notre processus de nanofabrication permet d'obtenir des piliers cylindriques de 200-300 nm de diamètre en gardant un produit RA similaire à celui mesuré dans les échantillons macroscopiques (14 $Ohm\mu m^2$). Cela signifie qu'aucune résistance parasite n'a été introduite au cours de la nanofabrication, et que les propriétés de la barrière ont été préservées. Les piliers de 100 nm de diamètre présentent une plus grande dispersion de résistances, et ceux de 50 nm de diamètre ne donnent aucun signal. La nanofabrication ou la réduction de la taille semblent affecter les propriétés de TMR par rapport aux échantillons macroscopiques. Cela pourrait provenir de l'oxydation partielle de la couche de TbCo, conduisant à un couplage d'échange plus faible de la couche de référence, ou à une inclinaison partielle de l'aimantation de la couche douce sur les bords des piliers. Il en résulte

une réduction du rapport de TMR de 80% dans les échantillons macroscopiques à 50% en piliers. Toutefois, l'épaisseur critique magnétique (réorientation de l'aimantation dans le plan) augmente légèrement après nano-structuration, indiquant une augmentation de l'anisotropie perpendiculaire ou de la stabilité thermique.

Des expériences de commutation par couple de transfert de spin ont été réalisées sur de telles structures. De faibles temps de commutation (10 ns), avec des tensions de commutation assez basses (430 mV pour écrire l'état P, correspondant à des densités de courant de 2,4 MA/cm^2), ont été obtenus sur des piliers de 200-300 nm de diamètre pour 0,86 nm d'épaisseur les couches de CoFeB avec un très bon facteur de stabilité thermique de 75. La tension critique de commutation augmente (540 mV) pour une épaisseur de 1,0 nm de CoFeB pour la même durée d'impulsion, mais reste dans les limites des exigences industrielles. Ces résultats préliminaires sont très encourageants. Ils indiquent également que l'augmentation de l'anisotropie et de l'amortissement pour les couches magnétiques les plus fines pourrait être plus que compensée par la diminution observée de l'aimantation à saturation.

La tension critique de commutation pour des durées d'impulsion de 10 ns augmente avec la diminution de la taille (augmentation de la résistance), en désaccord avec le modèle mono-domaine, et est probablement due aux défauts induits au cours du processus de nano-fabrication. Cela pourrait être aussi la raison de la forte dispersion du facteur de stabilité thermique entre les piliers, et pour les comportements inhabituels observés comme les phénomènes de commutation inverse.

Références

[Bai_88] M.N. Baibich, J.-M. Broto, A. Fert, F. Nguyen Van Dau, F. Petroff, P. Etienne, G. Creuzet, A. Friederich and J. Chazelas, *Giant magnetoresistance of (001)Fe/(001)Cr magnetic superlattices,* **Phys. Rev. Lett.** **61** (1988) 2472.

[Ber_96] L. Berger, *Emission of spin waves by a magnetic multilayer traversed by a current,* **Phys. Rev. B** **54** (1996) 9353.

[Bin_89] G. Binasch, P. Grünberg, F. Saurenbach and W. Zinn, *Enhanced magnetoresistance in layered magnetic structures with antiferromagnetic interlayer exchange,* **Phys. Rev. B** **39** (1989) 4828 (R).

[Bru_93] P. Bruno, *Oscillations of interlayer exchange coupling vs. ferromagnetic-layers thickness*, **Europhys. Lett.** **23** (1993) 615.

[Bru_95] P. Bruno, *Theory of interlayer magnetic coupling*, **Phys. Rev. B** **52** (1995) 411.

[But_01] W.H. Butler, X.-G. Zhang, T.C. Schulthess and J.M. MacLaren, *Spin-dependent tunneling conductance of Fe|MgO|Fe sandwiches,* **Phys. Rev. B** **63** (2001) 054416.

[Car_08] B. Carvello, C. Ducruet, B. Rodmacq, S. Auffret, E. Gautier, G. Gaudin and B. Dieny, *Sizable room-temperature magnetoresistance in cobalt based magnetic tunnel junctions with out-of-plane anisotropy,* **Appl. Phys. Lett.** **92** (2008) 102508.

[Che_06] T.-J. Chen, A. Canizo-Cabrera, C.-H. Chang, K.-A. Liao, S.C. Li, C.-K. Hou and T.-H. Wu, *Comparison of the interfacial structure between MgO and Al–O oxidation layers for perpendicular magnetic tunnel junction,* **J. Appl. Phys.** **99** (2006) 08T313.

[Die_91] B. Dieny, V.S. Speriosu, B.A. Gurney, S.S.P. Parkin, D.R. Wilhoit, K.P. Roche, S. Metin, D.T. Peterson and S. Nadimi, *Spin-valve effect in soft ferromagnetic sandwiches*, **J. Magn. Magn. Mat.** **93** (1991) 101.

[End_10] M. Endo, S. Kanai, S. Ikeda, F. Matsukura and H. Ohno, *Electric-field effects on thickness dependent magnetic anisotropy of sputtered MgO/$Co_{40}Fe_{40}B_{20}$/Ta structures,* **Appl. Phys. Lett.** **96** (2010) 212503.

[Eve_06] **http://everspin.com/press.php?ppo=2006&qtype=press**

[Fau_02] J. Faure-Vincent, C. Tiusan, C. Bellouard, E. Popova, M. Hehn, F. Montaigne and A. Schuhl*, Interlayer magnetic coupling interactions of two ferromagnetic layers by spin polarized tunneling,* **Phys. Rev. Lett.** **89** (2002) 107206.

[Fuj_06] *Storage Systems and HDD Technologies,* **Fujitsu Sci. Tech. J.** **42** (2006) 122.

[Gra_68] U. Gradmann and J. Müller, *Flat ferromagnetic epitaxial 48Ni/52Fe(111) films of few atomic layers*, **Phys. Stat. Sol.** **27** (1968) 313.

[Hat_07] T. Hatori, H. Ohmori, M. Tada and S. Nakagawa, *MTJ elements with MgO barrier using RE-TM amorphous layers for perpendicular MRAM,* **IEEE Trans. Magn.** **43** (2007) 2331.

[Her_10] J. Alvarez-Hérault, PhD Thesis, Grenoble University (2010).

[Hum_04] R.E. Hummel, *Understanding Materials Science - History, Properties, Applications*, 2nd Edition, Springer-Verlag, New York, (2004).

[Ike_10] S. Ikeda, K. Miura, H. Yamamoto, K. Mizunuma, H.D. Gan, M. Endo, S. Kanai, J. Hayakawa, F. Matsukura and H. Ohno, *A perpendicular-anisotropy CoFeB–MgO magnetic tunnel junction,* **Nature Mater.** **9** (2010) 721.

[Joh_96] M.T. Johnson, P.J.H. Bloemen, F.J.A. den Broeder and J.J. de Vries, *Magnetic anisotropy in metallic multilayers,* **Rep. Prog. Phys.** **59** (1996) 1409.

[Kat_00] J.A. Katine, F.J. Albert, R.A. Buhrman, E.B. Myers and D.C. Ralph, *Current-driven magnetization reversal and spin-wave excitations in Co/Cu/Co pillars,* **Phys. Rev. Lett.** **84** (2000) 3149.

[Kat_06] T. Katayama, S. Yuasa, J. Velev, M.Ye. Zhuravlev, S.S. Jaswal and E.Y. Tsymbal, *Interlayer exchange coupling in Fe/MgO/Fe magnetic tunnel junctions*, **Appl. Phys. Lett.** **89** (2006) 112503.

[Liu_03] Z.Y. Liu and S. Adenwalla, *Oscillatory interlayer exchange coupling and its temperature dependence in $[Pt/Co]_3/NiO/[Co/Pt]_3$ multilayers with perpendicular anisotropy,* **Phys. Rev. Lett.** **91** (2003) 037207.

[Liu_09] L. Liu, T. Moriyama, D.C. Ralph, and R.A. Buhrman, *Reduction of the spin-torque critical current by partially cancelling the free layer demagnetization field*, **Appl. Phys. Lett.** **94** (2009) 122508.

[Man_06] S. Mangin, D. Ravelosona, J.A. Katine, M.J. Carey, B.D. Terris and E.E. Fullerton, *Current-induced magnetization reversal in nanopillars with perpendicular anisotropy,* **Nature Mater.** **5** (2006) 210.

[Man_07] A. Manchon, *Magnétorésistance et transfert de spin dans les jonctions tunnel magnétiques,* **PhD Thesis, Grenoble University** (2007).

[Man_08a] A. Manchon, C. Ducruet, L. Lombard, S. Auffret, B. Rodmacq, B. Dieny, S. Pizzini, J. Vogel, V. Uhlir, M. Hochstrasser and G. Panaccione, *Analysis of oxygen induced anisotropy crossover in Pt/Co/MOx trilayers,* **J. Appl. Phys.** **104** (2008) 043914.

[Man_08b] A. Manchon, S. Pizzini, J. Vogel, V. Uhlir, L. Lombard, C. Ducruet, S. Auffret, B. Rodmacq, B. Dieny, M. Hochstrasser and G. Panaccione, *X-ray analysis of oxygen-induced perpendicular magnetic anisotropy in Pt/Co/AlOx trilayers,* **J. Magn. Magn. Mater.** **320** (2008) 1889.

[Mat_01] J. Mathon and A. Umerski, *Theory of tunneling magnetoresistance of an epitaxial Fe/MgO/Fe(001) junction*, **Phys. Rev. B** **63** (2001) 220403 (R).

[Mir_10] I.M. Miron, G. Gaudin, S. Auffret, B. Rodmacq, A. Schuhl, S. Pizzini, J. Vogel and P. Gambardella, *Current-driven spin torque induced by the Rashba effect in a ferromagnetic metal layer,* **Nature Mater.** **9** (2010) 230.

[Mon_02] S. Monso, B. Rodmacq, S. Auffret, G. Casali, F. Fettar, B. Gilles, B. Dieny and P. Boyer, *Crossover from in-plane to perpendicular anisotropy in Pt/CoFe/AlO_x sandwiches as a function of Al oxidation: A very accurate control of the oxidation of tunnel barriers,* **Appl. Phys. Lett.** **80** (2002) 4157.

[Moo_95] J.S. Moodera, L.R Kinder, T.M. Wong and R. Meservey, *Large magnetoresistance at room temperature in ferromagnetic thin film tunnel junctions*, **Phys. Rev. Lett.** **74** (1995) 3273.

[Mor_04] J. Moritz, F. Garcia, J.-C. Toussaint, B. Dieny and J.-P. Nozières, *Orange peel coupling in multilayers with perpendicular magnetic anisotropy: Application to (Co/Pt)-based exchange-biased spin-valves*, **Europhys. Lett.** **65** (2004) 123.

[Mor_06] A. Morisako and X.X. Liu, *Sm-Co and Nd-Fe-B thin films with perpendicular anisotropy for high-density magnetic recording media,* **J. Magn. Magn. Mater.** **304** (2006) 46.

[Mot_36] N.F. Mott, *The electrical conductivity of Transition Metals,* **Proc. Roy. Soc. A** **153** (1936) 699.

[Nak_98] N. Nakajima, T. Koide, T. Shidara, H. Miyauchi, H. Fukutani, A. Fujimori, K. Iio, T. Katayama, M. Nývlt and Y. Suzuki, *Perpendicular magnetic anisotropy caused by interfacial hybridization via enhanced orbital moment in Co/Pt multilayers: Magnetic circular X-ray dichroism study,* **Phys. Rev. Lett.** **81** (1998) 5229.

[Nak_08] M. Nakayama, T. Kai, N. Shimomura, M. Amano, E. Kitagawa, T. Nagase, M. Yoshikawa, T. Kishi, S. Ikegawa and H. Yoda., *Spin transfer switching in TbCoFe/CoFeB/MgO/CoFeB/TbCoFe magnetic tunnel junctions with perpendicular magnetic anisotropy,* **J. Appl. Phys.** **103** (2008) 07A710.

[Née_54] L. Néel, *Anisotropie magnétique superficielle et surstructures d'orientation*, **J. Phys. Rad.** **15** (1954) 225.

[Née_62] L. Néel, *Sur un nouveau mode de couplage entre les aimantations de deux couches minces ferromagnétiques*, **C. R. Hebd. Séances Acad. Sci.** **255** (1962) 1676.

[Nis_09a] L.E. Nistor, B. Rodmacq, S. Auffret and B. Dieny, *Pt/Co/oxide and oxide/Co/Pt electrodes for perpendicular magnetic tunnel junctions,* **Appl. Phys. Lett.** **94** (2009) 012512.

[Nis_09b] L.E. Nistor, B. Rodmacq, S. Auffret, A. Schuhl and B. Dieny, *Antiferromagnetic coupling in sputtered MgO tunnel junctions with perpendicular magnetic anisotropy,* **IEEE Trans. Magn.** **45** (2009) 3472.

[Nis_10a] L.E. Nistor, B. Rodmacq, S. Auffret, A. Schuhl, M. Chshiev and B. Dieny, *Oscillatory interlayer exchange coupling in MgO tunnel junctions with perpendicular magnetic*

anisotropy, **Phys. Rev. B** **81** (2010) 220407 (R).

[Nis_10b] L.E. Nistor, B. Rodmacq, C. Ducruet, C. Portemont, I.L. Prejbeanu and B. Dieny, *Correlation between perpendicular anisotropy and magnetoresistance in magnetic tunnel junctions,* **IEEE Trans. Magn.** **46** (2010) 1412.

[Nis_11] L.E. Nistor, B. Rodmacq, S. Auffret and B. Dieny, *Low effective demagnetizing field in magnetic tunnel junctions,* Intermag Conference, Taipei (Taiwan) Apr. 25-29 (2011).

[Noz_06] J.-P. Nozières, B. Dieny, O. Redon, R.C. Sousa and I.L. Prejbeanu, *Magnetic memory with a magnetic tunnel junction written in a thermally assisted manner, and method for writing the same*, **US Patent 7,411,817** (2006).

[Ohm_08] H. Ohmori, T. Hatori and S. Nakagawa, *Fabrication of MgO barrier for a magnetic tunnel junction in as-deposited state using amorphous RE–TM alloy*, **J. Magn. Magn. Mater.** **320** (2008) 2963.

[Oun_02] K. Ounadjela, B. Dieny and O. Redon, *High density MRAM using thermal writing,* **US Patent 20020281603** (2002).

[Par_91] S.S.P. Parkin, *Systematic variation of the strength and oscillation period of indirect magnetic exchange coupling through the 3d, 4d, and 5d transition metals*, **Phys. Rev. Lett.** **67** (1991) 3598.

[Pre_04] I.L. Prejbeanu, W. Kula, K. Ounadjela, R.C. Sousa, O. Redon, B. Dieny and J.-P. Nozières, *Thermally assisted switching in exchange-biased storage layer magnetic tunnel junctions*, **IEEE Trans. Magn.** **40** (2004) 2625.

[Puf_03] M.R. Pufall, W.H. Rippard and T.J. Silva, *Materials dependence of the spin-momentum transfer efficiency and critical current in ferromagnetic metal/Cu multilayers,* **Appl. Phys. Lett.** **83** (2003) 323.

[Rod_03] B. Rodmacq, S. Auffret, B. Dieny, S. Monso and P. Boyer, *Crossovers from in-plane to perpendicular anisotropy in magnetic tunnel junctions as a function of the barrier degree of oxidation,* **J. Appl. Phys.** **93** (2003) 7513.

[Rod_09] B. Rodmacq, A. Manchon, C. Ducruet, S. Auffret and B. Dieny, *Influence of thermal annealing on the perpendicular magnetic anisotropy of Pt/Co/AlOx trilayers,* **Phys. Rev. B** **79** (2009) 024423.

[Slo_89] J.C. Slonczewski, *Conductance and exchange coupling of 2 ferromagnets separated by a tunnelling barrier*, **Phys. Rev. B** **39** (1989) 6995.

[Slo_95] J.C. Slonczewski, *Overview of interlayer exchange theory*, **J. Magn. Magn. Mat.** **150** (1995) 13.

[Slo_96] J.C. Slonczewski, *Current-driven excitation of magnetic multilayers,* **J. Magn. Magn. Mater.** **159** (1996) L1.

[Sun_00] J.Z. Sun, *Spin-current interaction with a monodomain magnetic body: A model study*, **Phys. Rev. B** **62** (2000) 570.

[Sun_02] J.Z. Sun, D.J. Monsma, D.W. Abraham, M.J. Rooks and R.H. Koch, *Batch-fabricated spin-injection magnetic switches,* **Appl. Phys. Lett.** **81** (2002) 2202.

[Wei_07] M. Weisheit, S. Faehler, A. Marty, Y. Souche, C. Poinsignon and D. Givord, *Electric field-induced modification of magnetism in thin-film ferromagnets*, **Science** **315** (2007) 349.

[Wu_08] H.-C. Wu, S.K. Arora, O.N. Mryasov and I.V. Shvets, *Antiferromagnetic interlayer exchange coupling between Fe3O4 layers across a nonmagnetic MgO dielectric layer*, **Appl. Phys. Lett.** **92** (2008) 182502.

[Yan_07] H. Yanagihara, Y. Toyoda and E. Kita, *Antiferromagnetic interlayer coupling through a thin MgO layer in γ-Fe2O3/MgO/Fe(001) multilayers*, **J. Appl. Phys.** **101** (2007) 09D101.

[Yan_11] H.X. Yang, M. Chshiev, B. Dieny, J.H. Lee, A. Manchon and K.H. Shin, *First-principles investigation of the very large perpendicular magnetic anisotropy at Fe/MgO and Co/MgO interfaces*, **Phys. Rev. B** **84** (2011) 054401.

[Ye_08] L.-X. Ye, C.-M. Lee, J.-W. Syu, Y.-R. Wang, K.-W. Lin, Y.-H. Chang and T.-H. Wu, *Effect of annealing and barrier thickness on MgO-based Co/Pt and Co/Pd multilayered perpendicular magnetic tunnel junctions*, **IEEE Trans. Magn.** **44** (2008) 3601.

[Yoo_05] I. Yoo, D.K. Kim and Y.K. Kim, *Switching characteristics of submicrometer magnetic tunnel junction devices with perpendicular anisotropy,* **J. Appl. Phys.** **97** (2005) 10C919.

[Zha_03] X.-G. Zhang, W.H. Butler and A. Bandyopadhyay, *Effects of the iron-oxide layer in Fe-FeO-MgO-Fe tunneling junctions*, **Phys. Rev. B 68** (2003) 092402.

ABSTRACT

The aim of this thesis is the study of magnetic tunnel junctions with perpendicularly magnetized electrodes (pMTJ), using perpendicular magnetic anisotropy (PMA) arising from the magnetic metal/oxide interfaces. For magnetic memories applications, it was predicted in theory that perpendicular junctions should need less energy (current) for spin transfer torque (STT) writing applications. However, the engineering of such structures is a real challenge and a difficult task since simultaneous transport (TMR) and PMA properties impose constraints on materials being used and also limit the working window of the device, especially in terms of magnetic layer thickness. In order to reach our goal we first studied different properties of these structures, such as the origin of PMA from the metal/oxide interface, tunnel transport and interlayer exchange coupling phenomena. The PMA at magnetic metal/oxide interface was showed to strongly depend on different parameters like annealing temperature, oxygen concentration, layer thickness etc. Several pMTJ structures were tested in order to choose the best one for MRAM memories applications. A correlation between TMR and PMA was observed and confirms the PMA origin from the magnetic metal-oxygen bond formation at the interface. Furthermore, antiferromagnetic interlayer exchange coupling was observed in our structures in the presence of out of plane anisotropy. A detailed study was made as a function of annealing temperature and layers thickness, in order to understand the origin of this coupling and its possible relationship to the anisotropy strength. Finally the STT-pMTJ concept was validated and low critical currents were observed on submicronic dots prepared by electron beam lithography.

Keywords: Oxides, Magnetic Tunnel Junctions, MRAM, Perpendicular Magnetic Anisotropy, Interlayer exchange coupling, Spin Transfer Torque Switching

RESUME

Le but de cette thèse est l'étude des propriétés de jonctions tunnel magnétiques à aimantation perpendiculaire, en utilisant l'anisotropie perpendiculaire présente à l'interface entre un métal magnétique et un oxyde. En théorie, dans le cas des applications mémoires, les jonctions tunnel perpendiculaires devraient nécessiter moins d'énergie (courant) pour l'écriture par courant polarisé en spin. Mais la fabrication de telles structures représente un défi et une tâche difficile puisque les propriétés de transport (TMR) et d'anisotropie imposent des contraintes sur les matériaux utilisées en limitant la fenêtre de travail, notamment en ce qui concerne l'épaisseur des couches magnétiques. Pour atteindre cet objectif nous avons tout d'abord étudié les propriétés de ces structures comme l'anisotropie de l'interface métal magnétique-oxyde, le transport tunnel et le couplage entre les couches magnétiques à travers la barrière isolante. L'amplitude de l'anisotropie d'interface entre un métal magnétique et un oxyde dépend de l'épaisseur des couches magnétiques, de la température de recuit et la concentration de l'oxygène à l'interface. Différentes structures ont été réalisées afin de choisir la structure la mieux adaptée pour les applications mémoires MRAM. Une corrélation entre la TMR et l'anisotropie a été observée permettant de valider l'origine de l'anisotropie perpendiculaire : la formation de liaisons métal magnétique-oxygène. Un couplage antiferromagnétique à été aussi observé entre les couches magnétiques à anisotropie perpendiculaire à travers l'oxyde. Une étude détaillée sur le couplage a été faite en fonction de la température de recuit et de l'épaisseur des couches magnétiques pour mieux comprendre l'origine du couplage et une possible relation avec l'amplitude de l'anisotropie perpendiculaire. Finalement des jonctions perpendiculaires ont été nano-lithographiées et des mesures de commutation d'aimantation par transfert de spin sur des piliers nanométriques ont été réalisées avec de faibles courants critiques.

Mots-clés: Oxydes, Jonctions Tunnel Magnétiques, MRAM, Anisotropie Magnétique Perpendiculaire, Commutation par Couple de Transfert de Spin